Investigating the Deleterious Effects of Type 1 Diabetes Mellitus on Microvascular Repair in the Mouse Cortex

by

Eslam Mehina

B.Sc., University of Calgary, 2014

M.Sc., University of Calgary, 2016

A Dissertation Submitted in Partial Fulfillment

of the Requirements for the Degree of

DOCTOR OF PHILOSOPHY

in the Division of Medical Sciences (Neuroscience)

University of Victoria

I acknowledge with respect the Lekwungen peoples on whose traditional territory the university stands and the Songhees, Esquimalt and W̱SÁNEĆ peoples whose historical relationships with the land continue to this day.

Supervisory Committee

Investigating the Deleterious Effects of Type 1 Diabetes Mellitus on Microvascular Repair in the Mouse Cortex

by

Eslam Mehina

B.Sc., University of Calgary, 2014

M.Sc., University of Calgary, 2016

Supervisory Committee

Dr. Craig E. Brown, Supervisor

Division of Medical Sciences

Dr. Leigh Anne Swayne, Departmental Member

Division of Medical Sciences

Dr. Robert L. Chow, Outside Member

Department of Biology

Abstract

Microglia and brain-resident macrophages are the sentinel immune cells of the central nervous system (CNS), and are ideally situated to respond to any damage to the brain parenchyma or vasculature. Circulating leukocytes are generally excluded from the CNS environment under homeostatic conditions but can gain access to this region in diseases that disrupt immune system function and blood-brain barrier integrity. Although these diverse immune cells exhibit properties that may engender them to be well-suited to resolve microcirculatory insults, their relative contributions to the recanalization of capillary rupture in the cortex, known as cerebral microbleeds (CMBs), has yet to be described. CMBs are particularly concerning in conditions, such as diabetes mellitus (DM), in which these insults occur more frequently and potentially underlie the onset and progression of cognitive decline.

Using *in vivo* 2-photon microscopy and confocal imaging, here I highlight the compromised repair of CMBs in a mouse model of type 1 DM and characterize the robust, heterogeneous macrophage response to these insults. Specifically, 20% of damaged capillaries were eliminated from the circulation in the diabetic cortex and chronic insulin treatment failed to prevent this microvascular loss. Administration of interferon-α or interferon-γ neutralizing antibodies to dampen inflammatory signalling, or dexamethasone to reduce global inflammation, also failed to improve repair rates of damaged microvessels in diabetic mice. In contrast, CMBs in nondiabetic mice repaired without exception. Interestingly, depletion of CNS macrophages using the colony stimulating factor-1 receptor antagonist PLX5622 resulted in microvascular elimination in nondiabetic mice. Given the robust depletion of brain macrophage populations with this treatment, at first these data suggested that these cells were necessary for microvascular repair since their elimination produced vessel loss. However, by parsing the data I identified that

microvessels repaired in all cases where macrophages were not identified at the CMB; when CX3CR1+ aggregate was localized to the injury, ~20% of microvessels were eliminated. These findings show that CNS macrophages are not required for microvascular repair following CMB.

Immunofluorescent co-labelling of various microglial and macrophage markers within the diabetic CMB milieu revealed a novel population of Mac2+/TMEM119- cells, distinct from homeostatic TMEM119+ microglia. These cells reliably localized to CMBs that failed to repair and rarely associated with vessels that recanalized; Mac2+/TMEM119- cells were not found within nondiabetic CMBs. Treatment of diabetic mice with clodronate liposomes (CLR) to deplete circulating phagocytic leukocytes prevented aggregation of Mac2+/TMEM119- cells to CMBs and improved capillary repair rates. The efficacy of CLR in excluding these cells from the CMB aggregate, coincident with eradication of monocytes from circulation, indicated that these cells likely arose from the periphery. *In vivo* 2-photon imaging revealed significant increases in lipofuscin at the site of diabetic CMBs relative to the nondiabetic context; other phagocytic markers including CD68 and TREM2 were also upregulated. Mac2+/TMEM119- cells showed elevated lipofuscin content relative to homeostatic microglia; their association with CMBs may thus signal an increase in phagocytosis that contributes to capillary pruning.

Taken together, these data identify a novel Mac2+/TMEM119- macrophage associated with pathological microvascular elimination following CMB in the diabetic neocortex. These findings highlight the diversity of immune cell responses to CNS injury and provide insights into the cellular mechanisms of capillary pruning. Furthermore, these advances in our understanding of the regulation of microvascular elimination in the diabetic brain may have clinical implications for patients with DM as they provide evidence for putative adjuvant anti-inflammatory treatments, such as CLR, in mitigating cerebrovascular pathology.

Table of Contents

Supervisory Committee ii
Abstract iii
Table of Contents v
List of Tables viii
List of Figures ix
List of Abbreviations xi
Acknowledgements ii
Dedication iv
Epigraph v
CHAPTER 1: GENERAL INTRODUCTION 1
1.0 Rationale 1
1.1 The cerebrovascular network 3
1.1.1 Blood supply to, and within, the brain 3
1.1.2 Structure and function of the blood-brain barrier 6
1.2 Diabetes mellitus: an overview 12
1.2.1 Hyperglycemia has pervasive effects on cell signalling and function 17
1.2.2 Insulin and its limitations 25
1.2.3 Mouse models of type 1 diabetes 29
1.3 Diverse immune cell populations interact with the brain 34
1.3.1 Characterizing microglia and brain macrophages 35
1.3.2 The great migration: developmental origins of microglia and brain macrophages from yolk sac to maturation 41
1.3.3 Microglia as a diverse cell population 46
1.3.4 Microglial interactions with the vasculature 49
1.3.5 Peripheral phagocytes and the central nervous system 52
1.4 Vascular repair and immune cell function in diabetes 58
1.4.1 Diabetes as a disease of the vasculature 59
1.4.2 Diabetes and cerebral microbleeds 61
1.4.3 Inflammation in diabetes: implications for CNS-immune cell interactions 63

1.4.4 Immune cells in microvascular repair: help or hazard? 65
1.5 Project objectives 69
CHAPTER 2: MATERIALS AND METHODS 70
2.1 Animals 70
2.2 Craniotomies 70
2.3 *In vivo* 2-photon imaging and cerebral microbleed induction 72
2.4 Induction and treatment of type 1 diabetes mellitus 75
2.4.1 Streptozotocin treatment 75
2.4.2 Subcutaneous slow-release insulin administration 78
2.4.3 Drugs 78
2.5 Immunofluorescence and confocal imaging 79
2.6 Diff Quik histology 81
2.7 Data analysis 84
2.7.1 Determination of microvascular parameters 84
2.7.2 Morphological characterization of cerebral microbleed responses 86
2.7.3 Cell counting 89
2.7.4 Particle analysis *in vivo* and immunostained cortical sections 90
2.8 Data analysis and statistics 91
CHAPTER 3: TYPE 1 DIABETES MELLITUS MARS MICROVASCULAR REPAIR FOLLOWING CEREBRAL MICROBLEED 92
3.1 Abstract 92
3.2 Introduction 93
3.3 Results 95
3.3.1 Type 1 diabetes mellitus disrupts microvascular repair following microbleed in the mouse cortex 96
3.3.2 Morphological characteristics of microbleed responses do not predict microvascular loss 101
3.3.3 Anti-inflammatory treatment with dexamethasone or blockade of interferon signalling fails to rescue microvascular loss 106
3.3.4 Brain macrophage responses are not necessary for long-term microbleed repair 114
3.4 Discussion 119
CHAPTER 4: MAC2+ MACROPHAGES OF PERIPHERAL ORIGIN ARE ASSOICATED WITH MICROVASCULAR ELIMINATION IN TYPE 1 DIABETES MELLITUS 123
4.1 Abstract 123

4.2 Introduction 124
4.3 Results 127
4.3.1 Mac2+/TMEM119- macrophages are associated with microbleed responses in the diabetic cortex 127
4.3.2 Elimination of peripheral phagocytic leukocytes rescues pathological microvascular elimination in diabetes 139
4.3.3 Markers for phagocytosis are enhanced in the diabetic microbleed response, particularly in Mac2+/TMEM119- macrophages 150
4.4 Discussion 162
CHAPTER 5: GENERAL DISCUSSION 165
5.1 Summary 165
5.2 Type 1 diabetes mellitus disrupts repair of cerebral microbleeds with implications for impaired cognitive function 170
5.3 Heterogenous immune cell phenotypes respond to cerebral microbleeds 173
5.4 Phagocytic markers are upregulated in cells associated with microvascular elimination. 177
5.5 Limitations and Future Directions 180
5.6 Significance 182
REFERENCES 183

List of Tables

Table 1. Primary antibody concentrations and incubation conditions...... 80
Table 2. Summary of the proportion of microvessels repaired following microbleed in individual experimental animals. 113

List of Figures

Figure 1. General vascular architecture. 5
Figure 2. Cellular components and properties of the CNS blood-brain barrier. 9
Figure 3. Etiology of type 1 and type 2 diabetes mellitus. 16
Figure 4. Hyperglycemia affects numerous, diverse cell types and signalling pathways. 20
Figure 5. Insulin synthesis and general insulin receptor signalling. 27
Figure 6. Summary chart of common mouse models of type 1 diabetes mellitus. 32
Figure 7. Innate CNS immune cell localization and general homeostatic functions. 38
Figure 8. Ontogeny of innate brain macrophages. 44
Figure 9. Leukocyte ontogeny and hematopoiesis. 53
Figure 10. Example of cortical microvessel targeted for CMB and confirmation of ablation. 74
Figure 11. General experimental and longitudinal 2-photon imaging timeline. 76
Figure 12. STZ induces hyperglycemia in mice without significantly affecting weight. 77
Figure 13. Diff Quik histological stain visualized peripheral leukocytes and red blood cells. 83
Figure 14. Calculation of microvessel width and length. 85
Figure 15. Calculation of 2-dimensional area of eGFP aggregate at damaged microvessel. 87
Figure 16. Calculation of percentage of vessel coverage by eGFP+ processes. 88
Figure 17. Capillaries are repaired following cerebral microbleed in the healthy cortex, but eliminated in the diabetic condition. 98
Figure 18. Diabetes results in a significant loss of microvessels following microbleed that is not rescued by insulin treatment. 99
Figure 19. Microvascular parameters of targeted capillaries did not differ across groups. 100
Figure 20. Morphological characteristics of microbleed responses do not predict vessel fate. 104
Figure 21. Anti-inflammatory treatment did not rescue microvascular loss following microbleed in the diabetic cortex. 110
Figure 22. Anti-inflammatory treatments modulate microvessel fates following microbleed, but do not significantly affect microbleed response characteristics. 112
Figure 23. PLX5622 treatment significantly reduces cortical brain macrophage density. 115
Figure 24. PLX5622 depletion reveals CNS macrophages are not required for vessel repair. 118
Figure 25. CD206-expressing macrophages do not comprise the microbleed response. 129
Figure 26. Mac2+ cells are more resistant to CSF1R inhibition via PLX5622 treatment than homeostatic TMEM119-expressing cells. 133
Figure 27. Mac2+/TMEM119- cells are present in the brain parenchyma of untreated diabetic and PLX5622-treated brains in the absence of injury. 135
Figure 28. TMEM119-/Mac2+ cells are associated with eliminated microvessels in the diabetic cortex. 138

Figure 29. CX3CR1+ eGFP-expressing leukocytes stall in diabetic microvessels and near microbleed responses. 140
Figure 30. CLR depletes monocytes but not neutrophils, lymphocytes, or red blood cells. 141
Figure 31.CLR treatment effectively deplete tissue-resident macrophages of the spleen but not the brain parenchyma. 144
Figure 32. Depletion of peripheral phagocytes via clodronate treatment rescues diabetic microvessel loss following microbleed. 146
Figure 33. Clodronate treatment prevents aggregation of Mac2+/TMEM119- cells to diabetic microbleeds. 149
Figure 34. Lipofuscin autofluorescence reliably co-localizes with CD68 immunolabelling in CX3CR1+ cells. 154
Figure 35. Clodronate treatment normalizes pathologically elevated lipofuscin content in CX3CR1+ macrophages associated with microbleeds. 156
Figure 36. Lipofuscin content is significantly elevated in Mac2+/TMEM119- cells compared to homeostatic Mac2-/TMEM119+ cells. 158
Figure 37. CD68 and TREM2 immunostaining are significantly increased in diabetic microbleeds and normalized with clodronate. 161
Figure 38. Summary model of the effects of type 1 diabetes mellitus on cerebral microbleed repair. 169

List of Abbreviations

ACSF: Artificial cerebrospinal fluid

AD: Alzheimer's disease

ADP: Adenosine diphosphate

AGE: Advanced glycation endproducts

AGM: Aorto-gonado-mesonephros

ALS: Amyotrophic lateral sclerosis

ATP: Adenosine triphosphate

BAM: Barrier-associated macrophage

BBB: Blood-brain barrier

BM: Basement membrane

CCR2: CC-chemokine receptor-2

CD: Cluster of differentiation

CLR: Clodronate liposomes

CNS: Central nervous system

cpMΦ: Choroid plexus macrophages

CSF1: Colony stimulating factor-1

CSF1R: Colony stimulating factor-1 receptor

CX3CR1: CX3C chemokine receptor-1/ fractalkine

CXCL: Chemokine ligand

DAM: Disease-associated microglia

DB: Diabetic

DC: Dendritic cell

DEX: Dexamethasone

DM: Diabetes mellitus

DNA: Deoxyribonucleic acid

E: Embryonic day

EC: Endothelial cell

eGFP: Enhanced green fluorescent protein

eNOS: Endothelial nitric oxide synthase

ERK: Extracellular signal-regulated kinase

Fiji: Is just ImageJ

GAS6: Growth arrest-specific protein 6

GLUT: Glucose transporter

HbA_{1c} : Hemoglobin A1c

Hexb: Hexosaminidase subunit beta

HIF: Hypoxia-inducible factor

H_2O_2: Hydrogen peroxide

HSC: Hematopoietic stem cell

Iba-1: Ionized calcium-binding adaptor molecule-1

ICAM-1: Intracellular adhesion molecule-1

IFN: Interferon

IL: Interleukin

i.m.: Intramuscular

iNOS: Inducible nitric oxide synthase

INS: Insulin-treated diabetic

i.p.: Intraperitoneal

IR: Insulin receptor

i.v.: Intravenous

JAM: Junctional adhesion molecule

LFA-1: Lymphocyte function-associated antigen-1

LPS: Lipopolysaccharide

MAPK: Mitogen-activated protein kinase

MDM: Monocyte-derived macrophage

MHC: Major histocompatibility complex

mMΦ: Meningeal macrophages

MMP: Matrix metalloproteinase

MS: Multiple sclerosis

NADPH: Nicotinamide adenine dinucleotide phosphate

NDB: Nondiabetic

NFκB: nuclear factor κ-light-chain-enhancer of activated B-cells

NGP: Neurosciences Graduate Program

NKC: Natural killer cell

NMDAR: N-methyl-D-aspartate receptor

NO: Nitric oxide

NOD: Non-obese diabetic

NRROS: Negative regulator of reactive oxygen species

NSERC: Natural Sciences and Engineering Research Council

O_2*-: Oxygen free radical

***OH:** Hydroxyl radical

PARP: Poly(ADP-ribose) polymerase

PBS: Phosphate-buffered saline

PFA: Paraformaldehyde

PI3K: Phosphoinositide 3-kinase

PKB: Protein kinase B

PKC: Protein kinase C

pvMΦ: Perivascular macrophage

RAGE: Receptor for advanced glycation endproducts

RBC: Red blood cell

ROI: Region of interest

ROS: Reactive oxygen species

s.c.: Subcutaneous

STZ: Streptozotocin

TAM: TYRO3/AXL/MERTK receptor tyrosine kinases

TGF: Transforming growth factor

THIK: TWIK-related halothane-inhibited K^+

TJ: Tight Junctions

TMEM119: Transmembrane protein-119

TNFα: Tumour necrosis factor-α

TNFαR: Tumour necrosis factor-α receptor

TREM2: Triggering receptor expressed on myeloid cells-2

VCAM-1: Vascular adhesion molecule-1

VEGF: Vascular endothelial growth factor

VLA-4: Very late antigen-4

Acknowledgements

Several agencies provided funding to make this research possible. It has been a privilege to be supported by the Natural Sciences and Engineering Research Council (NSERC) through a Vanier CGS-D award and from UVic through the Edythe Hembroff-Schleicher and James A. & Laurette Agnew Memorial awards. The Brown Lab is funded by NSERC, the Canadian Institutes for Health Research, Canadian Foundation for Innovation, and Heart and Stroke Foundation. I would like to thank my supervisor, Dr. Craig Brown, for his patience, guidance, and support, as well as my committee members, Drs. Leigh Anne Swayne and Bob Chow, for their time, insights, and advice on this work. Furthermore, it is with much gratitude that I would like to acknowledge Emily White for her assistance with the chronic cranial window surgeries, and Taimei Yang, Dr. Michele Martin, and all of the amazing animal care staff for their excellent work in managing the mice and taking care of them with such compassion. I would also like to acknowledge Stephanie Taylor who collected the preliminary data for this project.

There is no doubt that this work would not have been possible without the extraordinary community of mentors and peers who have so generously supported me during this time, and who are an endless source of inspiration and joy. I would like to express my immense gratitude to Drs. Grant Gordon, Quentin Pittman, Roger Thompson, Jaideep Bain, and Janni Aragon for their ongoing support of my academic pursuits, all the last-minute reference letters, and their excellent advice and guidance. To my Gordon Lab buddies, Steven Shin and Drs. Adam Institoris, David Rosenegger, and Cam Ha Tran, thank you for your friendship, for making conferences so fun, and for being such outstanding humans. To Dr. Bruce Wright, thank you for all the time you have taken to meet with me and hear my ideas, for your encouragement and the jokes that went over my head, and for all the reference letters.

It has been a privilege to share this experience with an amazing cohort of peers in the Neuroscience Graduate Program. To Katie Neale, in particular, you are truly an 11/10 human and I am so grateful to have gotten to know you and to be inspired by your exceptional achievements and your commitment to making the world a better place. Thank you for your wisdom and for always knowing the right things to say, for your unwavering encouragement, and for dreaming with me of a healthier work-life balance and adventures beyond academia. To Dr. Bridget Ryan, thank you for your companionship and for being such a great listener during a particularly challenging time. I am so grateful for our mushroom foraging walks and I am continuously inspired by your breadth of knowledge and talents, and your wisdom.

To my Brown lab buddies, Emily, Alejandra, Mo, Pat, Reza, Rubina, Sunny, Ben, Sima, Maddy, and Sorabh, thank you all for your companionship, for being such great listeners, and for your enthusiasm for coffee walks. Each of you has made this experience special and meaningful. Alejandra, thank you for your compassion, your amazing insight, and your dauntless energy and commitment to brightening peoples' days. Sunny, thank you for laughing at my puns, for your patience with me, and for always making summer even more worth looking forward to. Ben, thank you for your ardent support of your friends and for making welcoming spaces for people to be themselves, for your excellent advice and honesty, and for all the golf and the memes.

Finally, I want to acknowledge all the mice that gave their lives for this research and the fundamental role that each one played in making the discoveries of this work possible.

A short sentence in this document is not sufficient to express my appreciation to each of you who has helped me to achieve all that I have and inspired me to push myself beyond my perceived limitations. I look forward to every opportunity in the future to continue to share my gratitude with you and to make you proud of me.

Dedication

To my family, with gratitude for the ongoing support of my academic pursuits – especially my sister Nabiha, for sharing the ups and downs of our mutual mental health journeys in grad school.

To Alex, my favourite human, with much love and appreciation for all the adventures we have shared and all the adventures still to come. Thank you for all of your enthusiastic encouragement and support, your patience, and your good humour.

Epigraph

Fortitude is key. More than anything, be consistent. Go at it. Go at it. Go at it. When you succeed, don’t forget the responsibility of making someone else succeed with you.

Antonia Novello

Discussing stuff is even harder in the midst of a global pandemic.

Eslam Mehina

CHAPTER 1: GENERAL INTRODUCTION

1.0 Rationale

Diabetes mellitus (DM) is a prevalent metabolic disorder that has reached epidemic proportions worldwide[1]. Commonly associated with a host of vascular complications, DM has important consequences to brain function as it is linked with increased incidences of neurovascular pathologies including stroke and cerebral microbleeds (CMBs)[2–5]. CMBs are hemorrhages that occur in penetrating arterioles or capillaries, resulting in a disruption of cerebral blood flow which may be temporary, if the vessel is repaired, or permanent if it is not[6,7]. Although strokes generally present immediate, overt clinical symptoms, CMBs likely impact brain function through in a more latent, protracted manner[7]. Indeed, although individual CMBs may be asymptomatic when they occur, compounding incidences have been positively correlated with cognitive decline and the onset or progression of dementias[7–10]. Of note, while insulin treatment is crucial for maintaining normoglycemia in type 1 DM, it does not abrogate diabetic pathology[11–16]. Since diabetic patients are at higher risk of experiencing CMBs[2,3], it is therefore imperative to develop effective strategies to prevent or repair these microvascular injuries.

The blood-brain barrier (BBB) is comprised of endothelial cells (ECs), astrocytes, mural cells, and basement membrane (BM)[17]. This crucial structure protects the central nervous system (CNS) from pathogens and potentially toxic molecules in circulation under healthy conditions[17]. Incidents of vascular rupture cause damage to this structure[6,7], resulting in the extravasation of blood plasma and other intravascular constituents into vulnerable tissues[18–21]. Brain-resident microglia are rapidly recruited to sites of tissue injury by local increases in cytokines and adenosine triphosphate (ATP)[22–24]. Once aggregated near the insult, these cells extend processes

to enwrap the microvessel in 3-dimensions, stemming leakage and restoring BBB cohesion[24,25]. Notably, this response is impaired in type 1 DM, resulting in prolonged BBB disruption[25]. The renewal of BBB integrity has been qualified as evidence of microvascular repair, but studies examining this phenomenon have restricted their analyses to the immediate few hours following rupture. Since vascular repair is an ongoing process, and because the restoration of blood flow to an impacted vessel may take days to weeks, it remains unknown whether microglial responses are necessary or sufficient for the ultimate recanalization of microvessels following CMB.

Due to their rapid, kinetic responses to CMBs and their juxtavascular localization, microglia have been the preferred candidates for study in the context of microvascular repair[24–26]. However, characterization of the plurality of immune cell phenotypes and functions that may be involved in the resolution of CNS injury has recently emerged as a major topic of research. For example, in addition to CNS-resident macrophages, peripheral leukocytes may also play a role in the repair of damaged microvessels. In fact, monocyte-derived macrophages (MDMs) have been shown to physically ligate the severed ends of damaged ECs following microbleeds in zebrafish[27]. Furthermore, during acute trauma or prolonged disease states, circulating immune cells have been shown to infiltrate the brain via upregulation of adhesion factors expressed on ECs[28–30]. As a chronic inflammatory disease, DM may produce conditions amenable to this process, facilitating peripheral leukocyte diapedesis into CNS tissues[31–34]. Paradoxically, microglia and macrophages have been assigned both supportive and detrimental roles in CNS injury repair[24,27,35–39], and further research is necessary to understand the involvement and relative contributions of these different cells in the context of CMB repair.

The goal of this work was to test the hypothesis that type 1 DM compromises repair of damaged microvessels following CMB via the disruption of immune cell responses to the injury.

Specifically, this dissertation sought to characterize the long-term repair of CMBs, and associated cellular responses, in mice over the course of weeks and identify the effects of type 1 DM on these processes. The diverse phenotypes of immune cells responding to CMBs were also examined and a putative cellular mechanism regulating microvascular repair in DM is proposed.

1.1 The cerebrovascular network

Before we begin exploring cerebrovascular dysfunction and mechanisms of repair, we must first discuss the CNS vascular architecture and its unique role in supplying the body's most energetically selfish organ - the brain - with the metabolic housekeeping required to sustain the intensive demands of neuronal processing[40]. The energetic costs of neurotransmission, the fundamental process underlying our perception of the world, cognition, and memories, are extraordinary; in fact, 20% of the body's metabolic activity at rest is attributed to the brain's functions[41]. Despite these demands, the brain is remarkably ill-equipped to store metabolic substrates and, besides sparse stores of glycogen in astrocytes, essentially relies on a constant supply of oxygen and glucose from vasculature[42,43]. This is also necessary for the removal of metabolic waste products and prevents their build-up in neural tissue. For these reasons, even small perturbations in CNS blood flow can significantly disrupt brain function, resulting in lasting implications for neurological health[7,9,44].

1.1.1 Blood supply to, and within, the brain

In order to supply the CNS with adequate blood flow, hundreds of kilometers of vasculature perfuse neural tissue. The internal carotid arteries and the vertebral arteries are the primary conduits of oxygenated blood to the brain, supplying anterior, middle and posterior territories[45]. These major arteries are joined by communicating arteries at the Circle of Willis, located on the ventral aspect of the brain; additional arteries branch from this structure to perfuse

distinct regions of brain tissue[45,46]. A key protective feature of the Circle of Willis is implicit in its "circular" structure: if a segment of the pathway is obstructed by a blockage, flow can still proceed along an alternative path. This redundancy prevents catastrophic disruptions in blood flow which would otherwise result in widespread ischemic tissue damage. Anastomoses, circular vascular structures formed by large pial arterioles on the brain's surface (Fig. 1), provide similar redundancy for crucial blood supplies[45,46]. Perpendicular branches from the surface vasculature form penetrating arterioles that dive down through most layers of the brain[47]. These arterioles are connected, via a network of microvessels, to penetrating venules which extract deoxygenated blood from CNS tissue for re-circulation[46,48]. Specifically, pre-capillary arterioles branch from penetrating arterioles and, through continuous degrees of bifurcation, form a network of capillaries that eventually leads to post-capillary and penetrating venules (Fig. 1)[48].

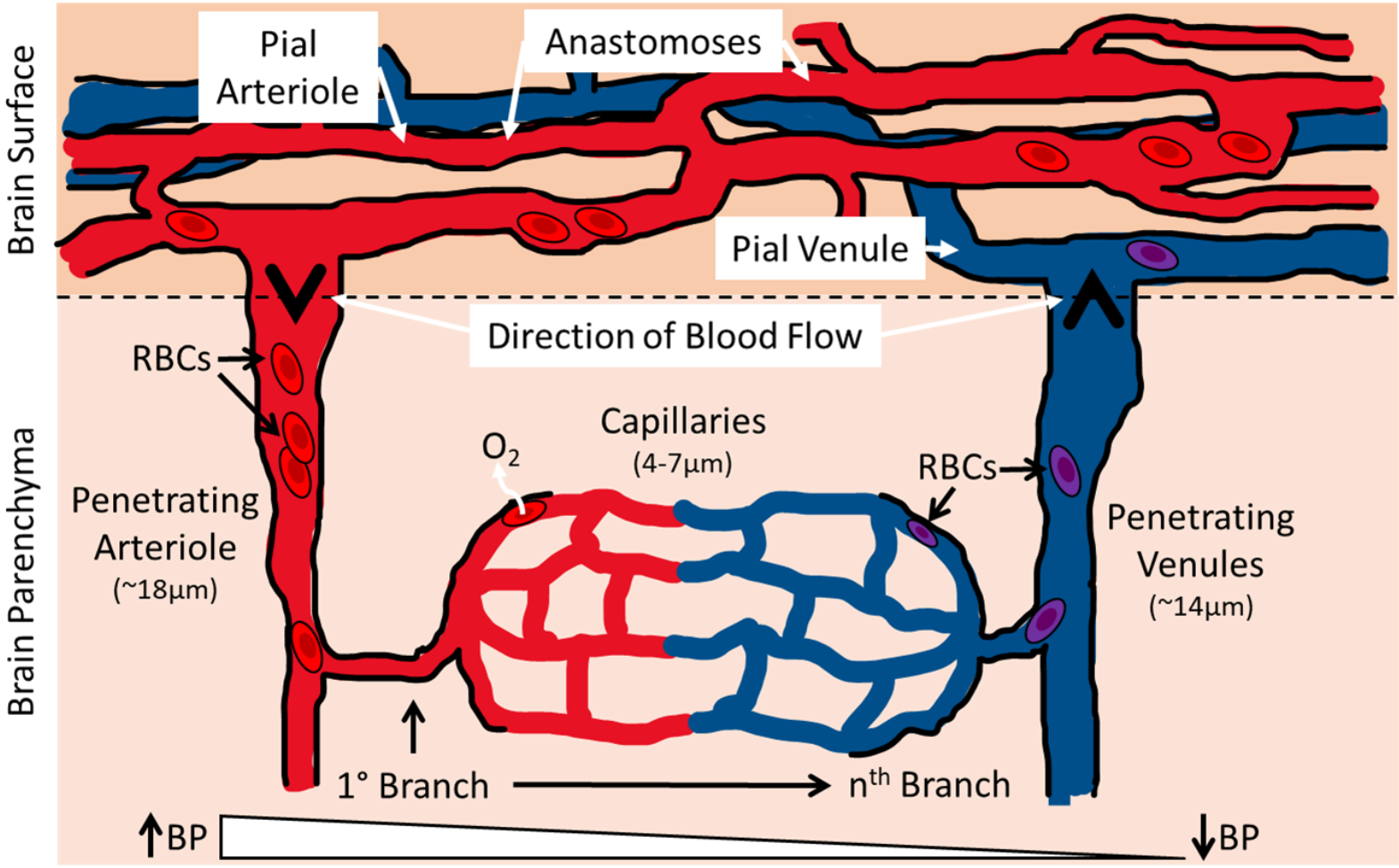

Figure 1. General vascular architecture.

Large pial arterioles and venules form circular structures, anastomoses, on the cortical surface. Penetrating arterioles and venules form perpendicular branches from the superficial vasculature and dive into the brain parenchyma. Beginning with the 1° pre-capillary arteriole branch, microvessels progressively branch into a complex network of capillaries that ultimately reach an n^{th} point that corresponds to the post-capillary venule. The flow of oxygenated blood is driven from the high pressure arteriolar aspect through the capillary network, where the exchange of metabolic products and O_2 occurs, to the low pressure venules. Deoxygenated blood is shunted away from the brain to the heart for recirculation to the lungs. RBC: Red blood cell.

The arterial and venous aspects of this network form essentially mirroring influx and efflux pathways of blood flow through the CNS. The capillary bed at the heart of this system is particularly noteworthy because this intricate web of microvessels (4-7 μm in diameter) is the primary site of gas and nutrient exchange in the brain (Fig. 1)[45]. The majority of the CNS vascular length is actually comprised of microvessels (>90%)[49,50] and, under healthy conditions, cell somas in the CNS are usually no more than 20 μm away from a capillary[51]. Between the first microvessel branching off of a pre-capillary arteriole to the last one before a post-capillary venule at the far end of the capillary bed there may be over a dozen consecutive capillary branches[48]. As in the context of anastomoses, the redundancy of the capillary network mitigates ischemic damage in the event of a loss of flow through an individual segment of the vasculature[7,52]. Indeed, the crucial role that capillaries play in supporting brain function is underscored by the fact that the compounding loss of capillaries can produce notable cognitive deficits in experimental animal models[6,7] and human disease[8,10,53]. The integrity and maintenance of these microvessels is, therefore, imperative for neurological health and brain function.

1.1.2 Structure and function of the blood-brain barrier

The primary feature of the CNS vascular architecture that sets it apart from peripheral vessels is a unique structure that rigorously segregates the brain from the general circulation: the BBB. The existence of a barrier structure in CNS vasculature was initially discovered in experiments conducted by Ehrlich in the early 1900s, wherein systemic dye perfusions failed to stain neural tissue coincident with the robust labelling of peripheral organs[54]. These findings suggested that a stringent barrier associated with the CNS circulation prevented the dye from accessing these privileged tissues, unlike the peripheral vasculature which was devoid of a comparable barrier structure and failed to exclude the dye[54]. Not only does the BBB tightly

regulate the quantities of ions and substrates in the brain parenchyma, to support signalling that relies on minute changes in the brain microenvironment, but it also protects vulnerable CNS tissue from potentially toxic substances and cells in circulation[45,55]. Broadly speaking, the BBB only permits the passage of water, lipid-soluble molecules, gases, and the selective transport of nutrients (ie. glucose, lactate, amino acids) from the vascular lumen to the brain parenchyma[45,55].

Several cellular constituents comprise the BBB including ECs, astrocytes, and mural cells (smooth muscle cells and pericytes); in conjunction with the BM, the highly selective "barrier" feature of this structure is a product of these cells' cumulative properties (Fig. 2A)[46]. Specifically, ECs are coupled by tight junctions (TJs) which closely fuse individual cells and restrict molecular diffusion and paracellular leukocyte transmigration (Fig. 2B)[46]. TJs are comprised of 3 integral membrane proteins, claudins, occludins, and junction adhesion molecules (JAMs), which can also associate with accessory proteins that regulate junctional permeability (Fig. 2B)[56]. EC transporters, necessary for shuttling glucose, lactate, and other molecules, regulate the passage of target substrates, further contributing to the selectivity of the barrier (Fig. 2B)[55]. Notably, CNS ECs demonstrate low rates of transcytosis and exhibit few vesicles and caveolae (Fig. 2B) relative to their peripheral counterparts[57].

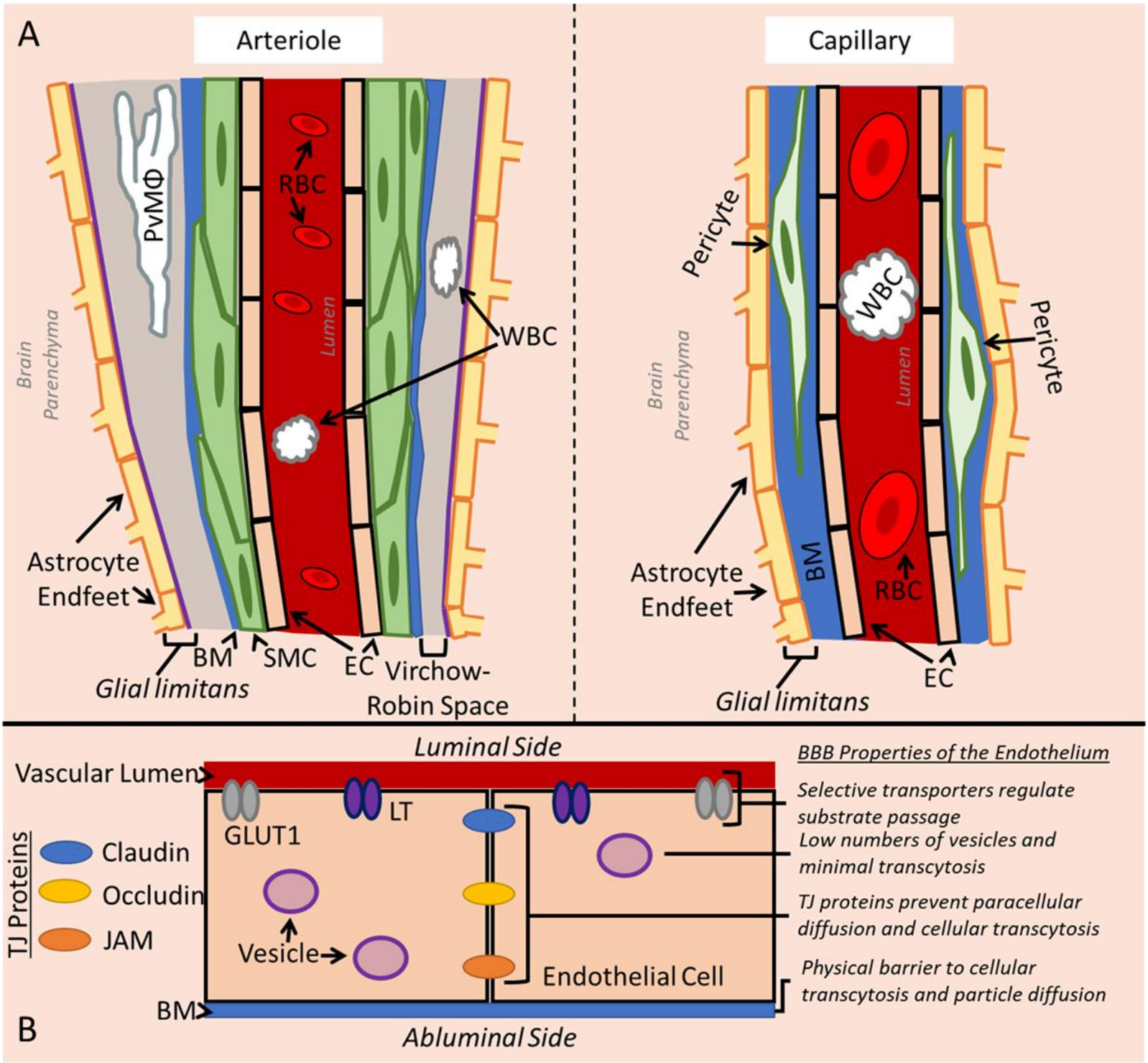
A
Arteriole
Capillary
PvMΦ
RBC
WBC
Lumen
Brain Parenchyma
Astrocyte Endfeet
BM
SMC
EC
Virchow-Robin Space
Glial limitans
Pericyte
Pericyte
WBC
Lumen
Brain Parenchyma
Astrocyte Endfeet
BM
RBC
EC
Glial limitans
B
Luminal Side
Vascular Lumen
GLUT1
LT
TJ Proteins
Claudin
Occludin
JAM
Vesicle
Endothelial Cell
BM
Abluminal Side
BBB Properties of the Endothelium
Selective transporters regulate substrate passage
Low numbers of vesicles and minimal transcytosis
TJ proteins prevent paracellular diffusion and cellular transcytosis
Physical barrier to cellular transcytosis and particle diffusion

Figure 2. Cellular components and properties of the CNS blood-brain barrier.

A. The cellular structure of the BBB between arterioles and capillaries in the CNS. The endothelium of arterioles is enwrapped by smooth muscle cells that control vascular tone. Between the BM and the *glial limitans*, which is comprised of astrocyte endfeet, is the Virchow-Robin space. Within this compartment, immune cells including perivascular macrophages and peripheral leukocytes exist and may interact with the local brain parenchyma via extensions of cell processes through the *glial limitans*. At the level of a capillary, the *glial limitans* fuses with the BM and the Virchow-Robin space disappears. To interact with the brain parenchyma, leukocytes in circulation must transmigrate across the BM as well as the *glial limitans*. Capillaries are associated with pericytes rather than smooth muscle cells. **B.** The endothelium of CNS vasculature exhibits several properties that contribute to the stringency of the BBB. Selective transporters on the luminal aspect of the vasculature regulate substrate passage to the brain parenchyma. Glucose transporter-1 (GLUT-1) and lactate transporters permit the influx of nutrients (glucose and lactate, respectively). Relative to peripheral ECs, their CNS counterparts exhibit low levels of transcytosis and contain few vesicles. TJ proteins, including claudins, occludins, and JAMs, couple ECs directly, eliminating paracellular spaces and minimizing molecular diffusion and cellular transmigration. The BM on the ablumenal aspect of ECs acts as a physical barrier to inhibit cellular infiltration and limit particle diffusion. RBC: Red blood cell. WBC: White blood cell. SMC: Smooth muscle cell. LT: Lactate transporter. JAM: Junctional adhesion molecule.

Astrocytes are intimately associated the CNS vasculature and their specialized processes, endfeet, create a physical barrier, the *glial limitans*, external to the BM and mural cells. Endfeet cover >90% of CNS blood vessels[58] and are responsible for the induction of the BBB properties of ECs during development[59], enhancing the expression of TJ proteins[59,60], sequestering glucose from blood vessels[61,62], and releasing vaso-active compounds that influence microvascular tone[63–65]. Indeed, extensive work has explored the putative mechanisms by which astrocytes may be involved in the regulation of stable or dynamic microvascular tone. Neurovascular coupling describes the phenomenon by which elevated neuronal activity prompts local vasodilation and increased blood flow[64]. Owing to their ideal positions around the vasculature, astrocytes serve as key conduits for these signals[66] and maintain the basal tone of microvessels[63,67]; they may even regulate vascular tone in the absence of changes in neuronal activity[65]. Notably, astrocytes also modulate dynamic changes in vascular tone in response to local neuronal activity by sensing synaptic glutamate via metabotropic glutamate receptors; subsequent astrocytic calcium signals prompt astrocytic release of vasoactive compounds, including arachidonic acid, prostaglandins, and epoxyeicosatrienoic acids which drive changes in arteriole tone[64,68]. There remains considerable controversy regarding the timescale on which astrocytes may influence changes in vascular tone (whether fast or slow), as well as whether, or which types of, astrocyte calcium responses are necessary for modulating these effects[69].

Finally, mural cells, including vascular smooth muscle cells along arteries and arterioles and pericytes that associate with capillaries, are also involved in the formation and stabilization of the BM during development[70,71] and in vascular tone regulation[72,73]. The diversity in distribution and morphology of mural cells has been highlighted, but specific roles for individual variants have yet to be reliably described[72,74]. Vascular smooth muscle cells have obvious roles

in regulating contractile responses in arteries and arterioles, via activity of α-smooth muscle actin, in response to signals from astrocytes, neurons, and sympathetic innervation[55,75,76]. The brain and retina demonstrate the greatest density of pericytes in the body[71]. Pericytes, particularly those localized to pre-capillary arterioles which have been shown to contain α-smooth muscle actin, may regulate capillary tone[72,73]. Electrical stimulation of pericytes in the retina and cerebellum produces capillary constriction along with a signal that propagates to distant pericytes[77]; these waves of activity may be capable of inducing significant changes in regional blood flow. Ischemic conditions are also capable of inducing pericyte-driven constriction of capillaries, which may contribute to the progression of neurovascular disease[77]. In addition to their profound roles in influencing microvascular tone, astrocytes and mural cells facilitate angiogenesis[78,79], engage in forms of phagocytosis[80–82], and protect against BBB degeneration[60,83].

The physical organization of the BBB differs between large CNS arterioles and microvessels. At the level of pial vessels and penetrating arterioles, smooth muscle cells are located below the BM and surround ECs (Fig. 2A), providing vascular contractility[77]. Pre-capillaries and capillaries, however, are associated with diverse classes of mural cells, including pericytes, which are embedded in the BM and extend sparse projections around ECs (Fig. 2A)[72,74]. Near the cortical surface penetrating arterioles are surrounded by Virchow-Robin space, a sinus that represents an extension of the subarachnoid space and separates the *glial limitans* and the BM[47]. Various immune cells exist within this niche, including resident perivascular macrophages (PvMΦ) and blood-borne leukocytes (Fig. 2A), that can influence cellular processes in the brain parenchyma and even local vascular tone[84,85]. As penetrating arterioles approach deeper cortical layers, the Virchow-Robin spaces progressively taper until the *glial*

limitans fuses with the BM at the capillary level (Fig. 2A)[47]. In capillary beds, vessel walls are only a single EC thick, allowing gas and nutrient diffusion to occur as permitted by the BBB[45,55].

Given the key role of the BBB in creating a relatively sterile and tightly regulated microenvironment in the brain, damage to its integrity and function can result in serious consequences to CNS homeostasis. Hemorrhagic stroke, or even the rupture of small blood vessels, creates a physical disruption in the BBB that permits the influx of toxins, including iron and fibrinogen, which may damage neuronal circuits[18,20,86,87]. The infiltration of peripheral leukocytes via these lesions can exacerbate inflammation and local cell damage[28,30,88]. Aging[89,90], as well as various disease conditions including Alzheimer's disease (AD)[19,91] and multiple sclerosis (MS)[18,92], are also associated with BBB breakdown. In these cases, the disruption of BBB integrity is correlated with the onset and progression of disease states and impairments in cognitive function. DM may also worsen BBB damage following vascular insults including microbleeds and stroke[15,25,93,94]. Coupled with the demonstrated upregulation of adhesion molecules on neurovascular ECs that occurs in DM[34], these conditions may facilitate aberrant leukocyte infiltration into the brain parenchyma. Taken together, the maintenance of vascular and BBB integrity is necessary for efficient brain function and health.

1.2 Diabetes mellitus: an overview

Diabetes has been described and treated as a physiological disorder since ancient times. Dubbed "honey urine" by Ayurvedic physicians, clinical symptoms of diabetes including glycosuria, diabetic gangrene, and emaciation are also described in *The Canon of Medicine* (1025 AD), the authoritative work of renowned Arab physician Ibn Sina[95–97]. Indeed, diabetes may have been referenced as early as 1552 BC in the Ebers Papyrus where a condition characterized by polyuria, a common symptom of diabetes, is treated with "water … elderberry,

fibers of the *asit* plant, fresh milk, beer-swill, [cucumber flowers], and green dates[97–99]." Joseph von Mering and Oskar Minkowski are generally credited with the discovery of the role of the pancreas in the manifestation of DM during their tenure at the University of Strasbourg in 1889[97]. DM was differentiated from diabetes insipidus by the progressive efforts of Frank and Farini. Working in the late 1700s, Frank observed that, although diabetes insipidus patients also produced high urine volumes and experienced polyuria, they did not excrete the hyperglycemic urine characteristic of DM patients[100]; Farini's isolation of vasopressin to treat this disease in 1913 confirmed the differential pathophysiological bases of DM and diabetes insipidus[100,101].

As of 2014, upwards of 8.5% of the global population suffered from some form of DM[1]. Type 1 and type 2 DM are the most prevalent forms of the disease, comprising ~10% and ~90% of DM cases, respectively; gestational diabetes and other types of diabetes resulting from genetic abnormalities, other diseases, or medications account for remaining diagnoses[102]. Although cases of type 1 DM can be diagnosed in adults, it is generally considered a disease of the young and pathophysiological features, such as islet autoantibodies, are identified in children <5-years-old in most individuals who later develop type 1 DM[103]. The cause of this disease remains unknown. A significant role for genetic factors has been identified, but genetics alone are regarded as insufficient; environmental factors, such as viral infection, have been hypothesized to trigger type 1 DM onset coincident with genetic susceptibility[104–107].

Elevated blood glucose, hyperglycemia, is the hallmark of all DM variants. It is generally accepted that this symptom manifests in type 1 DM as a result of the destruction of cells in the pancreas[108–110]. The pancreas is an organ with endocrine roles involved in the regulation of blood glucose; it also has important exocrine functions pertaining to digestion, including the secretion of enzymes necessary for this process[111,112]. Pancreatic endocrine tissues are organized in

clusters, referred to as islets of Langerhans, and contain α-, β-, and δ-cells which release the hormones glucagon, insulin, and somatostatin, respectively[111]. Pancreatic β-cells also co-release amylin with insulin at a ratio of 1:100 (amylin:insulin), and secrete c-peptide in equimolar quantities to insulin[112]. Amylin is produced post-prandially and slows the release of glucose into circulation through the coordinated inhibition of gastric emptying, digestive secretions, and glucagon release[111]. Notably, amylin is active in the hypothalamus and brainstem nuclei and modulates energy expenditure by reducing appetite and increasing sympathetic nervous system activity[113]. C-peptide facilitates the assembly, folding, and processing of insulin during its synthesis[114], and has been implicated as a protective factor in mitigating nerve damage; in fact, c-peptide administration in diabetic animals exhibiting early signs of neuropathy has been shown to improve nerve conduction velocities and mitigate structural degeneration[115].

The T-cell mediated autoimmune attack of pancreatic β-cells, the subsequent invasion of these lesions by mononuclear phagocytic leukocytes, and loss of β-cell mass are the mechanisms presumed to underlie the reduction or elimination of insulin production and secretion in type 1 DM[110]. Under healthy conditions, glucose uptake by skeletal muscle and fat occurs in a concentration-dependent manner via GLUT-4, which is trafficked to the cell membrane from intracellular storage vesicles by the activation of the transmembrane insulin receptor (IR)[116–118]. In the liver, glucose is transported from circulation in an energetically passive and insulin-independent manner (Fig. 3), predominantly mediated by GLUT-2 transporters which are permanently embedded in the plasma membrane[119]. By this mechanism, glucose is stored or metabolized, and glucose elevations are transient and tightly regulated. However, in the absence of insulin, this elegant control system is impaired and hyperglycemia manifests (Fig. 3)[116,117].

The concomitant absence of amylin secretion due to the loss of pancreatic β-cells may exacerbate the effects of hyperglycemia through uninhibited post-prandial glucose spikes[111].

Type 2 DM may also involve reduced secretion of insulin by pancreatic β–cells, but it is predominantly associated with the desensitization of IRs to circulating insulin (Fig. 3)[120]. The majority of individuals diagnosed with type 2 DM are obese and, although it is well known that the accumulation of intracellular free fatty acids is correlated with the degradation of effective IR signalling, the molecular mechanism underlying this process remains elusive[120,121]. Insulin resistance has been reproduced *in vivo* through manipulation of IR substrate-2, protein kinase B (PKB), and the transcription factor FOXO1a, suggesting that the activity of these downstream IR signalling molecules may play a key role in the manifestation of this condition[122–124]. Reduced IR signalling may also be caused by phosphorylation of protein kinase C (PKC), which leads to decreased IR gene expression, and, independently, the generation of by-products of mitochondrial dysfunction that prompt degradation of IR substrate proteins[123–126].

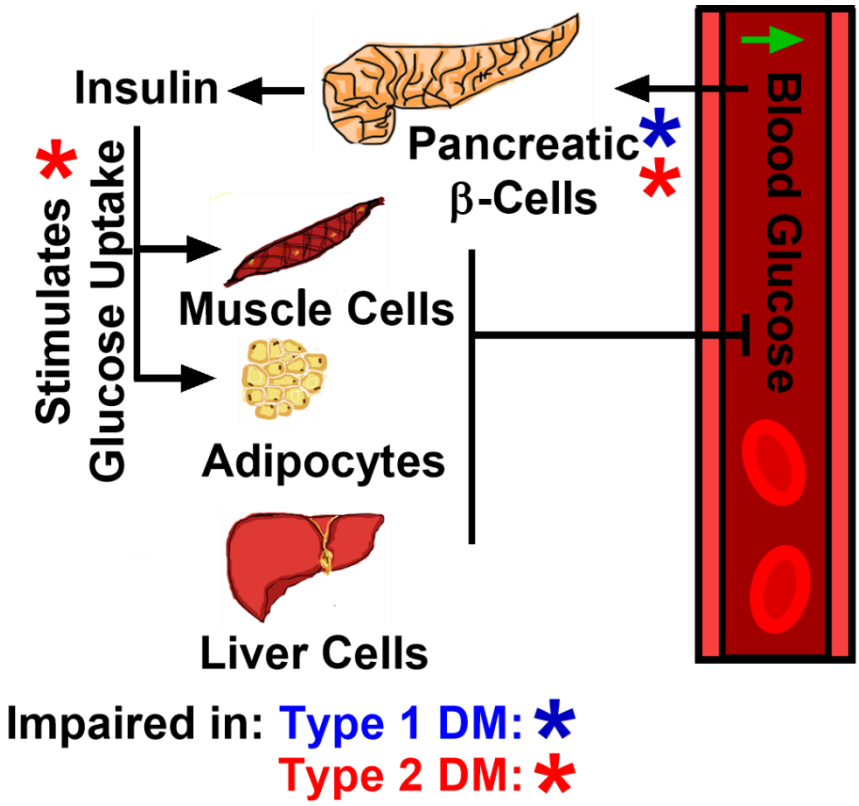

Figure 3. Etiology of type 1 and type 2 diabetes mellitus.

Type 1 and type 2 DM are both characterized by elevated blood glucose levels, but the pathological basis of this condition differs between disease variants. In type 1 DM, pancreatic β-cells in the islets of Langerhans are destroyed (*blue asterisk*) and thus cannot produce or secrete insulin or amylin in response to elevated blood glucose in circulation. In the absence of insulin, GLUT-4 transporters in muscle cells and adipocytes are not translocated to the plasma membrane to permit glucose uptake. The release of insulin by pancreatic β-cells may also be impacted in type 2 DM (*red asterisk, right*), but this disorder is primarily associated with IR insensitivity wherein skeletal muscle and fat tissue fail to sequester glucose even in the presence of normal insulin levels (*red asterisk, left*). Although glucose uptake by the liver is insulin-independent, it cannot compensate for the combined loss of homeostatic GLUT-4 activity and IR signalling in muscle cells and adipocytes, thereby leading to hyperglycemia.

For the purposes of this dissertation, I will focus on the effects of type 1 DM on microvascular repair. Type 1 DM it is an established risk factor for vascular pathology and is strongly correlated with increased incidences of stroke and CMB[2,3]. Of note, diabetic anomalies have been identified in the physiology of CNS-innate microglia and their responses to CMBs[25] and retinal microvascular disease[127], highlighting a candidate cell type whose dysfunction may be associated with poorer outcomes. Furthermore, since patients are generally diagnosed with type 1 DM at a younger age than those with type 2 DM, it affects them for a greater proportion of their lives and has been strongly correlated with mortality[11–13,128,129]. Additionally, although insulin provides a life-saving management technique for type 1 DM patients, it fails to completely mitigate complications [11–16,130,131]. It is, therefore, critical to understand the cellular and physiological changes contributing to type 1 DM pathology and facilitate the development of more effective management strategies for this disease and its debilitating comorbidities.

1.2.1 Hyperglycemia has pervasive effects on cell signalling and function

As highlighted above, the classical diagnostic criterion for DM is chronically elevated blood glucose: hyperglycemia. Understanding the cellular basis of hyperglycemia is thus imperative for determining how cellular pathology manifests in this disease. In biological processes, glucose is a primary energy source and serves as a key modulator of cell function. Notably, glucose is the brain's preferred metabolic substrate as it is poorly equipped to sequester energy from free fatty acids. Indeed, neurons have low energy storage capacity, relying instead on the regular import of glucose across the BBB from the circulation[132–134]. Interestingly, many CNS cells cannot directly gate glucose influx despite the crucial role that this molecule serves in supporting their function. Specifically, because the glucose transporters of CNS cells are concentration dependent they rely on transient increases in extracellular glucose concentrations

to drive appropriate levels of uptake[116–119,135–137]. Implicit to the nature of this mechanism, cells are exquisitely sensitive to fluctuations in circulating glucose levels. Cerebral ECs that line the vasculature, for example, express GLUT-1 and are bathed by hyperglycemic plasma, experiencing a chronic influx of glucose in diabetic conditions (Fig. 4A)[135–137]. Immune cells in circulation are also persistently inundated by the hyperglycemic environment[138–141].

Although the BBB provides a barrier between the CNS and blood plasma, it cannot prevent neural cells from hyperglycemic toxicity due to the way in which glucose moves in the brain. Specifically, increased glucose uptake by GLUT-1 in cerebral ECs is shuttled in greater concentrations into the perivascular space (Fig. 4A)[142]. Glucose is then taken up by GLUT-1 transporters on astrocyte endfeet, which systematically tile the vasculature; astrocytes may convert glucose into glycogen for storage or extrude it down its concentration gradient into the parenchyma to be utilized by other cells (Fig. 4A)[61,62]. GLUT-3, a high-affinity glucose transporter, is expressed by both neurons and microglia and ensures a constant influx of glucose even when extracellular concentrations are low[143]. Although microglia can utilize glucose, free fatty acids, and glutamine as metabolic substrates, they crucially rely on glucose for survival[144]. During microglial activation, when the energetic needs of these cells increase dramatically, they undergo a metabolic switch from oxidative phosphorylation to glycolytic metabolism of glucose and lactate production[145]. Interestingly, hyperglycemia has been shown to augment microglial activation in post-mortem brain tissue from patients, relative to those that were euglycemic before death[146]. Furthermore, in primary rat microglial culture, tumour necrosis factor-α (TNFα) secretion was amplified 4-fold by increasing extracellular glucose concentrations from 10 mM to 25 mM[147], further highlighting the sensitivity of these cells to hyperglycemic conditions. Taken

together, the activity of GLUT-1 and GLUT-3 systematically shuttle glucose throughout the extracellular and cellular compartments of the brain (Fig. 4A)[143,148].

It is worth noting that there is a debate in the literature regarding whether GLUT-1 transporters are downregulated in response to hyperglycemia[149,150], as this adaptive response could help to adjust glucose transport. Some studies have shown no difference, or a reduction, in GLUT-1 expression, but results also vary between regions (for review, see [149,150]); for example, Badr et al. demonstrated that GLUT-1 was downregulated in the retina, but not the cortex or microvascular ECs[151]. Despite these discrepancies pertaining to GLUT-1, there is general consensus that type 1 DM results in higher glucose uptake across the BBB[150,152,153]. These findings can be reconciled with the GLUT-1 debate given that, while GLUT-1 is the primary CNS glucose transporter, GLUT-3, as well as more sparsely expressed transporters such as GLUT-4 and GLUT-8, can also influence brain glucose levels[61,132,148].

In the periphery, which lacks a BBB correlate, cells, including neurons, are directly susceptible to hyperglycemic damage[11,13]. As a result of the significantly elevated glucose concentrations that build up in peripheral nerves, intracellular hexokinase becomes saturated and aldose reductase begins to convert glucose into sorbitol[148,154]. Since sorbitol is not readily cleared from affected cells, due to its low membrane permeability, its progressive accumulation exacerbates hyperglycemic toxicity and results in tissue swelling and damage due to osmotic stress[148,154]. The pathophysiological effects of sorbitol in the periphery have been linked to diabetic complications including nerve damage and cataracts[154,155]; notably, aldose reductase inhibitors, such as vitamin K1, have shown promise in preventing lens breakdown and cataract formation[155].

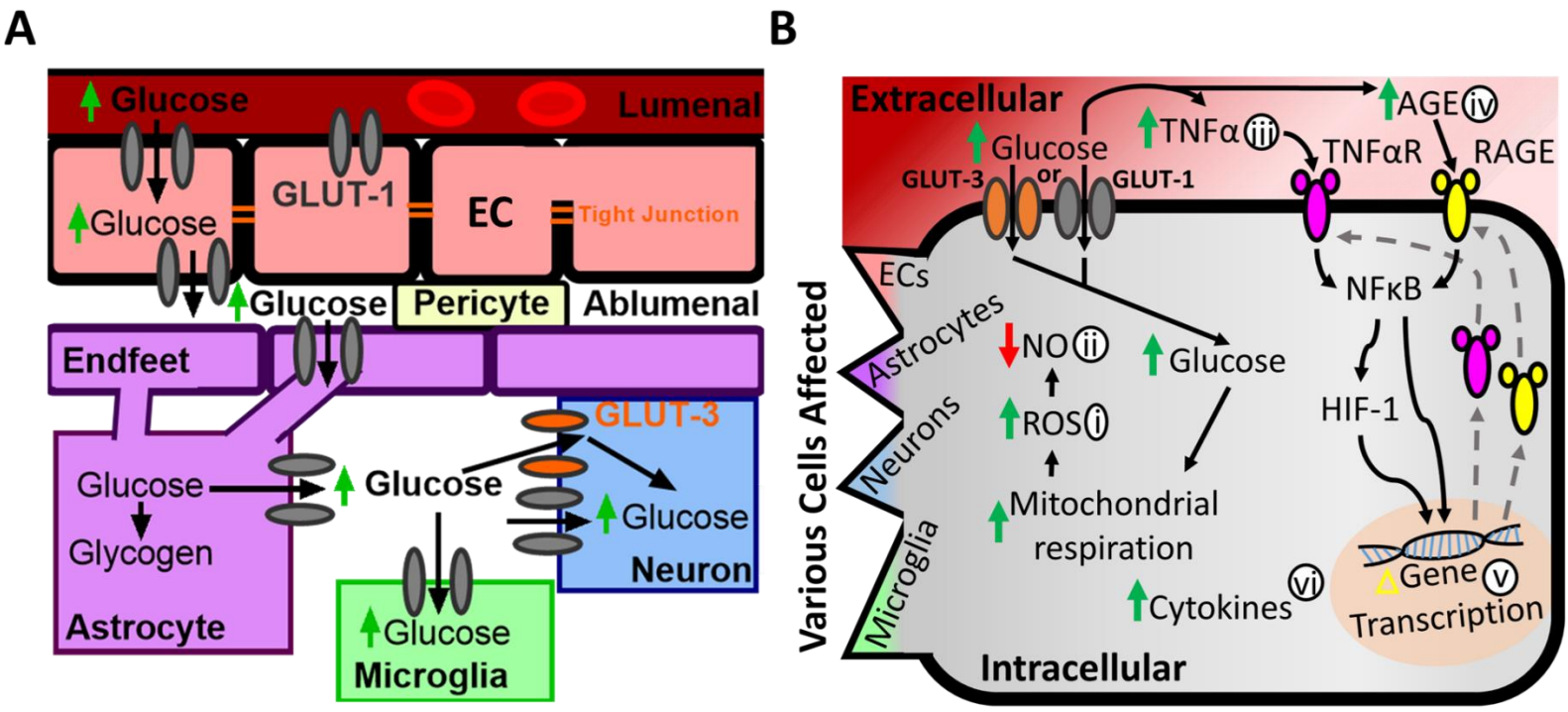

Figure 4. Hyperglycemia affects numerous, diverse cell types and signalling pathways.

A. Hyperglycemia in DM results in glucose being shuttled into ECs via passive GLUT-1. Glucose is then transported into the perivascular space and taken up by astrocyte endfeet; astrocytes may store glucose as glycogen or extrude it down its concentration gradient into the parenchyma. Other CNS cells increase glucose uptake via passive GLUT-1 and GLUT-3 as extracellular concentrations rise. **B.** High extracellular glucose prompts its influx via GLUT-1 and/or GLUT-3, resulting in progressively elevated intracellular concentrations. To clear excess glucose, mitochondrial respiration is elevated, and **i.** reactive oxygen species (ROS) are produced which **ii.** quench NO. Hyperglycemia prompts global activation of **iii.** TNFα and **iv.** advanced glycation endproducts (AGEs), which upregulate NFκB and hypoxia-inducible factor-1 (HIF-1). **v.** These molecules prompt translocation of nascent receptors for TNFα and AGEs (TNFαR and RAGE, respectively) to the plasma membrane via changes in gene transcription, and the **vi.** increased production of cytokines further amplifies inflammation.

The term “hyperglycemic toxicity” endeavours to broadly describe the pathological alterations and degradation of the integrity, viability, and functionality of many unique cell types in response to the diabetic condition. The generality of this term perhaps underscores the pervasive nature of these effects, and also hints at the uncertainty of the specific signalling pathways that drive these aberrations. Indeed, although a plethora of key targets have been identified, as both altered by hyperglycemia and contributing to cellular pathology[142,148,156–158], not one has been recognized as particularly superior to another. Similar to the pervasive way in which hyperglycemia directly affects all cells in the body, hyperglycemic toxicity conducts a concert of alterations in fundamental cellular signalling pathways. These effects are not only difficult to parse from one another, but underlie such key processes, including gene transcription and protein glycation, that their individual contributions are challenging to identify.

For the purpose of this introduction, I will focus on outlining 5 molecular mechanisms which have been implicated in vascular and immune cell dysfunction: ROS production; NO quenching; TNFα upregulation; protein glycation; cytokine generation. Firstly, ROS, major contributors to oxidative stress, are primarily generated as by-products of the reduction-oxidation reactions that occur during cellular respiration in mitochondria[159–162] (Fig. 4B). Elevated cellular metabolism in the mitochondria, which is required to clear high levels of intracellular glucose[142,162], produces increasing levels of superoxide dismutase, which generates hydrogen peroxide (H_2O_2)[148,163]. Generally, glutathione peroxidase effectively converts H_2O_2 into water; this reaction depends on nicotinamide adenine dinucleotide phosphate (NADPH), which is required to reduce glutathione peroxidase’s substrate, glutathione, from glutathione disulphide[148,164]. However, under conditions of increased oxidative metabolism, the polyol pathway is recruited instead of glycolysis, which requires less NADPH, and glutathione

production is diminished[164,165]. Therefore, during hyperglycemia H_2O_2 persists and produces reactive superhydroxyl radicals ($^{*}OH$) via the Fenton reaction[148,166]. Similarly, elevated metabolism also accelerates the production of oxygen free radicals (O_2^{*-}) from the reduction of O_2 during the mitochondrial electron transport chain step of cellular respiration[162,167,168] (Fig. 4B). Endogenous antioxidants may scavenge a proportion of these ROS,[165,169–172] but the chronic accumulation of cellular damage arising from escaped ROS contributes to progressive oxidative stress[164,172–174]. This damage triggers deoxyribonucleic acid (DNA) strand breakage[173,174] and activates poly(ADP-ribose) polymerase (PARP), which further slows glycolysis[148,156,164]. ROS interfere with vascular function by targeting astrocytes, inhibiting the folding of astrocytic gap junction proteins and degrading endfeet[156,175], and by inducing pericyte loss along capillaries[156].

NO, historically identified as endothelial-derived relaxing factor, is best known as a potent vasodilator that plays an important role in regulating vascular tone[176]. This readily diffusible free radical also acts as a modulator of cell signalling via its nitration of lipids and proteins[177]; for example, S-nitrosylation of N-methyl-D-aspartate receptors (NMDARs) results in their inactivation and can prevent excitotoxic cell damage via inhibition of excessive calcium influx through the receptor[178]. In the oxidative intracellular environment of diabetic cells, NO reacts with readily available ROS to form peroxynitrite (Fig.4B). The reaction of NO with O_2^{*-} is especially remarkable because it is so kinetically and thermodynamically favourable that it occurs spontaneously whenever these molecules are present within ~30 μm of one another; indeed, it is fast enough to always outcompete endogenous superoxide dismutase enzymes, making it essentially inevitable when the reactants are available[179–181]. In this way, sources of NO for housekeeping processes are diminished (Fig. 4B) and highly reactive peroxynitrite is formed, disrupting DNA, protein structure, and BBB integrity[181–184]. Notably, the inflammatory

interferon-γ (IFN-γ) pathway is activated by peroxynitrite and produces BBB permeability via breakdown of the BM[182,184]; this phenomenon can be inhibited by sequestering ROS [183,185].

In a hyperglycemic environment, TNFα production is induced in monocytes[157,158], reactive astrocytes[186], and vascular smooth muscle cells[187,188]and may be ROS-dependent or independent[158] (Fig. 4B). A key inflammatory molecule, TNFα induces p38 mitogen-activated protein kinase (MAPK) activity in monocytes and prompts their activation[158]; furthermore, since TNFα can be transported across the BBB, microglia are also affected. In support of this idea, Ibrahim et al. demonstrated that p38 co-localized with microglia in diabetic rat retinal sections, implicating TNFα in their activation[127]. Through its effects on the transcription factor NFκB, TNFα is also able to activate HIF-1 in muscle cells[189] and to regulate many genes, including those involved in monocyte activation[157,158], cytokine production[157,158], and adhesive integrin receptors on smooth muscle cells (Fig. 4B)[187,188,190]. Furthermore, although several studies showed that TNFα impacts EC integrity, with consequences to BBB permeability[191–193], Phares et al. found it neither necessary nor sufficient to produce these effects and, instead, identified oxidative stress resulting from excess peroxynitrite as the primary contributor[182]. Interestingly, NFκB also enhances transcription of TNFα mRNA, resulting in a positive-feedback loop that amplifies the inflammatory environment[158,194,195].

Non-enzymatic protein glycation can occur both extracellularly and intracellularly under conditions of hyperglycemia[196]. Glucose molecules can be spontaneously added to lysine groups on either structural or circulating proteins, producing glycated intermediates known as a Schiff base[197,198]. A stable AGE is subsequently produced via the slow Amadori rearrangement[197,198]. AGEs in circulation can bind to RAGEs to influence cell signalling and alter gene transcription through NFkB activation[199] (Fig. 4B). For example, the activation of RAGE on ECs may

increase permeability of capillaries through induction of vascular endothelial growth factor (VEGF)[200], and macrophage RAGE activity amplifies production of ROS, cytokines, and growth factors[201] (Fig. 4B). Cell-associated binding proteins for AGEs have also been identified which may further compound the signalling anomalies associated with AGEs[202]. AGEs also quench NO, diminishing its vasodilatory effects both *in vitro* and *in vivo*[203]. This deficit is exacerbated by the oxidative degradation of NO and contributes to the profound vascular pathology that manifests in DM. Intracellularly, AGEs can form from glucose-derived dicarbonyl precursors and the auto-oxidation of glucose to glyoxal[204], further destabilizing cellular processes by reacting with protein amino groups and altering their function[205,206]. Remarkably, intracellular AGE production has been identified in ECs following just 1 week of exposure to elevated glucose levels[207]. AGE concentration is increased in diabetic retinal microvessels[208], and studies investigating AGE inhibitors have shown promise in mitigating microvascular disease in retina, kidney, and peripheral nerves[209,210].

As highlighted in the mechanisms above, there are numerous ways in which cytokine production is amplified by hyperglycemia. Particularly, inflammatory cytokines including transforming growth factor-β (TGFβ), interleukins 1β, 2, 4, 6, and 18,[211–213] and IFNγ have been identified. These molecules induce chemokine expression, prompt immune cell recruitment to ECs, and facilitate leukocyte infiltration[194]. Importantly, as global cytokine levels increase throughout the diabetic body, which is in a constant state of low-grade inflammation[214–217], they may perturb efficient immune cell function.

In summary, high blood glucose induces numerous diverse changes in fundamental cell signalling pathways, resulting in far-reaching consequences to cell function and integrity. Of note, several key players that drive hyperglycemic toxicity in vascular and immune cells include

high levels of ROS, TNFα, AGEs, and cytokines, and NO quenching. These mechanisms have mutually amplifying relationships that perpetuate and compound diabetic pathology. Further research is necessary to disentangle their relative contributions to hyperglycemic toxicity and facilitate the identification of effective therapeutic targets.

1.2.2 Insulin and its limitations

Insulin is a large peptide hormone composed of 2 polypeptide chains (A and B), connected by disulfide bonds, and consists of 51 amino acid residues which are highly conserved across species[114,218] – even organisms in the Fungi and Protistia kingdoms have insulin-like proteins[219]. In mammals, insulin is produced by the β–cells within the pancreatic islets of Langerhans, and its release is triggered by glucose influx through GLUT-2 receptors in response to an increase in blood glucose following a meal[114]. Insulin is initially synthesized as a single polypeptide, preproinsulin (encoded by the *INS* gene on chromosome 11), which is subsequently cleaved upon translocation to the lumen of the rough endoplasmic reticulum to form proinsulin (Fig. 5A)[114,218,220]. The actions of carboxypeptidases and prohormone convertases then fold and modify the protein, removing the C-Chain embedded between A- and B-Chains, to form insulin, which is packaged in mature secretory granules along with C-peptide for storage and, ultimately, exocytosis[114,220]. Although insulin is synthesized and stored as a zinc-dependent hexamer, which exhibits long-term stability, it is active in its monomeric form (Fig. 5A)[114,218]. Once released into systemic circulation, insulin hexamers disassemble as they are progressively diluted in the plasma and the low concentration of zinc prevents their aggregation (Fig. 5A)[114].

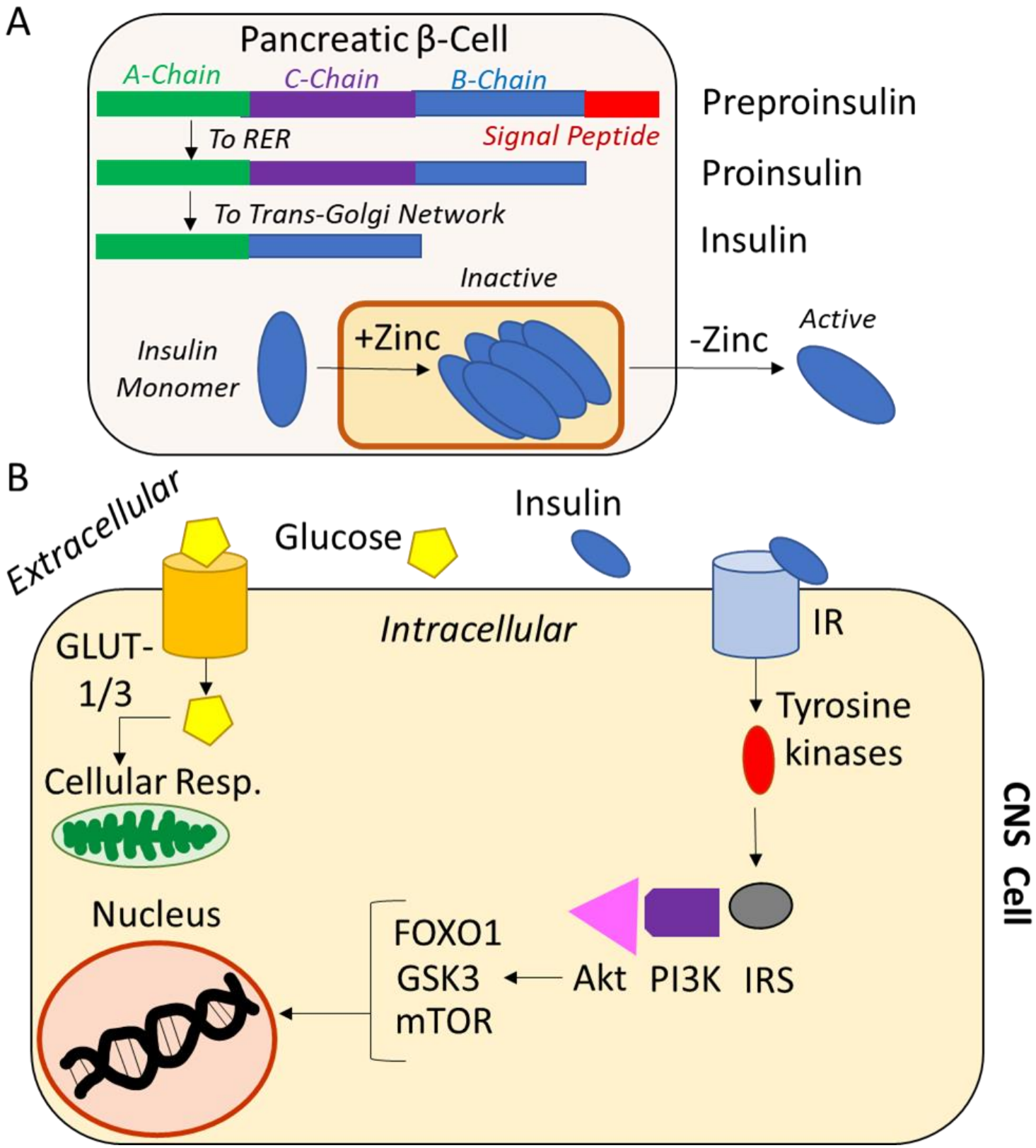
A
Pancreatic β-Cell
A-Chain
C-Chain
B-Chain
To RER
Signal Peptide
To Trans-Golgi Network
Preproinsulin
Proinsulin
Insulin
Inactive
Insulin Monomer
+Zinc
-Zinc
Active
B
Extracellular
Glucose
Insulin
Intracellular
IR
GLUT-1/3
Tyrosine kinases
Cellular Resp.
CNS Cell
Nucleus
FOXO1
GSK3
mTOR
Akt
PI3K
IRS

Figure 5. Insulin synthesis and general insulin receptor signalling.

A. Insulin is synthesized in pancreatic β-cells as a single protein comprised of A-, B-, and C-Chains as well as a signal peptide. The signal peptide targets the nascent protein to the rough endoplasmic reticulum and then is cleaved before the protein, now termed "proinsulin", is shuttled to the trans-Golgi network for processing; this includes removal of the C-Chain. Newly synthesized insulin monomers are stored as stable hexamers in mature secretory granules for release in response to increases in extracellular glucose concentrations. Once in circulation, insulin hexamers dissociate into active monomers. **B.** Insulin binding to the insulin receptor activates various tyrosine kinases that subsequently activate downstream signalling pathways including Akt, PI3K, and IRS. It may also elicit changes in gene transcription through the activation of transcription factors such as FOXO1, GSK3, and mTOR. CNS cells primarily express GLUT-1/3 which are insulin-independent transporters, allowing glucose influx required for cellular respiration to occur in the absence of this hormone

Insulin plays a fundamental role in regulating blood glucose levels by prompting the uptake of glucose from circulation by insulin-dependent glucose transporters[116–118]. In the CNS, insulin also serves as an important modulator of growth and metabolic function and its receptor is widely expressed, most abundantly in the cerebral cortex, olfactory bulbs, cerebellar cortex, hippocampus, and thalamus (Fig. 5B)[221,222]. Interestingly, insulin immunoreactivity has been observed in the brain, but whether this is the result of transport, uptake, or synthesis remains unclear[223,224]. Furthermore, although insulin-sensitive GLUT-4 transporters have been found in the brain, insulin-dependent glucose uptake has not yet been proven[223,225]. Although insulin-independent glucose transports have been identified throughout the body, the bulk of glucose uptake occurs in adipocytes and skeletal muscle and requires insulin[114,117]; thus, the loss of pancreatic β-cells results in chronic hyperglycemia and the onset of type 1 DM. The pathological consequences of lasting, unmitigated hyperglycemia are profound. Symptoms of weight loss, frequent urination, and poor would healing arise after only weeks to months of hyperglycemia, and progress to severe acute complications including coma, cerebral edema, and death[226,227]. Clinical trials strongly correlated the onset and progression of vascular complications, including macro- and micro-vascular pathology, with chronic hyperglycemia[130,228]. Notably, while the discovery of insulin by Banting and Best in 1922 provided an essential management technique for type 1 DM patients and drastically extended lifespans[229], it does not cure the disease.

Importantly, traditional insulin regimens have also proven ineffective at protecting against neurovascular disease in DM[11–16,130,131], and experimental intensive glycemic management therapies have only moderately improved prognoses[230,231]. A possible explanation for these findings is that insulin treatment alone fails to address the loss of additional signalling molecules, including c-peptide and amylin, that are also eliminated by the loss of pancreatic β-

cells[111]. Furthermore, although glycemic control may mitigate the immediate consequences of chronic hyperglycemia by generally maintaining levels within a normoglycemic range, it does not prevent glucose spikes which may be sufficient to induce diabetic pathology. Intermittent hyperglycemic spikes induce the glycation of blood proteins, such as hemoglobin A1c (HbA_{1c}), and the amount of glycated HbA_{1c} can be quantified to assess these events[232]. Indeed, elevated levels of HbA_{1c} have been recorded in type 1 DM patients prescribed insulin and were correlated with increased insulin requirements in the long term[131]. McCance et al. also found that higher levels of glycated HbA_{1c} in diabetic patients were predictive of greater risk for retinopathy or nephropathy[233]. Transient glucose spikes may represent sufficient, recurring hyperglycemic instances to alter gene expression and prompt the dysregulation of transcription, resulting in modifications which may persist even after normoglycemia is restored[234]. These cellular aberrations may then contribute to the progressive and severe pathology associated with DM.

Clearly, new strategies to mitigate neurovascular pathology in DM are necessary, and the first step to developing these alternatives will be improving our understanding of how DM may alter the repair and maintenance of the cellular constituents of CNS architecture.

1.2.3 Mouse models of type 1 diabetes

The development of animal models of type 1 DM in the 1960s-80s[235,236] marked a pivotal step in diabetes research and laid the foundation for our understanding of the genetics and pathogenesis of the disease. Furthermore, this led researchers to generate subsequent type 1 DM models that allowed for more control over disease onset and progression, setting the stage for specific features of this complex condition to be isolated and examined independently. Today there are spontaneous genetic, viral, and chemically-induced mouse models available to study type 1 DM, each with distinct advantages and limitations.

Several spontaneous genetic mouse models have been developed including the non-obese diabetic (NOD)[237] and Akita[238] mice (Fig. 6). The NOD mice, developed in Japan in 1974, are the most prevalent genetic model of spontaneous type 1 DM and exhibit hallmark features of the disease including insulitis, hyperglycemia, and ketonuria[237]. Generally used for the investigation of the genetic and immunological features of disease, NOD mice have been featured in more than 8000 publications[239]. Beginning around 5 weeks of age, an autoimmune response involving leukocyte aggregation to, and infiltration into, the pancreatic islets establishes initial insulitis[237,240]. Subsequently, waves of cluster of differentiation (CD)4^+ and $CD8^+$ lymphocytes, macrophages, natural killer cells (NKCs), and B-cells infiltrate the islets and cause destruction of β–cells; this response peaks at 10-14 weeks[240]. Notably, there is a stark sex-difference in DM incidence in this model with 60%-90% of females and only 10%-30% of males developing hyperglycemia within 40 weeks[237,241]. The incidence of DM is also highly dependent on the cleanliness of the colony, with viral infection and microbial exposure preventing disease development[242]. Hyperglycemia onsets when insulin production in the pancreas is reduced to <10% of normal levels[237]; at this point, animals rapidly lose weight and require insulin intervention for survival[243]. Using this model, 27 unique genetic loci involved in the onset and progression of type 1 DM have been identified[235], and over 200 different treatments have been discovered that prevent or reverse disease in these animals[244]. However, therapeutics derived from these findings have generally been disappointing in preclinical trials, prompting recommendations for diversifying the animal models[235,245], developing humanized variants of NOD mice[246], and revising treatment timelines[235].

Less commonly utilized than the NOD mice, the Akita model was generated in Japan from a mouse on a C57BL/6 background with a spontaneous mutation in the *Insulin 2* gene.

Akita mice develop spontaneous, severe insulin-dependent diabetes by 4 weeks of age, as well as characteristics of type 1 DM including hyperglycaemia, polyuria, and hypoinsulinemia; animals that do not receive insulin treatment perish within 12 weeks[238]. Disease onset is prompted by apoptosis of β-cells that results in reduced islet mass, comparable to what is observed in chemical models that target destruction of these cells[247]. Cell death occurs due to excessive endoplasmic reticulum stress resulting from an overload of misfolded proteins that are generated as a product of the mutant gene [238]. The earlier onset and faster progression of disease in the Akita model, relative to the NOD mice, allows for studies to be performed within an expedited time-course. However, it lacks the autoimmune features that render the NOD model more comparable to the human condition.

Viruses can be used to model type 1 DM in mice through direct infection of β–cells or by facilitating an autoimmune response against them[105,248,249] (Fig. 6). Perhaps unsurprisingly, these systems were developed to capitalize on the understanding that some environmental factors, including viruses, may contribute to type 1 DM susceptibility[250]. Various viruses have been utilized in these models, including the coxsackie B[105] and encephalomyocarditis viruses[248,249]. Additionally, transgenic mouse models have been developed in which a viral antigen is expressed under the insulin promoter[251]. Upon injection with the corresponding virus, an immune response is mounted that leads to the virus' reaction with the antigen in β–cells, where the insulin promoter is translated, resulting in the cells' destruction[251]. Although these models permit greater control of disease onset timing relative to the spontaneous genetic models, disease incidence and severity is dependent on viral replication levels which can be unpredictable.

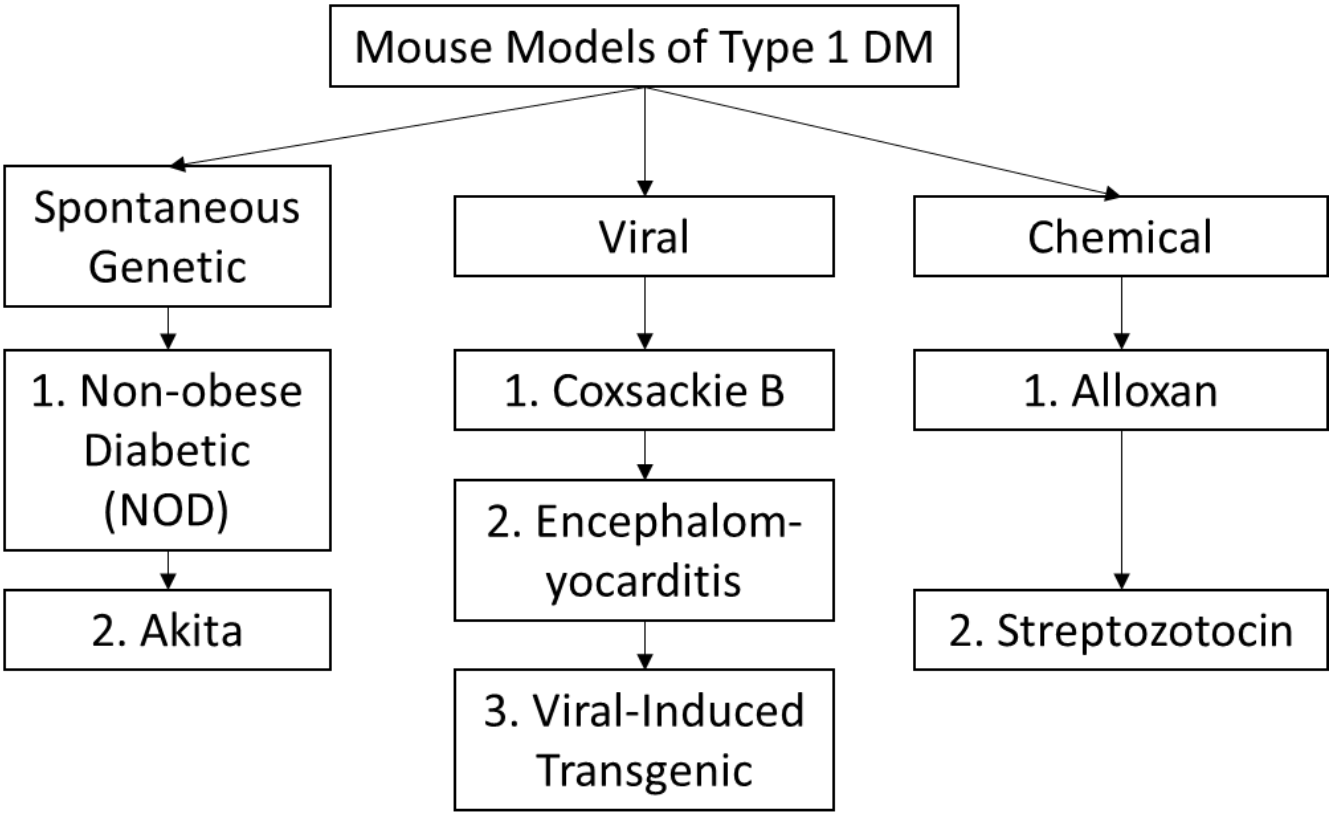

Figure 6. Summary chart of common mouse models of type 1 diabetes mellitus.

Spontaneous genetic, viral, and chemical models have been used to study type 1 DM in mice. Both the NOD and Akita strains of mice develop type 1 DM spontaneously, although the timelines for disease onset differ and Akita mice begin to exhibit diabetic pathology sooner than their NOD counterparts. Viral infection of pancreatic β-cells using coxsackie B or encephalomyocarditis viruses has been used to induce cell death and elicit the onset of type 1 DM. Transgenic incorporation of the gene encoding for a viral antigen ahead of the insulin promoter has also been used to create an inducible type 1 DM model; injection of the virus that corresponds to the expressed antigen results in β-cell death. Common means of chemical type 1 DM induction include alloxan and streptozotocin treatment. Both of these cytotoxic molecules are structural analogs to glucose and are preferentially accumulated in pancreatic β–cells, resulting in cell death via DNA alkylation and the development of insulitis.

Finally, common chemically-induced models of type 1 DM include alloxan (2,4,5,6-tetraoxypyrimidine; 5,6-dioxyuracil) and streptozotocin (2-deoxy-2-(3-(methyl-3-nitrosoureido)-d-glucopyranose; STZ) treatments (Fig. 6). Both of these cytotoxic compounds result in the destruction of a significant proportion of pancreatic β–cells and the subsequent onset of diabetic symptoms, including hyperglycemia and weight loss, within as little as 1 week[252,253]. However, due to its greater structural stability, STZ is the more widely-used agent[254]. Alloxan is a structural analog to glucose and readily taken up by β-cells; it achieves its effects through the production of free radicals, DNA fragmentation, and disruption of intracellular calcium signalling[253]. Notably, the liver is also a target for alloxan but, due to its greater anti-oxidant defenses, it is less susceptible to damage[254,255]. Highly specific dosage is required for alloxan's diabetogenic effects as it can induce dangerous toxicity with even mild overdosing[253]. This can make it challenging to troubleshoot in different animal strains, given that their tolerance to its effects may vary. STZ is selectively taken up GLUT-2 transporter on pancreatic β-cells and causes cell death via DNA alkylation[253]. Some free radical production may occur in concert with STZ treatment and, although these molecules may accelerate cell death, they are not known to play a central role in producing STZ's effects[254]. Insulin production is also inhibited due to the decrease in intracellular ATP in β-cells resulting from NAD^+ depletion following PARP activation in response to DNA alkylation[253]. STZ can be administered in a single high dose, which can result in an acute, transient increase in T-cells[256], or in multiple low doses which trigger glutamic acid decarboxylase autoantigens in β–cell and a subsequent autoimmune response[257]. These models grant researchers the capacity to induce rapid, controlled type 1 DM onset in experimental animals and can be utilized cheaply and reliably in large cohorts.

Taken together, numerous mouse models are available for the study of type 1 DM and include genetic strains that are spontaneously diabetic as well as virally- and chemically-induced models. Each system has unique features that render it suitable for the study of particular facets of the complex diabetic condition, and that make it more or less viable for investigators on the basis of cost and capacity. Ultimately, a greater understanding of the cellular mechanisms underlying diabetic pathology, along with successful treatments for this disease, will likely rely on the cumulative findings gleaned from the study of not just one, but many, of these models.

1.3 Diverse immune cell populations interact with the brain

The brain is an immunologically privileged organ under homeostatic conditions: leukocytes in circulation are generally excluded from the parenchyma by the BBB and CNS immune surveillance needs are served exclusively by innate macrophages. Microglia are the most common of these macrophages, comprising up to 12% of all cells in the mouse CNS[258]. Other resident brain macrophages include meningeal (mMΦ), choroid plexus (cpMΦ), and pvMΦ. Long believed to be a homogenous population, diversity within the overarching microglial schema has become a hot topic in the neurosciences and unique phenotypes, such as "dark microglia", are being proposed and characterized[259]. The extensive variation in microglial gene expression signatures, morphologies, and divergent responses to injuries provide ample support for these speculations[260,261]. Notably, various novel sub-groups of microglia have been attributed to neurological pathologies, and the misbehaviour of these cells is hypothesized to play an important role in disease manifestation and severity[260–262].

Although peripheral leukocytes have not been identified in the brain under healthy conditions, they can breach the BBB when its physical integrity is acutely disrupted (e.g. stroke) or homeostasis is chronically disturbed in inflammatory conditions such as MS[28–30,263,264].

Indeed, peripherally-derived phagocytes including neutrophils and monocytes have also been identified in the CNS following stroke[28,265] and during AD[266,267]. Once in the brain, monocytes can morph into MDMs with unique genetic signatures and features, including enhanced phagocytic capacity[35,268]. Interestingly, MDMs that infiltrate the CNS can acquire characteristics that make them nearly indistinguishable from resident microglia[268]. The presence of invading leukocytes has been associated with both beneficial[27,262,266,267] and adverse[167,263,264,269,270] outcomes in CNS disease, indicating that further research is required to better understand, and appropriately manage, the factors influencing these results.

As a disease characterized by chronic inflammation, type 1 DM could foster an environment ripe for deviant immune cell behaviour. Microglia and other innate CNS macrophages are affected by the pervasive effects of hyperglycemia[25,127,271], and may exhibit changes in gene expression and cell signalling that impact their responses to local injury. Furthermore, since the BBB may be compromised in this disease[15,272–274], peripheral immune cells may gain access to vulnerable brain tissues, with implications for prolonged inflammation and impaired CMB recovery. Alternatively, it is possible that the infiltration of circulating immune cells may be beneficial for healing following CMB, since others have described their direct role in tissue repair following CMB in healthy zebrafish[27] or in the hypoxic spinal cord[275]. Evidently, the role of both CNS and peripheral immune cells in CMB repair in the diabetic cortex requires further research. This dissertation contributes to these investigations.

1.3.1 Characterizing microglia and brain macrophages

Several types of macrophages, including microglia, comprise the innate immune cells of the CNS. These cells differ meaningfully in terms of their morphology, gene expression, and homeostatic functions; superficially, they can be differentiated by their unique regional

localization[276]. For example, mMΦ, cpMΦ, and pvMΦ are the 3 types of brain macrophages, named after the distinct anatomical niches that they occupy (Fig. 7)[276]. Since these cells are all associated with the interfaces of the CNS, they will be referred to cumulatively as barrier-associated macrophages (BAMs) in this document. Unlike BAMs, microglia mainly populate the brain parenchyma and exhibit varying density across brain regions, with the greatest numbers of microglia found in the white matter (Fig. 7)[258]. As an extension of the CNS, the neural retina also contains microglia and macrophages further populate the iris, ciliary body, and cornea of the eye[277–279]. Together, microglia and BAMs comprise a heterogenous population of brain macrophages that can protect neural tissue following acute insults; however, when aberrantly activated, they can also contribute to chronic, neurodegenerative conditions.

Identified by Spanish researcher Pío del Río-Hortega in 1919, microglia are one of the most dynamic, versatile cells in the body, rapidly morphing from a homeostatic, "resting" phenotype to an activated amoeboid one in response to various chemotactic signals (Fig. 7)[22,280,281]. The concept of microglia at rest seems to be a misnomer because these cells are perpetually in motion even when they are not activated: constantly extending and retracting their processes to scan the parenchymal microenvironment[22,281]. This surveillant behaviour is dependant on microglial resting membrane potential, which is predominantly maintained between -40mV to -60mV by the tonic activity of TWIK-related halothane-inhibited K^+ 1 (THIK-1) channels, depending on the cell's neuroanatomical localization[23,282]. Pharmacological blockade or genetic knock-out of THIK-1 channels in microglia results in a significant decrease in cells' ramification (including fewer processes and reduced process length) and a reduction in the volume of tissue surveyed by microglial processes[23]. Microglia exhibit a high input resistance which suggests that, like astrocytes, microglia do not express an abundance of voltage-gated

channels[23]. Although microglial cell bodies are generally stationary in their surveillant state, following activation they physically translocate their processes through the brain parenchyma towards an insult[22,283]. Once activated, microglial processes retract and swell then, guided by gradients of nucleotides, cytokines, and/or fibrinogen, encapsulate pathogens or cellular debris for clearance via phagocytosis[284,285] or enwrap ruptured microvessels in 3-dimensions to stem the extravasation of blood plasma and restore BBB integrity (Fig. 7)[24,25,286].

$P2Y_{12}$ is necessary for microglial activation and directed process outgrowth[22,284,285]. Specifically, in response to the local release of ATP or adenosine diphosphate (ADP), but not adenosine, microglial $P2Y_{12}$ receptors are activated and an outward K^+ current through THIK-1 channels hyperpolarizes the microglial membrane potential by ~30mV. This change in membrane potential is associated with reduced microglial ramification[23], and activation of integrin-1 by $P2Y_{12}$ receptors may further coordinate the cytoskeletal rearrangements associated with cellular and process motility[283]. Interestingly, although THIK-1 channels have been implicated in this response, they are not required and microglial activation can be achieved even when they are blocked[23]; whether cell function remains normal under these conditions is not known. The dramatic differences in microglial morphology and function between activation states led to the idea of dichotomous M1/M2 categorizations affiliated with anti- and pro-inflammatory microglial profiles, respectively[287]. Recently, however, researchers have moved beyond this simple model and tend to instead describe microglial phenotypes in more complex frameworks that better reflect the growing body of evidence showing microglia characterized by combinations of features once relegated to either an M1 or M2 phenotype[260,261]. A dedicated discussion of the heterogeneity of the microglial population follows in Section 1.3.3.

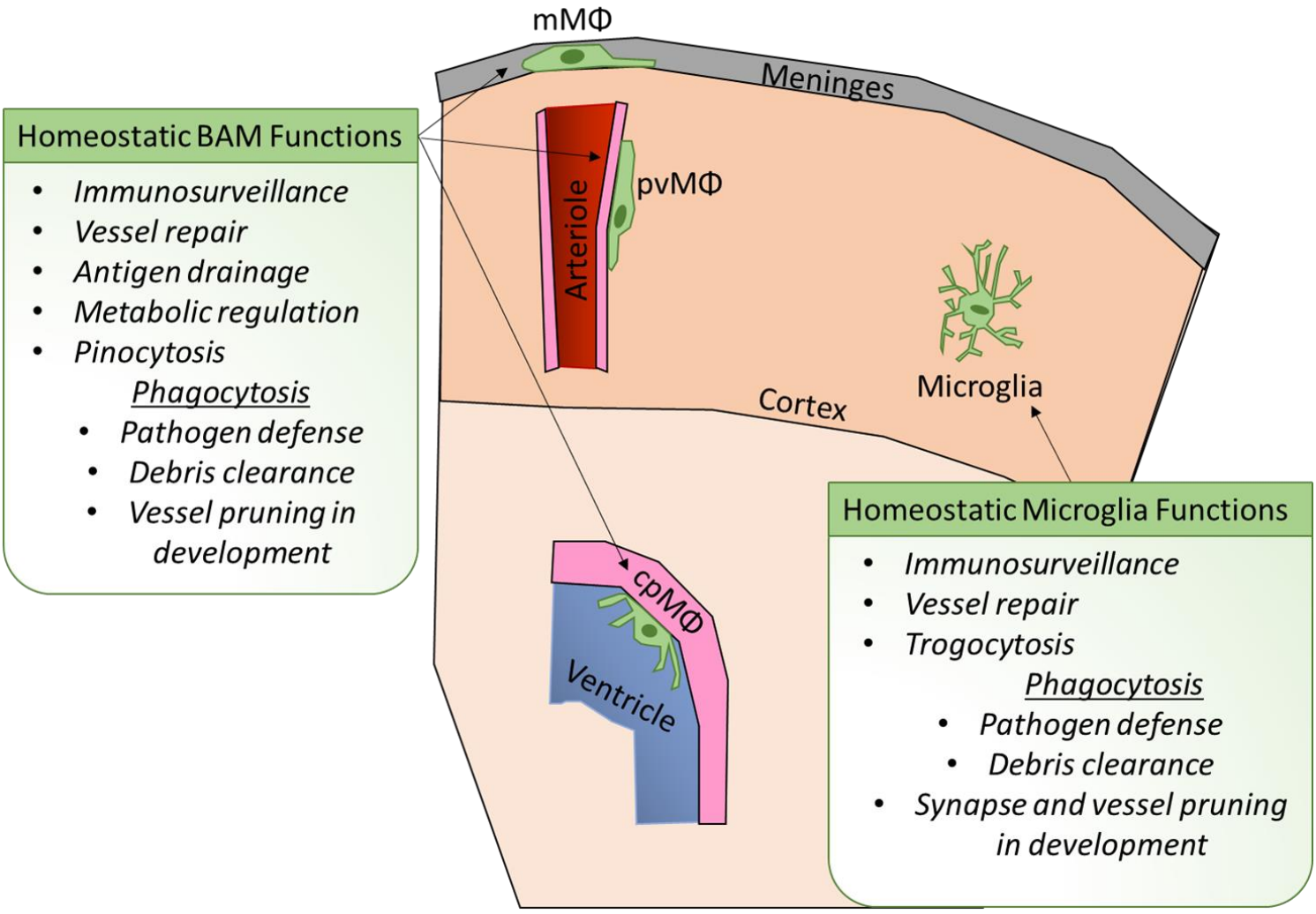

Figure 7. Innate CNS immune cell localization and general homeostatic functions.

Microglia and BAMs are the innate macrophages of the CNS. Generally, microglia are localized to the parenchyma while mMΦ populate the meninges, pvMΦ exist in the Virchow-Robin space of arterioles, and cpMΦ patrol the ventricular aspect of ependymal cells in the choroid plexus. Although the homeostatic functions of BAMs are not-well studied and research on this topic is evolving, they are hypothesized to engage in immunosurveillance, vessel repair, antigen drainage, metabolic regulation, pinocytosis, and various activities relating to phagocytosis. Homeostatic microglial functions are known to include immunosurveillance, vessel repair, trogocytosis, and numerous phagocytic behaviours.

Our current understanding of the physiological roles of BAMs is limited, but growing interest in their relationship with various neuropathologies has motivated novel, evolving investigations. In terms of the anatomical distribution of BAMs, their names provide good clues as to their localization: pvMΦ are found in the Virchow-Robin spaces along arterioles, cpMΦ localize to the choroid plexus (along ventricular ependymal cells), and mMΦ exist in the dura and arachnoid mater of the meninges (Fig. 7)[276]. Given their ideal positions at CNS interfaces, BAMs are hypothesized to contribute to brain homeostasis via immune surveillance[288], scavenging and clearing dead cells and debris via phago- and pino-cytosis[289,290], antigen drainage[291], and even metabolic regulation (Fig. 7)[292]. Interestingly, pvMΦ have been shown to secrete VEGF, enhance GLUT-1 expression by ECs, and promote glucose uptake in mice fed with a high-fat diet[292]. Taken together, BAMs not only protect neural tissue from pathogens and the build-up of cellular debris like microglia in the parenchyma, but they also act as cellular filters or "gate-keepers", augmenting and influencing the barrier functions of the BBB.

Under homeostatic conditions, pvMΦ and mMΦ exhibit a simpler morphology than the ramified parenchymal microglia, with some processes extending from their elongated cell bodies[276]. On the other hand, cpMΦ have a more stellate shape that bears closer resemblance to microglia and astrocytes[276]. Although pvMΦ are generally thought to be non-motile like surveillant microglia, they have been observed probing the perivascular space and vasculature with their limited processes[293]. A study by Barkauskas et al. indicated that during inflammation this projection of intravascular processes by pvMΦ increased, suggesting that these cells may react to cues in circulation[293]; given that pvMΦ can influence local BBB permeability[294,295], these findings have direct implications for the prevalence of neuropathology in inflammatory diseases. Although the motility of mMΦ has been described as limited, via *in vivo* imaging through

thinned skull preparations[296], their activity remains largely unexplored. Indeed, cpMΦ have been neglected from much of the research into BAM function and physiology, perhaps due to their inaccessibility for *in vivo* studies given that they are residents of the deeper brain structures.

A fundamental function shared by microglia and BAMs is their role as phagocytes; certainly, this is central to their identity as "macrophages" (Greek: "big eaters")[297]. Phagocytosis is the process by which macrophages clear dead cells and debris (particles >0.5μm in diameter) following injury, destroy invading pathogens, and restrict the spread of infiltrating toxins (Fig. 7)[298]. In the vicinity of phagocytic targets microglia secrete ROS in a process that is CD11b-dependent[299]. Subsequently, phagocytic engulfment and phagosome formation is mediated by activation of the TYRO3/AXL/MERTK (TAM) receptor tyrosine kinase family and growth arrest-specific protein 6 (GAS6)[300]. Following phagocytosis, microglia can secrete interleukin-1β (IL-1β), a potent pro-inflammatory cytokine that exacerbates tissue injury in degenerative conditions[23]. The release of this molecule requires activation of caspase-1 by the formation of an inflammasome complex; in microglia, this latter process essentially relies on K^+ efflux through THIK-1 channels which are activated by $P2Y_{12}$ receptors in response to local ATP[23]. Although IL-1β is generally produced by macrophages in response to infection, peritoneal macrophages were observed to secrete it after phagocytosis of latex particles[301]. BAMs are known to release ROS via NADPH oxidase-2 activity and also express MERTK, along with the phagocytic scavenger receptor CD36[302,303]. Microglia can recruit the complement pathway for phagocytosis and express component C1q as well as receptors CR3 and CR5[304]. In AD, for example, microglia tag synapses with C1q for engulfment via CR3[304]. Interestingly, microglia also perform trogocytosis (engulfment of particles ~250 nm in diameter) of presynaptic neuronal processes, which is independent of the CR3 pathway but could involve microglial recognition of "eat me"

signals, such as phosphotidylserine, on target membranes (Fig. 7)[305]. Phagocytosis by microglia during development is necessary for synaptic pruning[306] and pvMΦ phagocytose amyloid-β in AD, reducing the load of this inflammatory protein[302]. Dysregulation of this crucial process can result in the loss of healthy tissue and the onset of disease pathology[300].

In summary, microglia, cpMΦ, mMΦ, and pvMΦ coexist in the brain and occupy unique anatomical niches that compliment their immunosurveillant roles[276]. Microglial tissue surveillance processes and directed responses to CNS injury are well-characterized and the underlying molecular mechanisms driving these processes are rapidly being uncovered[22–25,281]. Much less is known about the physiological roles of BAMs; however, it is hypothesized that they also engage in active tissue surveillance and may even affect local metabolic processes[288,292]. Microglia and BAMs are phagocytes and may utilize this capacity for good (developmental programs, elimination of cellular debris buildup, etc.)[302,306] or evil (contributing to the onset or exacerbation of pathology in CNS disease)[307].

1.3.2 The great migration: developmental origins of microglia and brain macrophages from yolk sac to maturation

Developmentally, microglia and BAMs were once thought to represent ontogenetically distinct populations. The former was thought be derived from primitive yolk sac erythromyeloid progenitors that populate the brain parenchyma before birth, and the latter presumably arose postnatally from blood- and bone marrow-derived myeloid cells[36]. Remarkably, however, new fate-mapping and large-scale single-cell RNA-sequencing studies have shown that their developmental pathways are actually closely related[276,308,309]. These initial discrepancies likely arose due to the use of irradiation or chemotherapeutic conditioning in early transplantation studies[310–312]. These processes are now known to disrupt the BBB and permit the infiltration and

engraftment of peripheral leukocytes in the CNS[268]. The rapid evolution of this dogma is highlighted by the fact that a seminal review on microglia and BAMs by Prinz and Priller was published recently in 2014 stating that "microglia and CNS macrophages thus represent two ontogenetically distinct myeloid populations,[36]" notably, this work was followed by another comprehensive review from Prinz et al. in 2017 highlighting that "the classic view that non-parenchymal CNS macrophages are derived from the bone marrow has been now disproved[313]."

Based on the current literature it is thought that, microglia arise from erythromyeloid progenitors in the primitive blood islands of the embryonic yolk sac[314,315] and BAMs may derive from embryonic progenitor cells in the same region or their descendants in the fetal liver around embryonic day 7.0 (E7.0; Fig. 8)[276,309]. At this time these embryonic progenitors are $CD45^{-}$c-kit^{+} and already express the macrophage survival receptor colony-stimulating factor 1 (CSF1; Fig. 8)[315,316]. The unique ontogeny of microglia and brain macrophages, distinct from bone marrow-derived myeloid cells, was confirmed by studies showing that the transcription factor required for hematopoiesis of peripheral leukocytes, Myb, was not necessary for their engraftment in the CNS[276,317]. The transcription factor PU.1, however, is required for the development of all CNS innate immune cells[315]. Following the onset of a fetal heartbeat and prior to E8.5, these progenitors enter the circulation and surround the neuroepithelium of the nascent brain by E9.5 (Fig. 8)[314]. Following conversion to $CD45^{+}$c-$kit^{-}CX3CR1^{+}$ cells, they infiltrate the neuroepithelium via expression of matrix metalloproteinase (MMP) 8/9 (Fig. 8)[36].

It is worth noting that an alternative model has been proposed, suggesting that $F4/80^{+}CD11lb^{-}$ primary erythromyeloid progenitors arising in the blood islands at E7.0 colonize all tissues in the embryo including the brain[318]. These macrophages express CSF1R and are independent of the transcription factor Myb[318]. In this model, macrophage colonization of the

CNS occurs prior to the onset of a fetal heartbeat and the mechanism by which these cells would migrate to the tissue is unclear; chemotactic signals released by apoptotic neurons in the developing CNS may be a sufficient cue[319]. Regardless, microglial colonization of the parenchyma begins by E10.5 and continues via clonal expansion through postnatal day 28[314,315]; BAMs distribute throughout the CNS interfaces as these structures differentiate around E12.5 (Fig. 8)[276]. Nascent microglia exhibit an amoeboid morphology but become ramified by E14.5 (Fig. 8)[315]. The acquisition of microglial and BAM phenotypes is associated with local environmental factors including TGFβ and CSF1[320]. To induce a microglia-specific phenotype, SALL1 and the negative regulator of reactive oxygen species (NRROS) protein seem to play important roles[321,322]. Specifically, microglia from mice with a microglia-specific knockout of SALL1 downregulate canonical microglial gene signatures concomitant with the upregulation of a BAM phenotype[321]. Similar results are observed when NRROS signalling is knocked out, suggesting that it may exert its effects through SALL1[322]. The development and closure of the fetal BBB between E13.5-E14.5 likely signals the conclusion of erythromyeloid progenitor infiltration into the brain and prevents auxiliary influx of myeloid cells into the CNS under homeostatic conditions[318]. Survival of microglia and BAMs is dependent on the constitutive activity of the hematopoietic receptor for CSF1[314,323,324], given that genetic or pharmacological inhibition of this signalling pathway leads to robust elimination of these cells in the CNS.

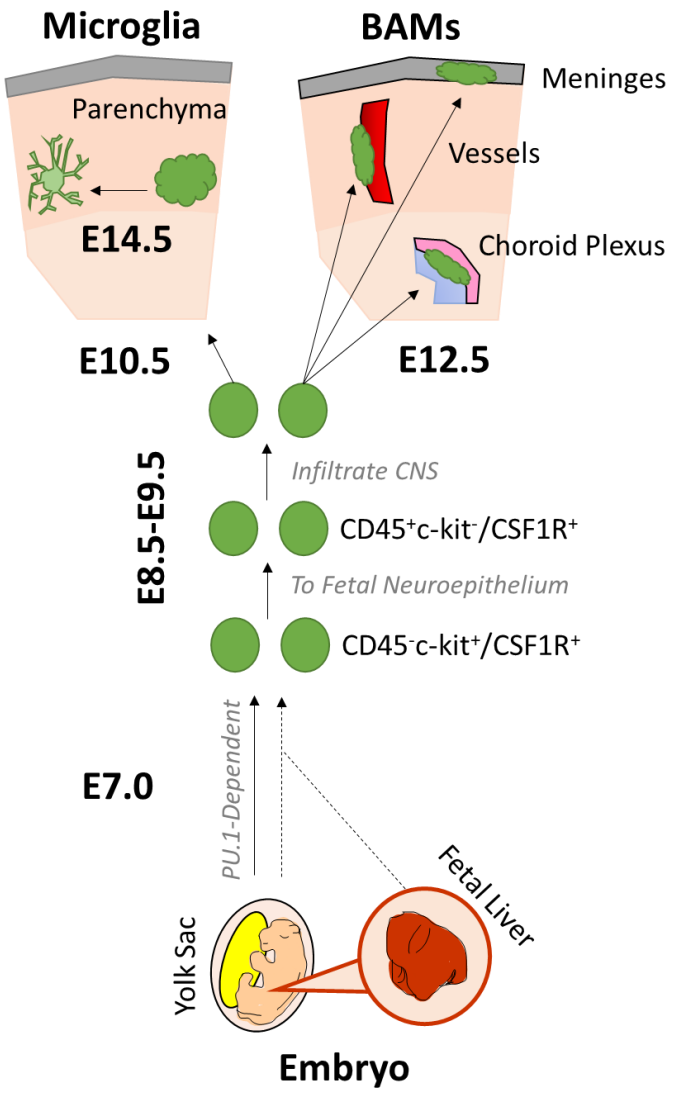

Figure 8. Ontogeny of innate brain macrophages.

Microglia and BAMs arise from PU.1 erythromyeloid progenitors that develop in the embryonic yolk sac or, in the case of BAMs, potentially the fetal liver. This primitive hematopoiesis begins around E7.0 and produces cells that are $CD45^{-}c\text{-}kit^{+}$ and express the receptor for CSF1. Around E8.0, these progenitors migrate to the fetal neuroepithelium and, following their conversion to $CD45^{+}c\text{-}kit^{-}$ cells, infiltrate the developing CNS. Microglial colonization of the parenchyma begins around E10.5 and the cells transform from amoeboid to ramified by E14.5. BAMs colonize their respective niches as these structures form around E12.5.

Once established, microglia, pvMΦ, and mMΦ are long-lived cells that show negligible replenishment by circulating bone marrow-derived progenitors under homeostatic conditions; their CNS populations are generally maintained throughout adulthood via proliferative self-renewal[276,325,326]. Interestingly, despite their similar embryonic origins, some cpMΦ do not share the longevity of other brain macrophages and exhibit turnover postnatally via contributions from peripheral progenitors (likely Ly6C^{hi} monocytes)[309]. The hypothesis of dual origins for cpMΦ is supported by the fact that activity of the myeloid CC-chemokine receptor-2 (CCR2) is necessary for maintenance of the population[276]. Mature microglia in the adult brain express pan-macrophage markers such as ionized calcium-binding adaptor molecule-1 (Iba-1), F4/80 (also known as EMR1), CD68, and CX3C chemokine receptor-1 (CX3CR1)[308]. To differentiate microglia from other brain macrophages, transmembrane protein-119 (TMEM119) has been used extensively as a microglia-specific marker[327]. Recently, however, Masuda et al. suggested that TMEM119 expression by microglia may be unstable when homeostatic brain conditions are perturbed, potentially rendering it unreliable as a unique identifier for microglia in disease[328]. Alternatively, the *Hexosaminidase subunit beta* (*Hexb*) gene was identified as an alternative, stably-expressed target for microglial discrimination from other brain macrophages in pathologies including MS and AD[328]. Like microglia, mature BAMs have been identified by their expression of CX3CR1, Iba-1, or F4/80, and largely differentiated by their anatomical localization[308]. Despite these similarities, BAMs otherwise have relatively distinct gene expression profiles from microglia. A popular marker for differentiating BAMs from microglia is the mannose receptor CD206, as well as CD36, carbonyl reductase 2, mannose receptor 1 C-type, and platelet factor-4[308]. Notably, in a comprehensive transcriptomic analysis of BAMs,

very few markers differed between pvMΦ, cpMΦ, and mMΦ under homeostatic conditions, despite their disparate localizations and unique morphologies[308].

In summary, the details of microglial and BAM development, particularly relating to the nature of their progenitor pools and timeline of events, are still under debate and the literature on these subjects is rapidly evolving. Despite ongoing controversies, these cells are known to arise from erythromyeloid progenitors that colonize the CNS before birth and, with the exception of cpMΦ, are not comprised of bone marrow-derived progenitors under homeostatic conditions. Furthermore, mature microglia and BAMs express unique gene expression signatures and can be readily differentiated by markers for TMEM119 and CD206, respectively. Since peripheral leukocytes can engraft in the brain during BBB disruption, and could become morphologically indistinguishable from microglia[268,329], it is important to understand whether the non-embryonic lineage of these can be identified by particular markers, coincident with any changes in function.

1.3.3 Microglia as a diverse cell population

The highly mutable gene profiles of microglia and their diverse range of functions under homeostatic and disease conditions have posed significant challenges to the development of reliable schemas for categorizing putative microglial subsets. With the help of novel technical advances, such as single-cell RNA sequencing and single-cell mass spectrometry, researchers have now been able to probe this subject with greater fidelity and resolution. Indeed, heterogeneous microglial phenotypes have been identified across anatomically distinct brain regions under healthy conditions, during aging, and in various disease conditions.

In the context of anatomical heterogeneity, region-specific differences in microglial gene expression profiles may provide clues regarding their unique physiological functions and local

environmental needs. For example, CD68 expression differs in microglia throughout the brain, implying variations in the phagocytic capacity of these cells in disparate regions. For example, cerebellar microglia express elevated F4/80[330], hippocampal microglia exhibit high levels of TNFα [331], and microglia in the white matter show increased expression of ubiquitin-specific protease 18, a negative regulator of type 1 IFNs [332]. Microglial morphology is also known to differ across brain regions, influenced by the cellular composition of the local milieu[330]. Furthermore, microglial turnover rates under homeostatic conditions vary in a region-specific manner, with the most rapid turnover observed in the dentate gyrus[333]. Interestingly, following microglial elimination via CSF1 receptor (CSF1R) inhibition, rapid proliferation of microglia leads to repopulation within 1 week of removing CSF1R blockade but generates a nearly homogenous population arising from a few CSF1R-resistant cells[334]. Since microglial dependence on the ligands for CSF1R (IL-34 and CSF-1) varies across brain regions it is possible that local populations may exhibit unique profiles as a result of these environmental cues; however, the authors of this study performed cluster analyses on bulk transcriptomic data from the whole brain and did not compare transcriptomes across anatomical regions[334].

A recent study examining microglial heterogeneity in the healthy human brain with single-cell RNA sequencing showed greater diversity throughout the population in comparison to mice, with gene expression profiles showing only partial overlap; regional diversity of microglia was not characterized in this study and tissue from temporal and frontal cortices was analyzed[335]. Interestingly, several subtypes of microglia were identified in humans that were not found in rodents. These populations were characterized by high expression of chemokine genes and zinc finger transcription factors[335]. Masuda et al. noted that these phenotypes, generally characteristic of an inflammatory microglial state in mice, may reflect a physiological state that has been

previously attributed to the normal human condition[335]. In studies of microglial diversity during aging, most cells exhibited homeostatic gene expression profiles but increased heterogeneity was noted, particularly pertaining to greater inflammatory subtypes of microglia[336]. These inflammatory phenotypes amplified expression of chemokines, ILs, and IFN-related genes[336].

"Disease-associated microglia" (DAM) were initially identified around amyloid plaques in a mouse model of AD[337] and have since been discovered in mouse models of amyotrophic lateral sclerosis (ALS) as well[338]. Characterized by elevated expression of APOE and triggering receptor expressed on myeloid cells-2 (TREM2), the gene profiles of these cells were shown to progress through distinct phases during disease[337]. The initial transition from healthy to a phase 1 disease profile was TREM2-independent, but the subsequent progression to phase 2 required TREM2 activity[337]. A unique population of myeloid cells with these DAM gene signatures, and which are of embryonic lineage, were also discovered in the choroid plexus epithelium of healthy mice; their physiological functions remain unknown[337]. During physiological aging white matter microglial diversity increases and cells show DAM-like gene signatures, including TREM2 expression and upregulation of other genes related to phagocytosis[339]. Interestingly, injection of lipopolysaccharide (LPS), which is commonly used to induce microglial activation and model their general morphological and phenotypic changes during inflammation, does not produce a DAM gene expression profile[340]. Specifically, expression of genes including *Trem2*, *Hif1a*, and *TYRO protein tyrosine kinase-binding protein* are generally upregulated in DAM but were actually downregulated in microglia following LPS injection[340]. In another disease model microglia from mice fed cuprizone, a chemical which causes oligodendrocyte cell death and demyelination (often used to study MS), exhibited 2 primary clusters of gene expression that were associated with the demyelination and remyelination phases of the treatment[335]. In this

study, the microglia assessed during the demyelination phase exhibited profiles akin to those of DAM but, during remyelination, microglia increased expression of *Cd74* and other major histocompatibility complex (MHC) class II genes[335]. In a mouse model of MS, microglial diversity increased and several clusters of distinct phenotypes were observed[308]. Notably, the core microglial gene signatures associated with this model showed a significant downregulation of typical microglial markers including *Tmem119* and *P2ry12*[308]. Taken together, these findings highlight the diversity of microglial phenotypes associated with disease states and caution against the overgeneralization of microglial profiles identified in particular conditions.

1.3.4 Microglial interactions with the vasculature

Microglia, best known as the resident macrophages of the CNS parenchyma, have important relationships with the vasculature in addition to their immunogenic roles. Unlike astrocytes and mural cells, microglia are not generally considered members of the neurovascular unit, nor have they been ascribed major roles in neurovascular coupling. Interestingly, recent research from the Dénes lab has identified specific interaction sites between microglial processes and neuronal cell bodies in mice and humans[341,342]. These $P2Y_{12}$ receptor-dependent sites were associated with neuronal mitochondria and identified as a mechanism by which microglia could sense and regulate neuronal calcium[341]. Microglia also make purinergic contacts with ECs and contribute to the regulation of cerebral blood flow in the mouse barrel cortex, thereby modulating neurovascular coupling[342]. Additionally, microglia directly contact capillaries and pericytes in the retina and stimulation of microglial CX3CR1 by fractalkine induces vasoconstriction in the rodent retina and cortex[271]. Notably, this effect was abolished in the retina of mice deficient in CX3CR1 signalling[271]. Microglia also release various small molecule messengers into the synaptic cleft through which they can influence neuronal activity[343,344].

Utilizing these same signals, microglia may also be capable of influencing vascular tone. For example, microglia can express inducible nitric oxide synthase (iNOS)[345] and could facilitate vasodilation by local release of nitric oxide (NO) near ECs. This may be particularly relevant to a subpopulation of microglia, termed juxtavascular microglia, which localize to the vasculature with their soma directly in contact with the *glial limitans*[346,347]. Taken together, these findings may constitute the foundation of our understanding of microglia as vasoregulatory cells.

During development microglia play a key role in sculpting the CNS cellular architecture, including the vasculature. Because the developing CNS has no intrinsic vasculature, blood vessel development progresses through angiogenesis. Notably, microglia migrate into the CNS prior to the appearance of blood vessels[314] and thus are poised to guide this process. In response to angiogenic guidance cues, such as hypoxia, increasing tissue mass, and VEGF-A, tip cells at the leading aspect of nascent vessels extend from perineural vessels into the neuroectoderm[348–350]. The tip cells of growing vessels connect with one-another, branching and forming anastomoses that result in the complex and highly ramified structure of the vasculature[348–350]. It has been suggested that microglia create physical bridges between vascular sprouts, facilitating vascular branching[351,352]. Indeed, microglia have been found to contact neighbouring endothelial sprouts and mice lacking microglia showed significantly decreased numbers of vascular branches[351]. Furthermore, the elimination of retinal microglia during development, through intravitreal injection of clodronate liposomes (CLR)[353] or in genetic models without microglia[351,352,354], resulted in reduced vascular complexity in the neonatal retina. However, the number of endothelial tip cells was not affected in any of these studies[351,353,354], suggesting that microglia facilitate vascular branching but not tip cell development or extension.

As extensive vascular networks are formed, immature vessels undergo significant pruning and regression to create an efficient, mature circulatory system[355,356]. Since microglia play an important role in pruning synapses during development[305,306], it would be reasonable to consider whether they could be involved in similar processes supporting the streamlining of CNS vascular systems. It is generally understood that vascular remodelling occurs through the migration of ECs to adjacent vessel segments in response to blood flow in those vessels[357–359]. In this way, functional blood vessels are reinforced and segments without reliable flow are lost. The role of microglia during angiogenesis may be restricted to the early stages of development since elimination of these cells 3 weeks after birth in conditional knock-out mice did not significantly alter the density or complexity of vascular networks compared to wild-type animals[354]. EC apoptosis has also been observed in the developing CNS vasculature of mice[357] and zebrafish[356,358] and may contribute to vessel pruning; however, the idea that microglia are required for this process remains contentious. A recent study by Zhang et al. investigated the role of microglia in EC apoptosis in the development of CNS vasculature in zebrafish and found that, although this phenomenon contributed to ~15% of pruning events, microglia were not required for the elimination of immature vessels but they contributed to the clearance of apoptotic debris[356]. Conversely, another group noted that the elimination of macrophages during development via diphtheria toxin resulted in the persistence of vasculature in the retina beyond the normal period for scheduled vascular regression, suggesting that they are necessary for inducing programmed apoptosis[360]. Indeed, others have shown that macrophages can induce programmed cell death in retinal ECs by activating the canonical WNT pathway[361]. Additional research is necessary to understand the nuances of microglial involvement in vascular pruning and network refinement during development and to reconcile these disparate findings.

In summary, although they are best known for their immunogenic properties, microglia have been recently ascribed putative roles in neurovascular coupling and vasoregulation. Furthermore, microglia facilitate angiogenesis during development, wherein they support vascular branching and complexity and modulate network density, although the details of their involvement in this latter process is controversial and requires further investigation.

1.3.5 Peripheral phagocytes and the central nervous system

Although peripheral phagocytes are generally excluded from the CNS under homeostatic conditions, they can gain access to this exclusive tissue following disruption of the BBB or in chronic inflammatory diseases[28–30]. There are 2 primary pools of peripheral leukocytes, distinguished by their developmental lineages: myeloid and lymphoid cells. During the first wave of hematopoiesis, which begins around E7.0, erythromyeloid progenitors are produced in the blood islands of the embryonic yolk sac (Fig. 9)[362]. These cells give rise to microglia, as described in Section 1.3.2, but also colonize the whole embryo with tissue-resident macrophages[362]. Early macrophages play fundamental roles in tissue remodeling and clearing apoptotic cells associated with developmental programs[306,360,363]. Notably, like CNS macrophages, most erythromyeloid progenitor-derived tissue macrophages in the periphery are long-lived, maintain proliferative capacity, and their development does not depend on the transcription factor Myb (Fig. 9)[324]; this latter point supports the idea that tissue-resident macrophage populations are not derived from bone marrow-borne progenitors under homeostatic conditions. However, in some barrier tissues, such as the gut and skin, postnatal macrophage replacement can occur progressively via differentiation of bone marrow-derived intermediates[362].

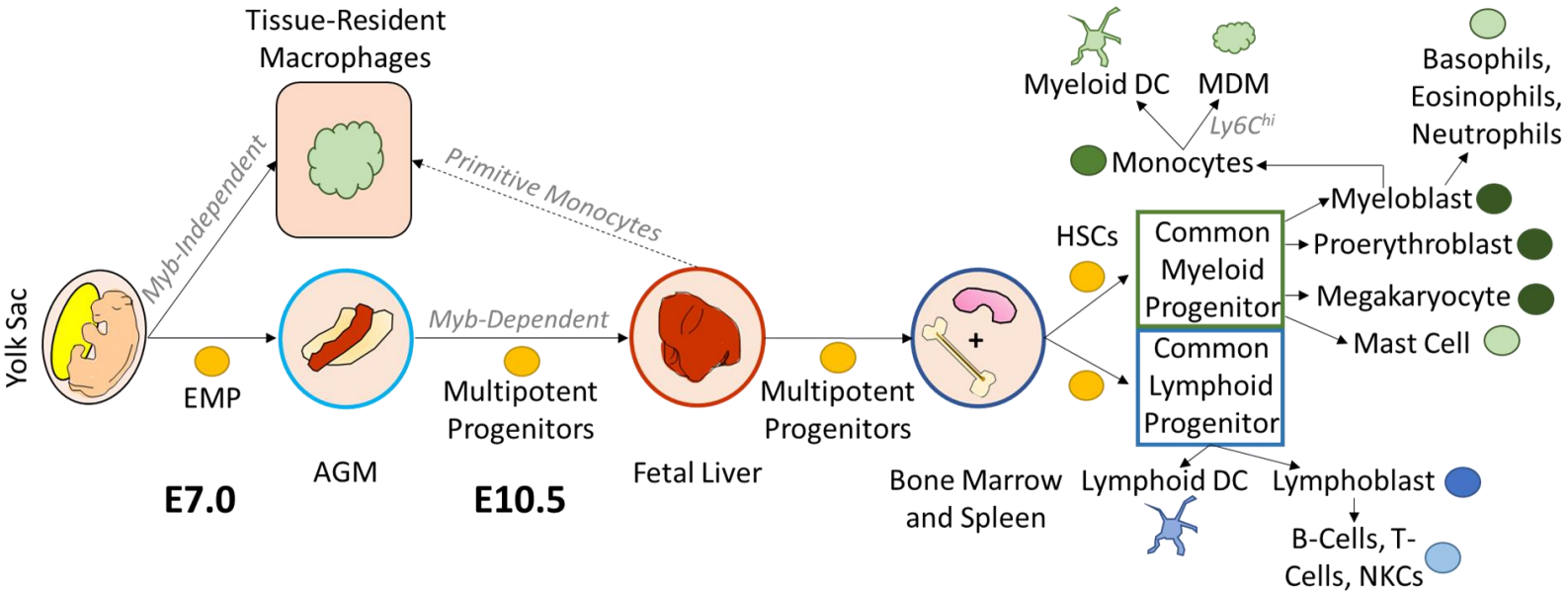

Figure 9. Leukocyte ontogeny and hematopoiesis.

Leukocyte development begins with the production of EMPs in the embryonic yolk sac at E7.0. In a Myb-independent manner, these EMPs colonize embryonic tissues and become resident macrophages that persist throughout adulthood. Other leukocytes require further, Myb-dependent differentiation. Following the onset of definitive hematopoiesis in the AGM and the production of multipotent progenitors by E10.5, these cells colonize the fetal liver and, subsequently, the bone marrow and spleen. Some primitive monocytes produced by the fetal liver may infiltrate embryonic tissues and contribute to resident macrophage populations. Within these structures, HSCs differentiate into either myeloid or lymphoid cells via respective common progenitors. Common myeloid progenitors produce mature mast cells as well as progenitors including megakaryocytes (generate platelets), proerythroblasts (produce red blood cells), and myeloblasts. Myeloblasts are the precursors of granulocytes (basophils, eosinophils, and neutrophils) as well as monocytes. Monocytes may differentiate into myeloid DCs or, if they are Ly6C^{hi}, MDMs. A common lymphoid progenitor exhibits the capacity to differentiate into a lymphoid DC or a lymphoblast, from which B-cells, T-cells, and NKCs arise. EMP: Erythromyeloid progenitor.

Although the first phase of hematopoiesis accounts for most tissue-resident macrophages, circulating leukocytes require additional developmental programs. The second wave of hematopoiesis, termed definitive hematopoiesis, begins in the embryonic aorto-gonado-mesonephros (AGM) region with the generation of multipotential hematopoietic progenitors around E10.5 (Fig. 9)[362]. Definitive hematopoiesis is Myb-dependent and all cells generated by this process require it for their development (Fig. 9)[318]. AGM progenitors seed the fetal liver, and then liver-derived cells colonize the bone marrow and spleen - the organs primarily responsible for adult hematopoiesis (Fig. 9)[362]. Some primitive monocytes are produced by the fetal liver to colonize tissues, except the CNS, where they may differentiate into long-lived macrophages that are indistinguishable from their yolk sac-derived counterparts; as necessary, these nascent MDMs may also replace primitive tissue-resident macrophages (Fig. 9)[364]. In the bone marrow, hematopoietic stem cells (HSCs) produce common myeloid and common lymphoid progenitors (Fig. 9)[365]. These progenitor populations represent the precursors of the distinct adult hematopoietic lineages: myeloid and lymphoid. In the myeloid context, the common myeloid progenitor yields megakaryoblasts, proerythroblasts, mast cells, and myeloblasts (Fig. 9)[365]. Myeloblasts further differentiate into basophils, neutrophils, and eosinophils via granulopoiesis and monocytes through monocytopoiesis (Fig. 9)[365]. Monocytes may be $Ly6C^{hi}$ or $Ly6C^{low}$ cells[366] and, following CCR2-dependent activation, enter the circulation from the bone marrow[367]. Subsequently, in response to local inflammation, $Ly6C^{hi}$ monocyte infiltrate tissues and environmental cues may prompt their differentiation into other mononuclear phagocytes including myeloid dendritic cells (DCs) and macrophages. On the other hand, the common lymphoid progenitor yields lymphoblasts or lymphoid DCs (Fig. 9)[365]. Lymphoblasts produce B-

and T-lymphocytes and NKCs through lymphopoiesis (Fig. 9)[365]. Of the mature leukocytes, monocytes, neutrophils, macrophages, and DCs engage in phagocytosis[362].

In the context of CNS disease and injury repair, infiltrating phagocytic leukocytes have been hailed as both supportive[27,262,266,267] and detrimental players[167,264,269,270]. MDMs in particular have been studied extensively[27,35]. As described previously, the BBB normally hinders the infiltration of these cells into the brain parenchyma; however, during acute trauma or in prolonged disease states it is no longer effective[28–30]. In these instances, local inflammatory molecules including ATP, TNF-α, IL-1β, and chemokine ligand-8 (CXCL-8) attract circulating immune cells to the CNS and stimulate the expression of adhesion molecules by ECs[27,368]. Specifically, the binding of P-selectin glycoprotein ligand-1 and very late antigen-4 (VLA-4) on leukocytes to endothelial P-selectin and vascular adhesion molecule-1 (VCAM-1), respectively, slows leukocyte rolling and permits activation by local chemokines[369]. Leukocytes halt and dock at the EC by upregulating VLA-4 and binding EC VCAM-1 as well as intracellular adhesion molecule-1 (ICAM-1) through lymphocyte function-associated antigen-1 (LFA-1)[369]. Leukocyte adhesion may be augmented by JAM-1 binding LFA-1[370]. Prior to transmigration, leukocytes may crawl along ECs via integrin/CAM interactions (ie. VLA-4/VCAM-1) to determine the optimal point for crossing[369], likely guided by a gradient of CXCL-1[371]. Transmigration itself may occur through either paracellular or transcellular routes and involves chemokine gradients that shepherd leukocytes to the abluminal aspect of the vasculature[372]. IL-1 has been described as a significant facilitator of macrophage transmigration[373]. Once leukocytes have traversed CNS ECs, they must also penetrate the BM and *glial limitan*s, a process which requires MMPs[374].

Once in the CNS proper, monocytes can transform into MDMs which exhibit morphological and genotypic similarities to resident microglia. For example, MDMs were found

to engraft in the brain following tissue preconditioning via irradiation, independently of any CNS degenerative pathology, and were almost indistinguishable from microglia[375]. Furthermore, uncommitted $KIT^{+}SCA1^{+}$ myeloid progenitor cells were found to contribute to long-lived MDMs in mice that had received myelosuppressive conditioning with busulphan[376,377]. Indeed, Shemer et al. described engrafted MDMs that acquired microglial characteristics including "ramified morphology, longevity, radio-resentence, and clonal expansion[329]." Although it is debated whether these cells truly are microglia, the semantic challenges of this discussion does not disqualify valid questions regarding whether they acquire homeostatic microglial functions and how they may engage with the local microenvironment[268,375]. For example, human HSC transplant recipients exhibit engrafted cells that remain distinct from yolk-sac derived host microglia, and engrafted MDMs in mice respond differentially to peripheral endotoxin administration when compared to innate microglia[329].

Importantly, the physiological properties of MDMs differ meaningfully from microglia. These cells demonstrate higher phagocytic capacity than microglia and the increased cellular load of phagocytic material renders them prone to apoptotic and necrotic cell death, which exacerbates local inflammation[269,270]. ROS are also generated as a product of NADPH oxidase activity from phagocytosis[177]; if neutrophils are present, ROS can also trigger their release of H_2O_2 and O_2^{*}, contributing to a positive feedback loop of local oxidative stress[378]. Furthermore, in response to various stimuli, monocytes generate O_2^{*}, even if they have not differentiated into MDMs[379]. If they retain these qualities following engraftment in the CNS, MDMs may have deleterious effects on the viability of nearby cells and injury recovery prognosis. For example, increased MDM infiltration was associated with memory deficits in the db/db mouse model of obesity; notably, pharmacologic inhibition of PKC-β prevented transmigration and enhanced

BBB integrity by preventing JAM degradation[380]. Following reperfusion injury infiltrating monocytes/MDMs have also been associated with neuronal loss and microglial activation[30].

From a regenerative perspective, MDMs have been ascribed supportive roles in AD. In this context, following irradiative preconditioning and bone marrow transplant, $CCR2^+$ monocytes/MDMs infiltrated the Virchow-Robin spaces and engrafted in the brain parenchyma, surrounding amyloid-β plaques[266,381]. Given the high phagocytic capacity of these cells, it has been suggested that MDMs may be particularly attracted to amyloid-β *in vivo* and more efficient at clearing the debris than resident microglia[266]. These findings are complimented by the evidence that CCR2 deficiency in a transgenic mouse model of AD accelerates amyloid-β deposition and contributes to disease progression[267]. In studies of a mouse model of Rett syndrome, a neurodevelopmental disease characterized by disruptions of synaptic plasticity and transmission, it has been hypothesized that decreased microglial numbers failed to effectively phagocytose debris during development, thereby contributing to impaired neuronal signalling[262]. Following bone marrow transplant in transgenic Rett mice, engraftment of wild-type MDMs in the CNS increased the lifespan of affected mice and ameliorated behavioral deficits[262]. It is worth noting that, despite confirming the infiltration and engraftment of MDMs in the CNS, some researchers have questioned the longevity of these cells in the parenchyma. Ajami et al. noted MDMs at the site of facial motor neuron axotomy, but found that these cells did not remain in the CNS under homeostatic conditions[382]. These researchers also discovered that recruitment of monocytes/MDMs to, and infiltration of, the spinal cord triggered the onset of MS pathology but found that they did not remain in the CNS following the resolution of an acute insult[264].

In summary, it is evident that the infiltration of the CNS by circulating phagocytes is possible when homeostasis is disturbed, but the desirability of this phenomenon in the context of

CNS repair and restoration remains unclear. Indeed, whether MDM engraftment contributes to better or worse outcomes in CNS disease or following injury is likely context-dependent and may be affected by various factors, such as the extent of pathology. Additionally, the question of MDM longevity in the CNS is an important one. If MDMs are reparative then supporting lasting engraftment may be desirable, but if they are detrimental then the transient nature of their residence in the CNS could imply that they are not a major obstacles to resolution of disease.

1.4 Vascular repair and immune cell function in diabetes

Having now reviewed the biochemical perturbations that contribute to diabetic pathology, as well as immune cell interactions with the CNS and its vasculature, this section will endeavor to bridge these topics. Furthermore, it will explore the mechanisms by which diabetes contributes to microvascular disease and immune cell dysfunction, specifically. ECs are particularly vulnerable to hyperglycemia's profound effects on cell signalling and function as they are perpetually and directly apposed to elevated glucose levels in the circulation[142]. These pathological perturbations can lead to impairments in BBB integrity and contribute to the onset or progression of microvascular disease[272,273]. CMBs are ruptures that occur in small cerebral blood vessels, including capillaries[383], and are clinically significant in DM since their incidence is significantly increased in patients relative to the healthy population; furthermore, their prevalence is positively correlated with cognitive decline[2,3]. Of note, CNS-resident immune cells and peripheral phagocytic leukocytes have been ascribed roles in modulating microvascular repair[24,25,27,275]. However, their chronic exposure to hyperglycemic toxicity in DM could have functional consequences to their capacity to facilitate the resolution of CMBs. In this way, the misbehaviour of immune cells in DM could contribute to disrupted microvascular repair and perpetuate cerebrovascular pathology in this disease.

1.4.1 Diabetes as a disease of the vasculature

ECs are a primary target for dysfunction in type 1 DM given their frontline situation along the lumenal aspect of the vasculature. Within ECs signalling changes resulting from hyperglycemic toxicity result in abnormal protein glycation, perturbed metabolism, and oxidative stress – all of which contribute to their susceptibility to damage and dysfunction[142]. Considering these pervasive effects, the prevalence of macro- and micro-vascular disease in DM may not be surprising. Although the pathological effects of hyperglycemia on general cell signalling and function were reviewed in depth in Section 1.2.1, it is worth discussing these pathological changes within the context of ECs specifically. One of the most prevalent changes in ECs that is associated with hyperglycemia is abnormally glycated proteins, including intracellular AGE formation, which accumulate rapidly following exposure to elevated glucose concentrations[207]. Notably, fibroblast growth factor is one of the primary proteins affected by abnormal glycation in ECs[207]. Additionally, proteins involved in macromolecule endocytosis are also targeted as AGEs and lead to a hyperglycemia-induced upregulation in endocytosis and increased BBB permeability[384]. Oxidative stress has been identified specifically by several studies as a key contributor to vascular complications in DM[385]. ECs cultured in hyperglycemic conditions exhibit irregular protein expression and activation of signalling pathways, such as ubiquitous MAPK, extracellular signal-regulated kinase (ERK)[386,387], and PKC activity[388]. Notably, changes to these pathways have implications to EC viability, gene expression, and function. *Angiotensinogen*, for example, is a gene involved in the regulation of capillary tone and its expression is perturbed in type 1 DM[271].

Along with the damage to cerebral ECs by hyperglycemic toxicity in DM, the integrity of the BBB as a whole is disrupted and has fundamental implications for the development of

vascular pathology[272,273]. One of the earliest recorded, and most ubiquitous, structural abnormalities of the BBB in DM is increased BM thickness, characterized via electron microscopy and quantified in many tissues including the CNS microvasculature[389]. BM thickening was observed in conjunction with increased vesicle-mediated transcytosis[390], indicative of greater permeability, and pericyte degeneration in multiple brain regions[274]; this latter point particularly bodes intuitive consequences for vessel function and maintenance. Expression of TJ proteins, including occludin and zona occludens-1, was decreased following 2 weeks of type 1 DM and associated with increased metalloproteinase-9 and elevated solute permeability across the BBB[380,391]. Though not generally considered members of the BBB, microglia may directly contribute to the maintenance of microvasculature in type 1 DM. For example, increased microglial contacts with blood vessels were observed in the retina of mice after 4 weeks of DM, even before these cells exhibited a reactive phenotype[271]. At these contact sites capillaries exhibited prolonged vasoconstriction following exposure to fractalkine; this phenomenon was observed in both retina and cortex[271]. In the retina, increased microvascular tone contributed to decreased blood flow and was hypothesised to contribute to early diabetic retinopathy in these animals[271]. Furthermore, elevated levels of angiotensin II have been found in the vitreous and retina of diabetic rodents[392,393]. In addition to promoting vasoconstriction, increased angiotensin II can prompt the uncoupling of pericytes from ECs, increase vascular permeability, and facilitate the formation of microaneurisms that can progress to CMBs[394].

In summary, hyperglycemic toxicity directly alters EC function and viability in type 1 DM, as well as the integrity of the BBB. Perturbations in cell signalling may be augmented by proliferation of oxidative species and aberrant protein glycation, leading to positive feedback

loops of inflammation that target the vasculature. The result is a weakened vascular unit which exhibits greater permeability and susceptibility to rupture, and worsening microvascular disease.

1.4.2 Diabetes and cerebral microbleeds

CMBs are hemorrhages in microvessels (arterioles, venules, and capillaries) that result in the efflux of blood constituents into the brain parenchyma[383] and a disruption of blood flow which may be temporary, if the vessel is repaired, or permanent if it is not[6]. These insults can be visualized as small (<1 mm diameter in rodents), round lesions in post-mortem histology or *in vivo* magnetic resonance imaging[383]. CMBs can occur due to physiological processes, such as vascular remodelling wherein ECs uncouple from one another and migrate to alternate vessel segments[275,395]. They also arise as a product of microvascular disease, a pathology that is common in various conditions including hypertension, hypoxia, and diabetes[383,396]. The basis of microvascular disease is endothelial dysfunction in small blood vessels[397]. Endothelial dysfunction broadly describes the shift in properties of the endothelium towards a pro-inflammatory state, coincident with reduced vasodilation[398]. Local inflammation augments oxidative stress and induces EC apoptosis, leading to the physical degradation of BBB integrity and the leakage of blood products into the brain[399,400]. Enhanced expression of adhesion proteins by ECs during inflammation may also facilitate leukocyte recruitment to CMBs, which could explain why these insults are usually associated with macrophages[396,398,399].

The most widely-described aetiologies of CMBs are cerebral amyloid angiopathy and hypertensive arteriopathy[383]. The former is characterized by amyloid-β plaques along the vasculature, which induces inflammation, and the latter is associated with arteriolosclerosis and related to vascular risk factors including aging, hypertension, and diabetes[399]. The timing of a CMB insult is unpredictable and their locations vary, making them a challenging phenomenon to

study. However, some distribution patterns have been observed when comparing different types of dementia. For example, CMBs resulting from cerebral amyloid angiopathy in AD have been found predominantly in lobar regions compared to the deep and infratemporal CMBs reported in vascular dementia patients[401]. During chronic mild hypoxia, which produces transient microvascular leakiness, CMBs are primarily observed in the white matter[402]. It has been proposed that this may be due to the lower vascular density of white matter (~25% of gray matter vascularization[403]); essentially, minor changes in oxygenation in this region drive stronger remodelling responses which are subsequently associated with microbleeds when ECs dissociate[402]. The leakage of blood plasma components, including iron and fibrinogen, into the sensitive cerebral microenvironment can disrupt local neuronal circuitry and impact brain function[15,86,404,405]. Microglia have been identified as important cellular responders, involved in stemming the release of vascular constituents following CMB by physically enwrapping damaged microvessels with their motile processes[24,25]; in essence, they act as a ligature that patches the ruptured vessel. In a mouse model of type 1 DM, the polarization and extent of these microglial responses were significantly impaired, resulting in the protraction of BBB disruption and increasing the exposure of vulnerable neuronal machinery to toxic plasma[25].

CMBs are particularly concerning in the context of type 1 DM because patients are known to experience significantly more CMBs than the healthy population[2,3]. In addition to increasing the likelihood of CMBs, diabetes may also disrupt the repair of damaged vessels, leading to a greater probability of vessel loss rather than maintenance. This shift may contribute to the reduced vascular density reported in DM patients[8,10]. Although an individual CMB may be asymptomatic, recent studies have found that CMBs compound over time[406,407]. The onset or progression of cognitive dysfunction could subsequently arise as a consequence of exacerbated

cerebral hypoperfusion due to cumulative vessel loss. Since the brain is an extraordinarily energetically demanding organ, and neural cells are poorly-equipped to store glucose, even small perturbations in blood flow can significantly affect brain function[9,40,134]. Notably, ≥4 coincident CMBs correlated with cognitive decline[8] and CMBs were identified in 20% of 90 cases of mild cognitive impairment[408] and in 85% of 86 patients with subcortical vascular dementia[409], compared to just 6% of 413 healthy people aged 45-50 years old[410]. This may help explain the increased risk of dementia in type 1 DM patients[2,3]. With this in mind, understanding the cellular basis of CMB repair in DM is a crucial step towards ameliorating this significant complication.

1.4.3 Inflammation in diabetes: implications for CNS-immune cell interactions

Inflammation is a complex process that involves the activation of the adaptive and/or innate immune system by inflammatory molecules generated during acute insults or chronic degenerative conditions[411]. As an autoimmune disease, type 1 DM is intrinsically characterized by the pathological recruitment of the adaptive immune system[108–110]. In adolescence, these inflammatory processes lead to the destruction of pancreatic β-cells and establish the hallmarks of this disease[108–110]. However, inflammation in type 1 DM is not restricted to the acute period of early life, but is chronically and incurably perpetuated by extensive hyperglycemic toxicity (reviewed in Section 1.2.1). Thus, the diabetic body is persistently exposed to elevated levels of inflammatory molecules (ie. TNFα, IFNγ, and various cytokines)[214–216], and in a constant state of low-grade inflammation that may compromise healthy CNS-immune cell interactions.

Immune cells, including CNS-resident macrophages, are exquisitely sensitive to inflammatory cues which serve as important chemotactic signals that are necessary for recruiting both peripheral and CNS immune cells to sites of injury[22–24,27,368]. Notably, since inflammatory molecules can be transported into the brain across the BBB[412,413], they may have far-reaching

consequences to immune cell functions. Indeed, disruption of the concentration gradients of these signals, which are essential for guiding focused cellular responses, may significantly impair immune cell activity[24,25]. In support of this idea, Ibrahim et al. identified phosphorylated ERK1/2 and p38 in microglia from the retinal sections of diabetic rats, implicating the activation of mitogen-activated ERK kinase 1/2 and mitogen-activated protein kinase kinase 3/6 in these cells[127]. These MAPK cascades are associated with microglial activation and suggest that inflammatory molecules infiltrated the retina to trigger this state[127]. Furthermore, the focused nature of microglial responses to CMBs in the diabetic brain were found to be compromised; however, they could be rescued with anti-inflammatory treatments (dexamethasone (DEX) or neutralizing antibodies for IFNs)[25]. This evidence further implicates inflammation in disrupting immune cell functions in DM, potentially via perturbation of chemotactic gradients.

Chronic inflammation also leads to greater BBB permeability, including elevated transcytosis of potentially toxic substrates, that may allow pathogens entry into the CNS when they would normally be excluded[15,18,275]. These aberrant conditions trigger numerous molecular mechanisms that increase the propensity for peripheral immune cells breaching the BBB. Indeed, in response to blood-borne inflammatory molecules, circulating leukocytes become activated and monocytes/MDMs have been found to infiltrate the brain parenchyma in various inflammatory conditions[264,380,414]. Complimenting these phenotypic changes, inflammation upregulates adhesion molecules, such as VCAM-1 and ICAM-1, on ECs, thereby facilitating the initiation of leukocyte transcytosis[415]. NO quenching, which is known to occur in type 1 DM and may contribute to reduced vascular motility in this disease[142,416,417], also has implications for leukocyte diapedesis. Specifically, NO activates cyclic guanosine monophosphate which decreases P-selectin expression by ECs and downregulates its ligand on neutrophils[418]. In

endothelial nitric oxide synthase (eNOS) null mice, 9-10 times more leukocytes were observed binding to ECs following an inflammatory stimulus[418]; other microvascular pathology, such as vessel stalls from leukocytes plugging the vascular lumen, may also increase in this context. Additionally, inflammation increases MMP expression, facilitating leukocyte degradation of the BM and further promoting their infiltration into the CNS[419]. TNFα in particular is known to facilitate the extravasation of mononuclear phagocytes via NFκB activation[194]. In concert with IL-1β secretion by local macrophages, this could increase expression of chemokines CXCL1 and CCL2, perpetuating the recruitment of circulating leukocytes to CNS ECs[194].

The precedent for immune cell dysfunction in inflammatory disease is extensive[263,264,420]. Interestingly, however, investigations of this nature in the context of CMB repair in type 1 DM are limited[25], despite the putative role for immune cell dysfunction in known diabetic neurological complications including cognitive decline[380], CMBs[24,25], and neuropathies[382]. Given that insulin treatment remains ineffective at fully mitigating diabetic pathology[11–16,130,131], alternative anti-inflammatory regimens are being explored. For example, a clinical trial utilizing a TNFα antagonist was successful in lowering HbA_{1c} levels and enhancing endogenous insulin production[215], and another involving the administration of a Vitamin D analogue, which has nonspecific anti-inflammatory effects, resulted in the reduction of patients' required daily insulin doses[421]. Building on these findings, it may be valuable to consider adjuvant treatments that target other aspects of the inflammatory phenotype, such as impaired immune cell function, in the quest to ameliorate the pervasive CNS vascular pathology associated with type 1 DM.

1.4.4 Immune cells in microvascular repair: help or hazard?

The purpose of the vasculature is to transport blood throughout the body, maintaining interstitial homeostasis; this requires an essentially continuous flow of blood through millions of

capillaries. In order for blood to flow through any blood vessel, an intact endothelial tube is required to transport it from one end of the capillary to the other. Thus, an injury such as a CMB, which results in the physical disruption of endothelial continuity in a microvessel, compromises blood flow through the capillary and deprives nearby cells of essential metabolic support. To restore microvascular function, effective reparative mechanisms must be undertaken. Although there has been increasing appreciation for the clinical significance of CMBs, our understanding of the cellular and molecular underpinnings of their repair remains in its infancy.

During ischemic neovascularization, endothelial network repair involves the proliferation of ECs or the differentiation of bone marrow-derived EC progenitors[422]. However, in the context of hemorrhagic insults, CNS microglia and MDMs play a central role in microvascular repair. Following CMB, both CNS innate immune cells and blood-borne leukocytes localize to the site of damage, guided by gradients of extracellular ATP[22,24,27]. In healthy mice, microglia envelop the rupture within an hour and stem the extravasation of blood plasma, restoring the integrity of the disrupted BBB[24,25]. In type 1 DM, microglial motility is suppressed, prolonging BBB closure[25]. Perpetuated vascular leakage is also observed when microglia are eliminated, resulting in astrocyte-vascular uncoupling and decreased expression of TJ proteins[275]. Similar results are observed with pharmacologic inhibition of purinergic $P2Y_{12}$ receptors[24] or peptide-based blockade of fibrinogen-Mac1 interactions[275]. Peripherally-derived phagocytes can access the brain directly during vascular rupture and aggregate to CMBs in arterioles progressively over days[28]. In zebrafish, macrophages extend processes to physically ligate the severed ends of ECs following laser-induced CMBs[27]. Both CNS-resident and blood-borne macrophages demonstrate the capacity to repair microvessels in the zebrafish brain, but successful repair was dependent on the adhesion of both endothelial ends to the same cell; in cases involving multiple macrophages

contacting the damaged ECs, the microvessel was not repaired[27]. Microvascular injury induced in a model of mild traumatic brain injury was also shown to attract anti-inflammatory mMΦ that mediated angiogenesis through local production of MMP-2[423]. Macrophages are also capable of secreting VEGF, which can serve to stabilize EC fusion and support recanalization[424].

Interestingly, macrophage-independent microvascular repair, via endothelial self-extension, has also been reported. Endothelial self-extension involves the continuous protraction of endothelial end cells, a process which depends on the reorganization of microtubules, towards one-another until they meet and connect[27]. This characterization of endothelial self-extension was performed in a genetic zebrafish model in which macrophages were absent, demonstrating that these cells were not required for microvascular repair[27]. Under physiological conditions, in which macrophages would be present, endothelial self-extension was observed immediately after laser-induced CMB, but was blocked by the physical contact of macrophages[27]. This suggests that endothelial self-extension may represent the initial stages of microvascular repair following CMB, but that immune cell-mediated processes are likely responsible for latent BBB closure and the restoration of EC continuity under physiological conditions.

Microglia, BAMs, and bone marrow-derived macrophages likely play both facilitative[24,25,27,275] and destructive[86,286,425] roles in injury repair. For example, microglia may be initially protective, facilitating repair processes as described above, but then they could adopt an activated and destructive phenotype, secreting pro-inflammatory cytokines and proteases and phagocytosing injured cells[269,270,285]. Macrophages can also induce apoptosis in target ECs during developmental vascular remodelling via activation of the canonical WNT pathway, a process known as macrophage-induced programmed cell death[361]. Since microglial developmental programs, such as synapse pruning, can be reactivated under pathological conditions[304] it is

possible that macrophage-induced apoptosis of ECs could also be resurrected outside its typical developmental window (ie. following hemorrhagic insult or in vascular dementia). Furthermore, AXL expression by microglia is upregulated in various neurological diseases, suggesting that enhanced phagocytosis may be involved in these conditions[300,426]. These findings could indicate that aberrant phagocytosis exacerbates pathology or that it is a compensatory response to cellular degeneration. On the other hand, Hilla et al. described microglia as "irrelevant" in either promoting or inhibiting degeneration or repair following an axonal crush injury in the retina[37].

This plurality of behaviours mirrors the fluidity in which CNS and peripheral macrophages adopt a spectrum of pro- and anti-inflammatory phenotypes and suggests that factors such as the severity of the injury, comorbid disease, or the prevalence of cytokines, chemokines, and ROS could determine their activities. In support of this idea, the Brown lab has previously shown that early microglial responses to CMBs are disturbed in the diabetic mouse brain, coincident with elevated levels of IFNγ, and that these responses were normalized with anti-inflammatory treatments[25]. Infiltrating peripheral leukocytes have also been associated with neuronal loss and microglial activation following reperfusion injury[30], and monocytes infiltrating the CNS in mice with experimental autoimmune encephalitis exacerbated disease progression[264].

Evidently, further investigation is necessary to determine the relationship between these diverse driving forces and CMB repair, particularly in the context of mechanisms involving immune cells. Additionally, studies examining microglial- and macrophage-meditated capillary repair have thus far been limited to the acute period of several hours following injury[24,25,27,275]. Since microvascular repair is an ongoing process that evolves over days and weeks, the relative roles of CNS and peripheral immune cells in the long-term functional reintegration of injured vessels into the cerebral circulation remains to be determined.

1.5 Project objectives

Type 1 DM is a prevalent metabolic disorder characterized by vascular complications, including increased risk of CMBs[2,3]. Notably, insulin therapy is not sufficient for mitigating diabetic pathology[11–16,130,131]. CMBs may lead to microvascular loss and their increasing incidence is correlated with declining cognitive function[7,8,10]. However, the long-term repair of vessels following CMB has yet to be characterized, and the cellular mechanisms underlying this process are poorly understood. Microglia are hypothesized to contribute to CMB repair due to their key role in restoring BBB integrity after damage[22,24,25]. Peripheral phagocytes and their derivatives, MDMs, may also modulate CMB repair[27,28]. Given that type 1 DM is characterized by persistent, low-grade inflammation[127,214–216], immune cell functions, including their putative reparative roles, may be disrupted. Vessel loss may lead to a decrease in cerebral perfusion that could precede or trigger cognitive impairment or dementia onset. Evidently, a greater understanding of the pathophysiological changes that contribute to this condition is impetrative.

Building on this context, the present work sought to improve our understanding of the vascular complications of type 1 DM by studying the cellular underpinnings of CMB repair. Whether long-term immune cell responses and microvascular repair functions are impaired in type 1 DM is unknown, but it is conceivable that a disruption of these processes could contribute to the prevalence of dementias in this disease. This research tested the general **hypothesis that type 1 DM disrupts microglial/macrophage responses to, and repair of, CMBs in the mouse cortex.** This hypothesis was addressed in 2 primary aims. The first aim characterized long-term repair of diabetic CMBs, and the second probed the mechanisms underlying this process:

Aim 1: Identify how type 1 DM affects microglial/macrophage responses to, and repair of, CMBs.

Aim 2: Determine cellular mechanisms that modulate repair of CMBs in type 1 DM.

CHAPTER 2: MATERIALS AND METHODS

2.1 Animals

2- to 3-month-old heterozygous CX3CR1$^{+/eGFP}$ male mice were utilized in all experiments. These transgenic animals were generated by inserting an enhanced green fluorescent (eGFP) reporter allele into the DNA locus for the *CX3CR1* gene. CX3CR1 is involved in leukocyte and macrophage migration; thus, eGFP is expressed in CNS-resident microglia and BAMs, as well as peripheral phagocytes including monocytes and neutrophils[427]. It has been previously shown that heterozygosity of the fractalkine allele does not significantly alter microglial responses to CMBs relative to animals with both alleles intact[25].

All animals involved in this work were used and cared for in accordance with approved guidelines set forward by the University of Victoria's Animal Care Committee and the Canadian Council on Animal Care. A 12-hour light/dark cycle was provided, and ventilated housing racks were located in a temperature- (21℃ – 23℃) and humidity-controlled (40% - 50% relative humidity) environment. Mice were group-housed and given *ad libitum* access to food and water. For microglia depletion experiments, PLX5622 diet (1200 ppm; generously provided by Plexxikon) was substituted for regular irradiated mouse chow. Specifically, for 3 weeks prior to *in vivo* imaging mice were given unrestricted access to the PLX5622 diet; animals were maintained on this regimen throughout the entire experiment[25].

2.2 Craniotomies

Chronic cranial windows or acute thinned-skull craniotomies were utilized for 2-photon imaging experiments and induction of CMBs, as described previously[25]. For both preparations the initial steps were the same: mice were anesthetized to surgical-depth using gaseous

isofluorane (2% for induction and 1.3% for maintenance) in medical air (80% N2, 20% O2) at a flow rate of 0.7 L/min and then head-fixed to a custom-built surgical stage. Animals' body temperature was maintained at 37℃ throughout the procedure using a rectal probe thermometer and a temperature feedback regulator. A 0.03 mL bolus of lidocaine was injected subcutaneously (s.c.) under the scalp at the surgical site before a lateral dorsoventral incision was made and the scalp was retracted. Muscle tissue and fascia were scraped from the skull using a Q-tip.

For mice that received chronic cranial windows, an additional 0.03 mL intramuscular (i.m.) injection of 2% DEX was also given to reduce acute inflammation. A custom metal ring (outer diameter 11.3 mm, inner diameter 7.0 mm, height 1.5 mm) was adhered to the skull over the right somatosensory cortex using Krazy Glue. A circular area of the skull, with a diameter of approximately 4 mm, was thinned in the center of the metal ring using a high-speed dental drill; cold HEPES-buffered artificial cerebrospinal fluid (ACSF) was regularly applied to the skull to cool the area. Once the vasculature could be visualized through the thinned skull fine forceps were used to remove the bone fragment. Gel foam soaked in cold ACSF was used to regularly moisten the brain and stem any subdural bleeds; the dura was kept intact for this procedure. Mice recovered under a heat lamp and were monitored regularly before being returned to their home cage for 5 weeks prior to beginning longitudinal 2-photon imaging experiments.

Thinned-skull preparations were used to generate tissue containing CMBs for immunofluorescence and confocal imaging. Once the skull was exposed, a square area of 16 mm^2 was marked over the right somatosensory cortex using a black permanent marker and thinned using a high-speed dental drill. Cold ACSF was applied to the skull during the drilling process to cool the area. The skull was deemed sufficiently thin when small meningeal blood vessels became visible through the skull with the application of ACSF. Anesthesia was reduced

to 1% isofluorane and the mouse was quickly transferred to a custom-built stage on the 2-photon microscope for CMB induction (described below). Once complete, the scalp was sutured closed, Polysporin was applied to the stitches, and the mouse was monitored regularly as it recovered under a heat lamp. Animals were returned to their home cage for 3 days prior to euthanasia and processing for immunofluorescence.

2.3 *In vivo* 2-photon imaging and cerebral microbleed induction

2-photon imaging and CMB induction were performed as per previous publications[25]. Mice were lightly anesthetized with gaseous ~1% isofluorane in medical air and fitted to a custom imaging stage for either thinned skull or cranial window preparations. High resolution images were acquired using an Olympus FV1000MPE laser scanning microscope fed by a mode-locked Ti:Sapph laser source (>1.5 W average output at 800 nm, ~80 MHz) and equipped with a water-dipping 40X objective lens (Olympus, NA=0.8); Olympus' proprietary software Fluoview FV10-ASW was utilized for laser scanning and image collection.

Vasculature was visualized with intravenous (i.v.) administration of 0.1mL Rhodamine-B Dextran (4% in saline or CLR solution for intervention group, Sigma Aldrich) and macrophages in transgenic animals expressed eGFP under the *CX3CR1* promoter (Fig. 10A; optimal coincident excitation of fluorescence for these entities was achieved at 880nm. eGFP alone was excited at 850 nm, lipofuscin autofluorescence at 750 nm, and the Cy5 fluorophore in immunofluorescence-labelled fixed tissue at 900 nm. Emitted light was split by a dichroic filter (552 nm) before it passed through either a 495-540 nm or 558-706 nm bandpass filter.

Microvessels to be targeted for CMBs were identified as flowing capillaries (3-7 µm width), confirmed by line-scans (Fig. 10A), 50-100 µm below the surface of the somatosensory cortex and were separated by a minimum of 200 µm. CMBs were induced by focusing the laser

to the center of the microvessel and increasing the power output (tuning the laser to 850 nm, ~220 mW at the back aperture) to a circular area with a diameter of 3 μm for ~6 s. Macrophage cell bodies apposed to microvessels were excluded from the circular ablation area. Successful microvascular ablation was confirmed by the rapid extravasation of intravascular fluorescent dye, visible upon completion of the CMB induction protocol (Fig 10B).

Imaging stacks with a depth of 45 μm were collected and consisted of individual images obtained at 1.5 μm z-plane intervals; acquired images represented an area of 144x144 μm^2 across the x-y planes and a resolution of 1024x1024 pixels. Each image was collected as the product of an average of 3 images per plane (Kalman= 3 frames). The same imaging area was relocated week-to-week using local landmarks and reference coordinates attributed to stable surface vessels. 2-photon imaging was performed on the day of CMB induction (images acquired before and after ablation; D0) and then 1, 3, 7, and 14 days later (Fig. 11).

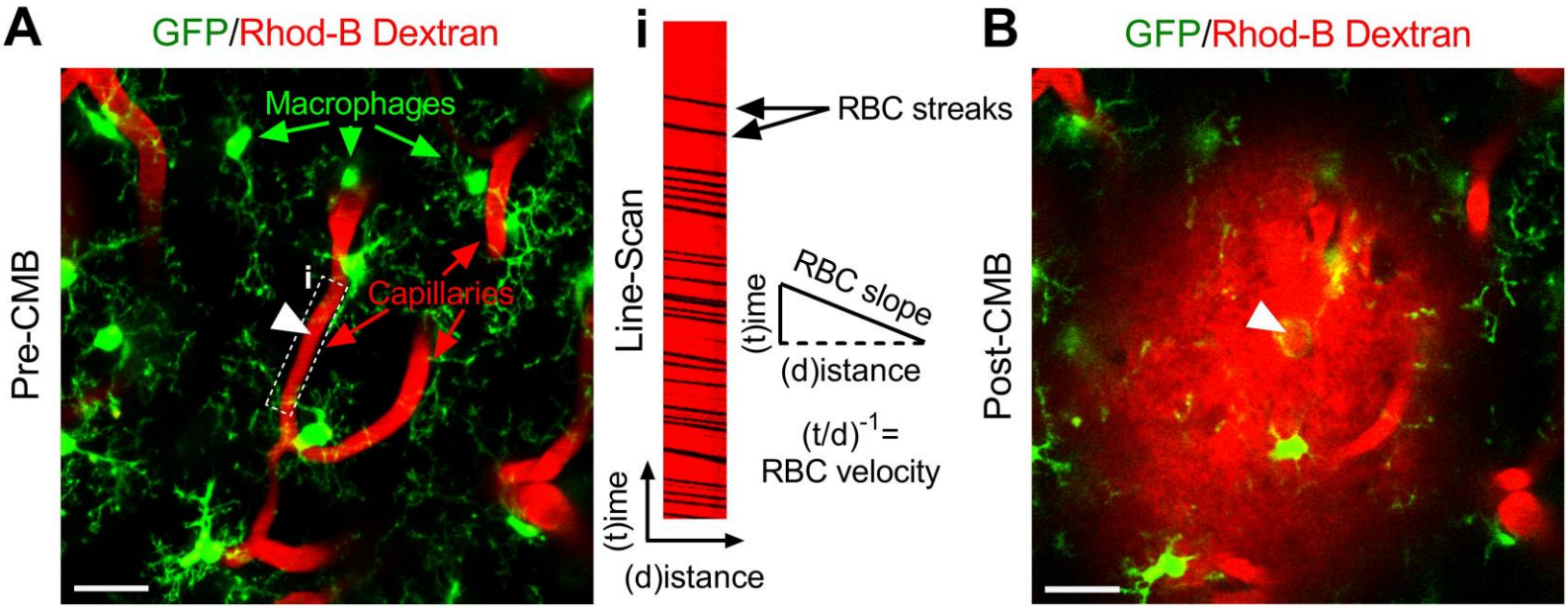

Figure 10. Example of cortical microvessel targeted for CMB and confirmation of ablation. **A.** Representative image of a capillary to be targeted for CMB induction (*white arrowhead*). Capillaries were visualized by labelling with intravascular Rhodamine-B (Rhod-B) Dextran and brain macrophages, such as microglia and BAMs, express eGFP in CX3CR1$^{+/eGFP}$ transgenic mice. Only flowing microvessels were targeted for ablation, determined by **i.** line-scans of vessels. **i.** Line-scans show RBCs as streaks of negative space through fluorescently-labelled vascular lumen. The inverse slope of RBC streaks approximates RBC velocity since time is represented on the y-axis of the line-scan and distance along the x-axis. **B.** Successful CMB induction was confirmed by rapid extravasation of intravascular dye from the target site (*white arrowhead*) following cessation of the ablation protocol. Scale bars represent 20 µm.

2.4 Induction and treatment of type 1 diabetes mellitus

Mice were randomly assigned to 3 treatment groups: nondiabetic (NDB), diabetic (DB), and insulin-treated diabetic (INS; Fig. 11). Type 1 DM was induced in transgenic CX3CR1$^{+/eGFP}$ mice, via the widely-utilized multiple low dose Streptozotocin model[428–430]; this strategy has been utilized extensively by the Brown lab[25,431]. This protocol permits tight control of DM onset, induced insulitis, and elicited reproducible, significant increases in blood glucose levels without causing weight loss (Fig. 12). Importantly, STZ does not cause toxicity to CNS cells since its effects targeting pancreatic β-cells are primarily the result of its uptake via GLUT-2[253], which is negligibly expressed in the brain[432]. Although STZ impacts the viability of hippocampal stem cells *in vitro*[433], it does not cause cellular degeneration at high concentrations (140 mg/kg) in cortical mouse brain slices, evidenced by an absence of Fluoro-Jade C staining in treated tissue[14].

2.4.1 Streptozotocin treatment

4 weeks prior to *in vivo* 2-photon imaging, mice assigned to DB or INS cohorts began STZ treatment to induce type 1 DM (Fig. 11). These animals received 2 consecutive daily doses of STZ (75 mg/kg) via intraperitoneal (i.p.) injection; animals were fasted for 5 hours prior to drug administration. STZ was dissolved in 50 mM citrate buffer (pH =4.5). A sucrose solution (5% in water), substituted for regular water, was provided overnight to mitigate acute hypoglycemia. Fasting blood glucose levels were monitored weekly using an Aviva™ Accu-Chek blood glucose meter on blood lanced from the tail vein. Type 1 DM onset was confirmed 1 week following the initial STZ injection (Fig. 12); mice that did not exceed the hyperglycemic threshold (defined as ≥15.0 mmol/L)[25] were given a single, additional dose of 110 mg/kg STZ. STZ-treated mice not surpassing the hyperglycemic threshold were included in the NDB group. NDB mice received equivalent injections of vehicle after 5 hours of food deprivation (Fig. 11).

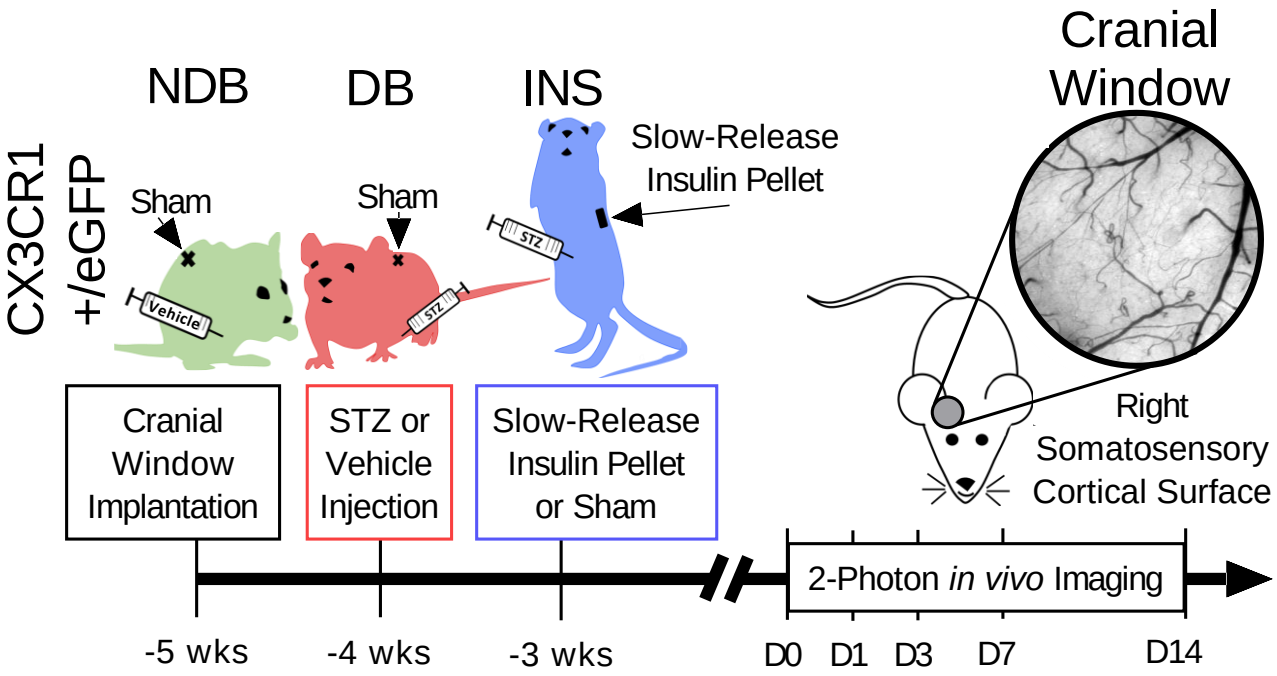

Figure 11. General experimental and longitudinal 2-photon imaging timeline.

Transgenic CX3CR1$^{+/eGFP}$ mice were randomly assigned to either NDB, DB, or INS cohorts. For longitudinal imaging experiments, chronic cranial windows were implanted over the right somatosensory cortex 5 weeks prior to beginning 2-photon imaging (D0). DB and INS mice received injections of STZ 1 week after surgery and NDB mice were given equivalent injections of vehicle. Mice assigned to receive implants of slow-release insulin pellets were treated 1 week after confirmation of DM onset; sham procedures were performed on DB and NDB mice. Longitudinal *in vivo* 2-photon imaging began on D0 with the induction of CMBs. These insults were relocated and imaged the next day and again 3, 7, and 14 days later.

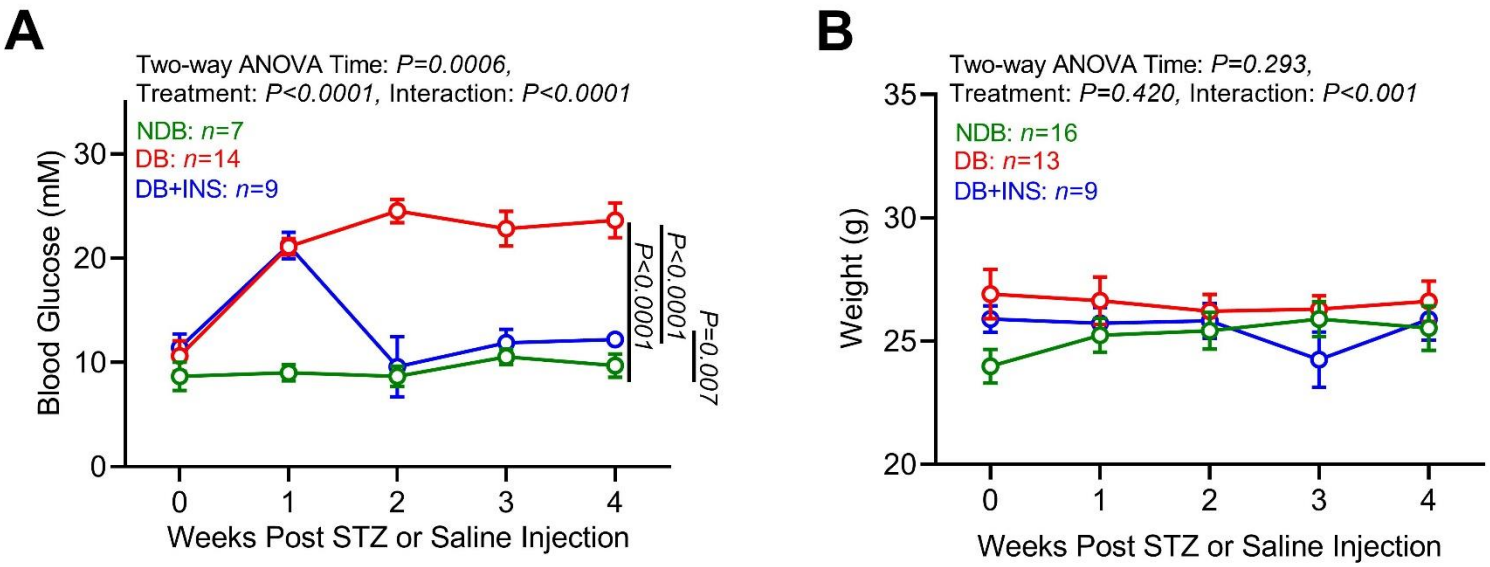

Figure 12. STZ induces hyperglycemia in mice without significantly affecting weight.

A. STZ injection induces a model of type 1 DM in mice, eliciting a significant increase in blood glucose levels 1 week following treatment relative to animals which receive saline. This hyperglycemia is sensitive to insulin treatment and can be normalized within 1 week using slow-release s.c. insulin pellets. **B.** Mice that receive STZ injections do not exhibit significant changes in weight relative to animals given saline; insulin treatment also does not affect body weight. Error bars represent ±SEM.

2.4.2 Subcutaneous slow-release insulin administration

A subset of DB mice, which were confirmed to have supra-threshold hyperglycemia (≥15.0 mM) 1 week following induction, were randomly chosen to receive chronic insulin treatment (Fig. 11). Insulin therapy was provided in the form of s.c. slow-release pellets (0.1U/24 hrs/pellet, LinShin). Using methods established previously[25], insulin pellets were implanted in mice that were anesthetized until toe-pinch reflexes were lost (1-1.3% isofluorane in medical air). The hair between the shoulder blades was trimmed with scissors and the area was cleaned with 70% ethanol and a 0.03 mL bolus of s.c. lidocaine was injected in the shaved area. A small incision was made in the skin and a hemostat was used to separate the fascia adhering the skin and muscle, creating a tissue pocket for the insulin pellets. A hemostat was used to insert the insulin pellets deep into the separated tissue; as per the manufacturer's instructions, dosing required 2 pellets per 20g bodyweight plus a supplementary pellet for each additional 5g[434]. The incision was sutured shut and stitches were secured with Krazy Glue. The mouse was regularly monitored as it recovered under a heat lamp before being returned to its home cage. Blood glucose levels were monitored weekly as described above (Fig. 12). If blood glucose exceeded 15.0 mM this procedure was repeated to insert additional pellets and reinstate normoglycemia.

2.4.3 Drugs

IFN signalling was manipulated *in vivo* using neutralizing antibodies. IFNγ (300µg in saline, Bio X Cell) or IFNα (300µg in saline, Bio X Cell) antibodies were injected i.v. twice, 2-3 days apart, during the 5-day period prior to CMB induction. A general anti-inflammatory intervention was provided by s.c. injection of 2 mg/kg DEX twice daily (12hrs apart) for 5 days before beginning imaging experiments. IFN and DEX controls received equivalent saline injections. These treatment schedules have been validated previously by the Brown lab[25]. To test

the involvement of peripheral immune cells in CMB repair, circulating phagocytic leukocytes were depleted using i.v. injections of 50 mg/kg CLR (Liposoma, B.V.). This treatment was provided 2 days prior to CMB induction, on the day of CMB induction, and 2 days later. Controls were given equivalent injections of PBS-encapsulated liposomes (Liposoma, B.V.).

2.5 Immunofluorescence and confocal imaging

Mice were euthanized using an approved protocol: i.p. injection of 240 mg/mL sodium pentobarbital (Euthanyl diluted 1:1 in sterile saline, Bimeda-MTC Animal Health Inc.). When no toe-pinch reflexes could be elicited, the mouse was transcardially perfused with 10 mL of phosphate-buffered saline (PBS) followed by 10 mL of 4% paraformaldehyde (PFA) in 0.1M PBS. Whole brains, liver, and spleen were extracted and fixed overnight in 4% PFA. Brains were transferred to a 30% sucrose solution (in 0.1 M PBS with 0.2% sodium azide), while livers and spleens were stored in 0.2% sodium azide (in 0.1 M PBS). Once brains were saturated with the sucrose solution they were sliced on a freezing microtome (American Optical Corp.) into 40 µm coronal sections, and liver and spleen were sectioned at 50 µm with a vibratome (Leica T1000); slices were stored in 12- or 24-well plates, submerged in 0.2% sodium azide solution.

For immunofluorescent processing, slices were washed with 0.1 M PBS for 10min before primary antibody incubation (Table 1). Following 3, 5min washes in 0.1 M PBS, incubation of secondary antibodies (1:400 Cy5 donkey anti-rat, Invitrogen; 1:400 Cy5 goat anti-rabbit, Invitrogen; 1:500 Cy5 donkey anti-sheep, Sigma Aldrich; 1:500 Alexa 488 goat anti-mouse, Invitrogen; 1:400 Alexa 568 goat anti-rabbit, Invitrogen) were performed at room temperature for 4hrs. After another series of washes, sections were stained with Hoescht 33258 (1:1000 in 0.1 M PBS; ThermoScientific), and then washed for 15 min in 0.1 M PBS. Slices were mounted on gelatin-coated glass slides with Fluoromount-G (Southern Biotech) and coverslipped.

Antibody	Supplier	Concentration	Antigen Retrieval?	Incubation Conditions
Rabbit anti-TMEM119	Abcam	1:1000	No	Overnight at room temperature in 0.1 M PBS
Mouse anti-Iba-1	Millipore	1:1000	No	Overnight at 4℃ in 0.1 M PBS
Rat anti-CD206	Bio-Rad	1:1000	No	Overnight at room temperature with 2% BSA and 0.2% TX-100 in 0.1 M PBS
Rat anti-CD68	Bio-Rad	1:1000	No	Overnight at room temperature with 2% BSA and 0.2% TX-100 in 0.1 M PBS
Rat anti-Mac2	Cedarlane	1:1000	No	Overnight at 4℃ in 3% NDS with 0.2% TX-100 in 0.1 M PBS
Goat anti-Axl	R&D	1:500	Required	Overnight at 4℃ in 0.1 M PBS with 0.2% TX-100
Sheep anti-TREM-2	R&D	1:200	Required	2 days at 4℃ in 5% NDS with 0.2% TX-100 in 0.1 M PBS

Table 1. Primary antibody concentrations and incubation conditions.

40 µm coronal sections of mouse brain and 50 µm slices of mouse liver and spleen were incubated with various primary antibodies in either 0.1 M PBS or 2% BSA, 0.2% TX-100, and/or 3% NDS in 0.1M PBS. To facilitate staining, some primary antibodies required antigen retrieval involving the incubation of slices in 10 mM sodium citrate buffer (pH=6.0) in a hot water bath at 75℃ for 30 min. BSA: Bovine serum albumin. TX-100: Triton X-100. NDS: Normal donkey serum.

Confocal imaging of immunofluorescence-labelled sections was performed on an Olympus FV1000BX61W1 microscope using either a 20X (Olympus, NA= 0.75) or a 60X objective (Olympus, NA= 1.35, oil). The proprietary FV10-ASW software was utilized for image capture and acquisition. The following settings were used for 20X or 60X image acquisition, respectively: zoom factor of 1.8X, 1024x1024 pixel resolution (0.345 µm/pixel), and 1 µm z-steps between subsequent sections or zoom factor of 2.0X 1024x1024 pixel resolution (0.103 µm/pixel), and 0.75 µm z-steps. 2 images were averaged per plane (Kalman = 2 frames) in both imaging contexts to generate an individual image.

2.6 Diff Quik histology

Peripheral leukocytes were identified using a Diff Quik staining kit (Electron Microscopy Sciences). A 1-3 µL drop of blood, collected by pricking the tail vein of a mouse, was smeared on a glass slide and allowed to air dry; 5 blood smears were performed for each animal. Slides were submerged for 1s 8 times in each of the solutions included with the kit: first the fixative (Fast Green in methanol), then Solution A (Eosin G in phosphate buffer), and finally Solution B (Thiazine Dye in phosphate buffer). Between consecutive dips, excess solution was allowed to drain from the slide. After dipping in Solution B slides were gently rinsed with distilled water and allowed to air dry on a rack.

Slides were imaged with a brightfield microscope (Olymps BX-51) using a 40X objective lens (Olympus; NA=0.65). Cells were identified by their morphological features, visualized using the histological stain: neutrophils contained distinct dark, multi-lobed nuclei, monocytes had large, dark purple nuclei with pale blue cytoplasm, lymphocytes had dark blue nuclei that comprised much of the cell area (pale purple cytoplasm was barely discerned around the predominant nucleus), and red blood cells (RBCs) exhibited a biconcave disc morphology that

did not react with the counterstain (Fig. 13). Images were acquired in the monolayer of the blood smear and 20 images were taken per slide, in a tiled manner. The total number of leukocytes and RBCs counted per slide were averaged across the 5 slides produced per animal to comprise an individual sample. The RBCs counted in each imaging area were used to standardize the number of leukocytes quantified.

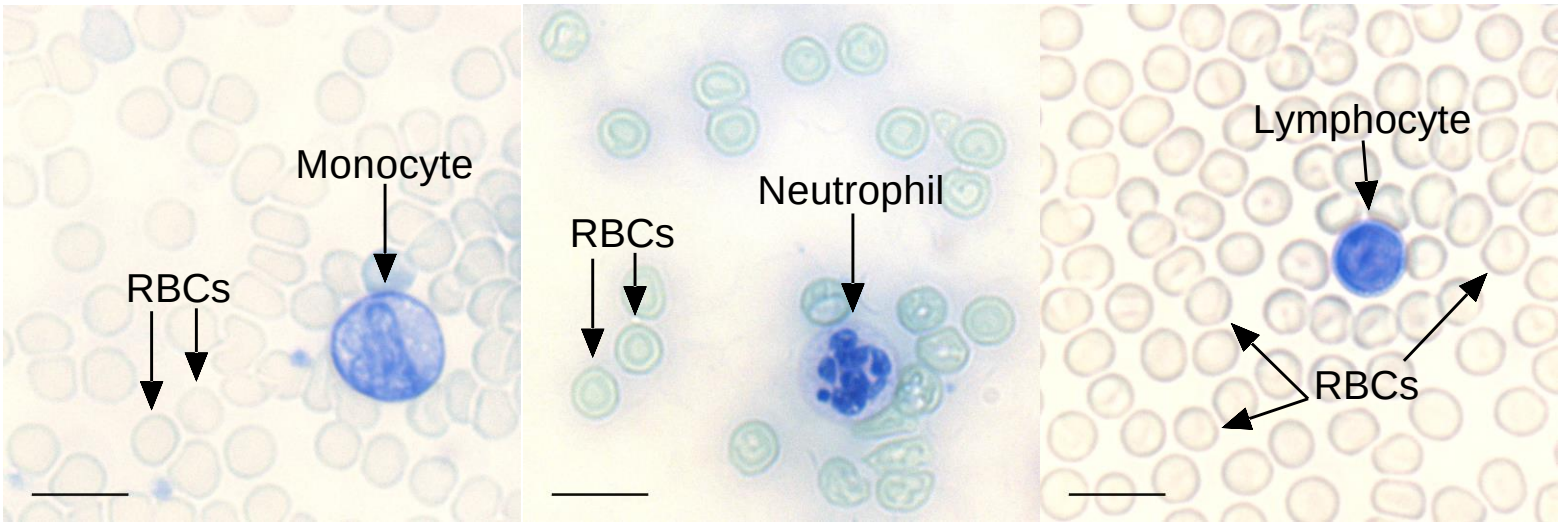

Figure 13. Diff Quik histological stain visualized peripheral leukocytes and red blood cells. Brightfield images obtained from the monolayer of mouse blood smears processed using the Diff Quick histological stain. Monocytes, neutrophils, lymphocytes, and RBCs were identified and differentiated by distinct morphological features. Specifically, (*left*) monocytes exhibited large, dark nuclei and abundant pale blue cytoplasm, (*middle*) neutrophils had dark blue multi-lobed nuclei, (*right*) lymphocytes were identified by their predominant dark nuclei and thin, barely-discernable ring of cytoplasm, and RBCs did not react with the counterstain and demonstrated a stereotypical biconcave shape. Scale bars represent 20 µm.

2.7 Data analysis

A variety of data pertaining to morphological, molecular, and functional features of cells and vasculature were extracted from individual images and z-stacks acquired from 2-photon, confocal, and brightfield microscopy using Olympus FV10-ASW or cellSens software. All data were stored on a computer for offline analysis. Image processing was performed manually using Olympus FV10-ASW and ImageJ (V1.52p; Fiji) functions, including automatic cell counting.

2.7.1 Determination of microvascular parameters

Blood flow velocity was calculated as the inverse slope of RBCs, visible as streaks of negative space in the fluorescent vascular lumen, identified by a line-scan of the target vessel (Fig. 10A). The vertical axis of a line-scan denotes time, while the position of a cell is plotted along the horizontal axis. The average velocity of a minimum of 3 RBCs were determined for each line-scan, and an average of 3 line-scans comprised a single blood flow velocity value. Olympus FV10-ASW software was used for these RBC velocity calculations.

To determine microvessel width and length, the red and green channels of an acquired image were split; only images from the red channel were retained for these calculations (Fig. 14A). Vessel width was determined by drawing a line perpendicular to the vessel's length in a single image, guided by a 90° angle plotted on the overlay layer (Fig. 14B). Using the "plot profile" function in Fiji, the half-maximum intensity of pixel grey values was determined (Fig. 14B). The full-width of half-maximum intensity values, generated by the "list values" function, was then calculated as equivalent to the vessel width (Fig. 14B). The length of a microvessel was determined by plotting a line along the vessel in 3-dimensions using a z-stack of images from the red channel (Fig. 14C). The "measure" function in Fiji provided an output of length (Fig. 14C).

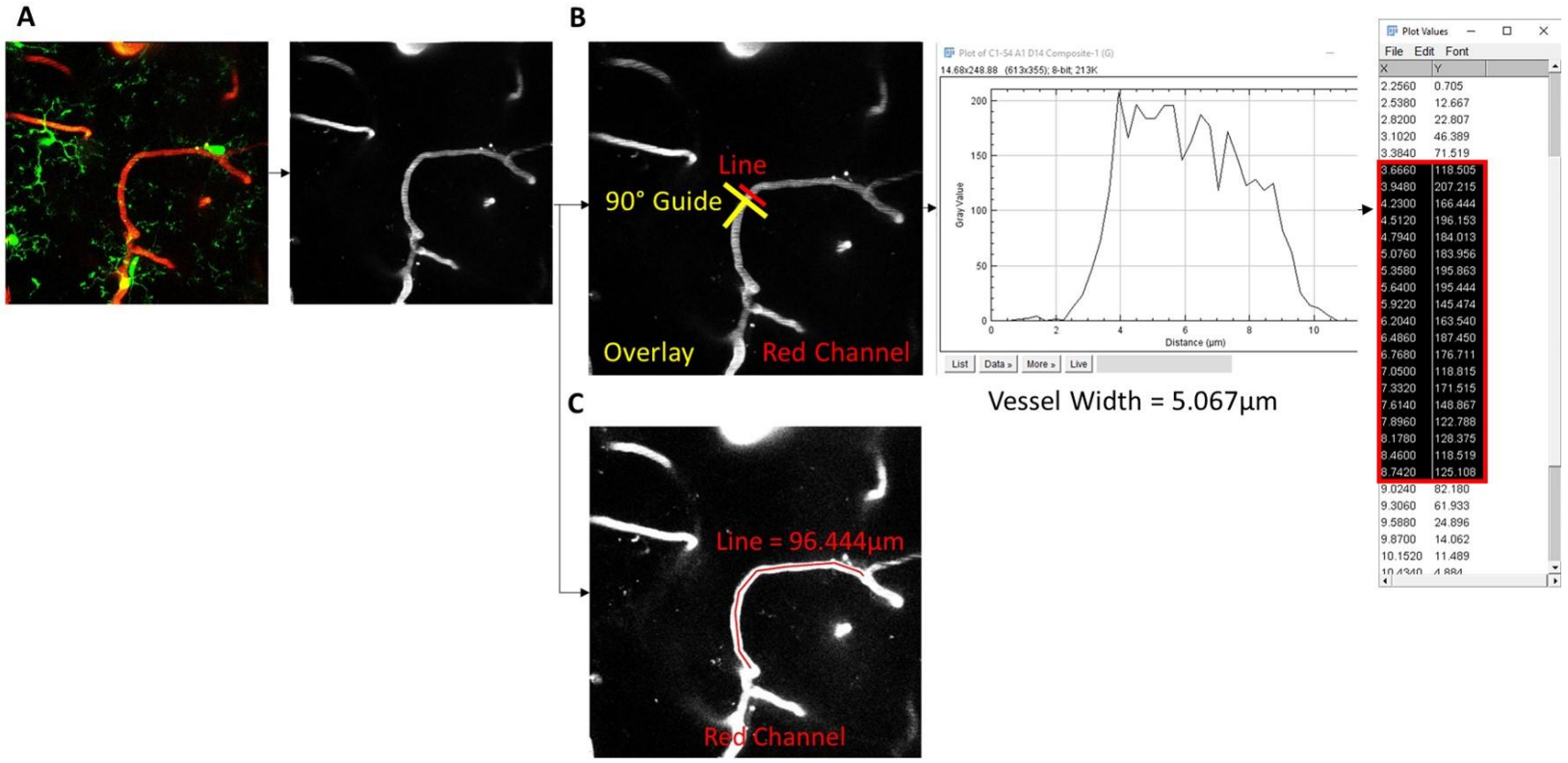

Figure 14. Calculation of microvessel width and length.

A. To calculate microvessel width and length, images were split into red (Rhodamine-B Dextran-labelled vessels) and green (eGFP-labelled macrophages) channels and only the red one (*right*) was used. **B.** (*left*) A line (*red*) perpendicular to the center of the target vessel, identified on the image in the center of the z-stack, was plotted using a 90° guide (*yellow*) drawn on the overlay. (*middle*) With the "plot profile" function in Fiji, the half-maximum intensity of pixel grey values was (*right*) used to determine the full-width of half-maximum values (*red selection*) plotted via the "list values" function. The difference of selected x-values provided the vessel width. **C.** Vessel length was calculated by tracing the vessel with a line in 3-dimensions using a z-stack of red channel images. The "measure" function in Fiji yielded the length. In this example, the process was applied to an individual plane in lieu of a z-stack for this in-text illustration.

2.7.2 Morphological characterization of cerebral microbleed responses

Morphological features of macrophage responses to CMBs were characterized as the 2-dimensional area of aggregated eGFP to the target vessel and the percentage of the vessel covered by eGFP+ processes (Fig. 15). The 2-dimensional area of GFP fluorescence was determined using the central image of the z-stack, containing the target vessel in-plane. This image was split into red and green channels (Fig.15A). Both channels were smoothed using a Gaussian blur (radius =2.00) filter and subjected to a threshold function ("Li", Fiji) to convert them into binary images (Fig. 15B). For reference, the signal pixels are in black. The vessel region of interest (ROI) was selected from the red channel and applied, using an overlay, to the binarized green channel (Fig. 15B). The "measure" function in Fiji was used to count all the signal pixels directly apposed to the vessel ROI, and the sum of these pixels was determined to comprise the 2-dimensional area of eGFP aggregated to the damaged vessel (Fig. 15C).

To determine the percentage of vessel coverage by eGFP+ processes, only the central plane of the z-stack was used. This image was split into its red and green channel components, filtered, and a threshold applied as described above for the calculation of the 2-dimensional area of eGFP aggregate (Fig. 16A, B). In the red channel, the left and right ablumenal aspects of the vessel were traced, their length determined using the Fiji "measure" function, and saved as ROIs (Fig. 16B). These ROIs were added to the green channel overlay and the total length intersecting with black pixels was determined to yield the percentage of eGFP coverage: (sum of intersecting black pixels) / (total length of vessel ROIs) x 100 (Fig. 16B, C).

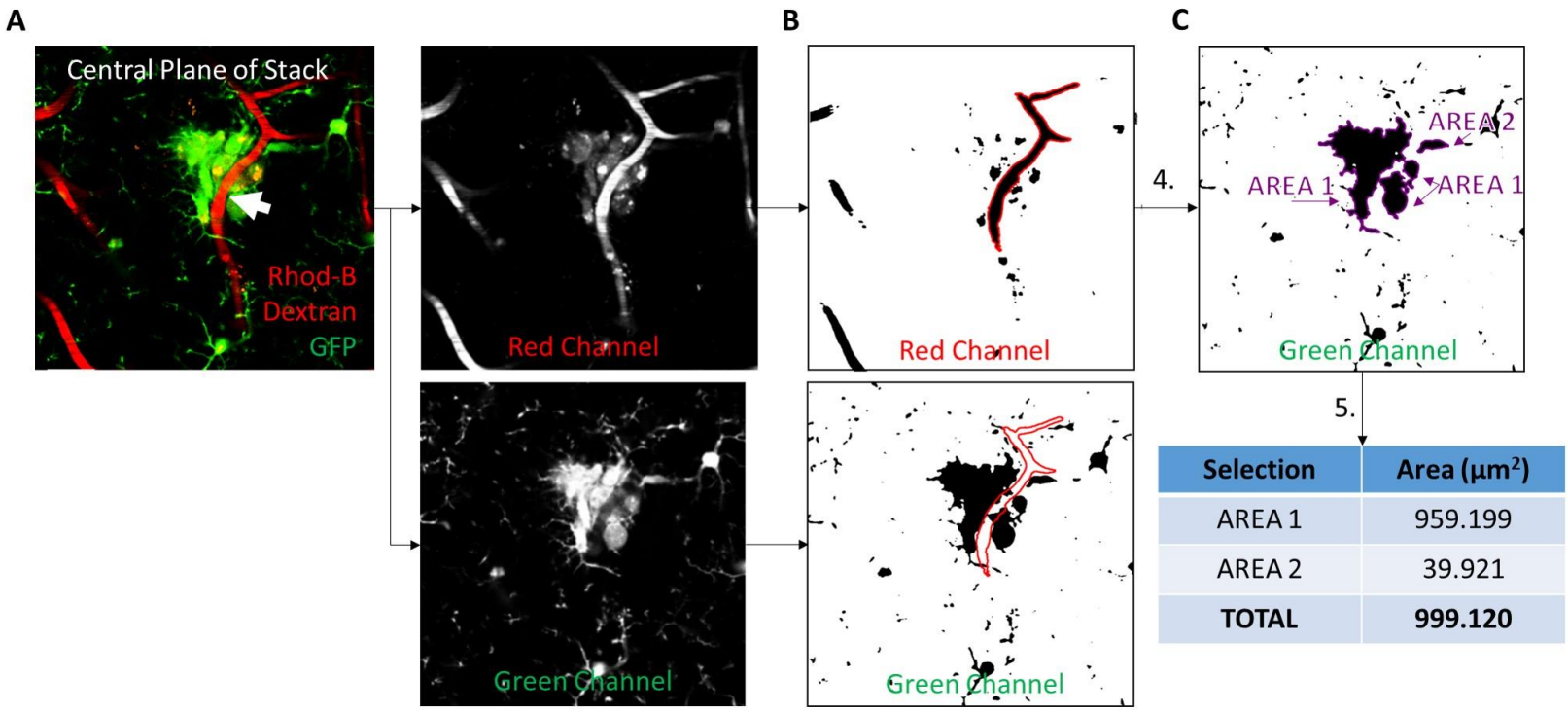

Figure 15. Calculation of 2-dimensional area of eGFP aggregate at damaged microvessel. **A.** Only the central plane of a z-stack, including the target vessel in-plane (*white arrow*), was used for these calculations. The image was split into its red (Rhodamine-B Dextran-labelled vessels) and green (eGFP-labelled macrophages) channel components. **B.** Individual channels were smoothed using a Gaussian blur filter and the "Li" function in Fiji was used to apply a threshold and convert the images into binary, where black pixels represented signal in the original image. The vessel ROI was selected in the red channel and overlaid on the binarized green channel. **C.** Using the "measure" function in Fiji, all signal pixels directly apposed to the vessel ROI, relating to the target vessel, were selected. The sum of these signal pixels comprised the 2-dimensional area of eGFP aggregate.

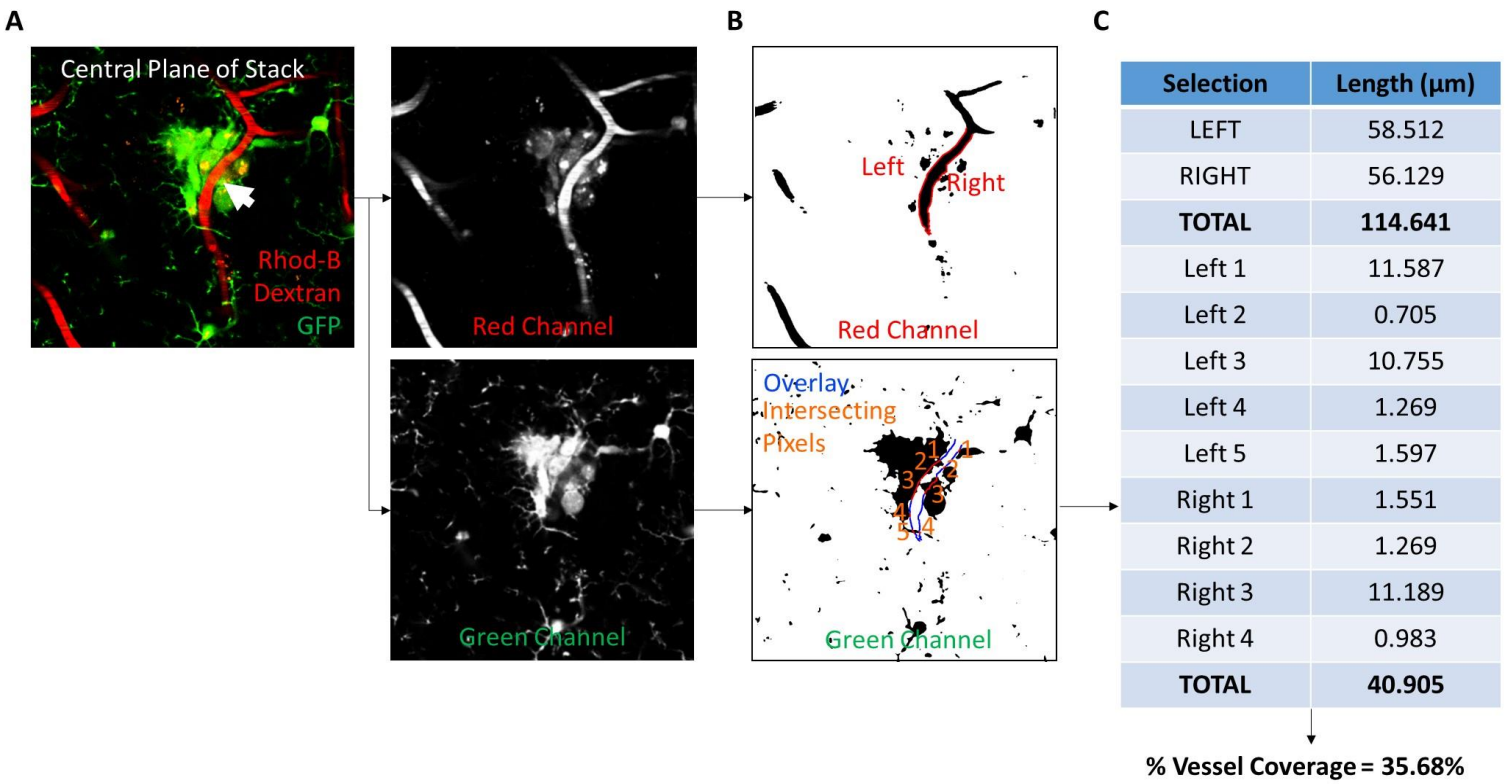

Figure 16. Calculation of percentage of vessel coverage by eGFP+ processes.

A. The central plane of a z-stack containing a target vessel (*white arrow*) was used for this calculation. This image was split into its red (Rhodamine-B Dextran-labelled vessels) and green (eGFP-labelled macrophages) channel components. **B.** Individual channels were processed using a Gaussian filter and converted to binary with the "Li" function in Fiji. Black pixels represented signal. The left and right ablumenal aspects of the vessel were traced in the red channel and their length determined with the "measure" function. The lines were saved as ROIs and transferred to an overlay (*blue*) in the green channel. The length of the overlaid lines that intersected with black pixels (*orange)* was quantified using the "measure" function. **C.** The sum of the length of overlaid lines intersecting with black pixels was divided by the total length of the vessel ROIs to determine the percentage of vessel coverage by eGFP+ processes.

2.7.3 Cell counting

Cells were counted in 3 contexts: immunofluorescence-labelled coronal sections with and without CMBs, and peripheral leukocytes visualized with the Diff Quik histological stain. In brain sections that did not contain CMBs, cells were counted plane-by-plane by scrolling through the z-stack. A cell was counted if the soma was fully contained within the acquired z-stack; that is, the cell body was not bisected by the edges of the imaging area and no part of it extended beyond the top or bottom of the stack. A cell was determined to be localized to the meninges if its soma was directly apposed to the autofluorescent aggregate along the cortical surface of a coronal section. If a cell soma was within the bounds of a penetrating arteriole, identified by the dense, dorsal-ventral arrangement of Hoechst 33342–labelled endothelial soma, it was qualified as being associated with a vessel. In the event that neither of these criteria were met, the cell was determined to be parenchymal.

In coronal sections containing CMBs, these insults were localized to layers 1-2 of the right somatosensory cortex. The eGFP+ aggregate associated with the CMBs was used to define the edges of the cellular milieu. Specifically, the eGFP signal was converted to a binary image using the “Li” function in Fiji and saved as an ROI. The ROI was then overlaid on individual images in the z-stack and cell somas that were fully contained within the area were counted. To assess the colocalization of immunofluorescent markers for Mac-2 and TMEM119 in CMBs, single planes from acquired z-stacks were split into individual channels and smoothed with a Gaussian blur filter (radius =1.00). These images were converted to binary using the “Li” threshold function in Fiji and ROIs containing signal pixels from the channel representing TMEM119 were measured, saved, and overlaid on the channel containing signal pertaining to Mac-2. The area of signal pixels within the overlaid ROIs was quantified and this process was

repeated for each plane containing portions of the contiguous eGFP+ aggregate. The total area of TMEM119 ROIs and the sum of Mac-2 pixels contained within the overlaid ROIs were calculated; the latter was divided by the former and converted to a percent, thus yielding the proportal colocalization of these markers in a CMB.

Finally, to count peripheral leukocytes individual images acquired using Olympus cellSens software were converted to binary using the "Triangle" threshold function in Fiji. Since most images contained hundreds of cells, the vast majority of which were round RBCs, the total cells contained in an image were counted automatically. Using the "Analyze Particles" function, cells (defined as having an area of 20-200 pixels) were counted, excluding those bisected by the edges of the image. Individual leukocytes were identified and differentiated manually and subtracted from the total cells, thereby also yielding the number of RBCs. 20 images were acquired in the monolayer of each blood smear, and the sum of cells in these images was calculated. The average of sums across 5 blood smears per animal yielded an individual sample.

2.7.4 Particle analysis *in vivo* and immunostained cortical sections

Particle analysis was performed *in vivo* to assess lipofuscin content at the site of a CMB and *in situ* for immunofluorescence-labelled coronal slices with markers for CD68, Axl, and TREM2. Firstly, to determine the colocalization of lipofuscin autofluorescence with CX3CR1+ cells, an image containing eGFP+ aggregate contiguous with the ablation site was split into individual red (autofluorescent lipofuscin particles) and green (eGFP-labelled macrophages) channels. Images were smoothed with a Gaussian blur filter (radius =1.00) and binarized using the "Li" threshold in Fiji. ROI selections of the relevant eGFP signal were made in the binary green channel, saved, and overlaid on the binary red channel. The area of signal pixels from the latter channel, contained within overlaid ROIs, was determined and the sum of these areas over

all planes in the z-stack containing the cellular milieu of the CMB was calculated. This process yielded both the percent area of lipofuscin colocalized with eGFP, as well as the number of lipofuscin particles in the CMB; particles <1.0 μm^2 were excluded. Using this process, the colocalization of lipofuscin with CD68, CD68 with eGFP, and Axl or TREM2 with Iba-1 were also assessed; a required minimum area of 1.0 μm^2 was applied for counting CD68 particles.

2.8 Data analysis and statistics

Data were analyzed and graphed using Graphpad Prism (Version 8.2.0). Statistical analyses included: unpaired Student's t-tests when comparing two groups, Chi-squared analyses to assess whether microvessel elimination rates differed, one-way ANOVAs for comparing 3 or more groups, and two-way mixed effects model ANOVAs to assess group differences over time. Significant main effects from ANOVAs were followed-up with post-hoc Tukey's multiple comparisons tests. $p<0.05$ was accepted as statistically significant. Experimental values are presented as mean ±SEM.

CHAPTER 3: TYPE 1 DIABETES MELLITUS MARS MICROVASCULAR REPAIR FOLLOWING CEREBRAL MICROBLEED

3.1 Abstract

Wound healing is significantly impaired in patients with Type 1 DM, and whether this diminished regenerative capacity is also translated to the vasculature in the context of CMB recovery is unknown. If microvessels fail to repair following CMB, they may be eliminated from the circulation, reducing vascular density and, consequently, cerebral perfusion. Microglia have been identified as key players in the restoration of BBB integrity and may play a facilitative role in the context of CMB repair. Notably, the vigorous responses that these cells exhibit following vascular injury are significantly blunted in type 1 DM but could be rescued with anti-inflammatory treatments. However, microvascular repair is an ongoing process, and it may take days or weeks before a damaged capillary is functionally reintegrated into the circulation. Since microglial responses to CMBs have thus far been characterized only in the acute (~1 hour) period after injury, their long-term contributions to vascular repair have yet to be determined.

Using longitudinal *in vivo* 2-photon imaging, microvascular repair following CMB was characterized in a mouse model of type 1 DM. A significant proportion (20%) of injured capillaries were found to be eliminated within 3 days following CMB induction; this phenomenon was not ameliorated by chronic insulin treatment. In contrast, all injured microvessels from healthy animals reliably repaired and were functionally reintegrated into the cerebral circulation. A robust, kinetic CX3CR1+ cellular response to induced microbleeds was observed in all treatment groups, and morphological features of this aggregate were characterized over a 14-day period. The 2-dimensional area of accumulated CX3CR1+ cells was greatest the first day after injury and gradually declined over the imaging period; similarly, a

significant increase in eGFP+ processes contacting the targeted microvessel was observed following the injury, peaking 1 day post-CMB and subsiding progressively thereafter. These characteristics did not differ significantly between groups and failed to predict microvascular fate. Anti-inflammatory interventions including blocking IFNγ and IFNα signalling, as well as global suppression via DEX treatment, failed to ameliorate microvascular elimination in diabetic animals. Extensive elimination of CNS CX3CR1+ cells via CSF1R inhibition revealed that their responses to CMBs were not necessary for vascular recanalization since injured microvessels without any eGFP+ aggregate reliably reintegrated into the circulation. These results show that type 1 DM significantly mars microvascular repair following CMB and underscore the complexity of the repair process given that treatments which effectively ameliorate other complications of the diabetic condition failed to mitigate this pathology. Additionally, the fact that innate CNS macrophages were nonessential to microvascular repair indicates that a better understanding of the cellular mechanisms underlying this process is required since modulation of microglial responses has been a central strategy in efforts to improve CMB healing thus far.

3.2 Introduction

Type 1 DM is a significant risk factor for a variety of vascular pathologies, including cerebral microbleeds[2,3]. Although these ruptures occur in small vessels in the brain, their compounding incidence is positively correlated with poorer cognitive scores[7,8,10]. These neurological symptoms may manifest due to the leakage of toxins, such as fibrinogen and iron, from the damaged vasculature into the brain parenchyma where they may induce demyelination and neuronal degeneration[16,18–20,87,92]. An alternative mechanism that could also explain how CMBs contribute to declining cognitive function is through reduced cerebral perfusion: a decrease in vascular density resulting from failed microvascular repair deprives neurons of

crucial nutrients and as local blood flow is lost, cognitive function declines. In the context of type 1 DM, which is known to slow wound healing and could impact vascular repair[435,436], either of these mechanisms could help explain the prevalence of dementias in this disease.

Microglia, the resident immune cells of the brain parenchyma, exhibit rapid, kinetic responses to CMBs and the extent of their physical association with injured vessels has been shown to mitigate secondary hemorrhage and reduce vascular leakage resulting from the damage[24,25]. This evidence indicates that they play an important role in restoring BBB integrity. With this in mind, a key question is: how does type 1 DM affect microglial responses to CMBs? Microglial responses to microbleeds have been characterized in the healthy[24] and diabetic brain[25], as well as the diabetic retina[127], over the time-scale of several hours following injury; however, the ultimate fate of the damaged vessel (whether it is reintegrated into the circulation or not) was not determined. Therefore, it remains an integral goal to characterize the evolving nature of these responses over days and weeks following the insult. Microglial responses to tissue damage, including CMBs, crucially depend on gradients of inflammatory molecules, such as IFNs and ATP released from lysed cells[22,23,281]. These necessary chemotactic signals may be disrupted in diabetes since it is characterized by persistent systemic inflammation[214–217]. Essentially, the fine gradients of cytokines required to accurately guide microglial responses to sites of injury could be blunted in an environment where these cells are persistently surrounded by elevated levels of inflammatory molecules. In support of this idea, it has been shown that type 1 DM impairs microglial responses to CMBs during the early stages after injury (<1 hour), but this deficit was normalized with treatment by DEX as well as specific blocking antibodies for IFNγ[25]. The lasting success of these treatments at reinvigorating diabetic microglial responses and facilitating vascular repair has yet to be determined, however.

The results of the present study reveal that type 1 DM induces the pathological elimination of damaged microvessels following CMB, a phenomenon that was never observed in healthy animals. In the nondiabetic brain, damaged microvessels reliably recanalized and were reintegrated into the cerebral circulation over a 2-week period. However, 20% of capillaries targeted with CMBs were eliminated from the diabetic cortex within 3 days and insulin did not ameliorate this microvascular loss. Morphological features of the CX3CR1+ cellular response to CMBs, including the 2-dimensional area of cellular aggregate and the extent of vessel coverage by CX3CR1+ cell processes, did not differ between groups and failed to predict vessel fate. Treatment of diabetic animals with blocking antibodies for IFNs γ or α, or general anti-inflammatory therapy via DEX injection, failed to prevent microvascular loss following CMB although they modulated aspects of the cellular response to these insults. Furthermore, although microglia exhibit a key capacity to mitigate vascular leakage following CMB, CNS macrophage responses to injury were ultimately unnecessary for recanalization and functional repair. These data underscore the pervasive nature of vascular pathology in type 1 DM and highlight the challenges of ameliorating microvascular loss associated with CMBs, particularly given the current, limited understanding of the cellular mechanisms involved in their repair.

3.3 Results

I would like to express my sincere gratitude to Emily White for performing the majority of the chronic cranial window surgeries for the mice used in the imaging experiments described in this section. Furthermore, I would also like to acknowledge Stephanie Taylor who carried out the longitudinal 2-photon imaging of 12 nondiabetic, 10 diabetic, and 7 insulin-treated mice at the outset of this project.

3.3.1 Type 1 diabetes mellitus disrupts microvascular repair following microbleed in the mouse cortex

To determine the effect of type 1 DM on microvascular repair in the cortex, CMBs were induced in 3 groups of mice: nondiabetic (NDB), mice with uncontrolled diabetes (DB), and diabetic animals receiving chronic insulin treatment (INS). Subsequently, the long-term reintegration of damaged microvessels into the cerebral circulation was characterized over 14 days (Fig. 17). CMB induction reliably elicited an aggregation of CX3CR1+ cells to the site of the injury within 1 day; since both innate CNS macrophages and circulating phagocytes express *CX3CR1*, it was not possible to determine the specific identity of the cells comprising the aggregate in this context (Fig. 17). Diabetes induced a significant loss of microvessels (20%, Chi-squared test: NDB versus DB, p=0.0020) following CMB that was not mitigated by chronic insulin treatment (18%, Chi-squared test: NDB versus INS, p=0.0041; Figs. 17, 18A). Notably, microvascular loss was never observed in healthy mice and all targeted capillaries were reliably recanalized (Figs. 17, 18A-B). These significant differences in microvascular repair rates between groups were evident if events from all animals within a group were pooled (Fig. 18A) or if the proportion of repaired vessels per animal was averaged across a group (Kruskal-Wallis test, p=0.0026; NDB versus DB: p=0.0367, NDB versus INS: p=0.0045; Fig. 18B). In cases where microvessels in DB and INS animals were eliminated, microvascular regression was evident within 1-3 days post-CMB (Fig. 18C). These group differences in microvascular repair could not be simply explained by the innate properties of the targeted vessels since there were no significant group differences in their blood flow velocity (One-way ANOVA, p=0.0824), diameter (One-way ANOVA, p=0.0523), or length (One-way ANOVA, p=0.5658; Fig. 19A-C).

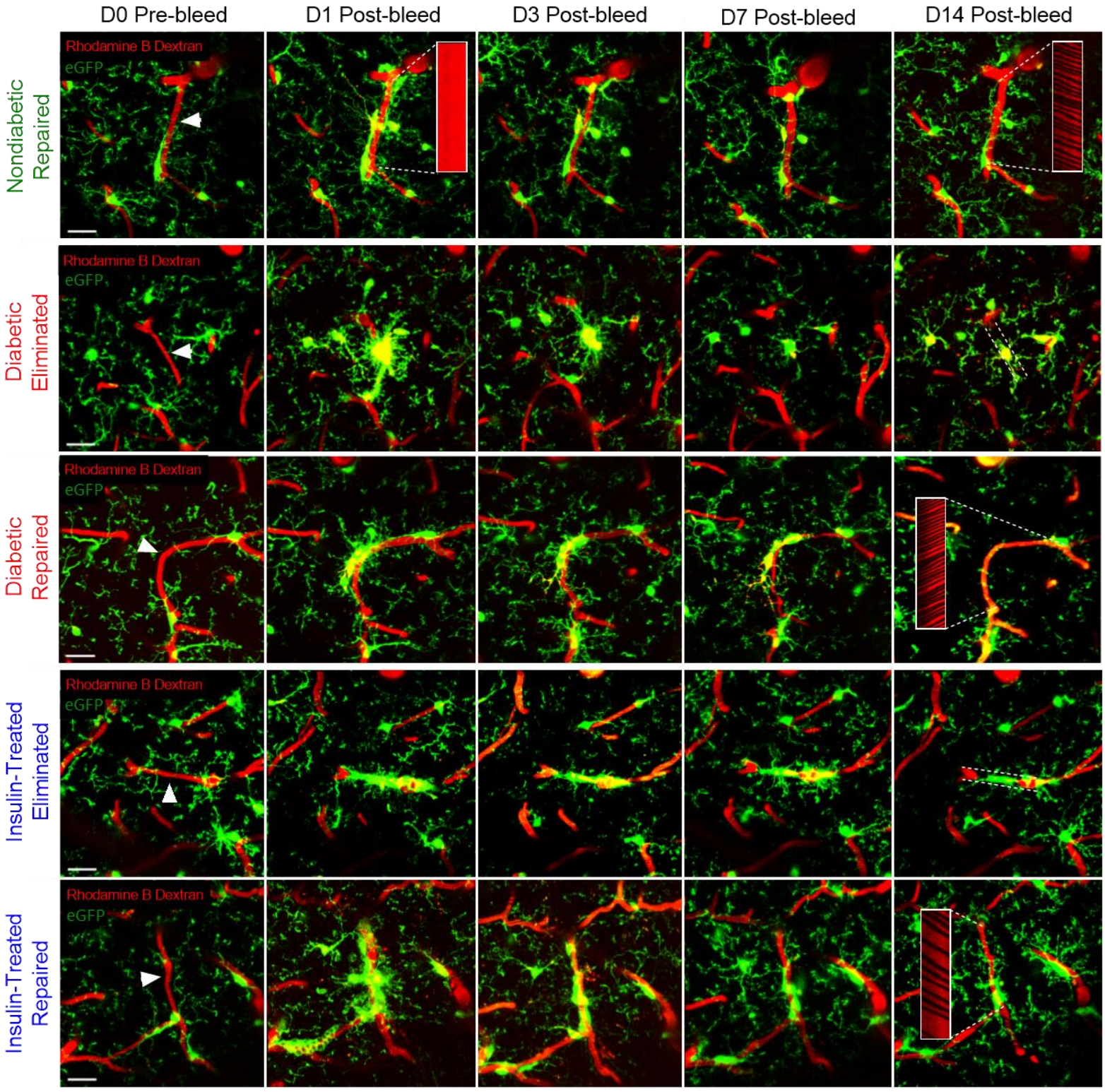
D0 Pre-bleed
D1 Post-bleed
D3 Post-bleed
D7 Post-bleed
D14 Post-bleed
Nondiabetic Repaired
Diabetic Eliminated
Diabetic Repaired
Insulin-Treated Eliminated
Insulin-Treated Repaired
Rhodamine B Dextran
eGFP

Figure 17. Capillaries are repaired following cerebral microbleed in the healthy cortex, but eliminated in the diabetic condition.

Montages of 2-photon images showing the evolving CX3CR1+ cellular response to CMBs (*induction site indicated by white arrows*) over 14 days in vessels that were repaired from nondiabetic, diabetic, and insulin-treated diabetic mice as well as vessels that were ultimately eliminated (*dashed white lines track original vessel lumen at D14*) in diabetic and insulin-treated conditions. CX3CR1+ cells express eGFP and microvessels were visualized via intravenous injection of Rhodamine B Dextran. Inlays show line-scans of blood flow in a vessel that was not flowing at D1 post-CMB and in recanalized vessels 14 days after insult. Scale bars represent 20 μm.

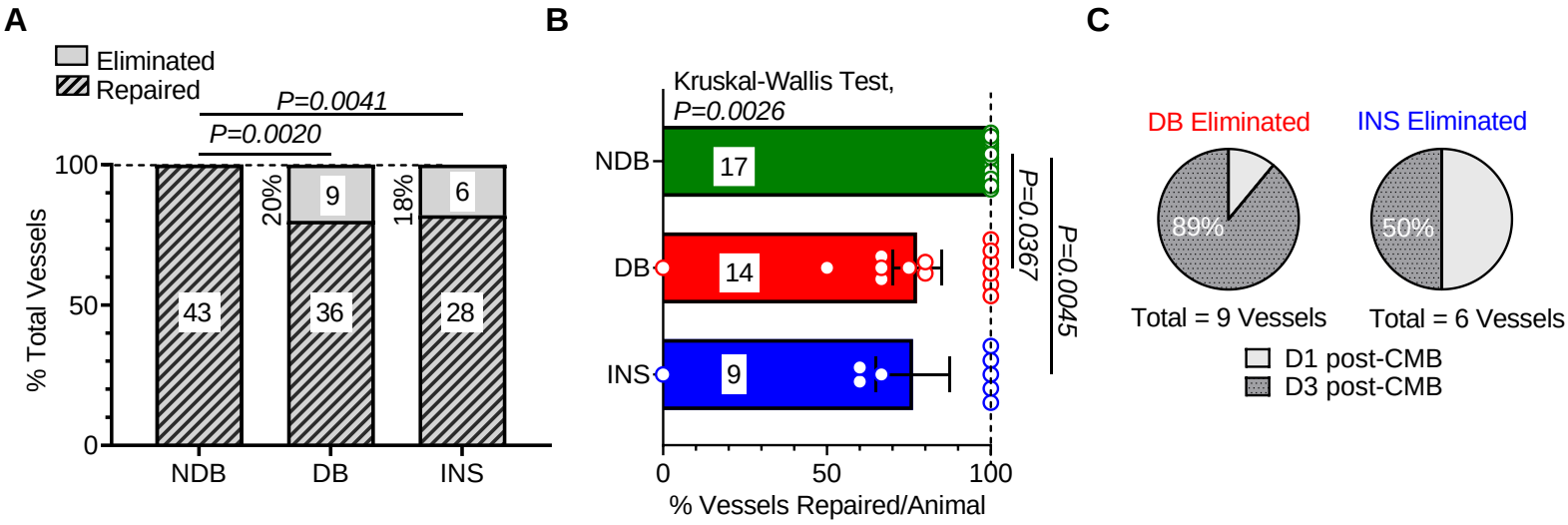

Figure 18. Diabetes results in a significant loss of microvessels following microbleed that is not rescued by insulin treatment.

A. Bar graph summarizing the proportion of targeted microvessels that were repaired or eliminated following induction of 1-5 CMBs per animal in NDB (*n*=17 mice), DB (*n*=14 mice), and INS (*n=9* mice) groups. The number of targeted microvessels is indicated on respective columns. **B.** Bar graph showing the average percentage of microvessels targeted with CMBs that were repaired in individual animals. 1-5 CMBs were induced per animal, data points represent individual mice and animal numbers are provided on columns. **C.** Pie charts indicate the proportion of eliminated vessels in DB (*left*) and INS groups (*bottom*) that were lost 1 or 3 days after CMB induction. Analyses performed in panels **A.** and **B.** assessed vessel repair at 14 days post-CMB. Data were analyzed using a Chi-squared test to compare ratios of repaired microvessels between groups and a non-parametric Kruskal-Wallis test with post-hoc Dunn's multiple comparisons test to determine differences in the percentage of vessels repaired between groups. Error bars represent mean± SEM

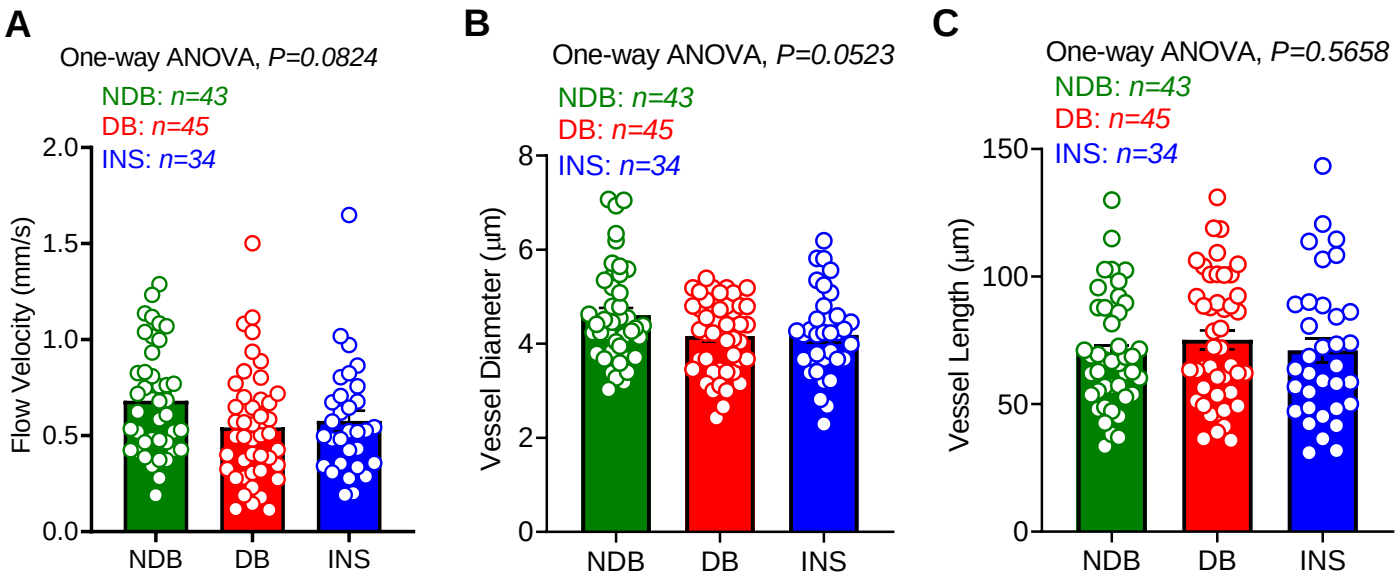

Figure 19. Microvascular parameters of targeted capillaries did not differ across groups.

A. Summary bar graph illustrating that there were no significant differences in blood flow velocity prior to CMB induction in targeted microvessels across treatment groups. **B.** Summary bar graph demonstrating that the average diameter of targeted microvessels did not vary significantly between experimental groups. **C.** Summary bar graph showing that the average length of targeted microvessels did not vary significantly between NDB, DB, and INS groups. All data points represent individual vessels in NDB (n=17 mice), DB (n=14 mice), and INS (n=9 mice) groups. Analyses were performed using images of vessels acquired prior to CMB induction (D0). One-way ANOVAs were used to assess group differences. Error bars represent mean± SEM.

3.3.2 Morphological characteristics of microbleed responses do not predict microvascular loss

Microglial aggregation to sites of microvascular injury has been associated with the restoration of BBB integrity, and blunted responses are known to contribute to prolonged vascular leakiness[24,25]. Furthermore, microglia inhibit the infiltration of the CNS by aggressive circulating leukocytes, which have been linked to the exacerbation of CNS injury[263,437]. Since acute (<1 hour post-injury) microglial responses to CMBs are specifically impaired in type 1 DM, it is conceivable that the perpetuation of this phenotype may be linked to the significant disruption in microvascular repair identified in this study.

To assess this possibility, the 2-dimensional area of eGFP+ aggregate at the site of the CMB and the percentage of the damaged vessel covered by eGFP+ processes were determined (Fig. 20A). This analysis revealed that all groups showed the greatest aggregation of CX3CR1+ cells to the lesion 1 day following the insult, and that this response gradually subsided over the 14-day imaging period (Two-way mixed effects model ANOVA, main effect of time: $F_{(1.754, 171.4)} = 18.07$, $p<0.0001$; main effect of treatment: $F_{(2, 114)} = 0.3255$, $p=0.7228$; Fig. 20B). Although the extent of vessel coverage by eGFP-expressing processes prior to CMB induction was significantly higher in NDB animals relative to their diabetic counterparts, this difference did not hold after the injury. Specifically, vessel coverage increased significantly 1 day after CMB when it reached its maximum in all groups (NDB: 53.461 ± 3.579%, $n=41$; DB: 56.490 ± 3.698%, $n=44$; DB+INS: 58.647 ± 4.694%, $n=23$), and then declined over the 14-day imaging period (Two-way mixed effects model ANOVA, main effect of time: $F_{(3.165,288)} = 126.6$, main effect of treatment: $F_{(2, 109)} = 0.06862$, $p=0.9337$, Fig. 20D). To determine whether either of these parameters was associated with vessel repair or elimination, the average area of eGFP aggregate

on D1 and D3 and the average percentage of vessel coverage at these time-points were compared in vessels that were repaired or eliminated across groups (Fig. 20E-F). Interestingly, neither the area of eGFP-expressing cells aggregated to the CMB (One-way ANOVA, p=0.8209; Fig. 20E) nor the percentage of the vessel covered by their processes (One-way ANOVA, p=0.0883; Fig. 20F) were predictive of microvascular fate. Since the velocity of blood flow in a microvessel prior to ablation could conceivably influence recanalization after injury, this metric was compared across groups (Fig. 20F). This analysis showed that intrinsic blood flow velocity also failed to predict microvessel fate following CMB (One-way ANOVA. p=0.1352; Fig. 20G).

Given that DM can affect gene transcription through a variety of disruptions in signalling pathways[157,158,187,188,190], and that IR activation specifically modulates transcription factors[117,118], it is possible that eGFP expression may be altered in DB and INS mice. In this way, CX3CR1+ cells that have downregulated transcription of the transgenic *eGFP* gene may exist in these groups and would be undetectable with 2-photon imaging. Therefore, to confirm that there were no significant differences in microglial density prior to CMB induction, fixed coronal slices from DB, INS, and NDB groups were labelled with the microglia-specific marker TMEM119 (Fig. 20H)[327]. This data showed that TMEM119+ cells reliably co-expressed eGFP in all groups, and that there were no significant differences in microglial density (One-way ANOVA, p=0.6012; Fig. 20I). Labelling CMBs in fixed coronal slices with Hoechst 33342 also indicated that there were no significant differences in the number of cells responding to these injuries between groups (One-way ANOVA, p=0.1712; Fig 20J-K). These findings further support the idea that the morphological characteristics of the CMB response do not effectively predict vessel fates.

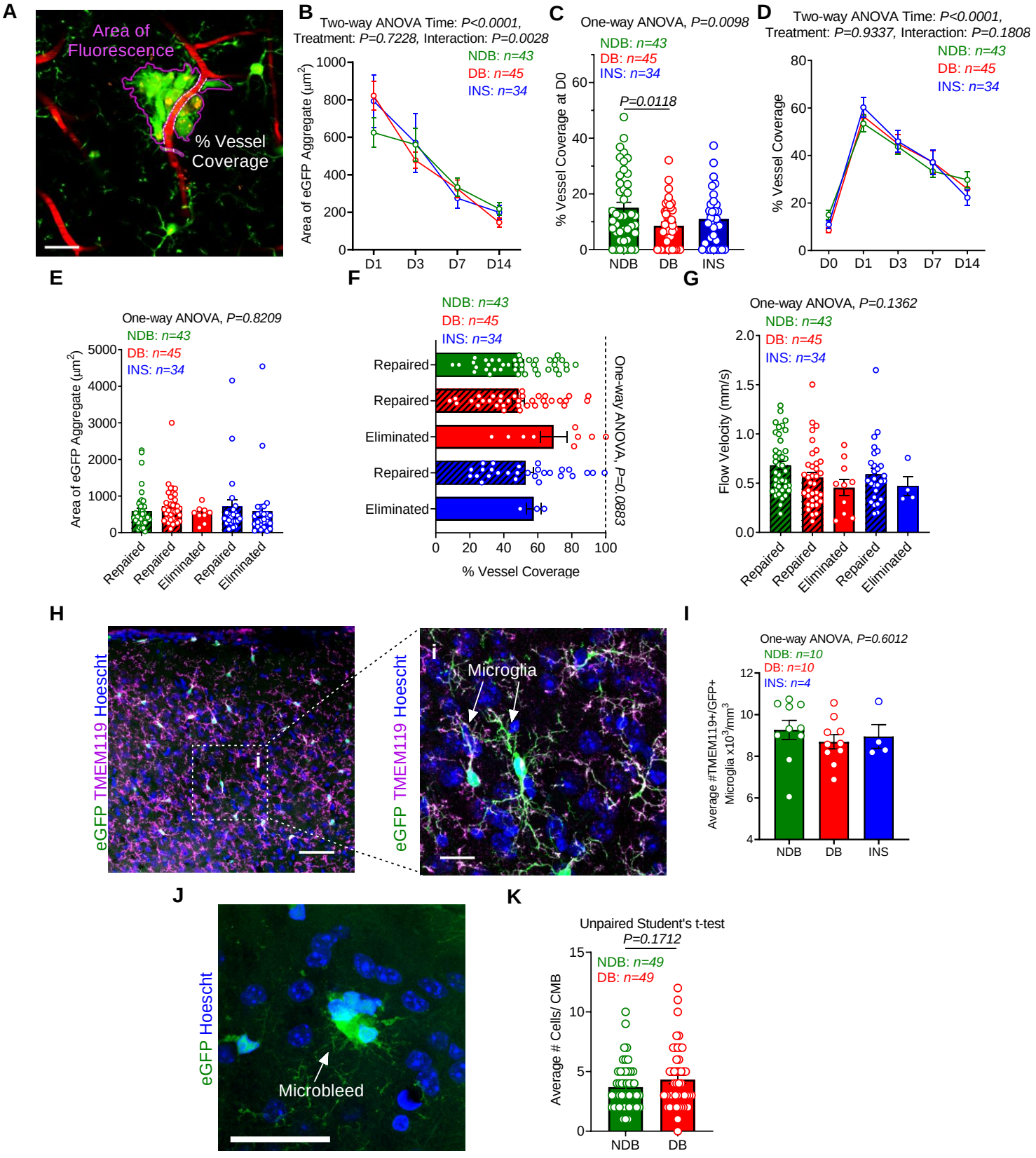
A
Area of Fluorescence
% Vessel Coverage
B
Two-way ANOVA Time: P<0.0001,
Treatment: P=0.7228, Interaction: P=0.0028
NDB: n=43
DB: n=45
INS: n=34
Area of eGFP Aggregate (µm²)
D1
D3
D7
D14
C
One-way ANOVA, P=0.0098
NDB: n=43
DB: n=45
INS: n=34
P=0.0118
% Vessel Coverage at D0
NDB
DB
INS
D
Two-way ANOVA Time: P<0.0001,
Treatment: P=0.9337, Interaction: P=0.1808
NDB: n=43
DB: n=45
INS: n=34
% Vessel Coverage
D0
D1
D3
D7
D14
E
One-way ANOVA, P=0.8209
NDB: n=43
DB: n=45
INS: n=34
Area of eGFP Aggregate (µm²)
Repaired
Repaired
Eliminated
Repaired
Eliminated
F
NDB: n=43
DB: n=45
INS: n=34
Repaired
Repaired
Eliminated
Repaired
Eliminated
One-way ANOVA, P=0.0883
% Vessel Coverage
G
One-way ANOVA, P=0.1362
NDB: n=43
DB: n=45
INS: n=34
Flow Velocity (mm/s)
Repaired
Repaired
Eliminated
Repaired
Eliminated
H
eGFP TMEM119 Hoescht
i
Microglia
I
One-way ANOVA, P=0.6012
NDB: n=10
DB: n=10
INS: n=4
Average #TMEM119+/GFP+ Microglia x10³/mm³
NDB
DB
INS
J
eGFP Hoescht
Microbleed
K
Unpaired Student's t-test
P=0.1712
NDB: n=49
DB: n=49
Average # Cells/ CMB
NDB
DB

Figure 20. Morphological characteristics of microbleed responses do not predict vessel fate. **A.** Representative 2-photon image of CX3CR1+ cellular response to damaged microvessel 3 days post-CMB illustrating the in-plane 2-dimensional area of fluorescence (*purple outline*) and vessel coverage by eGFP-expressing processes (*dashed white line*) that comprise the data represented in panels ***B-D.*** Scale bar represents 20 µm. **B.** Summary of changes in the area of CX3CR1+ cells aggregated at the site of the CMB over 14 days after induction in NDB, DB, and INS groups. **C.** Summary bar graph illustrating the extent of vessel coverage by eGFP-expressing processes prior to CMB in NDB, DB, and INS mice. **D.** Summary of the evolution of vessel coverage by eGFP-expressing processes before, and up to 14 days following, CMB in NDB, DB, and INS groups **E.** Summary bar graph showing the average area of CX3CR1+ cells aggregated to a vessel post-CMB in instances where it was ultimately repaired or eliminated. The average of data from D1 and D3 comprise each point. **F.** Summary bar graph describing the average extent of vessel coverage by eGFP-expressing processes in instances where vessels were repaired or eliminated. The average of data from D1 and D3 comprise each point. **G.** Summary bar graph illustrating the average blood flow velocity at D0, prior to CMB, in instances where vessels were repaired or eliminated. **H.** (*left*) Representative maximum intensity projection of a confocal image of microglial density in coronal slice of NDB cortex immunostained for TMEM119 with cell nuclei labelled by Hoechst 33342. Acquired at 20X magnification. Scale bar represents 50 µm. *(i)* Maximum intensity projection of a high resolution confocal image, acquired at 60X magnification, showing fine processes of microglial cells labelled by TMEM119 immunostaining. Scale bar represents 10 µm. **I.** Summary bar graph highlighting no significant group differences in the average density of microglial cells in the cortex. Animal numbers are indicated on the graph and data from 4-6 slices were averaged per animal to comprise an individual data point. **J.** High magnification confocal image of a representative CMB in fixed

tissue acquired from a transgenic CX3CR1$^{+/eGFP}$ mouse. Cell nuclei were labelled with Hoechst 33342. Scale bar represents 40 µm. **K.** Summary bar graph quantifying the average number of Hoechst 33342-labelled nuclei within the eGFP+ aggregate in CMBs from NDB and DB mice. Each data point represents a vessel and the number of CMBs analyzed per group is indicated on the graph. Data for panels **B.-F.** were collected from *n*=17 NDB, *n*=14 DB, and *n=9 INS* mice. Two-way mixed effects model ANOVAs were used to determine that there were no differences in 2-dimensional area of eGFP+ aggregate or vessel coverage by eGFP-expressing processes between groups over time. One-way ANOVAs were used to compare group differences in vessel coverage by CX3CR1+ processes at D0 and microglial density, followed by Tukey's multiple comparisons tests as appropriate. An unpaired Student's t-test was used to compare the average number of cells within a NDB and DB CMB. Error bars represent mean± SEM.

3.3.3 Anti-inflammatory treatment with dexamethasone or blockade of interferon signalling fails to rescue microvascular loss

It has been shown previously that the early stages of microglial responses to CMBs (<1 hour post-injury) are disrupted in type 1 DM[25]. These deficits were recovered by blocking IFNγ signalling and by treating diabetic animals with the broad-spectrum anti-inflammatory drug, DEX[25]. Given this precedent, the restoration of these acute responses could contribute to lasting microvascular repair and may rescue the vessel loss identified in type 1 DM.

To pursue this opportunity, NDB and DB animals were treated with IFNα/γ neutralizing antibodies to dampen these respective signalling pathways. IFNα and IFNγ constitute type I and type II IFNs, respectively, and are both released by various leukocytes to activate macrophages and initiate an innate immune response[438,439]. Since leukocytes in circulation are persistently exposed to hyperglycemic toxicity, the upregulated release of these cytokines could conceivably contribute to impaired microglial function in type 1 DM. Treatment with DEX was also used to induce a general anti-inflammatory state. Since microvessels to be eliminated regressed within 3 days following injury, the timeline of *in-vivo* 2-photon imaging was shortened to 7 days instead of 2 weeks (imaging time-points at D0, D1, D3, and D7).

As characterized in Section 3.3.1, CX3CR1+ cells aggregated to the site of CMB within 1 day following the insult and a proportion of injured microvessels from DB mice treated with IFNα, IFNγ, or DEX were found to repair while others were eliminated (Fig. 21). Remarkably, blocking IFNγ signalling resulted in microvascular loss in NDB animals – a phenomenon which was not observed previously in untreated healthy animals (Fig. 22A, Table 2). Furthermore, treatment of DB animals with IFNγ or IFNα blocking antibodies or DEX failed to significantly improve repair rates (Chi-squared test: DB versus IFNγ DB: p=0.7958; DB versus IFNα DB:

p=0.1213; DB versus DEX DB: p>0.9999; Fig. 22A). Indeed, none of the interventions attempted in DB mice were successful in rescuing microvascular repair rates to within comparable levels of those characterized in healthy animals (Chi-squared test: NDB versus IFNγ DB: p=0.0048; NDB versus IFNα DB: p<0.0001; NDB versus DEX DB: p=0.0026; Fig. 22A).

Interestingly, DB mice treated with DEX or IFNα showed faster blood flow velocity when compared to their untreated counterparts, but these values did not vary significantly relative to untreated NDB animals (One-way ANOVA, p<0.0001; DB versus IFNα DB: p= 0.0018; DB versus DEX: p=0.0005; NDB versus IFNα DB: p= 0.1663; NDB versus DEX: p=0.1018; Fig. 22B). As described previously in DB and NDB untreated animals, the greatest extent of vessel coverage by eGFP+ processes was observed 1 day following CMB for most intervention groups (IFNα NDB: 86.202 ± 18.821%, n=10; IFNα DB: 63.164 ± 6.896%, n=12; IFNγ DB: 74.402 ± 5.245%, n=23; DEX: 60.86 ± 7.029%, n=15; Fig. 22C); however, an exception were NDB animals treated with IFNγ. In this latter group, vessel coverage by eGFP+ processes continued to increase during the imaging period and peaked at the final D7 time-point (IFNγ NDB: 90.221 ± 4.101%, n=10; Fig. 22C). A significant main effect of treatment was determined pertaining to the percentage of vessel coverage by eGFP+ processes, but post-hoc analyses did not reveal any specific group differences (Two-way mixed-effects model ANOVA, main effect of treatment: $F_{(6, 150)}$= 2.493, p=0.0250; interaction: $F_{(18, 373)}$= 3.816, p<0.0001; Fig. 22C). The greatest amount of CX3CR1+ cells aggregated to the CMB was observed 1 day after induction, and this response subsided over the course of a week (Two-way mixed-effects model ANOVA, main effect of time: $F_{(1.618,202.2)}$= 48.20, p<0.0001; Fig. 22D). Perhaps unsurprisingly, the 2-dimensional area of the eGFP+ aggregate at the site of the CMB did not differ significantly between groups and, although a substantial collection of CX3CR1+ cells were observed in IFNγ-

treated DB animals following CMB (Figs. 21, 22D), this observation was not complimented by statistical significance (Two-way mixed-effects model ANOVA, main effect of treatment: $F_{(6,150)}$=, 1.969, p=0.0735; Fig. 22D). A summary of the proportion of targeted microvessels that repaired in each animal from all groups characterized in this section is provided in Table 2. Given that DEX treatment failed to rescue microvascular loss in DB animals that received this intervention, control experiments in a NDB cohort were not pursued.

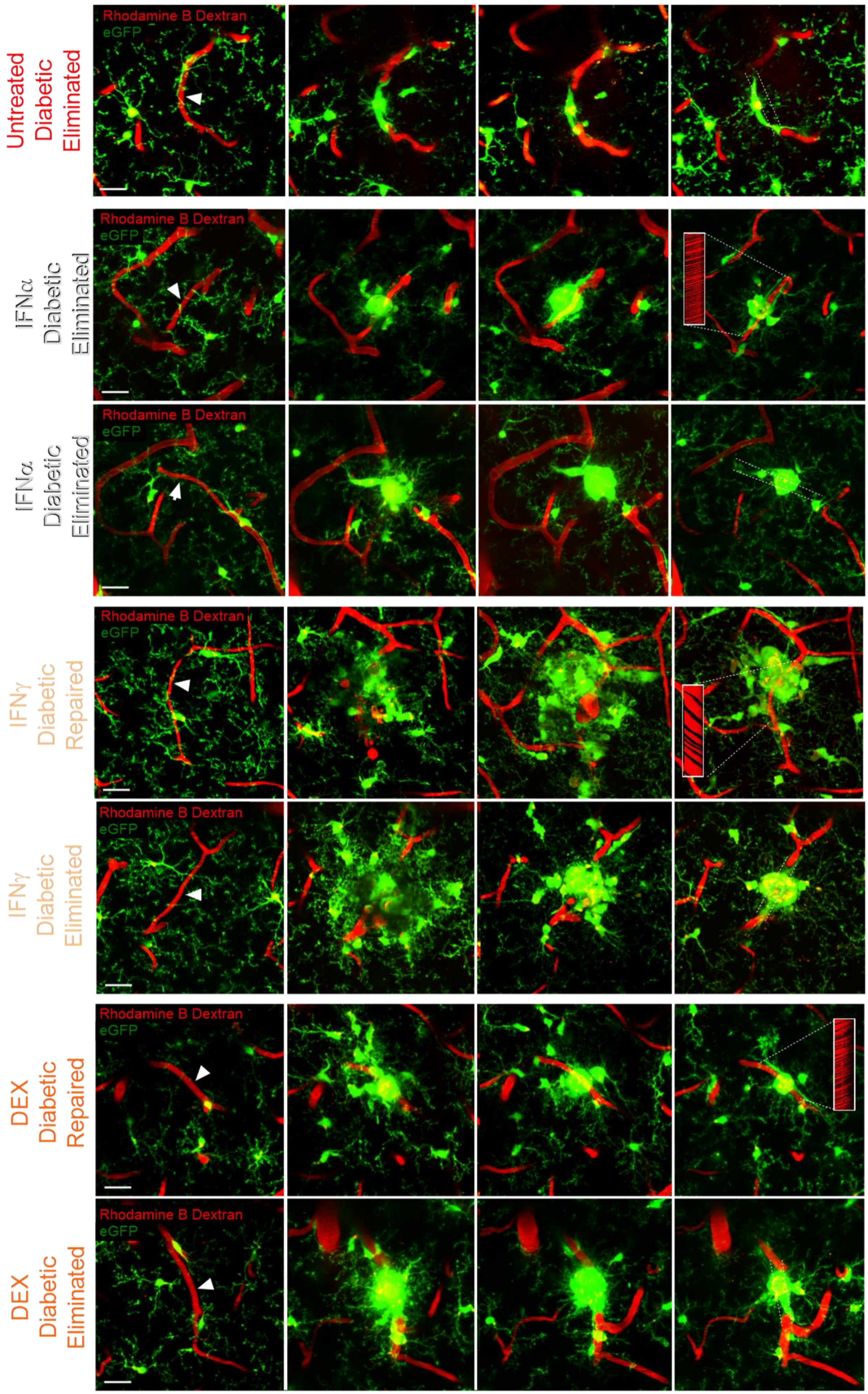
Untreated Diabetic Eliminated
IFNα Diabetic Eliminated
IFNα Diabetic Eliminated
IFNγ Diabetic Repaired
IFNγ Diabetic Eliminated
DEX Diabetic Repaired
DEX Diabetic Eliminated
Rhodamine B Dextran
eGFP

Figure 21. Anti-inflammatory treatment did not rescue microvascular loss following microbleed in the diabetic cortex.

Montages of 2-photon images illustrating the representative aggregation of CX3CR1+ cells to the site of CMBs (*site of induction indicated by white arrows*) in untreated diabetic mice and diabetic animals that received IFNγ or IFNα blocking antibodies, or DEX. The evolution of these responses is characterized over a period of 7 days and each group showed both elimination (*dashed white lines indicate previous vessel*) and repair (*inlays show line-scans of blood flow in recanalized vessels 14 days post-CMB*) of injured vessels. A particularly extensive aggregation of CX3CR1+ cells was noted in diabetic animals treated with IFNγ neutralizing antibodies. CX3CR1+ cells express eGFP and microvessels were visualized with intravascular injection of Rhodamine B Dextran. Scale bars represent 20 μm.

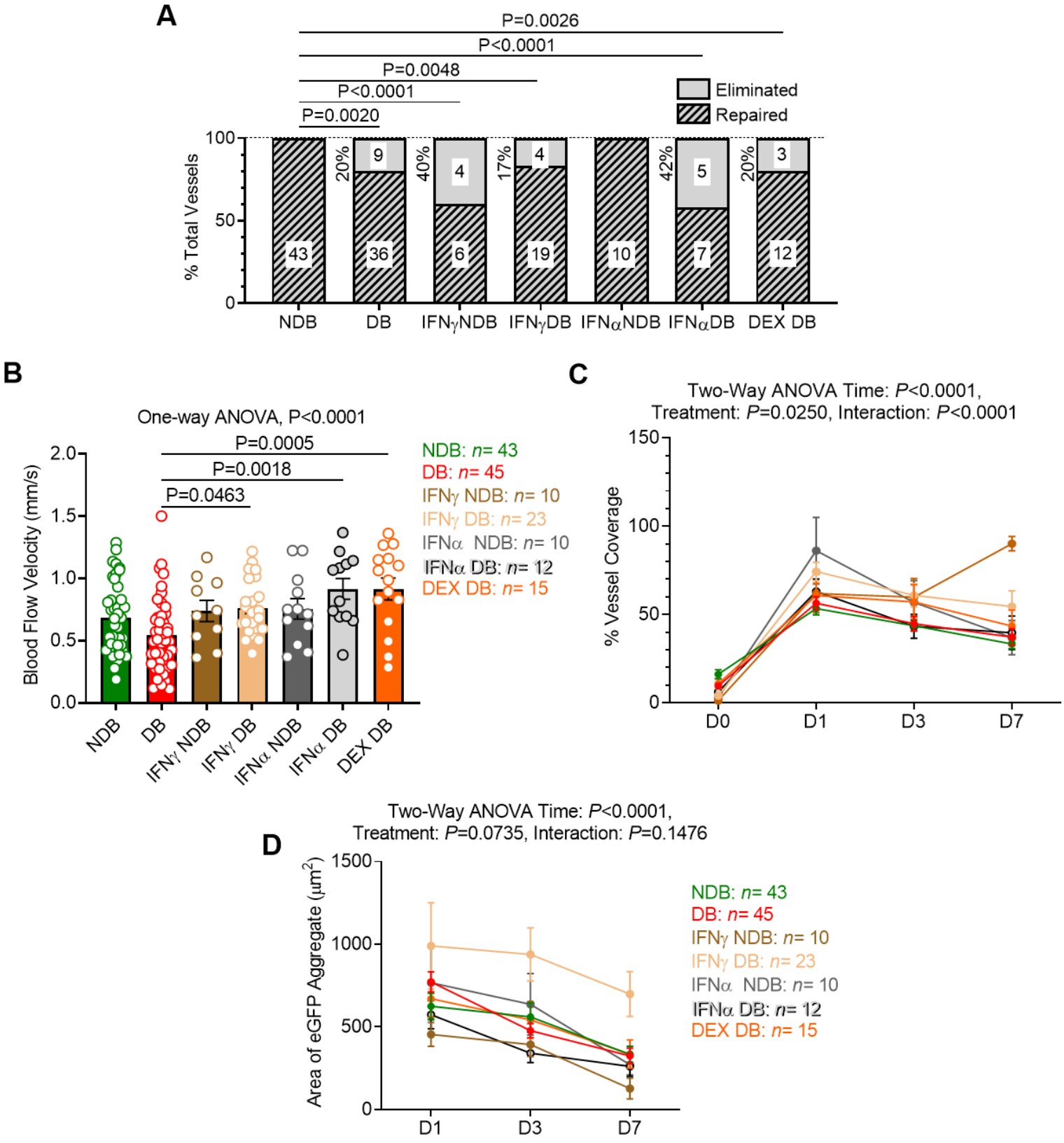
A
P=0.0026
P<0.0001
P=0.0048
P<0.0001
P=0.0020
Eliminated
Repaired
% Total Vessels
100
50
0
20%
40%
17%
42%
20%
43
9
36
4
6
4
19
10
5
7
3
12
NDB
DB
IFNγNDB
IFNγDB
IFNαNDB
IFNαDB
DEX DB
B
One-way ANOVA, P<0.0001
P=0.0005
P=0.0018
P=0.0463
Blood Flow Velocity (mm/s)
2.0
1.5
1.0
0.5
0.0
NDB
DB
IFNγ NDB
IFNγ DB
IFNα NDB
IFNα DB
DEX DB
NDB: n= 43
DB: n= 45
IFNγ NDB: n= 10
IFNγ DB: n= 23
IFNα NDB: n= 10
IFNα DB: n= 12
DEX DB: n= 15
C
Two-Way ANOVA Time: P<0.0001,
Treatment: P=0.0250, Interaction: P<0.0001
% Vessel Coverage
150
100
50
0
D0
D1
D3
D7
D
Two-Way ANOVA Time: P<0.0001,
Treatment: P=0.0735, Interaction: P=0.1476
Area of eGFP Aggregate (μm²)
1500
1000
500
0
D1
D3
D7
NDB: n= 43
DB: n= 45
IFNγ NDB: n= 10
IFNγ DB: n= 23
IFNα NDB: n= 10
IFNα DB: n= 12
DEX DB: n= 15

Figure 22. Anti-inflammatory treatments modulate microvessel fates following microbleed, but do not significantly affect microbleed response characteristics.

A. Summary bar graph highlighting the proportion of targeted microvessels that were repaired or eliminated, assessed 7 days post-CMB, following the induction of 1-5 CMBs per animal in NDB and DB mice that were untreated or received IFNγ or IFNα blocking antibodies or DEX. **B.** Summary bar graph depicting the average blood flow velocity in each treatment group at D0, prior to CMB induction. Each data point represents an individual vessel; total vessel numbers indicated to the right of the graph. **C.** Summary of changes in the extent of vessel coverage by eGFP processes over 7 days after CMB in NDB and DB controls and each treatment group. Individual data points represent the average of vessels from all animals in each group. Vessel numbers indicated to the left of the graph. **D.** Summary of the evolution of the 2-dimensional area of eGFP-expressing cellular aggregate associated with the CMB over 7 days following insult in NDB and DB controls and each treatment group. Individual data points represent the average of vessels from all animals in each group. Vessel numbers are indicated to the right of the graph. All data presented was collected from n=43 NDB, n=45 *DB,* n=10 IFNγ NDB, n=23 IFNγ DB, n=10 IFNα NDB, n=12 IFNα DB, and n=15 DEX DB mice. Chi-squared tests were used to compare ratios of repaired microvessels between groups. One-way ANOVA was utilized to compared blood flow velocities, followed by post-hoc Tukey's multiple comparison test to determine specific group differences. Two-way mixed effects model ANOVAs determined differences in 2-dimensional area and extent of vessel coverage by eGFP processes between groups over time; significant main effects were analyzed with a multiple comparisons tests to determine specific differences. Comparisons were performed between all relevant groups, but only significant results are depicted on graphs. Error bars represent mean± SEM.

	# Vessels Repaired/ Total Vessels Targeted						
Animal #	**NDB**	**DB**	**IFNγ NDB**	**IFNγ DB**	**IFNα NDB**	**IFNα DB**	**DEX DB**
1	1/1	5/5	5/5	4/5	5/5	2/3	5/5
2	3/3	3/4	1/5	3/6	5/5	2/3	3/5
3	3/3	4/6		4/4		3/6	4/5
4	1/1	2/3		4/4			
5	3/3	1/1		4/4			
6	3/3	1/2					
7	2/2	0/1					
8	2/2	2/3					
9	2/2	4/4					
10	2/2	3/3					
11	1/1	2/2					
12	4/4	1/1					
13	1/1	4/5					
14	3/3	4/5					
15	3/3						
16	4/4						
17	5/5						

Table 2. Summary of the proportion of microvessels repaired following microbleed in individual experimental animals.

Each animal received 1-5 CMBs, and groups contained 2-17 subjects. The proportion of targeted microvessels that repaired is expressed as a fraction of the total CMBs induced in each animal. Table rows indicate individual subjects, as outlined by the left-hand column. Since DEX failed to rescue microvascular loss in DB mice, treatment of a healthy control group was not pursued.

3.3.4 Brain macrophage responses are not necessary for long-term microbleed repair

Having identified a negligible relationship between characteristics of the CX3CR1+ cellular response to CMBs and the ultimate fate of damaged vessels, it is possible that brain macrophages are not necessary for microvascular repair and lasting recanalization. Other studies have identified microglia as key players in microvascular repair, but have considered the acute restoration of BBB integrity, rather than long-term reperfusion, as the definition of vessel repair[24,25]. Indeed, macrophage-independent repair of injured capillaries has been previously described in zebrafish[27]. To answer the question of whether brain macrophages are required for functional microvascular repair following CMB, these cells were depleted in the cortex using PLX5622 treatment. The activity of this CSF1R inhibitor leads to brain macrophage elimination because signalling through this receptor is necessary for the survival of these cells in the adult brain[440,441]. As expected, over 3 weeks PLX5622 treatment resulted in a progressive, significant decrease in brain macrophage density in both healthy (87.368±1.604%, n=19) and diabetic (84.781±1.329%, n=32) mice (Two-way mixed effects model ANOVA, main effect of time: $F_{(1.625,42.24)} = 172.6$, $p<0.0001$, main effect of treatment: $F_{(1, 49)} = 0.4135$, $p= 0.7449$; Fig. 23A-B).

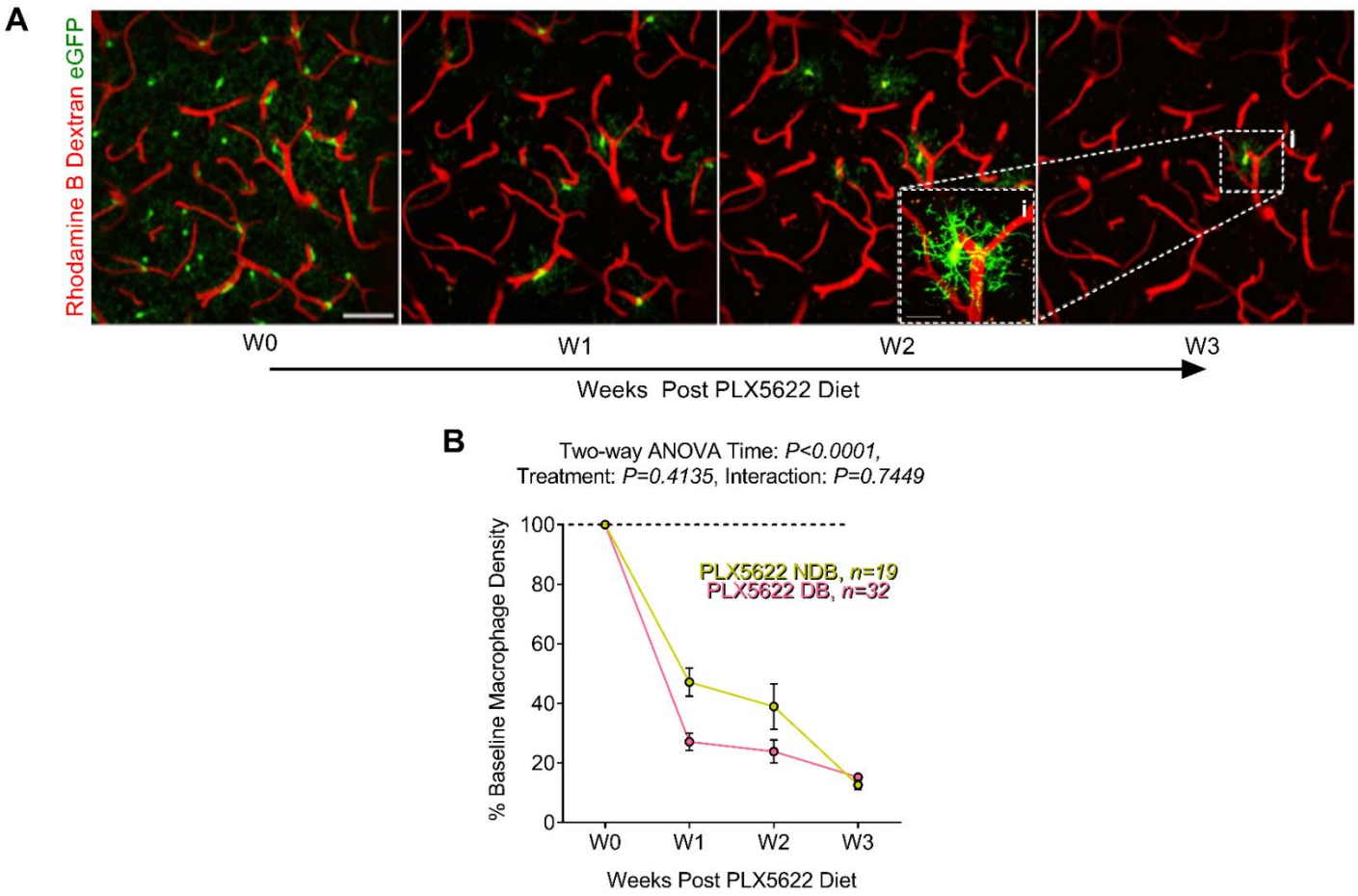

Figure 23. PLX5622 treatment significantly reduces cortical brain macrophage density. **A.** Representative 2-photon images characterizing the depletion of macrophages in the same imaging area over weeks following PLX5622 treatment in the NDB mouse brain. *Inlay (i)* is a magnified depiction of a remaining CX3CR1+ cell, highlighting its numerous, ramified processes. Scale bar represents 50 µm in main image and 20 µm in *(i)*. **B.** Summary graph quantifying the significant reduction in macrophage density relative to pre-treatment baseline over weeks with PLX5622 diet in NDB (n=6) and DB (n=6) animals. Individual data points represent the average density across all imaging areas (indicated on the graph) examined per group. Two-way mixed effects model ANOVA was used to confirm depletion over time. Error bars represent mean± SEM.

Following 3 weeks of macrophage depletion, CMBs were induced in NDB and DB mice and resulted in microvascular elimination rates in both groups (27% and 18%, respectively) comparable to those observed in untreated DB (20%) mice (Fig. 24A-C). The significant effect of PLX5622 treatment on microvascular repair in healthy animals was significant if considered across the whole group (Chi-squared test, p=0.0071; Fig. 24B), but not when analyzed as a proportion of vessels eliminated per animal (Kruskal-Wallis test, p=0.0015; NDB versus NDB PLX5622: p=0.0714; Fig. 24C). At first, this discovery of microvascular elimination following CMB in healthy mice appears to indicate that CNS macrophages are necessary for microvascular repair. However, when the data was parsed further this was not the case. Surprisingly, the small population of remaining CSF1R-resistant CX3CR1+ cells in the CNS exhibited remarkable migratory capacity and the majority of CMBs induced in PLX5622-treated mice exhibited an aggregation of eGFP-expressing cells (68/75 total CMBs) despite extensive brain macrophage depletion (Fig. 24A, D-E). Indeed, although ~20% of damaged microvessels with eGFP-associated responses were lost after CMB, remarkably, all vessels without this aggregate were successfully repaired and were functionally reintegrated into the cerebral circulation (Fig. 24D-E). These findings suggest that pathological changes to the CX3CR1+ cellular response may drive microvascular elimination and, in absentia, injured vessels may engage in reparative processes unhindered. Interestingly, although injured vessels regained flow without macrophage responses, they exhibited obvious secondary hemorrhages and vessel leakage (Fig. 24E). These observations, indicative of poor BBB integrity, recapitulate previous findings that microglial aggregation to sites of vascular rupture is crucial for restoring the damaged BBB[24,25].

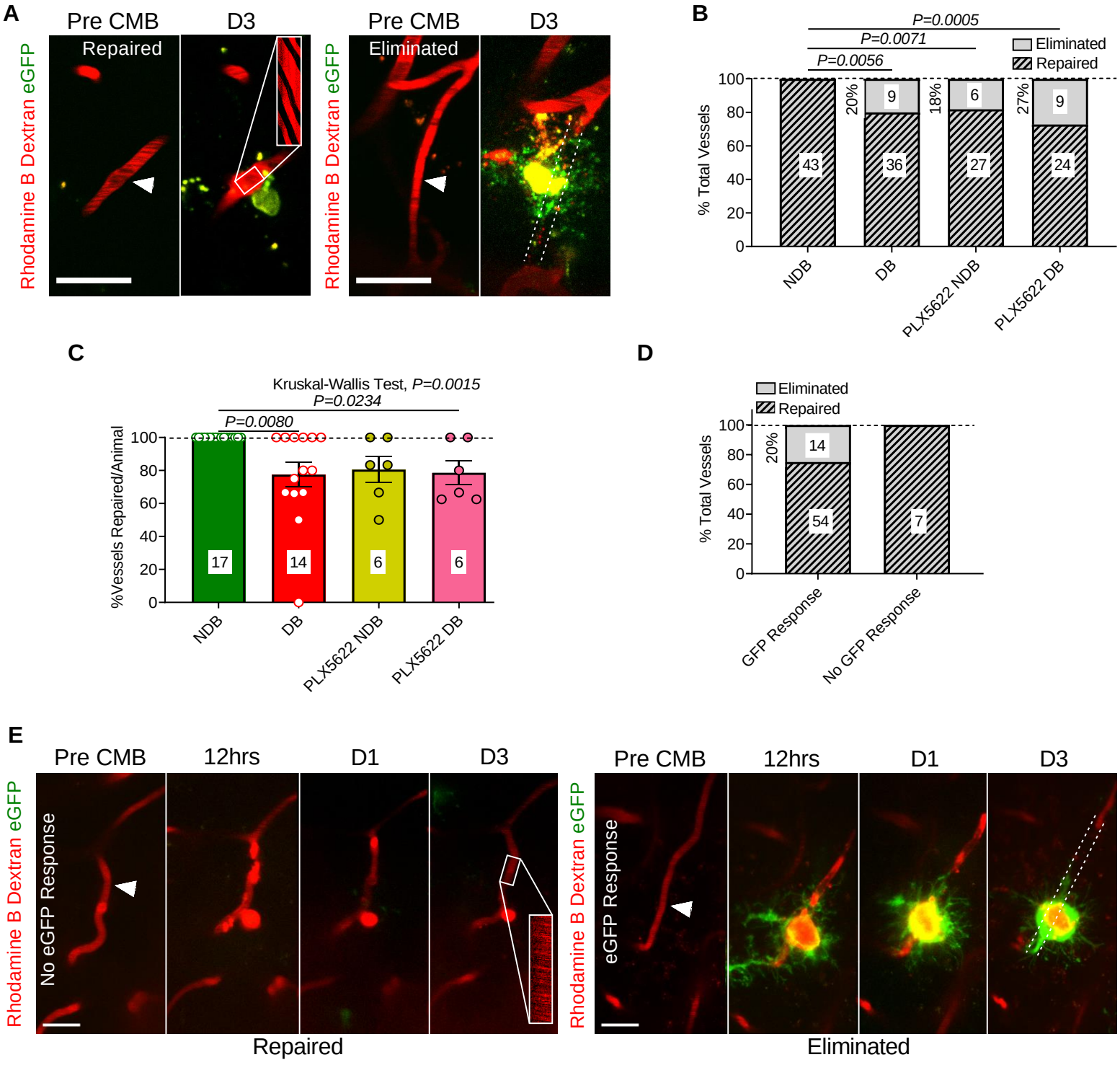
A
Pre CMB
D3
Repaired
Rhodamine B Dextran eGFP
Pre CMB
D3
Eliminated
Rhodamine B Dextran eGFP
B
P=0.0005
P=0.0071
P=0.0056
Eliminated
Repaired
% Total Vessels
100
80
60
40
20
0
20%
18%
27%
43
9
36
6
27
9
24
NDB
DB
PLX5622 NDB
PLX5622 DB
C
Kruskal-Wallis Test, P=0.0015
P=0.0234
P=0.0080
%Vessels Repaired/Animal
100
80
60
40
20
0
17
14
6
6
NDB
DB
PLX5622 NDB
PLX5622 DB
D
Eliminated
Repaired
% Total Vessels
100
80
60
40
20
0
20%
14
54
7
GFP Response
No GFP Response
E
Pre CMB
12hrs
D1
D3
Rhodamine B Dextran eGFP
No eGFP Response
Repaired
Pre CMB
12hrs
D1
D3
Rhodamine B Dextran eGFP
eGFP Response
Eliminated

Figure 24. PLX5622 depletion reveals CNS macrophages are not required for vessel repair.

A. Representative 2-photon images of microvessels in the PLX5622-treated NDB brain before CMB (*white arrow*) that *(left)* recanalized within 3 days (*inlay* line-scan confirms blood flow return) or *(right)* were eliminated 3 days after CMB *(white dashed lines trace lost vessel)*. Scale bars represent 20 µm. **B.** Summary bar graph indicating the fates of ablated vessels following CMB in NDB (n=17) and DB (n=14) untreated mice, and NDB and DB PLX5622-treated (n=6 and n=6, respectively) animals; outcomes assessed 7 days post-CMB. Number of vessels are indicated on respective columns. **C.** Summary bar graph of the average percentage of vessels that repaired per animal in NDB and DB untreated, and NDB and DB PLX5622-treated groups. Number of animals represented on respective bars; each animal received 1-5 CMBs. **D.** Summary bar graph highlights that all blood vessels without eGFP visible near the CMB in PLX5622-treated animals repaired. 33 vessels from NDB PLX5622-treated (n=6) mice and 33 vessels from their DB (n=6 mice) counterparts were pooled for this data; vessel numbers indicated on columns. **E.** *(left)* 2-photon images before, and 3 days after, CMB *(white arrow).* Latent aneurisms visible along the vessel, but no eGFP+ response noted at the CMB. *Inlay* line-scan shows streaking RBCs in the repaired vessel. *(right)* Representative 2-photon images of a microvessel with CX3CR1+ cells aggregated at the CMB. No intravascular fluorescence was identified 3 days post-CMB, confirming the vessel was eliminated (*white dashed lines*). Images acquired in PLX5622-treated NDB mice. Scale bars represent 20 µm. A Chi-squared test compared ratios of repaired microvessels between groups and a Kruskal-Wallis test with post-hoc Dunn's multiple comparisons qualified group differences in vessel repair rates. Comparisons were performed between all relevant groups, but only significant results are depicted on graphs. Error bars represent mean± SEM.

3.4 Discussion

Type 1 DM is a known risk factor for vascular pathology, and patients with this condition experience significantly more CMBs compared to healthy controls[2,3]. The present study provides further evidence that the reparative processes associated with these insults are compromised in DM, leading to the elimination of damaged microvessels from the cerebral circulation. Specifically, following CMB, 20% of ruptured capillaries were eliminated in the diabetic group, a phenomenon which was not observed in healthy animals; all damaged microvessels recanalized in the latter condition and their lasting reintegration into the cerebral circulation was recorded. Although CMBs also occur spontaneously in the healthy brain[409,442], these data suggest that capillaries generally recanalize under homeostatic conditions. Of note, insulin treatment did not mitigate microvascular elimination in diabetic mice and 18% of damaged capillaries were lost within 3 days following the injury. This observation builds on existing literature which describes how, although insulin treatment is crucial for controlling hyperglycemia, it is ineffective at ameliorating type 1 DM comorbidities[11–16,130,131]. Taken together, these data provide a rationale for the prevalence of cognitive decline and dementias in patients with diabetes. Essentially, as microvascular loss compounds over time it could contribute to the progressive reduction in microvascular density observed in aging patients with type 1 DM, resulting in concomitant cortical hypoperfusion that may compromise cognitive function as neurons are deprived of essential metabolic substrates.

Microglia responding to CMBs form a dense matrix of processes surrounding the lesion, necessary for the rapid closure of the BBB after insult[24,25]. In the context of CMB repair, these innate CNS macrophages prevent infiltration of blood-borne leukocytes into the exposed brain parenchyma[263,437] or they may be required to physically ligate the severed endothelial cells of a

ruptured vessel[27]. Furthermore, the Brown lab has shown previously that the extent of CX3CR1+ cellular aggregation to the site of a CMB is impaired in diabetic animals, particularly with regards to cell polarization to, and accumulation at, the site of damage[25]. Therefore, the morphological features of the evolving, long-term macrophage response to CMBs were characterized on the basis that they may be altered in the diabetic condition and could predict microvascular elimination. Although these evolving eGFP+ responses are evidently 3-dimensional in nature, with processes enwrapping the circumference of the vessel and extending above and below the plane of ablation, given the limitations of 2-photon microscopy in z-plane resolution, analyses was restricted to in-plane eGFP fluorescence. This work revealed that the CX3CR1+ eGFP-expressing cellular aggregate responding to CMBs peaked 1 day following injury, in terms of both the extent of vessel coverage by eGFP+ processes as well as the 2-dimensional area of the milieu, before it gradually regressed over the course of the 14-day imaging period. Notably, no significant differences were noted between microbleed responses in healthy and diabetic animals and these characteristics did not correlate with microvascular fate.

These findings compliment the results of CMB induction in PLX5622-treated animals showing that CNS macrophage responses to CMBs are not necessary for lasting vessel repair. Indeed, others have also shown that endothelial repair can occur in the absence of macrophages[27]. Rather than directly repairing the endothelium, BAMs and microglia may play a supportive role and augment the process via the release of trophic factors or the provision of mechanical support[27,423,424]. Furthermore, microglial responses likely protect vulnerable neuronal circuitry from toxic substances in the circulation, such as iron and fibrinogen, by rapidly sealing off the damaged BBB, essentially acting as a ligature to prevent plasma extravasation[16,18–20,87,92]. This latter hypothesis is supported by the present findings that in the absence of CX3CR1+ cell

responses to CMBs, even in cases where the vessels ultimately recanalized, capillaries exhibited lasting vascular leakage and major secondary hemorrhages. Additionally, in consideration of the recent characterization of changes in microglial phenotypes following PLX5622 treatment, it is possible that some of the CSF1R-resisistent cells that persisted in this condition constitute a Mac2+ population with monocyte-like gene expression profiles[443]. It is conceivable that these proliferative macrophages may respond differently to CMBs compared to homeostatic microglia and could shift microvascular fate towards elimination instead of repair. Given their upregulation of genes such TREM2, these Mac2+ cells resemble DAM and could promote microvascular degradation via enhanced phagocytic activity[269,443]. Taken together, these results show that microglial responses to CMBs alone are insufficient for ensuring vessel repair and imply that more nuanced cellular mechanisms likely drive microvascular elimination in diabetes.

Type 1 DM is associated with persistent inflammation as a product of chronic hyperglycemic toxicity, and various clinical trials are investigating the efficacy of anti-inflammatory treatments in mitigating disease pathology[214,215,421]; this research is further motivated by the aforementioned limitations associated with insulin therapy[11–16,130,131]. Furthermore, blunted microglial responses to CMBs in the diabetic brain were found to be reinvigorated by blocking IFNγ signalling and with corticosteroid treatment (DEX)[25]. IFNs α and γ are both released by circulating leukocytes to mount an innate immune response[438,439] and, since these cells are chronically exposed to the toxic effects of hyperglycemia in type 1 DM, it was worth considering whether blocking these signalling pathways could improve long-term microvascular repair in the diabetic cortex. Interestingly, systemic inhibition of IFNγ signalling produced a markedly increased aggregation of CX3CR1+ cells to the site of CMBs in both DB and NDB animals. This effect did not correspond with improved microvascular repair in DB

mice, however. Indeed, dampening IFNγ signalling and DEX treatment both proved ineffective at ameliorating pathological vessel loss in type 1 DM; inhibiting IFNγ activity actually induced microvessel elimination in NDB controls. These data further support the idea that the physical association of CX3CR1+ cells with a damaged microvessel and the acute restoration of BBB integrity does not correspond to the lasting functional repair of CMBs. Moreover, given the minute gradients of cytokines required for directing focused macrophage responses[22,23,281], it is likely that a "Goldilocks Zone" of sensitivity is necessary for effective function . Essentially, excessive suppression of these pathways may lead to impairments in macrophage function that may also be induced by the global overexpression of inflammatory molecules

Lastly, although the present study was limited to the investigation of neocortical CMBs, due to the important impact that they may have on cognitive function, it would be valuable to consider the state of microbleed repair in other regions of the diabetic CNS. For example, leveraging microglial-based repair functions has been posited as a means of improving retinal microbleed outcomes to combat diabetic retinopathy[26]. Clinical studies have also shown that various risk factors for cerebrovascular disease increase the prevalence of microbleeds differentially across brain regions. For example, while hypertension was associated with microbleeds in deep grey matter and in the brainstem, cerebral amyloid angiopathy was correlated with CMBs and microbleeds in the lobar regions[444,445]. Similarly, Schager and Brown recently demonstrated that ischemic capillary loss is heterogeneous across brain regions, with areas such as the white matter and cortical grey matter being especially vulnerable to reductions in microvascular density with aging[50]. This solicits consideration of whether a similar trend may be observed with hemorrhagic microvascular elimination, especially given the diverse immune cell populations that comprise different brain regions[36,260,261,446–449].

CHAPTER 4: MAC2+ MACROPHAGES OF PERIPHERAL ORIGIN ARE ASSOICATED WITH MICROVASCULAR ELIMINATION IN TYPE 1 DIABETES MELLITUS

4.1 Abstract

Microglia, resident immune cells of the CNS parenchyma, exhibit rapid, extensive morphological and functional changes in response to tissue damage or microvascular rupture. Other innate CNS macrophages, BAMs, may also respond to tissue injury and could contribute to vascular repair. Circulating phagocytic leukocytes are generally excluded from the immune-privileged CNS under homeostatic conditions but can gain access to this region in chronic inflammatory diseases and during acute disruptions of BBB integrity. Although these diverse immune cells are ideally suited to resolve microvascular insults, their relative contributions to the lasting recanalization of CMBs have yet to be fully described. A better understanding of the cellular mechanisms underlying CMB resolution is particularly key in conditions such type 1 DM, wherein these insults occur more frequently, and ineffective repair could lead to decreased microvascular density and the onset and progression of cognitive decline.

Using *in vivo* 2-photon microscopy and confocal imaging, a robust CX3CR1+ cellular response to CMBs was characterized in a mouse model of type 1 DM and a novel Mac2+/TMEM119- population of cells, distinct from homeostatic TMEM119+ microglia, was discovered in the CMB milieu. Of note, CMBs induced in healthy, nondiabetic mice repaired without exception and Mac2+/TMEM119- cells were not observed in the associated CX3CR1+ cellular aggregate. Treatment of diabetic mice with CLR to deplete circulating phagocytic leukocytes prevented the association of Mac2+/TMEM119- cells with CMBs and rescued capillary repair. The efficacy of CLR in excluding Mac2+/TMEM119- cells from CMB responses, combined with its thorough

eradication of monocytes from circulation, suggests that these cells originate in the periphery and may represent MDMs. CD206+ BAMs were not found in the CMB response of any group, and likely do not contribute to vascular repair in this context. Interestingly, Mac2+/TMEM119- cells were observed in the uninjured cortical parenchyma of diabetic and PLX5622-treated mice but not in healthy, untreated animals. These cells could represent MDMs that engrafted in the brain following CMB resolution or a phenotype of DAM-like cells that arises in these conditions. *In vivo* 2-photon imaging further revealed significant increases in lipofuscin content in CX3CR1+ cells at the site of diabetic CMBs; other phagocytic markers including CD68 and TREM2 were also upregulated, suggesting that changes in phagocytosis could be associated with pathological vessel loss. Mac2+/TMEM119- cells specifically exhibited greater lipofuscin content relative to homeostatic Mac2-/TMEM119+ microglia. Taken together, these data uncover a unique Mac2+/TMEM119- macrophage phenotype in diabetic CMBs that was strongly associated with pathological microvascular elimination, potentially via upregulated phagocytic activity. The findings of this study highlight the diversity of immune cell responses to CNS injury and underscore the complexity of the dynamic cellular mechanisms that modulate capillary pruning.

4.2 Introduction

The immune system is comprised of a heterogeneous population of cells including bone marrow-derived circulating myeloid and lymphoid leukocytes, as well as long-lived tissue resident macrophages. In response to injury or during chronic disease conditions, myeloid monocytes can infiltrate tissues and transform into MDMs with unique properties that are shaped by local environmental cues[268,377,450]. All of these cells are exquisitely sensitive to inflammatory molecules and mount robust responses to tissue injury or pathogen invasion[22–24,27,368]. In addition to their immune roles, the contributions of phagocytic leukocytes (monocytes, neutrophils,

MDMs, and tissue-resident macrophages) have been highlighted in the context of vascular pathology. In type 1 DM, high levels of blood glucose result in a global increase in the generation of inflammatory compounds including cytokines[214–217], which may affect the function of circulating immune cells that are perpetually inundated in a toxic hyperglycemic environment; furthermore, since cytokines can be transported across the BBB[412,413], the resident immune cells of the CNS are also chronically exposed to this inflammatory environment.

Microglial involvement in the restoration of BBB integrity after injury is well-described[24,25,275], and their anti-inflammatory phenotype has been associated with better outcomes in AD[437]. Furthermore, BAMs including pvMΦ and mMΦ could facilitate microvascular repair. Although the range of their functions has yet to be fully characterized, pvMΦ are known to modulate BBB permissiveness to solutes and circulating immune cells[294,295], engage in phagocytosis[312,451], and respond to central and peripheral inflammation[312] and mMΦ have been shown to support microvascular repair following mild traumatic brain injury[423]. Under homeostatic conditions, the specialized structure of the BBB hinders transmigration of circulating phagocytic leukocytes into the CNS. However, following instances of BBB disruption during acute trauma or prolonged disease states, circulating immune cells including monocytes, neutrophils, T-cells and B-cells may infiltrate the brain[28–30,265]. The local production of inflammatory molecules including TNF-α, IL-1β, and CXCL-8 attract immune cells to the CNS and stimulates the expression of adhesion molecules by endothelial cells to facilitate leukocyte diapedesis into the brain[368]. Once in the CNS proper, monocytes may transform into MDMs which have been characterized in both beneficial and detrimental roles in the context of CNS injury repair[35]. For example, MDMs have been identified as important mediators of microvascular repair in zebrafish, physically reconnecting the severed ends of damaged

endothelial cells and facilitating their ligation[27]. Furthermore, since these cells exhibit a higher phagocytic capacity than brain-resident microglia they have been demonstrated to clear amyloid-β more effectively in AD[302], mitigating disease progression. Conversely, the increased load of phagocytic material renders MDMs prone to apoptotic and necrotic cell death and could exacerbate local inflammation[269,270].

Given the putative effects of type 1 DM on immune cell function, the present work sought to investigate the cellular mechanisms of CMB repair in the diabetic brain and to disentangle the relative contributions of brain-resident and peripheral immune cells in this process. These investigations revealed a unique population of Mac2+/TMEM119- cells that were strongly associated with the pathological elimination of microvessels following CMB in the diabetic neocortex. Interestingly, Mac2+/TMEM119- macrophages were also found in the brain parenchyma of diabetic and PLX5622-treated mice, even in the absence of injury. Of note, these cells were never identified in the cellular milieu of nondiabetic CMBs and were not found in the uninjured brain parenchyma of healthy animals. Treatment with CLR, an anti-inflammatory drug which eradicates peripheral phagocytes, prevented the aggregation of Mac2+/TMEM119- constituents to CMBs and rescued microvascular repair in diabetic mice, suggesting that these cells were of peripheral origin. Increased expression of phagocytic markers including lipofuscin, CD68, and TREM2 were also observed in the diabetic CMB relative to the healthy condition and were particularly enriched in Mac2+/TMEM119- cells compared to homeostatic microglia. CLR treatment effectively normalized the upregulation of phagocytic markers in the diabetic CMB. In summary, these data highlight the complexity of cellular responses to CMBs and identify a novel population of phagocytic Mac2+/TMEM119- macrophages in the brain, which appear to play a key role in the pathological elimination of microvessels in the diabetic cortex.

4.3 Results

With gratitude I would like to acknowledge Emily White, who performed most of the chronic cranial window surgeries for the mice used in the imaging experiments in this section

4.3.1 Mac2+/TMEM119- macrophages are associated with microbleed responses in the diabetic cortex

Building on the previous findings of this work which demonstrate that microglial responses to CMBs are not necessary for lasting vascular recanalization, this section endeavours to further advance our understanding of the cellular mechanisms contributing to pathological microvascular elimination. Indeed, various circulating and tissue-resident immune cells besides microglia are attracted to CMBs and may contribute to the cellular response to insult[27,28,265,452]. Since these phagocytes are all CX3CR1+, and thus indistinguishable with 2-photon imaging alone given their ubiquitous eGFP expression in the present transgenic model[427], a more rigorous assessment of the cellular phenotypes comprising the CMB response was required.

Since mMΦ and pvMΦ have been ascribed roles in microvascular repair[27,84,423], it is conceivable that they may breach the brain parenchyma and migrate towards a distant CMB. To consider this possibility, immunostaining for CD206, a popular marker for differentiating BAMs from microglia, was examined[84]. As expected, CD206+ eGFP-expressing cells were identified along penetrating arterioles and the meninges along the cortical surface of fixed brain slices (Fig. 25A). PLX5622 treatment significantly reduced the density of CD206+ macrophages along relevant CNS interfaces relative to healthy and diabetic mice that did not receive PLX5622 (One-way ANOVA, $p = 0.0332$; NDB versus PLX5622 NDB; DB versus PLX5622 NDB, $p = 0.0086$; Fig. 24B). Since BAMs require constitutive CSF1R activity for survival in the adult brain, it is perhaps not surprising that its blockade with PLX5622 would eliminate these cells.

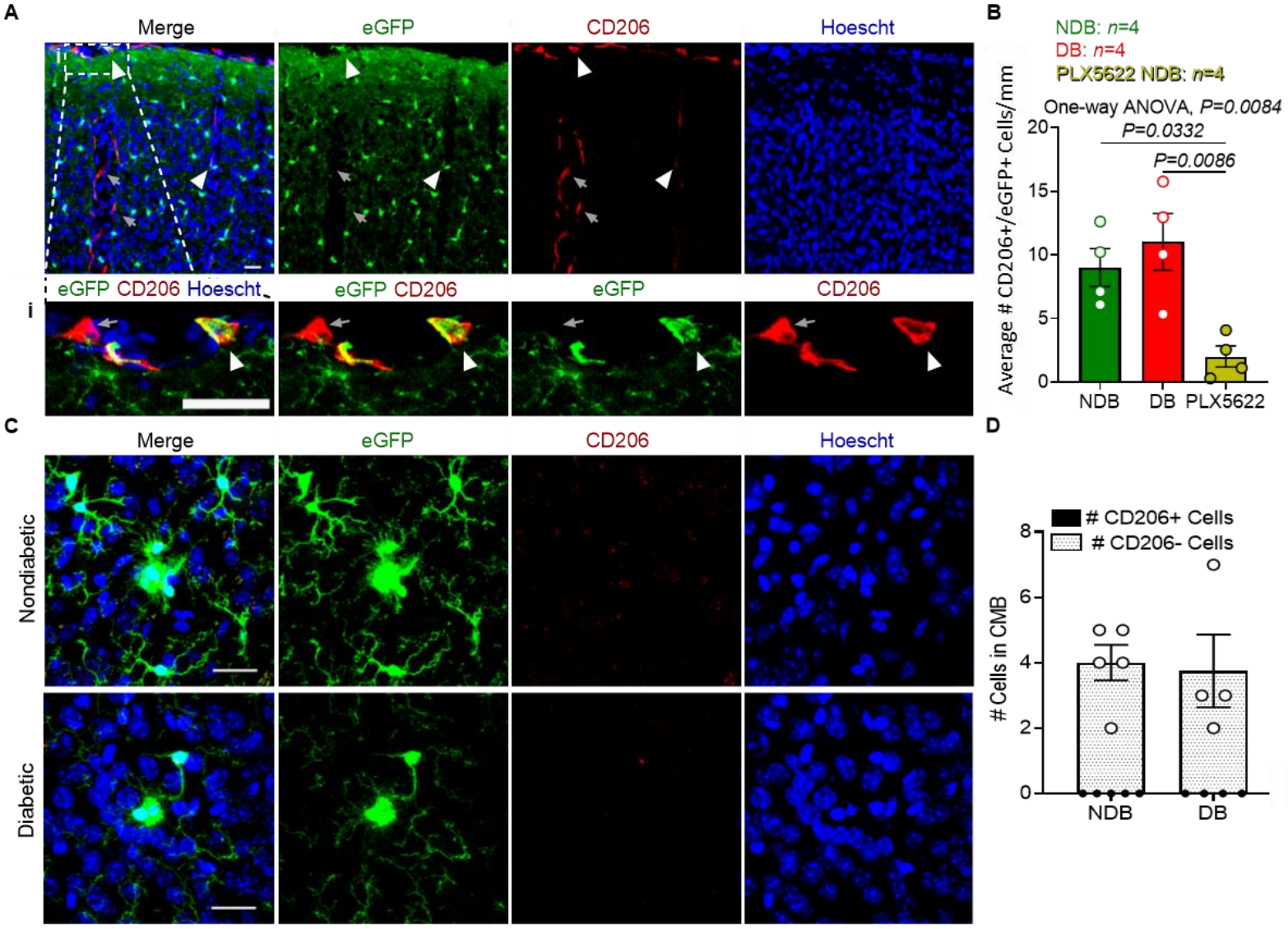
A
Merge
eGFP
CD206
Hoescht
i
eGFP CD206 Hoescht
eGFP CD206
eGFP
CD206
B
NDB: n=4
DB: n=4
PLX5622 NDB: n=4
One-way ANOVA, P=0.0084
P=0.0332
P=0.0086
Average # CD206+/eGFP+ Cells/mm
20
15
10
5
0
NDB
DB
PLX5622
C
Merge
eGFP
CD206
Hoescht
Nondiabetic
Diabetic
D
CD206+ Cells
CD206- Cells
Cells in CMB
8
6
4
2
0
NDB
DB

Figure 25. CD206-expressing macrophages do not comprise the microbleed response.
A. Representative maximum intensity confocal images of nondiabetic somatosensory cortex showing CD206-expressing cells situated on the pial surface and along a large penetrating blood vessel (*arrows*). Some, but not all, CD206+ cells were CX3CR1+ and expressed eGFP (*white arrowheads and grey arrows, respectively*). (*i)* A magnified image highlighting the colocalization of CD206 and eGFP in a CD206+ CX3CR1+ macrophage (*white arrow*). A CD206+ cell that does not co-express CX3CR1 is also visible (*grey arrow*). Scale bars represent 20 μm. **B.** Bar graph quantifying the average density of CD206+/CX3CR1+ eGFP-expressing cells along the meninges and vessels of NDB (*n=4* mice), DB (*n=4* mice), and PLX5622-treated NDB (*n=4* mice) cortices. Each data point represents the average of 4-6 areas per animal. **C.** Representative confocal images showing that CX3CR1+ eGFP-expressing, but not CD206+ cells, aggregate to the site of CMBs induced via thinned skull preparations in DB and NDB mice. Tissue was collected 3 days post-CMB. Scale bars represent 20 μm. **D.** Bar graph highlighting the absence of CD206+ cells in NDB (*n*=5 mice) and DB (*n*=4 mice) CMBs from tissue harvested 3 days post-ablation. Data points represent individual CMBs. One-way ANOVA compared the density of CD206+/eGFP+ cells between groups and was followed with a post-hoc Tukey's multiple comparison's test. Error bars represent mean± SEM.

In the context of CMBs specifically, no CD206+ cells were observed in the cellular responses to injury, characterized 3 days post-CMB, in either NDB or DB groups (Fig. 25C-D). Therefore, although BAMs do not generally appear to respond to CMBs, the discovery of cells with monocyte-like gene expression profiles that are Mac2+ (also known as Gal3) in the PLX5622-treated brain by Zhan et al.[443] provided another target phenotype that could contribute to the differential microvascular repair rates that this treatment induced in healthy animals. Mac2 is a β-galactoside binding protein involved in macrophage activation and adhesion that is expressed by cells of myeloid lineage and would, therefore, not generally be expected to be expressed by homeostatic microglia[141,453]. Indeed, since these cells showed upregulated TREM2 activity, it is possible that their responses to CMBs could disrupt microvascular repair by augmenting phagocytic processes[443]. Immunostaining of fixed coronal slices from PLX5622-treated and control animals revealed the presence of 2 phenotypes of Mac2+ cells: TMEM119+/Mac2+ and TMEM119-/Mac2+ variants (Fig. 26A). TMEM119 is widely considered to be a microglia-specific marker[327]. Both of these phenotypes were CX3CR1+ eGFP-expressing cells, and exhibited a branched phenotype that made them morphologically indistinguishable from neighbouring TMEM119+/Mac2- homeostatic microglia. In agreement with the findings of Zhan et al., PLX5622 treatment increased the proportional representation of Mac2+ cells in the remaining parenchymal CX3CR1+ population (Fig. 26B). This persistence suggests that Mac2+ cells exhibit greater resistance to CSF1R inhibition compared to most TMEM119+, which were significantly eliminated by PLX5622 (Student's t-test, TMEM119: Control versus PLX5622, $p<0.0001$; Fig. 26B).

To more rigorously characterize these Mac2+ cells, the density of both TMEM119- and TMEM119+ variants were quantified in the uninjured DB and NDB cortex. Although

macrophages in both DB and NDB brains without PLX56822 treatment expressed homeostatic microglial gene signatures (TMEM119+/Mac2-), half of the Mac2+ cells in the diabetic parenchyma were TMEM119- and, notably, these cells were not observed in the brain parenchyma of healthy mice (Figs. 27A-B). Furthermore, although PLX5622 treatment depleted Mac2+/TMEM119- cell density in the meninges (One-way ANOVA, p= 0.0326; DB versus PLX5622, p= 0.0423; Fig. 27C), the concentration of these cells did not vary between groups in terms of their localization to vessels or the parenchyma (Vessels: One-way ANOVA, p= 0.1555; Parenchyma: One-way ANOVA, p= 0.6919). However, DB and PLX5622-treated animals both exhibited significantly greater densities of Mac2+/TMEM119- cells in the uninjured brain parenchyma compared to NDB animals that did not receive PLX5622 (One-way ANOVA, p=; NDB versus DB, p= 0.0130; NDB versus PLX5622, p= 0.0256; Fig. 27D) With this in mind, it is possible that the Mac2+/TMEM119- population represents a type of DAM or an engrafted macrophage from the periphery. In either context, if these cells are sentinel in the uninjured brain parenchyma and are capable of influencing vessel fate, then their prevalence in non-homeostatic and disease conditions could help explain associated microvascular loss, given that this phenomenon was not observed in healthy animals which are devoid of Mac2+/TMEM119- cells.

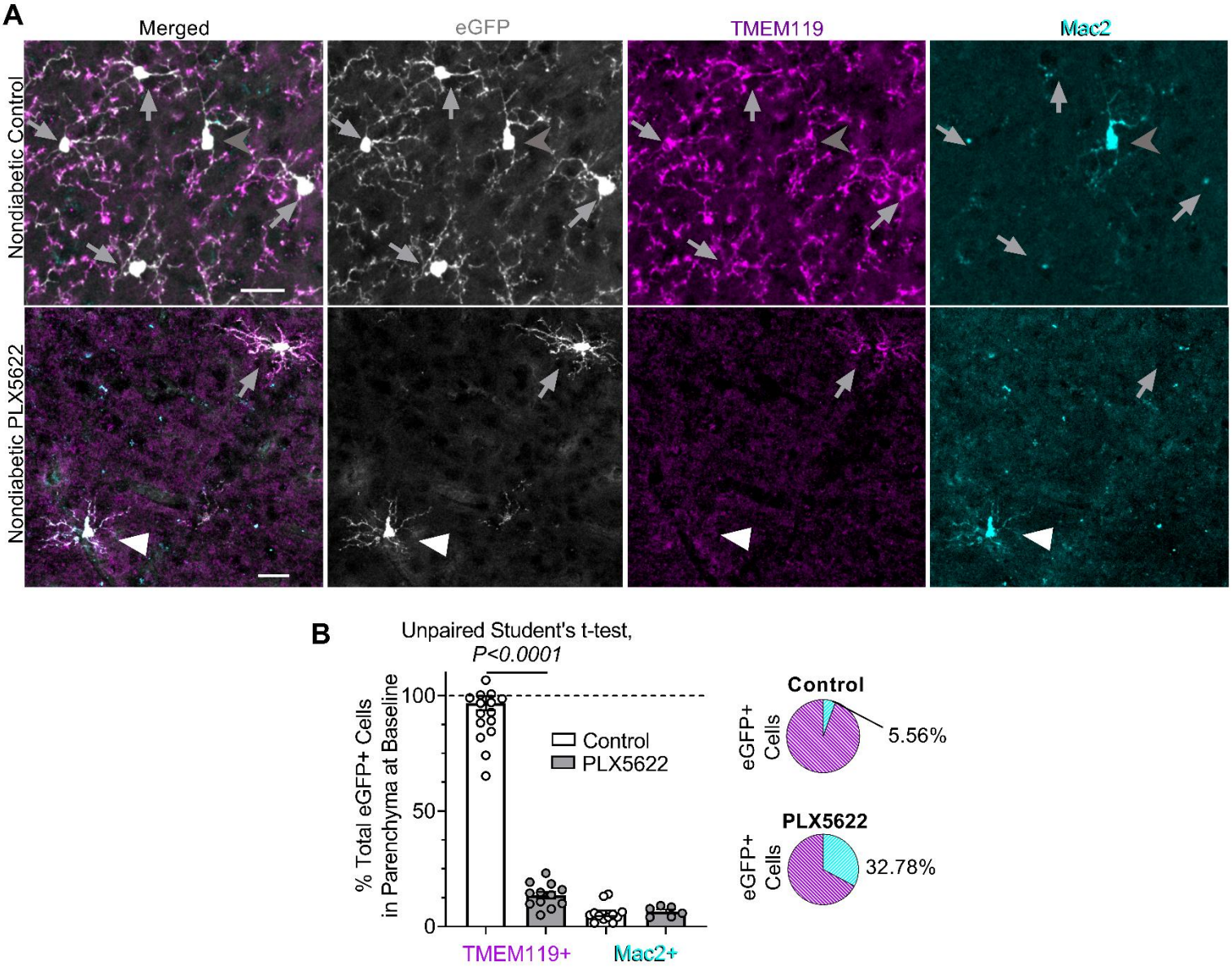
A
Merged
eGFP
TMEM119
Mac2
Nondiabetic Control
Nondiabetic PLX5622
B
Unpaired Student's t-test,
P<0.0001
% Total eGFP+ Cells
in Parenchyma at Baseline
100
50
0
Control
PLX5622
TMEM119+
Mac2+
Control
eGFP+
Cells
5.56%
PLX5622
eGFP+
Cells
32.78%

Figure 26. Mac2+ cells are more resistant to CSF1R inhibition via PLX5622 treatment than homeostatic TMEM119-expressing cells.

A. Maximum intensity projections of confocal images from uninjured somatosensory cortex showing eGFP, TMEM119, and Mac2 expression in untreated and PLX5622-treated nondiabetic groups. TMEM119-/Mac2+/eGFP+ cells (*white arrowheads*), TMEM119+/Mac2-/eGFP+ cells (*grey arrows*), and TMEM119+/Mac2+/eGFP+ cells (*grey arrowheads*) are indicated. Scale bars represent 20 μm. **B.** Graph showing the proportion of CX3CR1+ eGFP-expressing cells that were also labelled by TMEM119 (*purple*) or Mac2 (*cyan*) in the uninjured parenchyma of untreated (*white bar*) and PLX5622-treated (*shaded bars*) mice relative to pre-treatment density. Cell counts acquired from images of 24 coronal sections from 8 control mice (4 NDB and 4 DB) and 12 sections from 4 (2 NDB and 2 DB) PLX5622-treated mice comprise this data set. **C.** Pie charts illustrate that PLX5622-treated mice exhibit a non-homeostatic, large proportion of Mac2+ cells comprising the remaining CX3CR1+ eGFP-expressing cells relative to controls (32.8% vs 5.6%, respectively). Unpaired Student's t-tests were used to compare differences in cell counts between control and PLX5622 treated animals. Error bars represent mean± SEM.

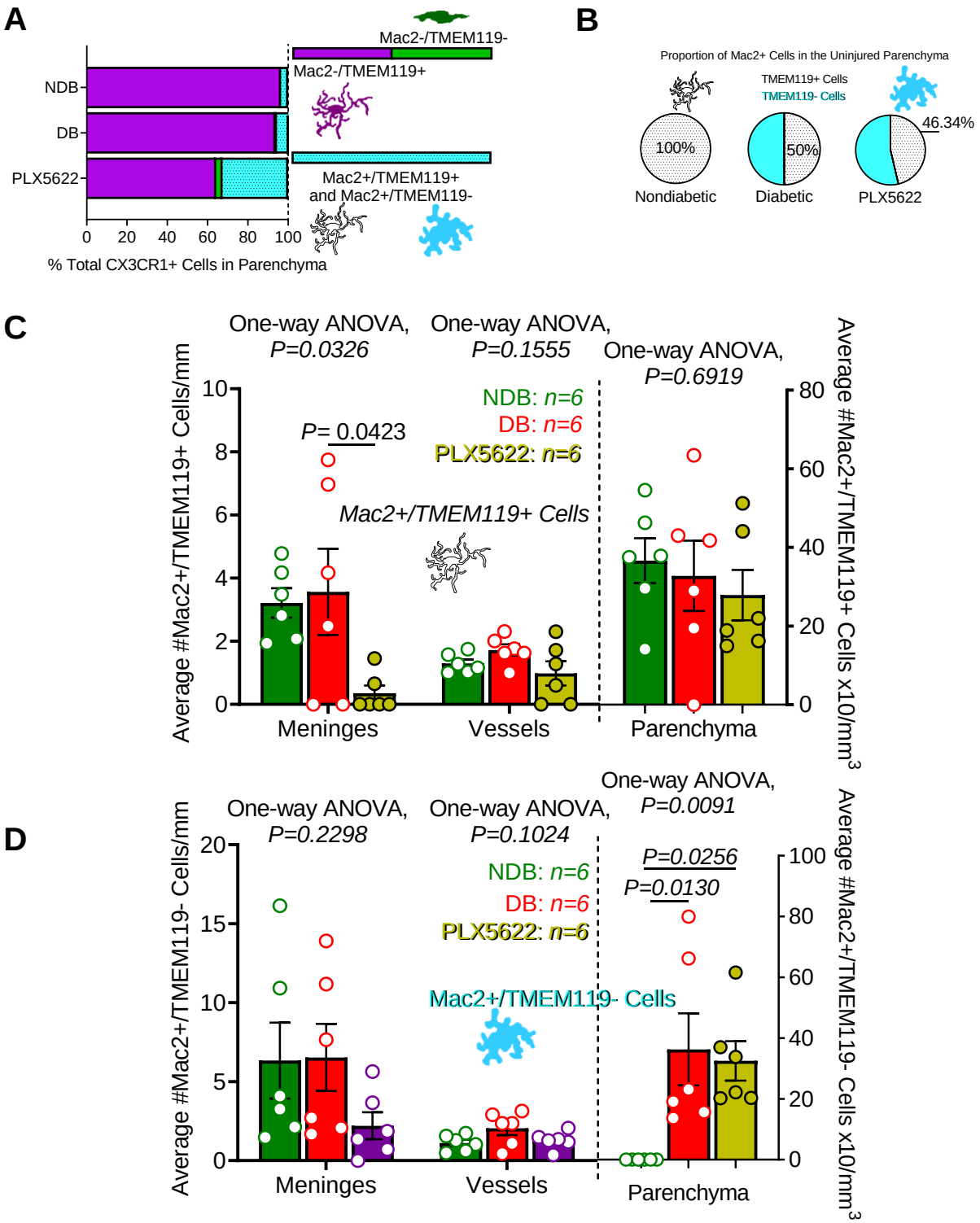
A
Mac2-/TMEM119-
Mac2-/TMEM119+
NDB
DB
PLX5622
Mac2+/TMEM119+
and Mac2+/TMEM119-
0 20 40 60 80 100
% Total CX3CR1+ Cells in Parenchyma
B
Proportion of Mac2+ Cells in the Uninjured Parenchyma
TMEM119+ Cells
TMEM119- Cells
100%
50%
46.34%
Nondiabetic
Diabetic
PLX5622
C
One-way ANOVA, P=0.0326
One-way ANOVA, P=0.1555
One-way ANOVA, P=0.6919
NDB: n=6
DB: n=6
PLX5622: n=6
P= 0.0423
Mac2+/TMEM119+ Cells
Average #Mac2+/TMEM119+ Cells/mm
Average #Mac2+/TMEM119+ Cells x10/mm3
Meninges
Vessels
Parenchyma
D
One-way ANOVA, P=0.2298
One-way ANOVA, P=0.1024
One-way ANOVA, P=0.0091
P=0.0256
P=0.0130
NDB: n=6
DB: n=6
PLX5622: n=6
Mac2+/TMEM119- Cells
Average #Mac2+/TMEM119- Cells/mm
Average #Mac2+/TMEM119- Cells x10/mm3
Meninges
Vessels
Parenchyma

Figure 27. Mac2+/TMEM119- cells are present in the brain parenchyma of untreated diabetic and PLX5622-treated brains in the absence of injury.

A. Summary bar graph quantifying the proportion of total cells identified as Mac2-/TMEM119+ microglia, Mac2-/TMEM119- cells, and Mac2+ cells in the uninjured parenchyma of NDB, DB and PLX5622-treated cortices. **B.** Pie charts showing the proportion of Mac2+ cells that co-express the homeostatic microglial marker TMEM119 (*grey*) or those that do not (*blue;* macrophages). Data comprising this figure were collected by confocal imaging of 4-6 coronal sections from 6 animals in each group. **C.** Summary bar graph showing the average density of Mac2+/TMEM119+ microglia quantified in the meninges, along penetrating arterioles, and in the brain parenchyma of NDB, DB, and PLX5622-treated animals. **D.** Summary bar graph highlighting that, although there were no significant differences in the average density of Mac2+/TMEM119- macrophages in the meninges or along the penetrating arterioles of NDB, DB, and PLX5622-treated cortices, these cells were identified in the uninjured brain parenchyma of DB and PLX5622-treated mice. Individual data points represent the average of data collected from 4-6 coronal sections per animal. In all figures, 6 animals were used per group; 3 NDB and 3 DB mice received PLX5622 treatment. One-way ANOVAs were used to compare group differences and followed with post-hoc Tukey's multiple comparisons tests as appropriate. Error bars represent mean± SEM.

To investigate the possibility that Mac2+ cells could be associated with microvascular elimination, CMBs were induced in DB and NDB mice via a chronic cranial window, with injuries staggered dorsoventrally (Fig. 28A). After determining the fate of the CMBs 3 days post-insult (Fig. 28B), brains were serially sectioned and the relative coordinates of the induced microbleeds were used to relocate them *in situ* (Fig. 28B). Confocal imaging of these coronal slices, immunostained for the microglial marker TMEM119 and the peripheral immune cell label Mac2, revealed a diverse collection of cells in the microbleed milieu that were indistinguishable from one another using 2-photon microscopy alone (Figs. 28B-C). In addition to homeostatic Mac2-/TMEM119+ microglia, Mac2-/TMEM119- cells that were CX3CR1+ were identified along with 2 subsets of Mac2+ cells: a group that co-expressed TMEM119 and another that did not (Fig. 28C). Although both eliminated and repaired microvessels were associated with every cell type, only Mac2+/TMEM119- cell were significantly increased at the site of CMBs which resulted in vessel loss (Unpaired Student's t-test, p=0.0006; Fig. 28C-D).

Furthermore, by quantifying Mac2 expression area as a function of TMEM119, it was evident that of Mac2+/TMEM119- cells were significantly more common at the site of microvessels that were eliminated than at those that repaired (Unpaired Student's t-test, $p<0.0001$; Fig. 28D). Furthermore, when the colocalization of Mac2+/TMEM119- cells in the CMB cellular response was binarized (present versus absent), it was evident that the majority of eliminated vessels (83%) were associated with these cells (Fig. 28F). By contrast, capillaries that ultimately recanalized following CMB were rarely associated with Mac2+/TMEM119- cell (11.11%; Fig. 28F). These results identify a population of Mac2+/TMEM119- cells that are particularly resilient to CSF1R inhibition when compared to Mac2-/TMEM119+ microglia, and are strongly associated with failed microvascular repair following CMB.

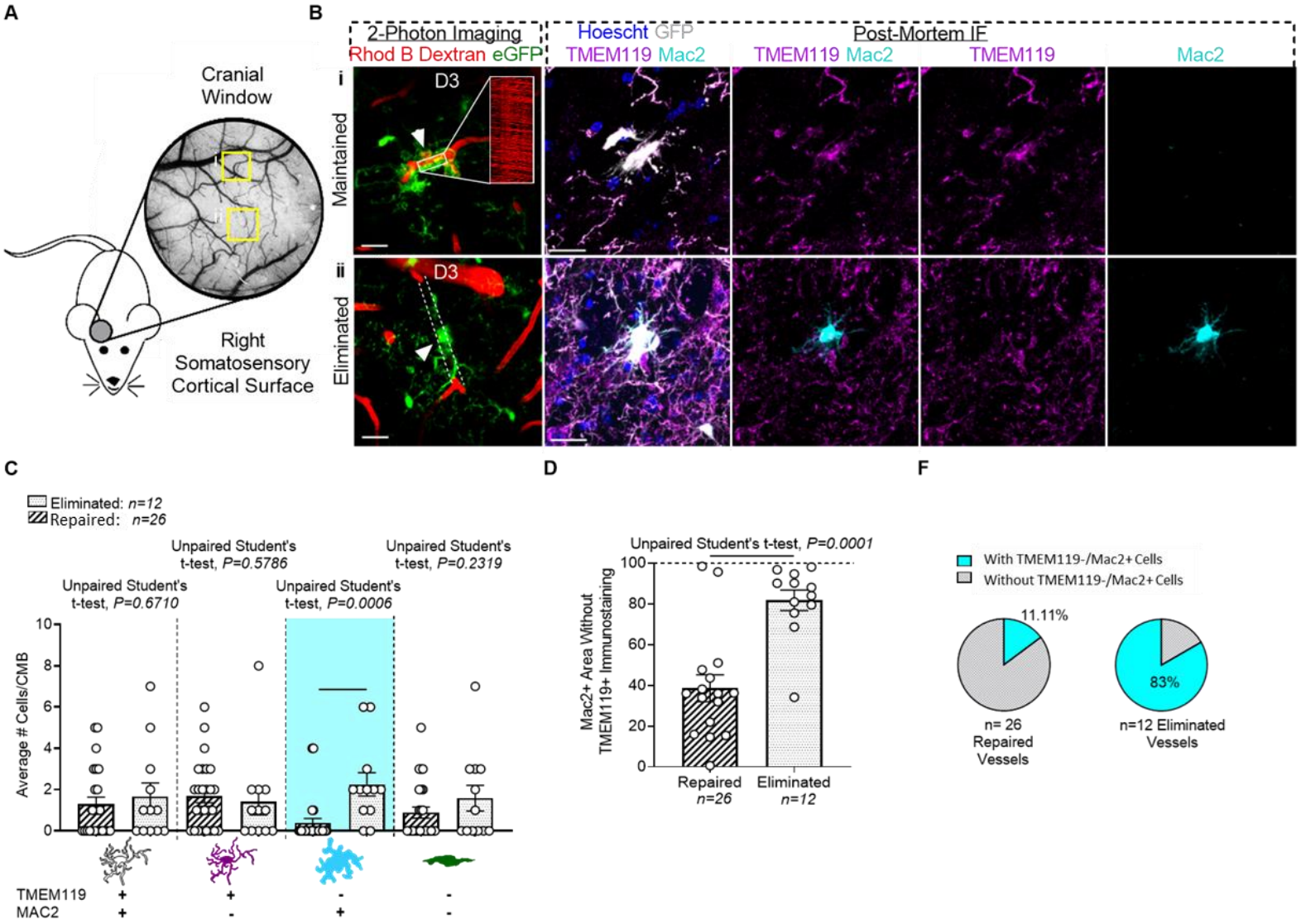
A
Cranial Window
Right Somatosensory Cortical Surface
B
2-Photon Imaging
Rhod B Dextran eGFP
Hoescht GFP
TMEM119 Mac2
Post-Mortem IF
TMEM119 Mac2
TMEM119
Mac2
i
Maintained
D3
ii
Eliminated
D3
C
Eliminated: n=12
Repaired: n=26
Unpaired Student's t-test, P=0.6710
Unpaired Student's t-test, P=0.5786
Unpaired Student's t-test, P=0.0006
Unpaired Student's t-test, P=0.2319
Average # Cells/CMB
TMEM119
MAC2
D
Unpaired Student's t-test, P=0.0001
Mac2+ Area Without TMEM119+ Immunostaining
Repaired n=26
Eliminated n=12
F
With TMEM119-/Mac2+ Cells
Without TMEM119-/Mac2+ Cells
11.11%
83%
n= 26 Repaired Vessels
n=12 Eliminated Vessels

Figure 28. TMEM119-/Mac2+ cells are associated with eliminated microvessels in the diabetic cortex.

A. Illustration demonstrating the staggering of 2 representative imaging areas where CMBs were induced through a chronic cranial window in the right somatosensory cortices mice. Following confirmation of repair or elimination of damaged microvessels by D3, the same imaging areas were found in fixed slices via their imaging coordinates and distinct locations. **B.** 2-photon and maximum intensity projections of confocal images showing the localization of CMBs induced in diabetic mice *in vivo* that were relocated in fixed slices and immunostained with TMEM119 and Mac2. Nuclei were labelled by Hoechst 33342. Scale bars indicate 20 μm. (***i***) 2-photon image of a repaired vessel at D3 (*white arrow indicates site of CMB induction*); *inlay* line-scan confirming blood flow. Post-mortem immunofluorescence of the CMB showed TMEM119+/eGFP+ microglia aggregated and no Mac2+ signal. (***ii***) 2-photon image of an eliminated microvessel (*dashed white lines show original vessel path*) at D3 (*white arrow indicates site of CMB induction*). Immunofluorescent labelling of the CMB in fixed tissue revealed that it contained TMEM119-/Mac2+/CX3CR1+ cells. **C.** Summary bar graph comparing the number of TMEM119+/Mac2+, TMEM119+/Mac2-, TMEM119-/Mac2+, and TMEM119-/Mac2- cells in CMBs from eliminated or repaired microvessels, as confirmed by longitudinal *in vivo* 2-photon imaging. **D.** Bar graph summarizing the average area of Mac2+ immunostaining that did not co-express TMEM119 in CMBs that were either repaired or eliminated. ***E.*** Pie charts visualizing the proportion of repaired (*left*) or eliminated (*right*) microvessels that were associated with TMEM119-/Mac2+ cells. Data for these analyses were generated from 5 DB (23 vessels) and 4 NDB (15 vessels) mice; 2-5 CMBs were induced per animal. Unpaired Student's t-tests were used to assess differences between groups and to compare the proportional area of lipofuscin associated with vessels that were repaired. Error bars represent mean± SEM.

4.3.2 Elimination of peripheral phagocytic leukocytes rescues pathological microvascular elimination in diabetes

Since the Mac2+/TMEM119- cells observed at the site of eliminated microvessels could be of peripheral origin, given that cells of myeloid lineage express Mac2[141,453], and others have shown that MDMs arising from the periphery may play a role in pruning CNS capillaries[27], it was necessary to investigate the source of these cells. Furthermore, sporadic observations of eGFP-expressing leukocytes stalled in diabetic vessels or near CMBs provided impetus to consider the involvement of these cells in injury repair (Fig. 29A-D). Therefore, to investigate the contributions of circulating leukocytes, peripheral phagocytes were depleted via i.v. injection of CLR. Mechanistically, when cells phagocytose CLR the liposomes are degraded within phagolysosomes, releasing encapsulated clodronate and initiating apoptosis in target cells[454–456].

Using the Diff Quik histology stain, it was determined that CLR significantly depleted circulating monocytes (One-way ANOVA: $F_{(3, 16)} = 4.865$, $p=0.0136$; NDB versus CLR, $p=0.0236$; DB versus CLR, $p=0.0128$; Fig. 30A) without affecting lymphocytes (One-way ANOVA: $F_{(3, 16)} = 0.07202$, $p=0.9741$; Fig. 30A) or RBCs (One-way ANOVA: $F_{(3, 16)} = 1.816$, $p=0.1849$; Fig. 30B); neutrophil numbers were also decreased by CLR, although not significantly (One-way ANOVA: $F_{(3, 16)} = 2.696$, $p=0.0807$; Fig. 30A). Of note, PLX5622 treatment did not deplete circulating phagocytes (Monocytes: One-way ANOVA: $F_{(3, 16)} = 4.865$, $p=0.0136$; NDB versus PLX5622, $p=0.8826$; DB versus PLX5622 , $p=0.6355$; Neutrophils: One-way ANOVA: $F_{(3, 16)} = 2.696$, $p=0.0807$; Fig. 30A).

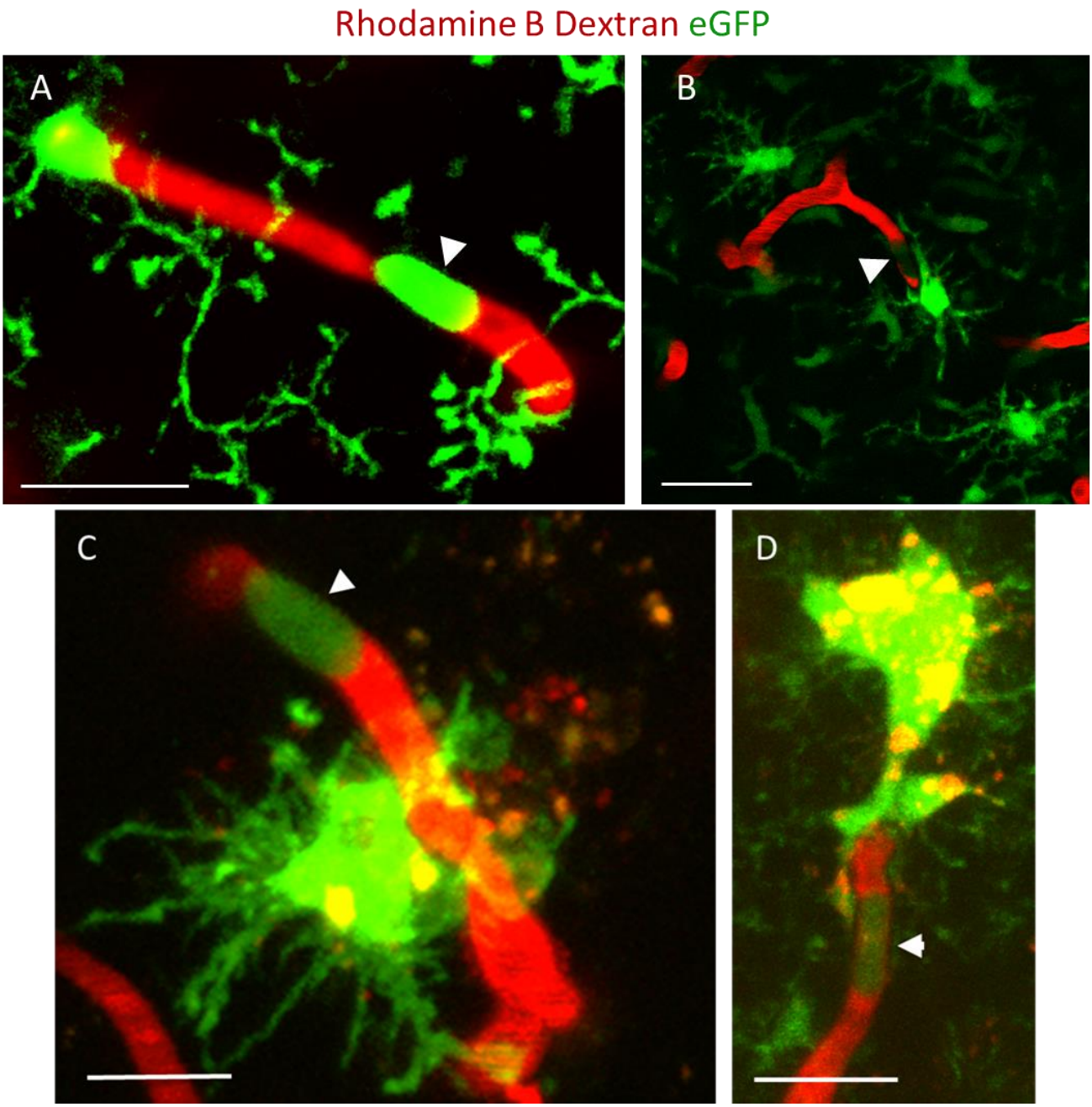

Figure 29. CX3CR1+ eGFP-expressing leukocytes stall in diabetic microvessels and near microbleed responses.

Examples of 2-photon images depicting eGFP-expressing CX3CR1+ cells (*white arrowheads*) stalled in **A.** a diabetic microvessel prior to CMB and near microbleed responses in **B.** IFNα blocking antibody-treated DB, **C.** PLX5622-treated, and **D.** INS mice. The vascular lumen is labelled with Rhodamine B dextran. Scale bars are 10 µm in **A.**, **C.**, and **D.** and 20 µm in **B.**

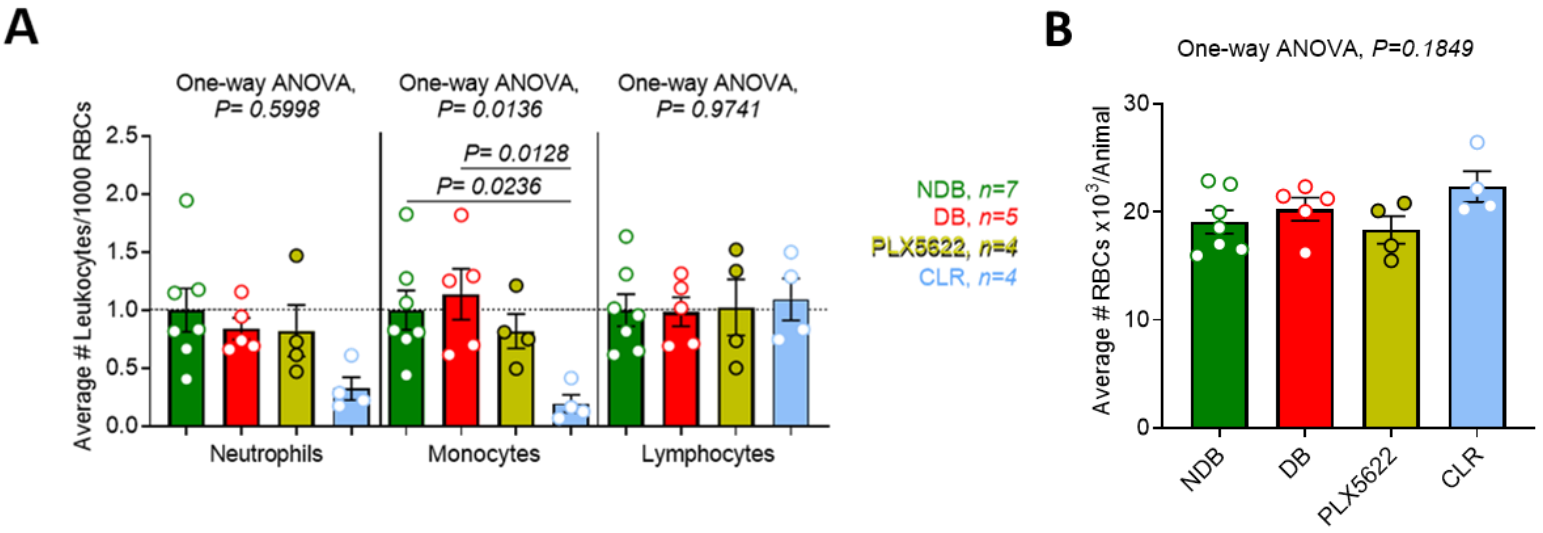

Figure 30. CLR depletes monocytes but not neutrophils, lymphocytes, or red blood cells. **A.** Summary bar graphs illustrating that CLR significantly depletes monocytes but circulating neutrophils and lymphocytes do not vary significantly between any groups. Averages are normalized to the NDB group. Leukocyte counts for each imaging area were normalized to the corresponding number of RBCs present. Animal numbers per group are represented to the right of the graph. **B.** Summary bar graph showing no significant differences in the average number of RBCs quantified in each blood smear in NDB, DB, PLX5622-treated, or CLR-treated animals. The number of mice comprising each group is indicated to the left of the graph. The total number of blood cells in 10 regions of the monolayer of a blood smear were averaged across 5 blood smears per animal to comprise a single data point in **A.** and **B.** The PLX5622-treated and CLR-treated groups each contained 2 DB and 2 NDB mice for a total of 4 animals. One-way ANOVAs followed by post-hoc Tukey's multiple comparisons tests, as appropriate, were utilized to assess group differences in leukocyte and RBC numbers. All relevant comparisons were performed, but only significant results are shown on the graph. Error bars represent mean± SEM.

In the spleen, Mac2+ resident macrophages were significantly depleted by CLR but not PLX5622 (One-way ANOVA: $F_{(2, 34)} = 10.41$, $p=0.0003$; VEH versus CLR, $p= 0.0043$; VEH versus PLX5622, $p= 0.6969$; CLR versus PLX5622, $p= 0.0004$; Fig. 31A-B). Importantly, however, CLR treatment did not impact cortical microglial density, a finding which has been similarly replicated by others in various rodent models (One-way ANOVA: $F_{(2, 9)} = 0.6762$, $p=0.5164$; Fig. 31C-D)[84,457,458].

Having confirmed that CLR effectively depletes circulating phagocytic cells but not CNS-resident microglia, CMBs were induced in diabetic mice treated with CLR (intervention provided 2 days prior to the insult, D0, and 2 days post-CMB). It is worth noting that CLR treatment could impact levels of circulating inflammatory factors by eliminating the phagocytes that secrete them, thereby potentially influencing vessel fates in a manner independent of the physical aggregation of target cells to injury sites. By following the resolution of these CMBs over 14 days, a significant increase in microvascular repair rates was noted in diabetic mice treated with CLR (94.87%) relative to untreated diabetic mice (80.00%; Chi-squared test: DB versus CLR DB, $p=0.0439$; Fig. 32A-B). Although most diabetic animals treated with CLR exhibited repair of all targeted vessels, an individual mouse lost 2/5 of damaged vessels, potentially indicating an ineffective administration of the drug (Fig. 32C). This possibility could have been tested by quantifying the depletion of Mac2+ macrophages in the liver or spleen, but those tissues were not harvested at the time of euthanasia. However, even when the proportion of vessels repaired per animal were considered, as opposed to the average repair rate across groups as a whole, CLR still significantly improved vessel repair relative to untreated DB mice (Kruskal-Wallis Test, $p<0.001$; DB versus CLR DB, $p=0.0128$; Fig. 32C).

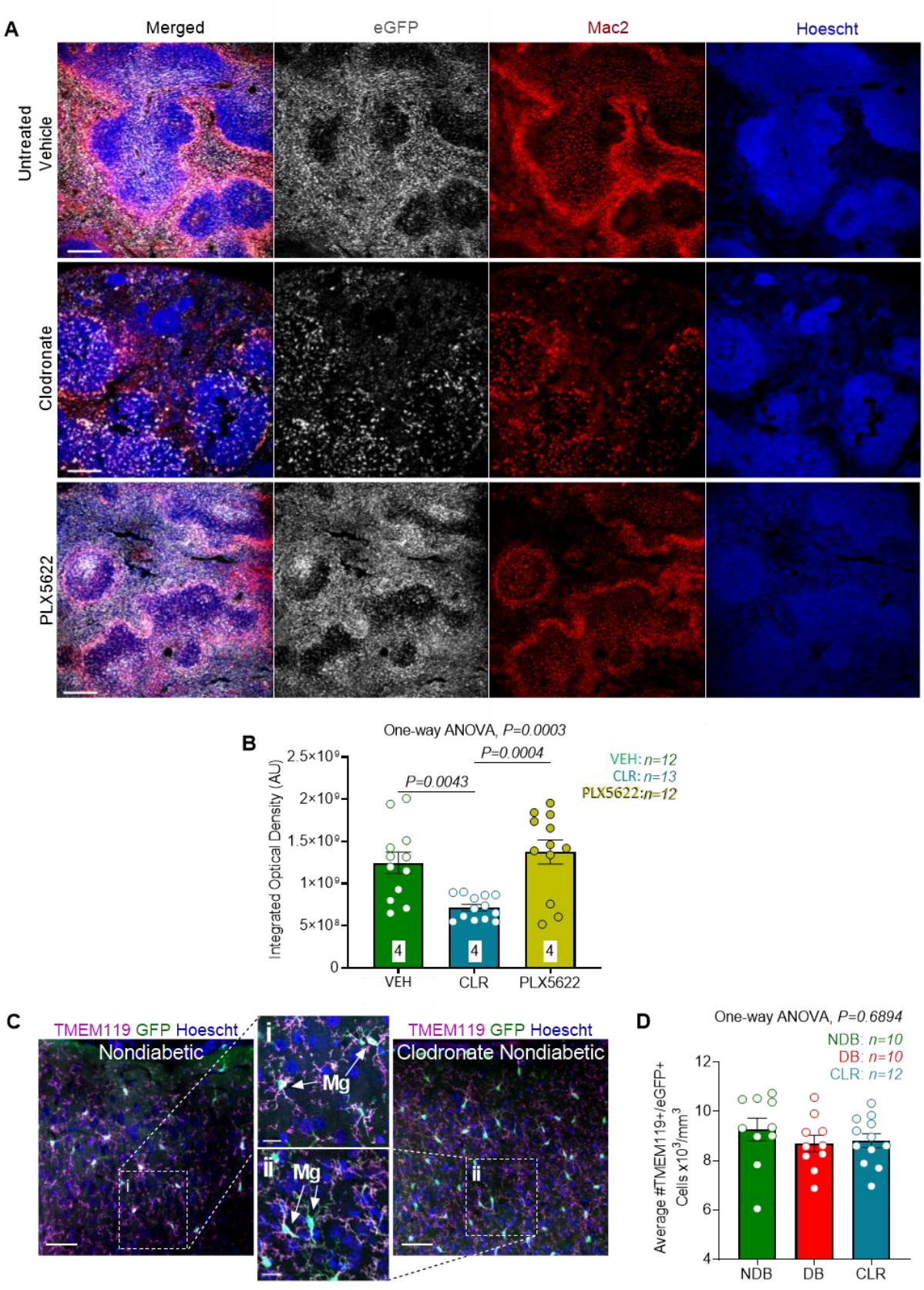
A
Merged
eGFP
Mac2
Hoescht
Untreated Vehicle
Clodronate
PLX5622
B
One-way ANOVA, P=0.0003
P=0.0004
P=0.0043
VEH: n=12
CLR: n=13
PLX5622: n=12
Integrated Optical Density (AU)
2.5×10⁹
2×10⁹
1.5×10⁹
1×10⁹
5×10⁸
0
4
VEH
CLR
PLX5622
C
TMEM119 GFP Hoescht
Nondiabetic
i
Mg
ii
Clodronate Nondiabetic
D
One-way ANOVA, P=0.6894
NDB: n=10
DB: n=10
CLR: n=12
Average #TMEM119+/eGFP+ Cells x10³/mm³
12
10
8
6
4
NDB
DB
CLR

Figure 31.CLR treatment effectively deplete tissue-resident macrophages of the spleen but not the brain parenchyma.

A. Maximum intensity projections of confocal images of coronal sections of spleen, labelled with immunofluorescent markers for Mac2, showing the profound depletion of CX3CR1+/Mac2+ macrophages following i.v. administration of CLR in a nondiabetic mouse. Mac2+ expression in the spleen of a nondiabetic PLX5622-treated mice was not significantly different from untreated healthy animals that received vehicle (VEH) injections. Scale bars indicate 200 μm. **B.** Summary bar graph showing the significant decrease in integrated optical density of Mac2 fluorescence in spleens of NDB mice treated with CLR compared to their NDB PLX5622-treated or NDB VEH counterparts. Animal numbers are reflected on respective columns; 3-4 images were acquired from each spleen. **C.** Representative maximum intensity projections of confocal images of uninjured somatosensory cortex, collected with a 20X objective and labelled with immunofluorescent markers for TMEM119, from NDB mice that received vehicle or CLR. (*center*) Maximum intensity projections of high-resolution images, acquired at 60X magnification, show TMEM119-labelled microglia at comparable densities in both (*i*) vehicle-treated NDB and (*ii*) CLR-treated NDB coronal sections. Scale bars represent 50 μm for 20X images and 20 μm for (*i*) and (*ii*). D. Summary bar graph showing no significant differences in microglial density between vehicle-treated NDB and DB, and NDB CLR-treated groups. Animal numbers are indicated above the graph; each data point is the average of images from 4-6 slices per animal. One-way ANOVAs with post-hoc Tukey's multiple comparisons tests, as appropriate were used to assess group differences. All appropriate comparisons were performed, but only significant results are shown on the graph. Error bars represent mean± SEM. Mg: microglia.

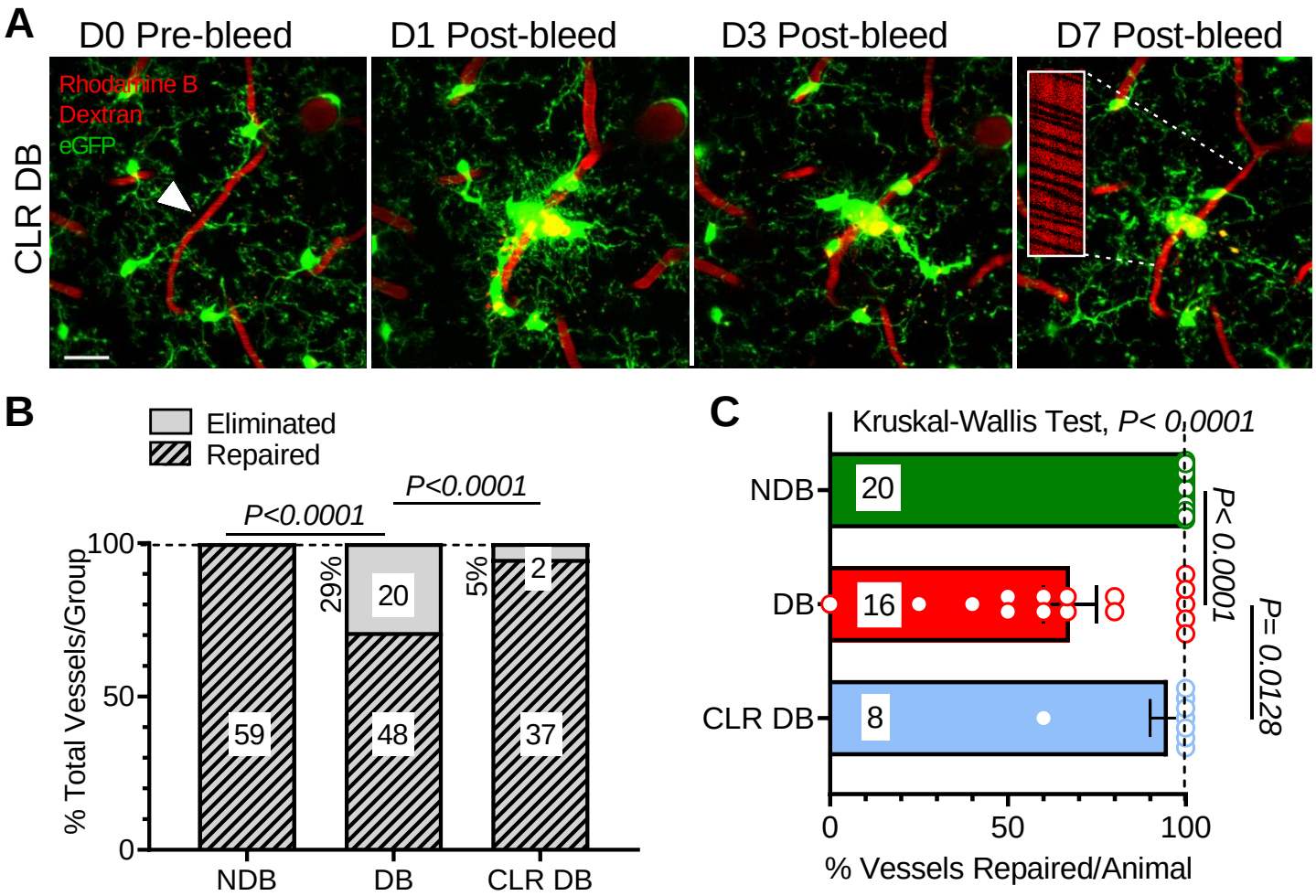
A
D0 Pre-bleed
D1 Post-bleed
D3 Post-bleed
D7 Post-bleed
CLR DB
Rhodamine B
Dextran
eGFP
B
Eliminated
Repaired
P<0.0001
P<0.0001
% Total Vessels/Group
100
50
0
29%
5%
59
20
48
2
37
NDB
DB
CLR DB
C
Kruskal-Wallis Test, P< 0.0001
NDB
DB
CLR DB
20
16
8
P< 0.0001
P= 0.0128
0
50
100
% Vessels Repaired/Animal

Figure 32. Depletion of peripheral phagocytes via clodronate treatment rescues diabetic microvessel loss following microbleed.

A. Montage of 2-photon images chronicling the CX3CR1+ eGFP-expressing macrophage response to CMB (*site indicated by white arrowhead*) in a diabetic mouse that received CLR treatment (CLR DB). The long-term vessel repair and recanalization is highlighted by the line-scan at D7 showing streaking RBCs *(inlay)*. **B.** Summary bar graph demonstrating a significant reduction in the proportion of eliminated microvessels in DB (n=14) mice when treated with CLR (n=8). Repair rates in diabetic mice treated with CLR did not differ significantly from NDB (n=17) mice. The number of vessels comprising each group is indicated on relevant columns. **C.** Summary bar graph describing the average percentage of vessels repaired per animal in NDB, DB, and CLR DB mice. Animal numbers are indicated on columns; each mouse received 1-5 CMBs. Vessel outcomes were assessed at 7 days post-CMB. A Chi-squared test compared ratios of repaired microvessels between groups and a non-parametric Kruskal-Wallis test with post-hoc Dunn's multiple comparisons determined group differences in repair rates. Bars represent mean± SEM.

Next, to determine whether these changes in microvascular fate were associated with alterations in the cellular milieu of the CMB aggregate, CMBs were induced via thin skull craniotomies, animals were euthanized 3 days post-CMB induction, and then injuries were relocated using confocal imaging. By immunostaining cortical sections for Mac2 and TMEM119, Mac2+/TMEM119- cells were discovered at the site of diabetic CMBs but could not be found in the NDB microbleed response (Figs. 33A-B). Notably, CLR significantly reduced the number of Mac2+/TMEM119- cells in diabetic CMBs, rendering them generally morphologically and phenotypically indistinguishable from NDB CMBs (One-way ANOVA: $F_{(2, 87)} = 14.48$, $p<0.0001$; DB versus CLR DB, $p=0.0344$; Figs. 33A-B). Interestingly, the presence of Mac2+/TMEM119+ cells was not affected by CLR (One-way ANOVA: $F_{(2, 87)} = 0.7862$, p=0.7862; Fig. 33B). This suggests that the Mac2+/TMEM119+ population may represent a subtype of microglia resident to the CNS, corresponding to the Mac2+ cells identified by Zhan et al., while Mac2+/TMEM119- cells likely arise from the periphery. The area of Mac2+ immunostaining in each CMB that did not co-express TMEM119 was also normalized in diabetic mice treated with CLR (One-way ANOVA: $F_{(2, 62)} = 45.49$, $p<0.0001$; DB versus CLR DB, $p<0.0001$; Fig. 33C). Taken together, these data suggest that Mac2+/TMEM119- cells in the diabetic CMB milieu arise from the periphery and that their aggregation to microvascular insults is associated with an outcome shift that favours loss rather than repair.

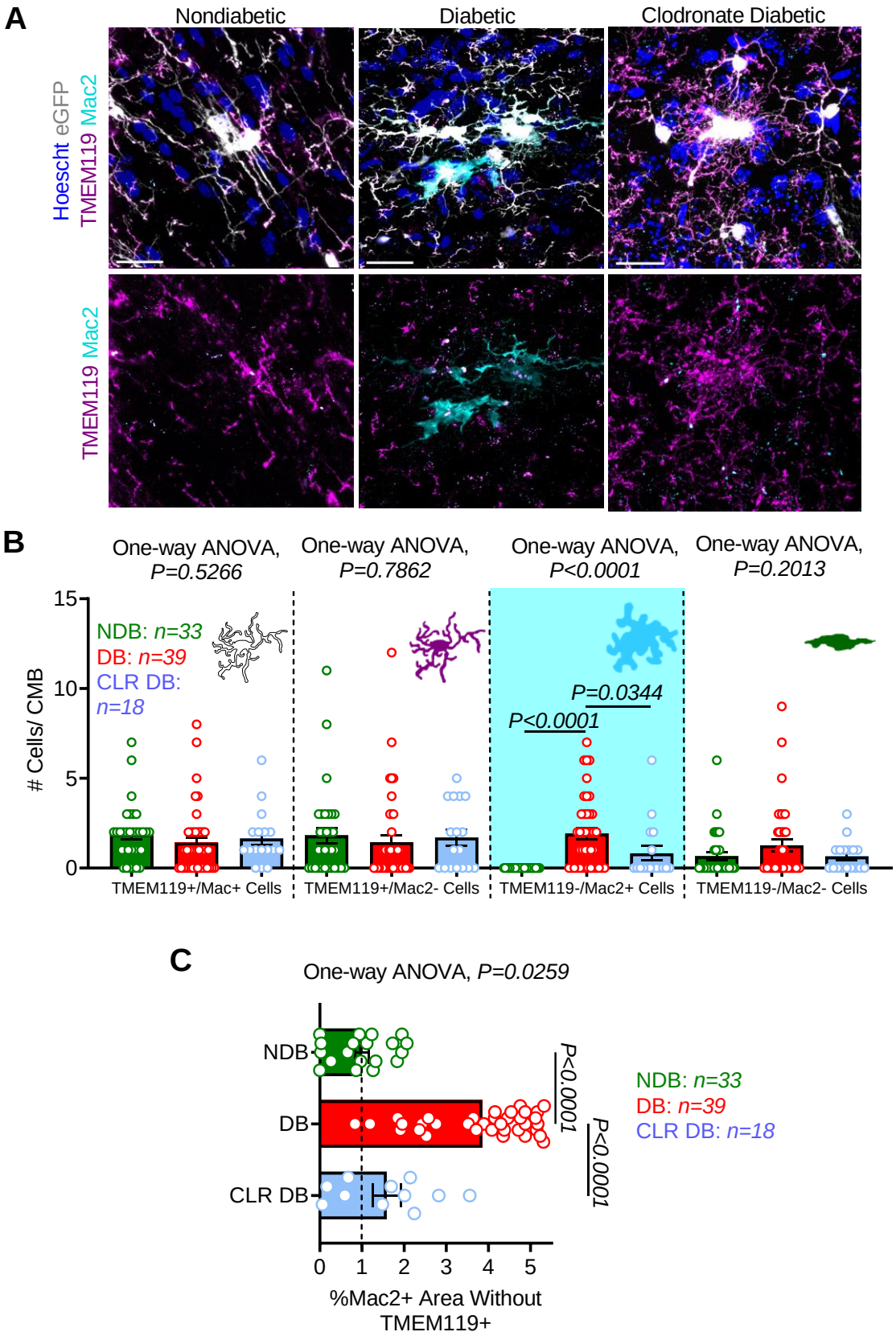
A
Nondiabetic
Diabetic
Clodronate Diabetic
Hoescht eGFP TMEM119 Mac2
TMEM119 Mac2
B
One-way ANOVA, P=0.5266
One-way ANOVA, P=0.7862
One-way ANOVA, P<0.0001
One-way ANOVA, P=0.2013
Cells/ CMB
NDB: n=33
DB: n=39
CLR DB: n=18
P=0.0344
P<0.0001
TMEM119+/Mac+ Cells
TMEM119+/Mac2- Cells
TMEM119-/Mac2+ Cells
TMEM119-/Mac2- Cells
C
One-way ANOVA, P=0.0259
NDB
DB
CLR DB
P<0.0001
P<0.0001
NDB: n=33
DB: n=39
CLR DB: n=18
%Mac2+ Area Without TMEM119+

Figure 33. Clodronate treatment prevents aggregation of Mac2+/TMEM119- cells to diabetic microbleeds.

A. Maximum intensity projections of confocal images of immunofluorescent staining for Mac2 and TMEM119 in microbleeds, induced in the somatosensory cortex via thin skull preparations with animals euthanized 3 days post-injury, from NDB, DB, and CLR DB mice. Hoechst 33342 was used to label cell nuclei. Scale bars indicate 20 μm. **B.** Summary bar graph describing the average number of TMEM119+/Mac+, TMEM119+/ Mac-, TMEM119-/ Mac+, and TMEM119-/ Mac- cells in CMBs in NDB, DB, and DB CLR cortices. 2-5 CMBs were used from each animal. **C.** Bar graph summarizing the proportion of Mac2+ immunostaining that does not colocalize with TMEM119 immunostaining in NDB, DB, and CLR DB mice. Averages are normalized to NDB values. Data comprising these figures were collected from $n=8$ NDB, $n=10$ DB, and $n=6$ CLR DB mice One-way ANOVAs with post-hoc Tukey's multiple comparisons tests were used to compare group differences. All relevant comparisons were performed, but only significant results are shown on graphs. Error bars represent mean± SEM.

4.3.3 Markers for phagocytosis are enhanced in the diabetic microbleed response, particularly in Mac2+/TMEM119- macrophages

Phagocytosis is a primary facet of microglial and macrophage function. Since dysregulation of this process has been connected with these cells' pathological roles in aberrant synapse pruning[300,304] or depletion of myelin[459], it may also contribute to microvascular elimination in diabetes. That is, hyperglycemic toxicity in type 1 DM, and the resulting inflammatory environment, may enhance phagocytic activity in macrophages and facilitate their degradation of tissue rather than supporting anti-inflammatory phenotypes that could augment repair. Furthermore, since the morphological features of microbleed responses could not reliably predict microvessel fate following CMB, phagocytosis was investigated as an alternative, functional mechanism that may more effectively predict microvascular elimination.

To probe phagocytic activity associated with CMBs *in vivo*, lipofuscin was used as an indirect marker of this process in CX3CR1+ cells because it is indicative of the accumulation of lipid particles within lysosomal compartments[460]. Firstly, to confirm that the autofluorescent signal of putative lipofuscin particles that could be visualized with 2-photon microscopy actually correspond to these entities, CD68 immunostaining was used to label lysosomal compartments[461,462] in fixed coronal sections and then these specimens were imaged with the 2-photon microscope. Penetrating arterioles were ablated *in vivo*, prompting a robust CX3CR1+ macrophage response, extensive tissue damage, and increased phagocytic activity, and then mice were euthanized 1 day later and brain tissue was collected and processed for immunostaining. A Cy5 secondary antibody was used to visualize CD68 immunostaining and excitation of this fluorophore was achieved by tuning the 2-photon laser to 900nm, generating a signal that could be easily separated from that of lipofuscin (excited at 750nm; Fig. 34A). The majority of

quantified CD68 immunostaining (72.86%) was localized to eGFP-expressing CX3CR1+ cells and, notably, all observed lipofuscin autofluorescence colocalized with CD68 immunostaining (Fig. 34A-C). Furthermore, a greater area of CD68 immunostaining was observed in comparison to the area of lipofuscin autofluorescence (Figs. 34A-C). Although all lipofuscin signal was observed within CD68+ particles, 64.34% of quantified CD68 immunostaining did not also exhibit lipofuscin autofluorescence (Fig. 34C). These findings indicate lipofuscin signal assessed with 2-photon imaging is reliably associated with lysosomal compartments and may underrepresent the degree of lysosomal activity given the extent of CD68 immunostaining that did not also exhibit lipofuscin autofluorescence.

Having confirmed that the lipofuscin signal acquired using 2-photon imaging corresponds with CD68+ lysosomes, it was then permissible to assess the lipofuscin content of CX3CR1+ cells responding to CMBs. By quantifying the percent area of lipofuscin puncta contained in the CX3CR1+ CMB aggregate, a significant increase in lipofuscin 1 day after CMB was quantified in all groups (Two-way mixed effects model ANOVA, main effect of time: $F_{(3.166, 326.9)} = 31.41$, $p<0.0001$; D0 versus D1: $p<0.0001$; Fig. 35A-B). Notably, in DB mice the increase in the proportional area of lipofuscin that co-localized with eGFP expression was significantly greater than that of the NDB group (Two-way mixed effects model ANOVA, main effect of treatment: $F_{(2,123)} = 7.708$, $p=0.0005$; NDB versus DB, , $p<0.0001$; Fig. 35A-B). Furthermore, CLR treatment effectively normalized this increase in lipofuscin in diabetic CMBs to NDB levels regardless of whether its effects were considered chronically (Two-way mixed effects model ANOVA, main effect of treatment: $F_{(2,123)} = 7.708$, $p=0.0005$; NDB versus DB, $p=0.0007$; Fig. 35B) or at the D1 peak in lipofuscin (One-way ANOVA: $F_{(2, 121)} = 4.313$, $p=0.0155$; NDB versus CLR DB, $p=0.0366$; DB versus CLR DB, $p=0.0322$; Fig. 35C). To confirm that these changes in

lipofuscin content related specifically to cells responding to a CMB, the lipofuscin content of other CX3CR1+ cells distal to the CMB (>40µm) was also examined (*Grey lines*, Fig. 35B). Small lipofuscin puncta were identified in these cells and, although a slight increase in lipofuscin content was observed after D1, it did not differ significantly between groups (Two-way mixed effects model ANOVA, main effect of treatment: $F_{(1,85)} = 1.449$, $p = 0.2321$, main effect of time: $F_{(2.838,210.7)} = 2.869$, $p = 0.0403$; Fig. 35B). This supports the notion that changes in lipofuscin content are a property of the CX3CR1+ cells near CMBs specifically, and that microbleeds in DB mice are associated with greater phagocytic activity than their NDB counterparts. In relation to microvascular fate following CMB, a significantly greater percent area of lipofuscin at D1 was recorded in CX3CR1+ cells associated with microvessels that were ultimately eliminated compared to those that repaired (Unpaired Student's t-test, $p < 0.0001$; Fig. 35D).

To extend the investigation of lipofuscin content in CMBs to the context of Mac2+/TMEM119- cells specifically, these cells, as well as Mac2+/TMEM119+ and Mac2-/TMEM119+ microglia, were identified via confocal imaging of immunofluorescence-labelled diabetic brain slices. Then, the same cells were relocated using 2-photon microscopy to determine their relative lipofuscin content (Fig. 36A-B). Although the percent area of lipofuscin did not vary significantly between the Mac2+ cell phenotypes, Mac2+/TMEM119- macrophages exhibited significantly greater lipofuscin content than Mac2-/TMEM119+ cells (One-way ANOVA: $F_{(2, 42)} = 3.627$, $p = 0.0352$; Mac2+/TMEM119- versus Mac2-/TMEM119+, $p = 0.0345$, Fig. 36B). Taken together, these findings suggest that the elevated lipofuscin content of Mac2+/TMEM119- cells specifically may contribute to the enhanced lipofuscin signal identified at the site of eliminated diabetic microvessels. Furthermore, the normalization of lipofuscin content by CLR may support this notion since it excludes Mac2+/TMEM119- cells from CMBs.

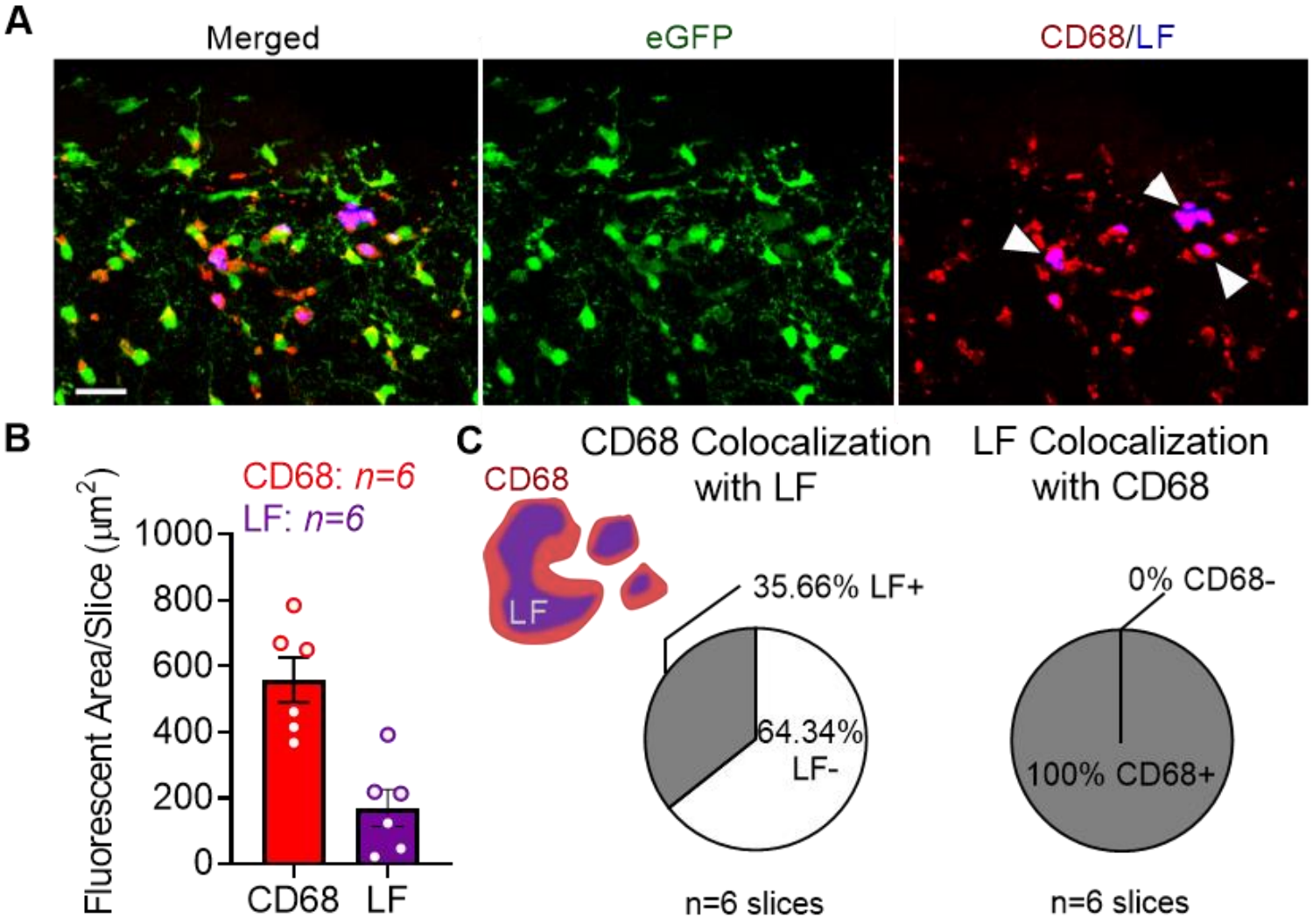
A
Merged
eGFP
CD68/LF
B
CD68: n=6
LF: n=6
Fluorescent Area/Slice (µm²)
1000
800
600
400
200
0
CD68
LF
C
CD68 Colocalization with LF
CD68
LF
35.66% LF+
64.34% LF-
n=6 slices
LF Colocalization with CD68
0% CD68-
100% CD68+
n=6 slices

Figure 34. Lipofuscin autofluorescence reliably co-localizes with CD68 immunolabelling in CX3CR1+ cells.

A. Maximum intensity projections of 2-photon images of brain slices from a nondiabetic mouse, fixed 1 day after the ablation of an arteriole, and labelled with immunofluorescent markers for CD68. Lipofuscin autofluorescence (LF) was imaged at 750nm and CD68 immunofluorescence was visualized at 900nm for excitation of a Cy5-conjugated secondary antibody. Colocalization of LF with CD68 immunofluorescence is indicated by *white arrowheads*. Scale bar indicates 20 µm. ***B.*** Summary bar graph describes the average area of CD68 fluorescence and LF in fixed brain slices imaged using 2-photon microscopy. Slices, relevant numbers indicated on the graph, were collected from *n=2* NDB mice. ***C.*** Illustration describes co-localization of LF with CD68+ lysosomes/endosomes of CX3CR1+ macrophages. (*left*) Pie chart summarizes the finding that there is a greater proportion of CD68+ particles that do not colocalize with LF, but that there is a substantial amount CD68 immunostaining that does contain LF. (*right*) Pie chart highlights the observation that all LF autofluorescence was identified in CD68+ particles within CX3CR1+ macrophages. Error bars indicate mean± SEM.

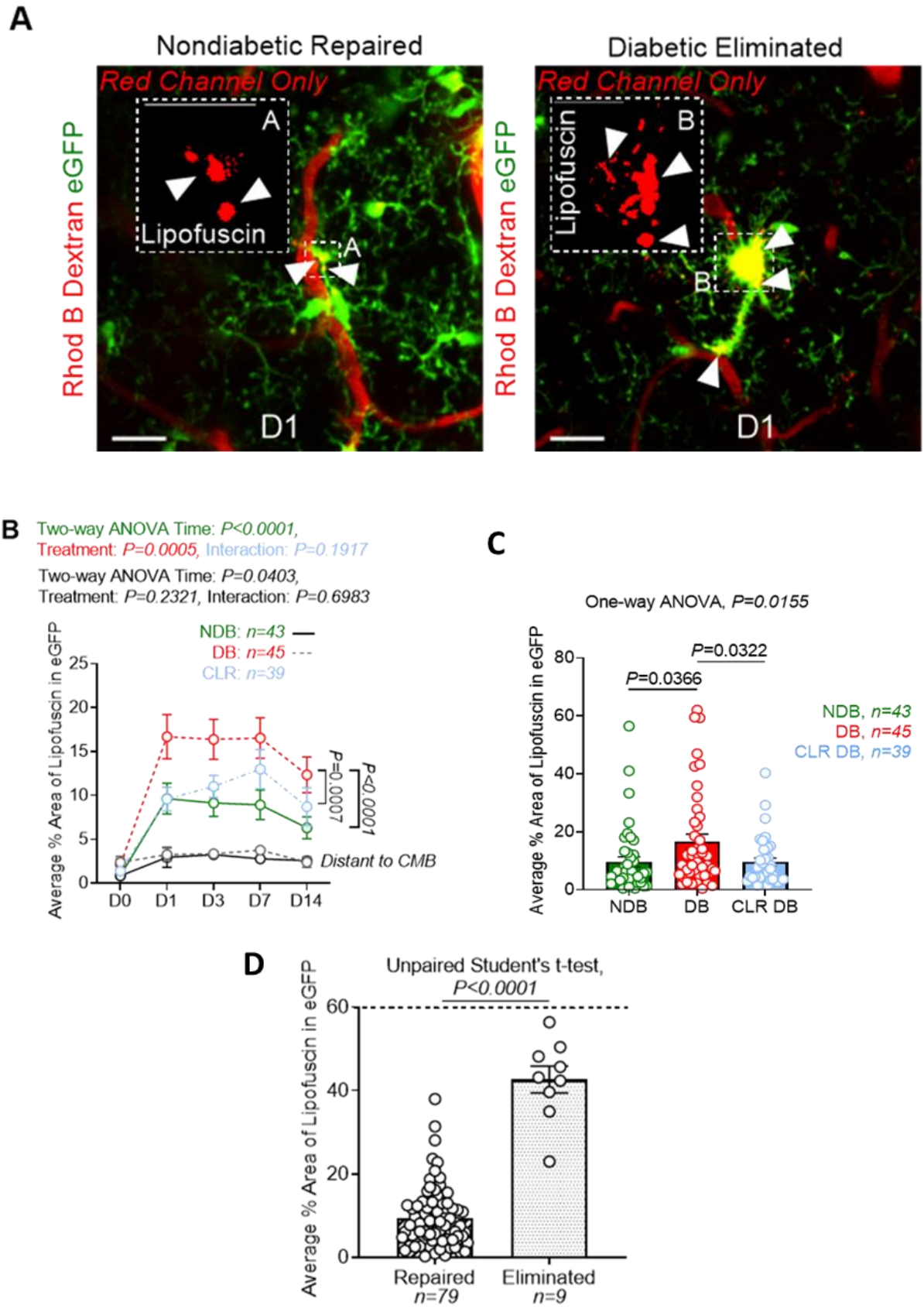
A
Nondiabetic Repaired
Diabetic Eliminated
Red Channel Only
Rhod B Dextran eGFP
Lipofuscin
A
B
D1
B
Two-way ANOVA Time: P<0.0001,
Treatment: P=0.0005, Interaction: P=0.1917
Two-way ANOVA Time: P=0.0403,
Treatment: P=0.2321, Interaction: P=0.6983
NDB: n=43
DB: n=45
CLR: n=39
Average % Area of Lipofuscin in eGFP
P=0.0007
P<0.0001
Distant to CMB
D0
D1
D3
D7
D14
C
One-way ANOVA, P=0.0155
P=0.0322
P=0.0366
NDB, n=43
DB, n=45
CLR DB, n=39
NDB
DB
CLR DB
D
Unpaired Student's t-test,
P<0.0001
Repaired
n=79
Eliminated
n=9

Figure 35. Clodronate treatment normalizes pathologically elevated lipofuscin content in CX3CR1+ macrophages associated with microbleeds.

A. Representative 2-photon imaging areas of NDB repaired and DB eliminated microvessels 1 day following CMB induction. Autofluorescent lipofuscin particles (*white arrowheads*) are yellow puncta in the eGFP-expressing aggregate of CX3CR1+ cells responding to the CMB. Scale bars represent 20 µm. *Inlays* show enlarged binarized and pseudo-coloured images of autofluorescent lipofuscin particles (*white arrowheads*) visible in the red channel during 2-photon imaging. Scale bars represent 10 µm. **B.** Graph summarizing changes in the proportional content of lipofuscin autofluorescence within eGFP-expressing cellular aggregate, over the 14-day imaging period, at the site of CMB (*coloured lines*) and in distant CX3CR1+ cell bodies (*grey lines*). **C.** Summary bar graph demonstrates that CLR returns lipofuscin content in diabetic CMBs to NDB levels when quantified 1 day post-CMB. **D.** Summary bar graph highlighting the significant increase in the proportional area of lipofuscin autofluorescence in the eGFP-expressing aggregate associated with eliminated microvessels relative to recanalized vessels. 1-5 CMBs were quantified in each animal; *n=17* NDB, *n=14* DB, and *n=8* DB CLR mice were used for **B.** and **C.** and vessels from *n=17* NDB and *n=14* DB were pooled to constituted **D.** Unpaired Student's t-tests assessed differences between 2 groups and one-way ANOVAs determined differences between 3 or more groups; post-hoc Tukey's multiple comparisons test was used to identify specific group differences. Two-way mixed-effects model ANOVA was used to qualify changes in lipofuscin content in CX3CR1+ cells between groups over time. All relevant comparisons were made, but only significant results are shown on the graphs. Error bars represent mean± SEM.

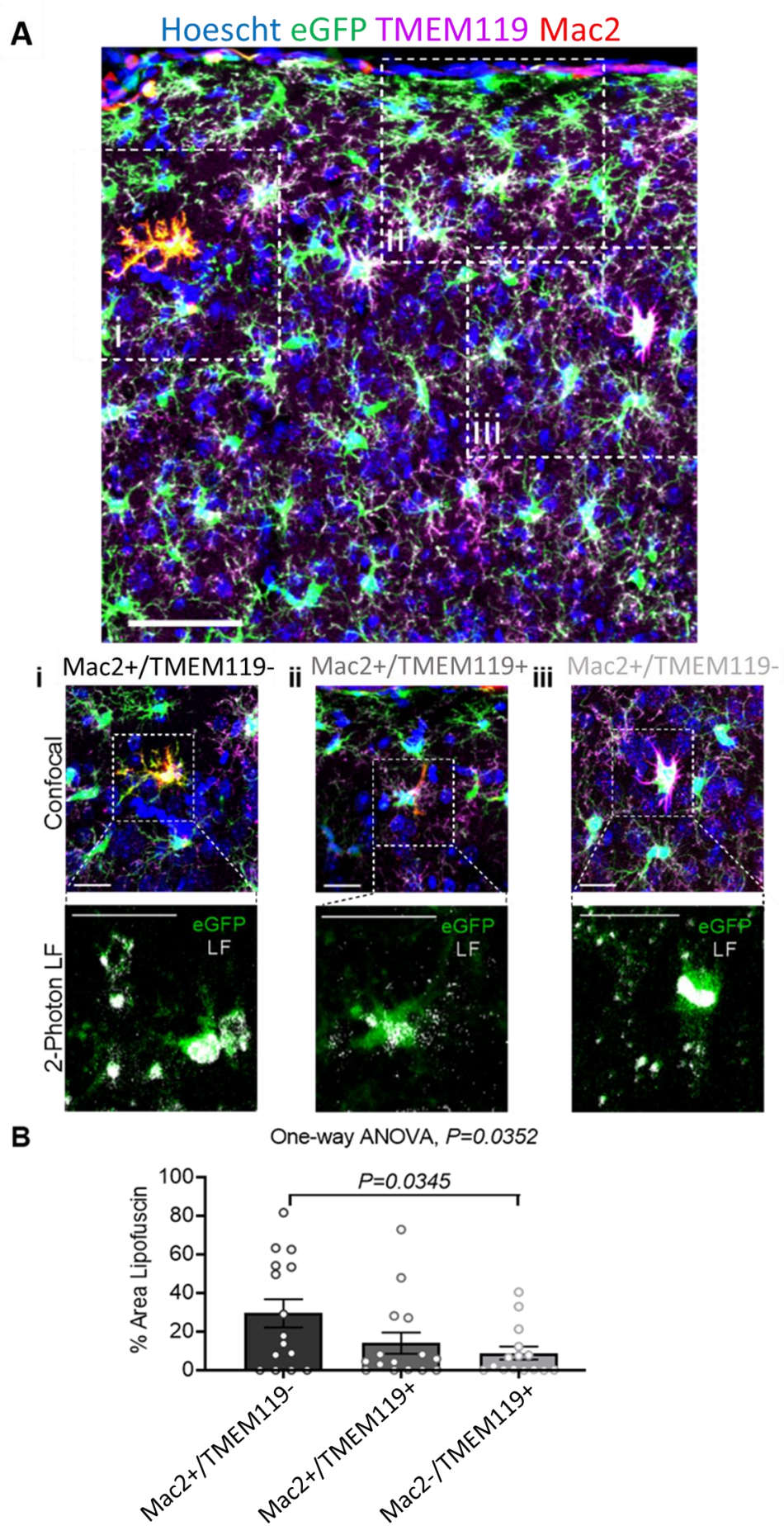
A
Hoescht eGFP TMEM119 Mac2
i
ii
iii
i Mac2+/TMEM119-
ii Mac2+/TMEM119+
iii Mac2+/TMEM119-
Confocal
2-Photon LF
eGFP
LF
B
One-way ANOVA, P=0.0352
P=0.0345
% Area Lipofuscin
100
80
60
40
20
0
Mac2+/TMEM119-
Mac2+/TMEM119+
Mac2-/TMEM119+

Figure 36. Lipofuscin content is significantly elevated in Mac2+/TMEM119- cells compared to homeostatic Mac2-/TMEM119+ cells.

A. Maximum intensity projection of a confocal image acquired in uninjured diabetic somatosensory cortex with examples of Mac2+/TMEM119-, Mac2+/TMEM119+, and Mac2-/TMEM119+ cells, visualized using immunofluorescent labelling. Scale bar represents 50 µm. (***i***) Mac2+/TMEM119- , (***ii***) Mac2+/TMEM119+, and (***iii***) Mac2-/TMEM119+ cells were identified using confocal microscopy and then located *in situ* with 2-photon imaging. eGFP fluorescence was excited by tuning the 2-photon laser to 900nm and a lipofuscin signal (*white puncta*) was elicited with an excitation wavelength of 750nm. Scale bars represent 20 µm. ***C.*** Summary bar graph depicting the average percent area of eGFP that also contained lipofuscin signal in Mac2+/TMEM119-, Mac2+/TMEM119+, and Mac2-/TMEM119+ cells. Data was acquired from 16 areas in 7 diabetic mice; 2-3 areas were averaged per animal to comprise an individual data point. One-way ANOVA with post-hoc Tukey's multiple comparison's test was used to compare the amount of lipofuscin observed in different cell types. Error bars represent mean± SEM.

To further explore the potential role of phagocytosis in microvascular elimination, changes in other relevant signalling pathways, TREM2 and Axl, were investigated. TREM2 has been implicated in microglial synaptic pruning[463] and is a characteristic marker of DAM[337,460], while AXL has been shown to act via an independent pathway to mediate phagocytosis of apoptotic neurons[300]. This extension beyond consideration of lipofuscin alone as an assessment of phagocytosis was necessary given that lipofuscin is, at best, an indirect gauge of this process. Using NDB, DB, and CLR DB mice, CMBs were induced through thin skull windows, brains were harvested 3 days post-CMB, and coronal slices of cortex containing CMBs were immunostained with various markers for phagocytosis prior to confocal imaging.

Analysis of the extent of CD68 immunostaining in CMBs confirmed the results of the lipofuscin analysis, showing a significant increase in DB CMBs relative to NDBs; CLR also effectively normalized diabetic CD68 expression (One-way ANOVA: $F_{(2, 51)} = 5.857$, $p=0.0051$; NDB versus DB, $p=0.0222$; DB versus CLR DB, $p=0.0078$; Figs. 37A-B). Interestingly, although they were generally larger in the DB condition, the number of CD68-labelled particles did not vary significantly between groups. (One-way ANOVA: $F_{(2, 51)} = 0.4932$, $p=0.6135$; Fig. 37A-B). This suggests that either it was not possible to resolve individual lysosomes/endosomes or that the number of these structures was not altered by DM. TREM2 expression was significantly elevated in diabetic CMBs relative to both NDB and CLR DB groups, indicating that increased phagocytosis may result from pathological activity of this receptor in response to inflammation during diabetes (One-way ANOVA: $F_{(2, 51)} = 7.112$, $p=0.0019$; NDB versus DB, $p=0.0058$; DB versus CLR DB, $p=0.0051$; Fig. 37C-D). Axl immunostaining, however, was only weakly or negligibly expressed in CMBs from all groups and no significant differences were discernable (One-way ANOVA: $F_{(2, 33)} = 1.407$, $p=0.2592$; Fig. 37E-F).

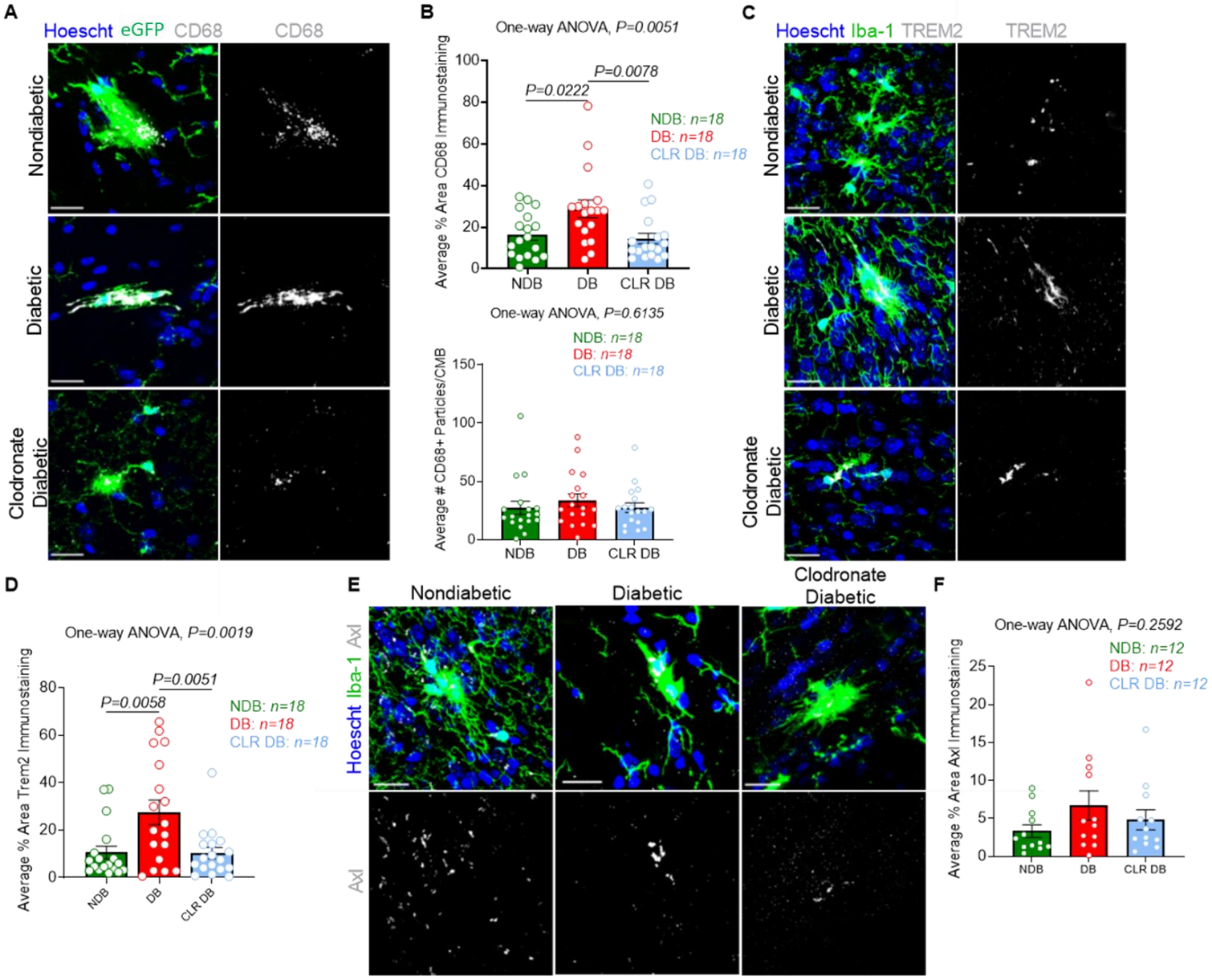
A
Hoescht eGFP CD68
CD68
Nondiabetic
Diabetic
Clodronate Diabetic
B
One-way ANOVA, P=0.0051
Average % Area CD68 Immunostaining
P=0.0222
P=0.0078
NDB: n=18
DB: n=18
CLR DB: n=18
NDB
DB
CLR DB
One-way ANOVA, P=0.6135
Average # CD68+ Particles/CMB
C
Hoescht Iba-1 TREM2
TREM2
D
One-way ANOVA, P=0.0019
Average % Area Trem2 Immunostaining
P=0.0058
P=0.0051
E
Nondiabetic
Diabetic
Clodronate Diabetic
Hoescht Iba-1 Axl
Axl
F
One-way ANOVA, P=0.2592
Average % Area Axl Immunostaining
NDB: n=12
DB: n=12
CLR DB: n=12

Figure 37. CD68 and TREM2 immunostaining are significantly increased in diabetic microbleeds and normalized with clodronate.

A. Representative maximum intensity projections of confocal images of CMBs in the somatosensory cortices of NDB, DB, and DB CLR mice; tissue was harvested 3 days post-CMB. Slices were immunolabelled for CD68 and cell nuclei were stained with Hoechst 33342. **B.** Summary bar graphs of (*top*) the average percent area of eGFP that also expressed CD68 in CMBs and (*bottom*) the average number of CD68 particles counted in the CX3CR1+ eGFP-expressing CMB cellular response. CMBs from NDB (*n=6*), DB (*n=6*), and CLR DB (*n=6*) mice were used. **C.** Representative maximum intensity projections of CMBs imaged in the somatosensory cortex of NDB, DB, and CLR DB mice; tissue was harvested 3 days post-CMB. Slices were immunolabelled for TREM2 and Iba-1, and cell nuclei were identified with Hoechst 33342. ***D.*** Summary bar graph highlighting a significant increase in the proportional amount of TREM2 immunostaining in CMBs from DB mice relative to those from either NDB or DB CLR groups. Mice from NDB (*n=6*), DB (*n=6*), and CLR DB (*n=6*) groups were used to generate this data. **E.** Representative maximum intensity projections of confocal images of CMBs in the somatosensory cortices of NDB, DB, and CLR DB mice; tissue was harvested 3 days post-CMB. Slices were immunolabelled for Axl and Iba-1, and cell nuclei were labelled with Hoechst 33342. ***F.*** Summary bar graph indicating trace amounts of Axl immunostaining in CMBs that did not vary significantly between NDB (*n=5* mice), DB (*n=5* mice), and CLR DB (*n=4* mice) groups. In all experiments, 2-3 CMBs were analyzed from each mouse and data points represent individual CMBs. Scale bars are 20 µm. One-way ANOVAs with post-hoc Tukey's multiple comparison's tests were used to assess group differences. All relevant comparisons were performed, but only significant results are indicated on graphs. Error bars represent mean± SEM.

4.4 Discussion

The present work sought to improve our understanding of the cellular mechanisms contributing to microvascular repair in the diabetic brain and uncovered a unique population of Mac2+/TMEM119- cells that were strongly associated with pathological capillary regression. Furthermore, although chronic insulin therapy failed to ameliorate microvascular loss, providing CLR as an intervention effectively rescued CMB repair in diabetics, likely by depleting infiltrative Mac2+/TMEM119- cells from the circulation. In addition to depleting peripheral macrophages, CLR, a bisphosphate commonly prescribed for rheumatic patients[464,465], reduces circulating levels of cytokines such as ILs 1 and 6, TNFα, and prostaglandins; these properties underlie its profound anti-inflammatory effects[464–466]. The efficacy of CLR in mitigating vascular pathology supports the direction of recent clinical studies which have sought to target inflammation in type 1 DM in efforts to ameliorate pervasive complications of the disease that are incurable with insulin therapy alone[214,215,421]. Although other anti-inflammatory treatments including DEX and blocking IFN signalling facilitated the acute recovery of BBB integrity following CMB[25], the fact that these drugs did not support the lasting repair of damaged microvessels underscores the putative role of peripherally-derived immune cells in this process.

The heterogeneity of microglia and BAM phenotypes under homeostatic and disease conditions has been increasingly highlighted[36,38,261,414,449]. Indeed, the present study is not the first to identify Mac2-expressing cells in the brain. A comprehensive characterization of microglial heterogeneity under CSF1R inhibition by Zhan et al. highlighted a population of Mac2+ microglia, present in the healthy CNS, that survived PLX5622 treatment[443]. These Mac2+ cells were highly proliferative, and following removal of PLX5622 the proportional contribution of these cells to the repopulated microglial pool increased significantly[443]. Others

have identified the key role that Mac2, also known as Galectin3, plays in regulating microglial activation and proliferation in stroke[467] and in transforming the microglial phenotype into its amoeboid, phagocytic form[468]. The present study bolsters these findings and further characterizes 2 phenotypes of Mac2+ cells: Mac2+/TMEM119+ cells observed in both healthy and diseased conditions and Mac2+/TMEM119- cells which act as key modulators of microvascular fate in diabetes, potentially through enhanced phagocytic activity. Since Mac2 is a secreted galactoside binding protein that is highly expressed on myeloid cells[73,74], whether these Mac2+ cells arise from peripherally-derived monocytes is an important question. Using lineage tracing[443] and a transgenic chimeric animal model[467], it has been suggested that Mac2+ cells in the homeostatic and PLX5622-treated brain represent a subpopulation of intrinsic microglia rather than infiltrating leukocytes. In the present study, Mac2+/TMEM119- cells were prevented from aggregating to diabetic CMBs by CLR, coincident with the significant depletion of circulating monocytes, but Mac2+/TMEM119+ cells were unaffected by this treatment. Given that MDMs are known to migrate to sites of cerebrovascular trauma[27,28,469,470], in combination with the CLR data, this implies that the unique population of Mac2+/TMEM119- cells responding to CMBs may arise from a bone marrow-derived myeloid lineage. However, it is likely that the Mac2+/TMEM119+ cells which were found in the healthy parenchyma, identified at CMBs in all groups, and which exhibited no response to CLR may represent a subtype microglia that are present under homeostatic conditions and exhibit a monocyte-like gene expression profile.

Given the hemorrhagic nature of CMBs, which invariably produce substantial cellular debris, and the fact that microglia, BAMs, and MDMs are professional phagocytes, assessment of phagocytosis pathways was a clear target for further understanding the extensive pruning of diabetic vessels. Indeed, studies of ischemic retinopathy highlighted the presence of

macrophages at the sites of regressing vessels[471]. Macrophages have also been observed to phagocytose EC membrane particles even before obvious vascular regression[472,473], and elevated phagocytic activity by CX3CR1+/CD11b+ macrophages in the diabetic rat retina is thought to precede the development of retinopathy[35,452]. Lipofuscin has been used as an indirect marker of phagocytosis because it represents the autofluorescent signal arising from the excitation of lipid particles encapsulated in lysosomal compartments[474–476]. Building on the finding that lipofuscin content was elevated in diabetic CMBs and normalized with CLR, it was not surprising to observe similar results with CD68 immunostaining, given the prior confirmation of the overlap between these markers. Support for this conjecture is further evidenced by results from stroke models indicating that the vasculature of the penumbra is phagocytosed by microglia, coincident with increased CD68 expression, even if vessels were still perfused[425]. AXL and TREM2 expression were also probed to expand the mechanistic scope of this analysis given their roles in independent phagocytic pathways, as well as the fact that they are both expressed by brain-resident macrophages as well as peripheral myeloid cells. Interestingly, although TREM2 expression increased at the site of diabetic CMBs, AXL immunostaining was negligible in the CX3CR1+ cellular aggregate at CMBs in all groups. Since Mac2 itself can mediate phagocytosis through the activation of phosphoinositide 3-kinase (PI3K), a pathway that is linked to TREM2 but not AXL,[307,459,468,477–481] these findings may indicate that upregulated phagocytosis in diabetic CMBs could occur in Mac2-expressing cells largely through the activity of TREM2.

In summary, these findings underscore the heterogeneity of the cellular constituents of CMBs and identify a novel cellular target, peripherally-derived Mac2+/TMEM119- macrophages, that exhibits upregulated phagocytic activity and is strongly associated with the pathological elimination of microvasculature in type 1 DM.

CHAPTER 5: GENERAL DISCUSSION

5.1 Summary

Micro- and macrovascular pathology is a common complication associated with type 1 DM[2,3]. CMBs are unpredictable microvascular hemorrhages that occur more frequently in the diabetic brain and their compounding incidence has been correlated with declining cognitive function[7,8,10]. Furthermore, since tissue repair is compromised by type 1 DM[482], a key question arises: how does this disease affect the resolution of microvascular insults in the cortex? Specifically, does the increased prevalence of vascular disease in type 1 DM combine with compromised repair mechanisms to exacerbate pathology, or are microvascular insults repaired effectively despite their elevated incidence? Furthermore, since various immune cells, particularly microglia, have been implicated as key players in healing the damaged vasculature [22,24,25,27,28], it is also crucial to understand whether these functions are perturbed in chronic inflammatory diseases such as type 1 DM. Indeed, even in the healthy brain our understanding of the cellular mechanisms involved in the repair of CMBs is limited. The present work sought to answer these pressing questions through the identification and completion of 2 aims: 1) identify how type 1 DM affects microglial/macrophage responses to, and repair of, CMBs and 2) determine the cellular mechanisms that modulate repair of CMBs in type 1 DM.

In aim 1, *in vivo* 2-photon longitudinal imaging of CMBs in a mouse model of type 1 DM revealed the diminished repair of microvessels in the diabetic brain. Indeed, 20% of vessels targeted with CMBs were eliminated from the cerebral circulation of diabetic mice within 3 days following the insult, while these injuries were always repaired in the healthy context (Fig. 38). Furthermore, the limitations of chronic insulin therapy in ameliorating diabetic complications were underscored by the fact that diabetic animals receiving this treatment still lost ~18% of

damaged vessels (Fig. 38). Building on previous work showing that anti-inflammatory treatments reinvigorate acute microglial responses to CMBs in type 1 DM[25], these regimens were replicated in an effort to improve long-term microvascular repair in this disease. Although these treatments modulated CX3CR1+ cellular responses to CMBs, they proved ineffective in restoring microvascular repair in diabetic animals. Notably, morphological characteristics of the CX3CR1+ cellular response to CMBs failed to predict microvascular fate, and elimination of brain-resident macrophages via PLX5622 treatment further supported the idea that the responses of innate CNS immune cells was not necessary for vascular repair since damaged vessels with no CX3CR1+ cellular aggregate reliably regained blood flow. However, the fact that microvessels without these responses exhibited lasting vascular leakage and aneurisms supports previous work highlighting the role of microglia in restoring BBB integrity[24,25].

By combining parallel approaches of longitudinal *in vivo* 2-photon imaging and confocal imaging of immunohistochemically-labelled cortical tissue in Aim 2, a unique population of Mac2+/TMEM119- cells were discovered in diabetic CMBs. The presence of these macrophages strongly associated with microvascular elimination and they were never identified in the CMB milieu of healthy animals (Fig. 38). Interestingly, these cells were also found in the uninjured parenchyma of diabetic and PLX5622-treated mice, but not in the nondiabetic brain (Fig. 38). Of note, CMBs in all groups, even healthy animals, were associated with heterogenous CX3CR1+ cell phenotypes including Mac2+/TMEM119+, Mac2-/TMEM119+, and Mac2-/TMEM119- variants (Fig. 38). CD206+ BAMs were not identified in the cellular responses to CMBs in any group, suggesting that these sentinel cells did not generally contribute to the resolution of these insults. Mac2 is expressed by peripheral immune cells[141,453] but, since others have identified diverse DAM phenotypes[337,460,483] and Mac2+ cells in the brain have been hypothesized to be of

microglial lineage[443], an investigation of their origin was necessary. Using CLR to deplete circulating phagocytic leukocytes, Mac2+/TMEM119- cells were reliably excluded from diabetic CMB responses but Mac2+/TMEM119+ cells were unaffected (Fig. 38). This dichotomous response suggests that the former phenotype may be bone marrow-derived MDMs, while the latter may constitute a previously described proliferative microglial subtype[443]. Phagocytosis was also investigated as a putative target for dysregulation in type 1 DM that may result in macrophage-induced vessel loss. Indeed, both lipofuscin and CD68 expression were enhanced in diabetic CMBs and the extent of lipofuscin autofluorescence specifically correlated with microvascular elimination (Fig. 38). MDMs may exhibit enhanced phagocytic capacity relative to homeostatic microglia[269,270,302]; this is in line with the present finding that Mac2+/TMEM119- cells contain significantly more lipofuscin than their Mac2-/TMEM119+ counterparts (Fig. 38). TREM2 expression, which has been identified as a common marker of DAM[337,460,483], was also increased in the diabetic CMB aggregate. CLR treatment normalized these phagocytic markers in diabetic mice, coincident with the normalization of microvascular repair (Fig. 38). These findings provide further evidence that the infiltration of the diabetic CMB milieu by phagocytic, peripherally-derived macrophages, may contribute to microvascular elimination.

Taken together, these data reveal that type 1 DM compromises microvascular repair in the neocortex and implicate a peripherally-derived, phagocytic Mac2+/TMEM119- macrophage in this phenomenon. Furthermore, this dissertation highlights the diverse immune cell response to CMBs and advances our understanding of the cellular mechanisms involved in pathological capillary pruning. These discoveries may have clinical implications for patients with type 1 DM as they improve our understanding of its associated microangiopathy and provide impetus for the use of adjuvant therapies, such as CLR, to ameliorate this insidious complication.

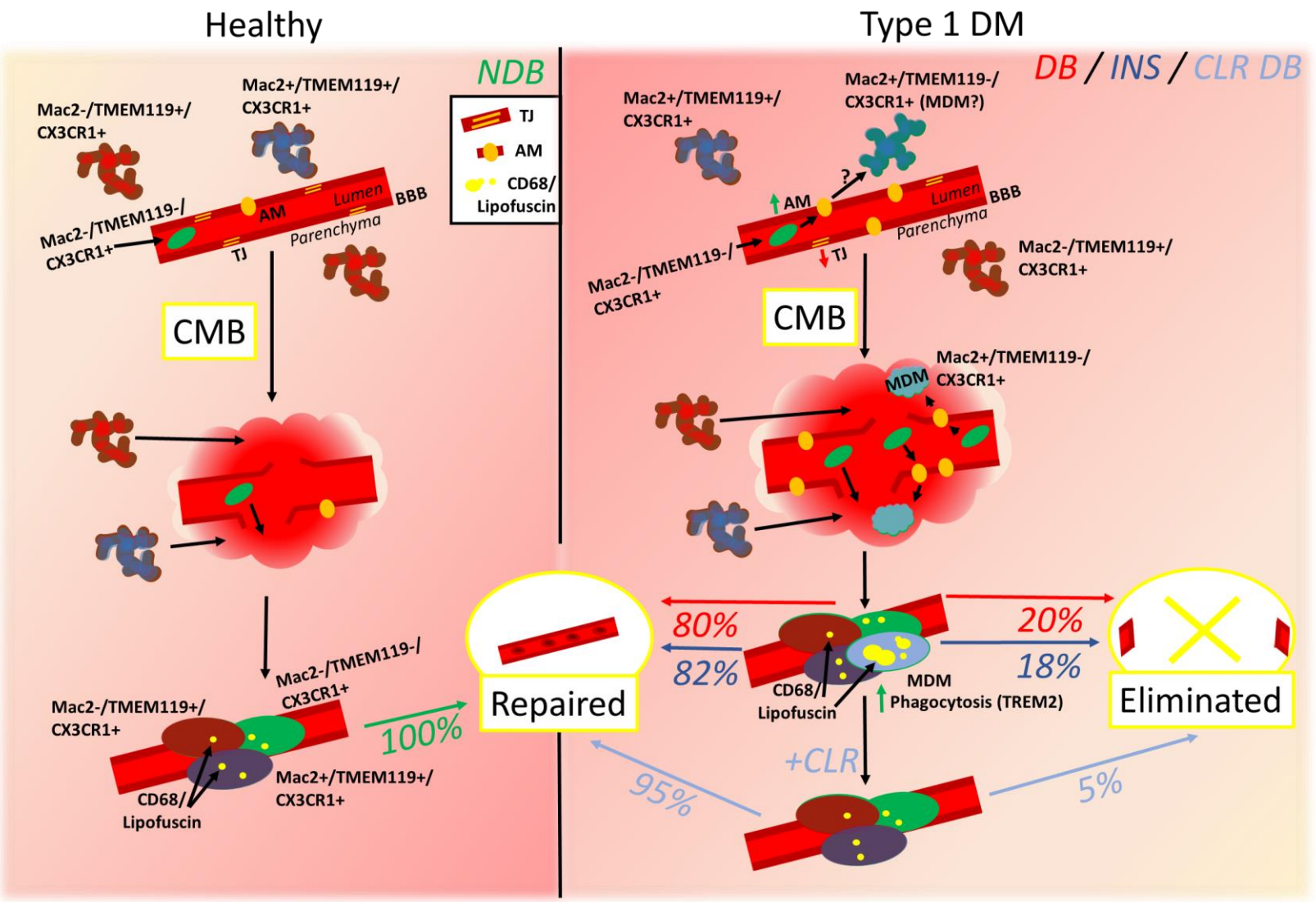
Healthy
Type 1 DM
NDB
DB / INS / CLR DB
TJ
AM
CD68/
Lipofuscin
Mac2-/TMEM119+/
CX3CR1+
Mac2+/TMEM119+/
CX3CR1+
Mac2-/TMEM119-/
CX3CR1+
Lumen
BBB
Parenchyma
TJ
CMB
Mac2+/TMEM119-/
CX3CR1+ (MDM?)
AM
?
MDM
Repaired
Eliminated
80%
82%
20%
18%
MDM
Phagocytosis (TREM2)
100%
+CLR
95%
5%

Figure 38. Summary model of the effects of type 1 diabetes mellitus on cerebral microbleed repair.

Illustration comparing microbleed repair in the neocortex of healthy and type 1 DM mice. (*left*) In the NDB parenchyma, Mac2-/TMEM119+/CX3CR1+ homeostatic and proliferative Mac2+/TMEM119+/CX3CR1+ microglia are present in the absence of injury, but Mac2-/TMEM119-/CX3CR1+ peripheral phagocytes are excluded from the CNS by the BBB. After a CMB, brain-resident microglia migrate towards the injury and circulating leukocytes may enter the brain via the physical disruption of the BBB and contribute to the CMB response. Some phagocytic activity occurs in the CMB milieu, indicated by lipofuscin content or CD68 expression, but 100% of CMBs induced in healthy, NDB (*green text*) mice are repaired. (*right*) In the diabetic cortex, Mac2-/TMEM119+/CX3CR1+ and Mac2+/TMEM119+/CX3CR1+ microglia can be found, as well as Mac2+/TMEM119-/CX3CR1+ macrophages, in the absence of injury. Hyperglycemic toxicity reduces TJ protein expression, coincident with an upregulation of endothelial AMs, and may facilitate the transmigration of leukocytes into the CNS; these cells transform into MDMs and could contribute to the parenchymal population of Mac2+/TMEM119-/CX3CR1+ cells. In response to a CMB, brain-resident microglia, putative engrafted MDMs, and circulating Mac2-/TMEM119-/CX3CR1+ phagocytic leukocytes infiltrate the microbleed milieu. Increased AM expression may further facilitate MDM binding near the bleed site. High phagocytic activity in MDMs, mediated by increased TREM2 expression and evidenced by elevated CD68/lipofuscin content, compromises microvascular repair and leads to elimination of 20% and 18% of injured vessels in untreated DB (*red text*) and DB mice receiving chronic insulin therapy (*dark blue text*), respectively. Treatment of DB mice with CLR (*light blue text*) rescues microvascular repair rates to 95% by reducing local phagocytic activity through the exclusion of MDMs from the CMB response. AM: Adhesion molecule.

5.2 Type 1 diabetes mellitus disrupts repair of cerebral microbleeds with implications for impaired cognitive function

The prevalence of microvascular disease throughout the body is well-described in type 1 DM and contributes to the manifestation of numerous complications including neuropathy, retinopathy, and CMBs[2,127,209,210,271]. Furthermore, diabetes impairs wound healing which, in the periphery, is hypothesized to arise, at least in part, as a product of chronic cytokine production and reduced blood flow due to microangiopathy[435,436]. Since CMBs occur with greater frequency in diabetic patients[2,3], the combination of an increased propensity for vascular insults and impaired resolution of pathology could progressively reduce microvascular density in the CNS. Bolstering these concerns are converging pieces of evidence that characterize diminished microvascular density in the brains of diabetic patients[8,10] and the prevalence of cognitive decline and dementia in this population[2,3]. Furthermore, although mechanisms of vascular dysregulation have been characterized in the development of diabetic retinopathy[127,271], studies examining the resolution of known vascular pathology, microbleeds, *in vivo* in the cortex are lacking.

The present work highlights a significant disruption in the repair of injured microvessels after CMB, leading to the penultimate elimination of impacted vessels from the cerebral circulation, in a mouse model of type 1 DM. Most patients with type 1 DM use chronic insulin treatment to manage their hyperglycemia; however, in the present study, normalizing murine blood glucose in this way failed to prevent microvascular loss. These findings are in line with various clinical studies that outline how insulin therapy is ineffective in mitigating the vascular risk factors associated with type 1 DM[14–16,130]. Capillaries are responsible for the delivery of metabolic substrates to the CNS and the removal of waste products, thereby playing a crucial role in sustaining neuronal activity[132–134]; remarkably, although they comprise >90% of the CNS

vascular length[49],the loss of even a few vessels can result in consequences for brain function[7]. Indeed, elimination of the microvascular arbour associated with a single penetrating arteriole is sufficient to induce behavioural deficits in rodents[7] and just 4 CMBs is correlated with impaired cognitive function in humans[8]. Although CMBs are known to occur spontaneously in the healthy brain, the fact that injured microvessels reliably repaired in nondiabetic animals in the present study suggests that they generally recanalize under nonpathological conditions. Taken together, these data provide a putative explanation for the manifestation of cognitive decline and dementia in patients with type 1 DM: compounding CMBs result in progressive microvascular loss that contributes to the reduced microvascular density observed in diabetic patients, and consequent cortical hypoperfusion compromises cognitive function.

An alternative mechanism by which CMBs could contribute to cognitive decline in type 1 DM is by releasing toxins from the circulation into the vulnerable brain parenchyma, resulting in damage to local neuronal circuits[15,484,485] (alternatively, see Rosidi et al. who showed that CMBs induced transient dendritic retraction but not lasting neuronal degeneration[405]). Specifically, the expulsion of fibrinogen during vascular rupture and the presence of iron released by lysed RBCs has been shown to contribute to neuronal degeneration and demyelination[16,18,20,87,92]. Increased microvascular insults in type 1 DM could propagate this damage and, given the poorer tissue healing prognosis in diabetes[435,436], lead to lasting cognitive impairments if neuronal components are not repaired. Microglial responses to CMBs are well-known to exhibit robust, rapid responses to vessel rupture and quickly stem the leakage of vascular constituents[22,24,25,28], likely protecting nearby neuronal circuitry from damage. The present data involving the characterization of microvascular repair in PLX5622-treated animals further underscores the important role that CX3CR1+ cells play in mitigating vascular leakage, since capillaries without

cellular responses exhibited prolonged leakage and hemorrhage. Moreover, the Brown lab has shown previously that the immediate microglial responses to CMBs are compromised in type 1 DM, leading to lasting extravasation of plasma from damaged vessels[25]. This observation supports the idea that impaired neuronal function arising from the leakage of toxins into the parenchyma could be exacerbated in diabetes due to a combination of increased CMB incidence and stunted microglial responses, thereby contributing to cognitive decline. Of course, it is conceivable that a combination of these mechanisms (hypoperfusion due to microvascular loss and neuronal damage arising from greater vascular leakage) could compound to trigger and/or exacerbate symptoms of dementia in type 1 DM. Future investigations may determine the relative contributions of these models to changes in cognitive function and behaviour.

It is worth considering as well that the increased permeability of the BBB, both in terms of compromised TJ protein expression[380,391] and elevated endothelial transcytosis[390], associated with type 1 DM could contribute to the chronic diffusion of toxins into the brain even in the absence of vascular rupture. In this context, cognitive decline may reflect BBB permeability and the extent of neuronal circuit exposure to plasma constituents. Since BBB disruption could also increase the risk of microbleeds, a greater prevalence of CMBs could correlate with cognitive decline without being its cause. Finally, whether the prevalence of spontaneous CMBs is increased in the STZ model of type 1 DM was not investigated in the present study due to their unpredictable nature, in terms of their incidence and localization, and the subsequent challenges associated with their accurate identification *in situ*. Therefore, although it was not possible to replicate clinical findings of increased CMB incidence in type 1 DM[2,408], this study represents an important characterization of comorbid deficits in microvascular repair that could, at least in part, explain the prevalence of cognitive decline in this disease.

5.3 Heterogenous immune cell phenotypes respond to cerebral microbleeds

The heterogeneity and dynamic nature of microglial phenotypes in the CNS has become increasingly appreciated as studies utilizing single-cell RNA sequencing and fate mapping techniques probe the diversity of this population with greater fidelity[276,308,309]. The present study underscores the plurality of microglial phenotypes in healthy and disease conditions, and in the context of acute CNS injury. Furthermore, the discovery of a bone marrow-derived Mac2+/TMEM119-/CX3CR1+ macrophage that is strongly associated with the pathological elimination of microvasculature following CMB highlights the functional differences between peripheral and brain-resident immune cells in the resolution of cerebrovascular insults.

Homeostatic microglia are classically identified by their expression of $P2RY_{12}$ and TMEM119[327,328]; Mac2, however, is particularly expressed by circulating myeloid cells[89,90]. Despite its general attribution to peripheral leukocytes, Mac2+ cells have been identified previously in the brain and presumed to represent a type of microglia. Specifically, Zhan et al. described a Mac2-expressing microglial subpopulation, with progenitor-like gene signatures, that was present in the brain under homeostatic conditions[486]. These findings were replicated by the present work which characterized Mac2+/TMEM119+/CX3CR1+ microglia in the nondiabetic parenchyma in the absence of injury. Interestingly, another population of myeloid-like cells with DAM gene signatures has also been discovered in the choroid plexus epithelium of healthy mice; although these cells were of embryonic lineage, like most BAMs, they were otherwise unique from cpMΦ[337]. The work of this dissertation also led to the discovery of Mac2+/TMEM119-/CX3CR1+ cells in the uninjured brain parenchyma of diabetic and PLX5622-treated mice; notably, this population was not found in the nondiabetic context. Given their lack of TMEM119 expression, a key question was: do these Mac2+/TMEM119-/CX3CR1+ cells actually represent

brain-resident microglia, or are they engrafted or infiltrative bone marrow-derived macrophages? Using a transgenic lineage tracing strategy, Zhan et al. found that most Mac2-expressing cells in the brain were long-lived and suggested that they were likely a subtype of microglia which retains their progenitor-like gene signatures[486]. However, Zhan et al. did not parse Mac2+ cells into TMEM119-expressing variants[486], so it is conceivable that the Mac2+/TMEM119+ population identified in all treatment groups corresponds to this microglial phenotype while the Mac2+/TMEM119- cells found only in the diabetic and PLX5622-treated brain may have disparate origins. Strong evidence for the peripheral origins of Mac2+/TMEM119- cells is provided by the fact that CLR effectively eliminated these cells from diabetic CMBs, coincident with the profound depletion of bone marrow-derived monocytes. Furthermore, since CLR did not affect the presence of Mac2+/TMEM119+ cells in CMBs from any groups, it is likely that this population represents a subtype of brain-resident microglia.

Although the Mac2+/TMEM119- cells found in diabetic CMBs and those identified in the uninjured parenchyma of diabetic and PLX5622-treated mice expressed similar protein signatures, they may not necessarily represent constituents of the same population. However, it is worth considering that old microbleeds are identified epidemiologically by the presence of iron-enriched macrophages that demarcate the location of a latent CMB[383,487,488]. Therefore, it is possible that, in the absence of induced CMBs, Mac2+/TMEM119- cells found in the parenchyma are examples of these engrafted macrophages: sentinel cells remaining at the original site of an insult that may have initially derived from infiltrating monocytes. Furthermore, once in the CNS, MDMs rapidly acquire microglial gene signatures and morphology upon exposure to environmental cues and become nearly indistinguishable from resident cells[488]. The fact that Mac2+/TMEM119- cells were not found in nondiabetic CMBs

could further explain why they were not observed in the brain parenchyma of these animals. In the context of PLX5622 treatment, microglial depletion could permit the chronic infiltration of peripheral leukocytes into the CNS since microglia have been shown to inhibit their transmigration[437]. Therefore, peripherally-derived MDMs could be identified in the brain parenchyma in this context, even in the absence of injury, and could coexist with brain-resident Mac2+/TMEM119- cells. It is worth considering that in disease states or during acute CNS injury microglia may downregulate homeostatic markers, such as TMEM119[38,261,489,490]. Thus, although Mac2+/TMEM119- cells found in the CMB milieu likely represent bone marrow-derived cells, as they were depleted by CLR, their parenchymal correlates could be microglia which dampened TMEM119 expression. Interestingly, Mac2-/TMEM119-/CX3CR1+ cells also responded to CMBs in all groups and could represent infiltrating immune cells or brain-resident microglia that have downregulated TMEM119 expression. Since the presence of these cells was not significantly impacted by CLR treatment though, they were likely CNS-derived.

There is evidence that unique microglial phenotypes and MDMs differ functionally from homeostatic microglia[262,266,329,381]. For example, Zhan and colleagues noted that the Mac2-expressing population was resistant to CSF1R inhibition and persisted during PLX5622-treatment[486]. During the clonal expansion phase of microglial re-establishment following removal of PLX5622, this led to a greater proportion of Mac2+ cells in the resulting population compared to control conditions[486]. These observations are in line with the present study which found that PLX5622 treatment eliminated most Mac2-/TMEM119+/CX3CR1+ cells without significantly affecting Mac2+ cells; in fact, this latter phenotype comprised the majority of remaining parenchymal CX3CR1+ cells. Furthermore, both Mac2+/TMEM119- and Mac2+/TMEM119+ cell types were resilient to CSF1R inhibition and were not significantly

depleted by PLX5622 treatment. Interestingly, Mac2+/TMEM119- cells contained more lipofuscin than TMEM119+ microglia, suggesting that their phagocytic capacities may differ and contribute to meaningful changes in function. In support of this idea, since Mac2+/TMEM119- cells were reliably associated with microvascular elimination following CMB in diabetes, it is possible that the prevalence of these cells in the PLX5622-treated brain was connected to the induction of vessel loss in nondiabetic mice that received PLX5622. Specifically, given their significant representation in the remaining CX3CR1+ population, it is conceivable that these cells may have been as likely to respond to CMBs as any remaining homeostatic microglia and could have associated with microvascular elimination as observed in the diabetic condition.

Taken together, the present study identified heterogenous CX3CR1+ cell populations in the uninjured parenchyma of healthy, diabetic, and PLX5622-treated mice. Although the Mac2+/TMEM119+/CX3CR1+ cells observed in these groups are likely a subtype of microglia, further research will be required to confirm the origins of the Mac2+/TMEM119-/CX3CR1+ cells characterized under non-homeostatic conditions. Notably, this work also discovered Mac2+/TMEM119-/CX3CR1+ cells in the CX3CR1+ aggregate at diabetic CMBs that were sensitive to CLR treatment, therefore likely bone marrow-derived, and strongly correlated with pathological microvascular elimination. Other Mac2+/TMEM119+/CX3CR1+ and Mac2-/TMEM119-/CX3CR1+ cells found in the heterogenous CMB milieu of all treatment groups were unaffected by CLR treatment and likely represent proliferative microglia and microglia that downregulated homeostatic TMEM119 expression, respectively. These data highlight the diverse phenotypes of immune cells implicated in responses to CMBs and underscore the importance of ongoing studies to characterize functional differences between cell types, particularly in the context of pathological conditions and CNS injury repair.

5.4 Phagocytic markers are upregulated in cells associated with microvascular elimination

Aberrant phagocytic activity by brain-resident microglia has been implicated in a host of disease conditions[23,300,304], and phagocytosis by MDMs has been touted as detrimental[425,471,472] or supportive[262,302] in different contexts. Since hemorrhagic insults, including CMBs, produce cellular debris which must be cleared by phagocytosis to restore interstitial homeostasis and protect tissue integrity[269,298], the dysregulation of this process was a strong candidate amongst the factors that could contribute to microvascular elimination. The present study correlated increased phagocytic activity, indirectly evidenced by elevated lipofuscin content in CX3CR1+ cells responding to a CMB, to microvascular elimination in the diabetic brain. CD68 and TREM2 expression were also increased in the cellular aggregate of diabetic CMBs and normalized to nondiabetic levels by CLR. Lipofuscin content in Mac2+/TMEM119-/CX3CR1+ cells specifically was enriched relative to homeostatic microglia, suggesting that upregulated phagocytosis by these MDMs could contribute to pathological microvascular elimination.

The quantification of lipofuscin content within CX3CR1+ cells responding to CMBs permitted the *in vivo* investigation of the relationship between phagocytosis and microvascular fate. Although lipofuscin is an indirect indicator of phagocytosis, its utility in this context provided some insight into the dynamic changes in this process over a 14-day period following a CMB. Specifically, lipofuscin content in CX3CR1+ cells responding to CMBs peaked 1 day after the insult and was greatest in diabetic CMBs, but normalized to nondiabetic levels by CLR. Moreover, elevated lipofuscin content was predictive of microvascular elimination. The fact that CD68 immunostaining was increased in diabetic CMBs and normalized by CLR, coincident with the effective colocalization of CD68 with lipofuscin that was characterized, compliments these

findings. Since lipofuscin and CD68 are both markers that reflect lysosomal activity and are not causally linked to molecular pathways that regulate phagocytosis[460,462], TREM2 and Axl were investigated as independent mechanisms that regulate this process. Both of these targets are expressed by microglia as well as peripheral myeloid cells, particularly monocyte-derived DCs and MDMs[491–494]. TREM2 signalling contributes to microglial pruning of synapses during development[463], clearance of apoptotic neurons[478], and is characteristic of DAM which are crucial for plaque clearance in AD[337,460]. Axl has also been attributed to microglial phagocytosis of apoptotic neurons[495] and, in MS, to myelin degradation[459]. Specifically, while TREM2 functions through the adapter protein DAP12 and activates numerous pathways including tyrosine protein kinase SYK, PI3K, PKB, and PLCβ[478,479,496], Axl, and other members of the TYRO3/AXL/MERTK family contribute to phagocytosis through Gas6 and require activation of Rac and Vav[480,481]. Notably, Mac2 itself is also involved in the regulation of phagocytosis via upregulation of PI3K and activation of K-Ras-GTP[468,477].

In the present work, TREM2 immunostaining was significantly increased in diabetic CMBs and normalized by CLR treatment, potentially via the exclusion of highly phagocytic Mac2+/TMEM119-/CX3CR1+ cells from the CMB response. On the other hand, Axl immunostaining was negligible in CMBs from all treatment groups. Despite its known connection to phagocytosis pathways, others have also described an insignificant role for Axl in regulating phagocytosis during neurological disease conditions[497]. For example, Axl did not play a major role in the phagocytosis of apoptotic neurons in an animal of AD but another TAM receptor tyrosine kinase, Mertk, was essential for this process[497]. Building on this precedent, the dichotomous immunostaining observed for Axl and TREM2 might be explained by the fact that increased TREM2 activity in Mac2-expressing cells may result in their converging activation of

PI3K to mediate phagocytosis and, in this way, Mac2 and TREM2 could act through a common pathway that excludes Axl and effectively upregulates phagocytic activity.

It is worth highlighting the fact that the increased expression of phagocytic markers at the site of an eliminated vessel following CMB does not indicate whether upregulated phagocytosis caused the vessel loss or whether it reflects a post-hoc response to a vessel that is already regressing for another reason. For example, if Mac2+/TMEM119- macrophages induced cell death in target ECs, potentially via activation of WNT signalling as during development[361], then the clearance of apoptotic cells would require increased phagocytosis but the vessel elimination itself was caused by another process. Conversely, macrophages are known to phagocytose EC membrane particles in the stroke penumbra prior to obvious vessel regression, suggesting that phagocytosis could indeed drive vascular elimination. Although increased lipofuscin was quantified in Mac2+/TMEM119- cells relative to homeostatic microglia, potentially reaffirming the elevated phagocytic capacity of MDMs that has been described previously,[269,270] this may not directly correlate with increased TREM2 activity in this population. That is, greater lipofuscin content in Mac2+/TMEM119- cells does not necessarily equate to elevated TREM2 activity in these cells specifically, even if TREM2 expression increased in the general CMB milieu. Indeed, MDMs can manipulate the phagocytic activity of juxtaposed microglia[270,498,499], so increased TREM2 immunostaining in the CMB aggregate as a whole could actually reflect changes in microglial phagocytosis induced by Mac2+/TMEM119- macrophages. Ultimately, the details of these findings regarding elevated phagocytic activity in diabetic CMBs and Mac2+/TMEM119- cells will require further, detailed characterization. Future studies with transgenic animals may overcome methodological limitations associated with antibody compatibility and could permit the direct investigation of key phagocytic mediators in Mac2-expressing cells.

5.5 Limitations and Future Directions

As this dissertation approaches its conclusion, several key limitations of the work are worth highlighting alongside opportunities for future investigations. Firstly, and perhaps most obviously, the present work was limited to the study of microvascular repair in male mice. This experimental design was reflective of the field of cerebrovascular research in general at that time, with female mice excluded on the basis of the estrous cycle having fluctuating protective or detrimental effects on vascular outcomes which would generate data that was too variable to interpret meaningfully[500]. Fortunately, this unfounded reasoning is being overturned and it is now being appreciated that males can have similar degrees of hormonal fluctuations that would similarly affect microvascular repair. In particular, group-housed male mice establish hierarchies that lead to significantly higher levels of testosterone in dominant males than in subordinate individuals[501]. Future studies replicating the long-term *in vivo* characterizations of microbleed resolution in female mice would be informative, as would the investigation of the cellular composition of CMB responses in these animals. Fortunately, in terms of the heterogeneity of the microglial population, there seem to be only minor sex differences in gene expression signatures during development and homeostasis as revealed by single-cell RNA sequencing[336].

Furthermore, in terms of considering whether 1) compounding microvascular loss and resultant hypoperfusion or 2) damage to neuronal circuitry near CMBs is the major contributor to cognitive degeneration in diabetes, several strategies could be employed to probe this clinically-relevant question. Cognitive function could be assessed using a battery of behavioural tasks (Barnes maze, novel object recognition, etc.) and changes in calcium activity in synaptic boutons near a CMB could be quantified directly in a transgenic mouse expressing a GCaMP reporter in neurons. In this mouse model, the fate of a targeted microvessel could still be determined via

longitudinal *in vivo* imaging and intravascular labelling with a fluorescent dye, so the relative contributions of compounding vessel loss or changes in synaptic activity could be assessed in combination with cognitive function. Additionally, although DEX treatment and interventions blocking IFN signalling did not rescue microvascular elimination, since they modulated the aggregation of CX3CR1+ cells to the site of CMBs, it would be possible to consider whether these responses had a protective effect on neuronal integrity. Furthermore, the Brown lab has shown that age-related vessel loss and angiogenesis can occur at varying rates in different brain regions[50]. An important question, then, is: can pathological microvascular loss following CMB in diabetes be compensated for by angiogenesis? Although the present work followed the resolution of CMBs for several weeks, it is possible that local hypoperfusion resulting from vessel loss eventually prompts angiogenesis after further weeks or months. Extending the imaging timeline and increasing the sampling area could augment the power of this investigation.

Lastly, a crucial limitation of other studies which the present work addresses, but is also limited by, is the use of the transgenic $CX3CR1^{+/eGFP}$ mouse to study brain macrophages. Indeed, a key contribution of this dissertation is its identification of heterogenous cell types within the CMB milieu, a discovery made possible by the combination of immunohistochemistry and *in vivo* imaging. However, the constraints of available antibodies limited the dimensions in which these cells could be characterized, preventing the discrimination of additional cell phenotypes. Single-cell RNA sequencing will be a fundamental tool to assess the diversity of the cellular constituents of CMB responses with greater fidelity. Moreover, the replication of these studies in other transgenic models (TMEM119, Hexb, Mac2, etc.) could provide insight into the dynamic expression of TMEM119 in CMBs, the bone marrow-derived origins of Mac2+/TMEM119- cells, and the histological analysis of other relevant targets such as $P2RY_{12}$.

5.6 Significance

Diabetes has become a world-wide epidemic and is commonly associated with a host of vascular complications, including CMBs[2,3]. Importantly, chronic insulin treatment is not a cure for type 1 DM and does not abrogate its vascular comorbidities[11–16,130,131]. In order to develop more effective treatments, it is imperative to understand the cellular and molecular changes that occur in this disease. Furthermore, various immune cells including brain-resident microglia, CNS BAMs, and circulating phagocytic leukocytes have been implicated CMB repair[24,25,27,423], but their relative contributions to the resolution of these insults has not been well described. It was therefore crucial to understand these interactions in more detail, particular in the context of a chronic inflammatory disease such as type 1 DM, given the opportunity that harnessing these cellular mechanisms may present for preventing the progression of microvascular disease.

The present work is significant because it describes the pathological elimination of microvessels following CMB in type 1 DM for the first time, and uncovers a peripherally-derived macrophage phenotype characterized by Mac2+/TMEM119- expression that is strongly associated with this vessel regression. Notably, it also identifies an effective intervention that rescues this pathology: CLR. A preliminary mechanistic explanation for these effects is also outlined, wherein depletion of circulating phagocytes excludes Mac2+/TMEM119- cells from the CMB milieu and reduces local TREM2-mediated phagocytic activity to rescue microvascular repair. This work addresses crucial gaps in our understanding of the cellular mechanisms underlying type 1 DM complications and, using powerful 2-photon microscopy, demonstrated the resolution of this pathology *in vivo.* Given the limitations of insulin treatment, these findings may have clinical implications for patients with type 1 DM as they provide further evidence for the use of adjuvant treatments, such as CLR, to mitigate cerebrovascular pathology

REFERENCES

1. World Health Organization. Global report on diabetes. *Publications of the World Health Organization* 1–83 https://www.who.int/publications/i/item/9789241565257 (2016).

2. Woerdeman, J. *et al.* Proliferative retinopathy in type 1 diabetes is associated with cerebral microbleeds, which is part of generalized microangiopathy. *Diabetes Care* **37**, 1165–8 (2014).

3. Cordonnier, C., Al-Shahi Salman, R. & Wardlaw, J. Spontaneous brain microbleeds: systematic review, subgroup analyses and standards for study design and reporting. *Brain* **130**, 1988–2003 (2007).

4. Brownlee, M., Cerami, A. & Vlassara, H. Advanced Glycosylation End Products in Tissue and the Biochemical Basis of Diabetic Complications. *N. Engl. J. Med.* **318**, 1315–1321 (1988).

5. Wang, Y., Chen, L. & Liu, M. Microvesicles and diabetic complications — novel mediators, potential biomarkers and therapeutic targets. *Acta Pharmacol. Sin.* **35**, 433–443 (2014).

6. Nishimura, N. & Schaffer, C. B. Big effects from tiny vessels: imaging the impact of microvascular clots and hemorrhages on the brain. *Stroke* **44**, S90-2 (2013).

7. Shih, A. Y. *et al.* The smallest stroke: occlusion of one penetrating vessel leads to infarction and a cognitive deficit. *Nat. Neurosci.* **16**, 55–63 (2013).

8. Akoudad, S. *et al.* Association of Cerebral Microbleeds With Cognitive Decline and Dementia. *JAMA Neurol.* **73**, 934 (2016).

9. Iadecola, C. Neurovascular regulation in the normal brain and in Alzheimer's disease. *Nat. Rev. Neurosci.* **5**, 347–360 (2004).

10. Qiu, C. *et al.* Cerebral microbleeds, retinopathy, and dementia: the AGES-Reykjavik Study. *Neurology* **75**, 2221–8 (2010).

11. Davies, M., Brophy, S., Williams, R. & Taylor, A. The prevalence, severity, and impact of painful diabetic peripheral neuropathy in type 2 diabetes. *Diabetes Care* **29**, 1518–22 (2006).

12. Harati, Y. Diabetic Peripheral Neuropathies. *Ann. Intern. Med.* **107**, 546 (1987).

13. Yagihashi, S., Mizukami, H. & Sugimoto, K. Mechanism of diabetic neuropathy: Where are we now and where to go? *J. Diabetes Investig.* **2**, 18–32 (2011).

14. Sweetnam, D. *et al.* Diabetes Impairs Cortical Plasticity and Functional Recovery Following Ischemic Stroke. *J. Neurosci.* **32**, 5132–5143 (2012).

15. Reeson, P. *et al.* Delayed Inhibition of VEGF Signaling after Stroke Attenuates Blood–Brain Barrier Breakdown and Improves Functional Recovery in a Comorbidity-Dependent Manner. *J. Neurosci.* **35**, 5128–5143 (2015).

16. Tennant, K. A. & Brown, C. E. Diabetes Augments In Vivo Microvascular Blood Flow Dynamics after Stroke. *Neurobiol. ofDisease Diabetes* **33**, 19194–19204 (2013).

17. Ballabh, P., Braun, A. & Nedergaard, M. The blood-brain barrier: An overview: Structure, regulation, and clinical implications. *Neurobiol. Dis.* **16**, 1–13 (2004).

18. Akassoglou, K. *et al.* Fibrin depletion decreases inflammation and delays the onset of demyelination in a tumor necrosis factor transgenic mouse model for multiple sclerosis.

Proc. Natl. Acad. Sci. U. S. A. **101**, 6698–6703 (2004).

19. Cortes-Canteli, M., Mattei, L., Richards, A. T., Norris, E. H. & Strickland, S. Fibrin deposited in the Alzheimer's disease brain promotes neuronal degeneration. *Neurobiol. Aging* **36**, 608–17 (2015).

20. Ryu, J. K. *et al.* Blood coagulation protein fibrinogen promotes autoimmunity and demyelination via chemokine release and antigen presentation. *Nat. Commun.* **6**, 8164 (2015).

21. Hawkins, B. T. & Davis, T. P. The blood-brain barrier/neurovascular unit in health and disease. *Pharmacol. Rev.* **57**, 173–185 (2005).

22. Davalos, D. *et al.* ATP mediates rapid microglial response to local brain injury in vivo. *Nat. Neurosci.* **8**, 752–758 (2005).

23. Madry, C. *et al.* Microglial Ramification, Surveillance, and Interleukin-1β Release Are Regulated by the Two-Pore Domain K + Channel THIK-1. *Neuron* **97**, 1–14 (2018).

24. Lou, N. *et al.* Purinergic receptor P2RY12-dependent microglial closure of the injured blood-brain barrier. *Proc. Natl. Acad. Sci. U. S. A.* **113**, 1074–9 (2016).

25. Taylor, S. *et al.* Suppressing Interferon-γ Stimulates Microglial Responses and Repair of Microbleeds in the Diabetic Brain. *J. Neurosci.* **38**, 8707–8722 (2018).

26. Ibrahim. Investigative Ophthalmology & Visual Science. *Invest. Ophthalmol.* **21**, 3 (1981).

27. Liu, C. *et al.* Macrophages Mediate the Repair of Brain Vascular Rupture through Direct Physical Adhesion and Mechanical Traction. *Immunity* **44**, 1162–1176 (2016).

28. Ahn, S. J., Anrather, J., Nishimura, N. & Schaffer, C. B. Diverse Inflammatory Response After Cerebral Microbleeds Includes Coordinated Microglial Migration and Proliferation. *Stroke* **49**, 1719–1726 (2018).

29. Moore, K. J. & Tabas, I. Macrophages in the Pathogenesis of Atherosclerosis. *Cell* **145**, 341–355 (2011).

30. Zhang, C. *et al.* Invasion of Peripheral Immune Cells into Brain Parenchyma after Cardiac Arrest and Resuscitation. *Aging Dis.* **9**, 412–425 (2018).

31. Baumgartner-Parzer, S. M., Wagner, L., Pettermann, M., Gessl, A. & WaldhÄusl, W. Modulation by high glucose of adhesion molecule expression in cultured endothelial cells. *Diabetologia* **38**, 1367–1370 (1995).

32. Takami, S., Yamashita, S., Kihara, S., Kameda-Takemura, K. & Matsuzawa, Y. High concentration of glucose induces the expression of intercellular adhesion molecule-1 in human umbilical vein endothelial cells. *Atherosclerosis* **138**, 35–41 (1998).

33. Esposito, C. *et al.* Long-term exposure to high glucose up-regulates VCAM-induced endothelial cell adhesiveness to PBMC. *Kidney Int.* **59**, 1842–1849 (2001).

34. Quagliaro, L. *et al.* Intermittent high glucose enhances ICAM-1, VCAM-1 and E-selectin expression in human umbilical vein endothelial cells in culture: The distinct role of protein kinase C and mitochondrial superoxide production. *Atherosclerosis* **183**, 259–267 (2005).

35. Corliss, B. A., Azimi, M. S., Munson, J. M., Peirce, S. M. & Murfee, W. L. Macrophages: An Inflammatory Link Between Angiogenesis and Lymphangiogenesis. *Microcirculation*

23, 95–121 (2016).

36. Prinz, M. & Priller, J. Microglia and brain macrophages in the molecular age: from origin to neuropsychiatric disease. *Nat. Rev. Neurosci.* **15**, 300–312 (2014).

37. Hilla, A. M., Diekmann, H. & Fischer, D. Microglia Are Irrelevant for Neuronal Degeneration and Axon Regeneration after Acute Injury. *J. Neurosci.* **37**, 6113–6124 (2017).

38. Deczkowska, A. *et al.* Disease-Associated Microglia: A Universal Immune Sensor of Neurodegeneration. *Cell* **173**, 1073–1081 (2018).

39. Schwartz, M. Macrophages and microglia in central nervous system injury: Are they helpful or harmful? *J. Cereb. Blood Flow Metab.* **23**, 385–394 (2003).

40. Attwell, D. & Laughlin, S. B. An energy budget for signaling in the grey matter of the brain. *J. Cereb. Blood Flow Metab.* **21**, 1133–1145 (2001).

41. Kuzawa, C. W. *et al.* Metabolic costs and evolutionary implications of human brain development. *Proc. Natl. Acad. Sci. U. S. A.* **111**, 13010–13015 (2014).

42. Kleinfeld, D. *et al.* A guide to delineate the logic of neurovascular signaling in the brain. *Front. Neuroenergetics* **3**, (2011).

43. Muoio, V., Persson, P. B. & Sendeski, M. M. The neurovascular unit - concept review. *Acta Physiol.* **210**, 790–798 (2014).

44. Lecrux, C. & Hamel, E. The neurovascular unit in brain function and disease. *Acta Physiol.* **203**, 47–59 (2011).

45. Kandel, E. R., Schwartz, J. H. & Jessell, T. M. *Principles of Neural Science*. *Neurology*

vol. 4 (2000).

46. Cipolla MJ. The Cerebral Circulation. in *Colloquium Series on Integrated systems Physiology: From Molecule to Function* vol. 1 1–59 (Morgan & Claypool Life Sciences, 2009).

47. Jones, E. G. On the mode of entry of blood vessels into the cerebral cortex. *J. Anat.* **106**, 507–20 (1970).

48. Blinder, P. *et al.* The cortical angiome: An interconnected vascular network with noncolumnar patterns of blood flow. *Nat. Neurosci.* **16**, 889–897 (2013).

49. Xiong, B. *et al.* Precise cerebral vascular atlas in stereotaxic coordinates of whole mouse brain. *Front. Neuroanat.* **11**, (2017).

50. Schager, B. & Brown, C. E. Susceptibility to capillary plugging can predict brain region specific vessel loss with aging. *J. Cereb. Blood Flow Metab.* **40**, 2475–2490 (2020).

51. Tsai, P. S. *et al.* Correlations of neuronal and microvascular densities in murine cortex revealed by direct counting and colocalization of nuclei and vessels. *J. Neurosci.* **29**, 14553–14570 (2009).

52. Shih, A. Y. *et al.* Robust and fragile aspects of cortical blood flow in relation to the underlying angioarchitecture. *Microcirculation* vol. 22 204–218 (2015).

53. Iadecola, C. The overlap between neurodegenerative and vascular factors in the pathogenesis of dementia. *Acta Neuropathol.* **120**, 287–96 (2010).

54. Davson, H. History of the Blood-Brain Barrier Concept. in *Implications of the Blood-Brain Barrier and Its Manipulation* 27–52 (Springer US, 1989). doi:10.1007/978-1-4613-

0701-3_2.

55. Daneman, R. & Prat, A. The blood–brain barrier. *Cold Spring Harb. Perspect. Biol.* **7**, (2015).

56. Luissint, A. C., Artus, C., Glacial, F., Ganeshamoorthy, K. & Couraud, P. O. Tight junctions at the blood brain barrier: Physiological architecture and disease-associated dysregulation. *Fluids and Barriers of the CNS* vol. 9 (2012).

57. CM de Lange, E. The Physiological Characteristics and Transcytosis Mechanisms of the Blood-Brain Barrier (BBB). *Curr. Pharm. Biotechnol.* **13**, 2319–2327 (2012).

58. Mathiisen, T. M., Lehre, K. P., Danbolt, N. C. & Ottersen, O. P. The perivascular astroglial sheath provides a complete covering of the brain microvessels: An electron microscopic 3D reconstruction. *Glia* **58**, 1094–1103 (2010).

59. Janzer, R. C. & Raff, M. C. Astrocytes induce blood-brain barrier properties in endothelial cells. *Nature* **325**, 253–257 (1987).

60. Lee, S. W. *et al.* SSeCKS regulates angiogenesis and tight junction formation in blood-brain barrier. *Nat. Med.* **9**, 900–906 (2003).

61. Bélanger, M., Allaman, I. & Magistretti, P. J. Brain Energy Metabolism: Focus on Astrocyte-Neuron Metabolic Cooperation. *Cell Metab.* **14**, 724–738 (2011).

62. Loaiza, A., Porras, O. H. & Barros, L. F. Glutamate triggers rapid glucose transport stimulation in astrocytes as evidenced by real-time confocal microscopy. *J. Neurosci.* **23**, 7337–42 (2003).

63. Rosenegger, D. G., Tran, C. H. T., Wamsteeker Cusulin, J. I. & Gordon, G. R. Tonic local

brain blood flow control by astrocytes independent of phasic neurovascular coupling. *J. Neurosci.* **35**, 13463–13474 (2015).

64. Attwell, D. *et al.* Glial and neuronal control of brain blood flow. *Nature* vol. 468 232–243 (2010).

65. Mulligan, S. J. & MacVicar, B. A. Calcium transients in astrocyte endfeet cause cerebrovascular constrictions. *Nature* **431**, 195–199 (2004).

66. Mishra, A. *et al.* Astrocytes mediate neurovascular signaling to capillary pericytes but not to arterioles. *Nat. Neurosci.* **19**, 1619–1627 (2016).

67. Mehina, E. M. F., Murphy-Royal, C. & Gordon, G. R. Steady-state free Ca2+ in astrocytes is decreased by experience and impacts arteriole tone. *J. Neurosci.* **37**, 8150–8165 (2017).

68. Iadecola, C. & Nedergaard, M. Glial regulation of the cerebral microvasculature. *Nature Neuroscience* vol. 10 1369–1376 (2007).

69. Koehler, R. C., Roman, R. J. & Harder, D. R. Astrocytes and the regulation of cerebral blood flow. *Trends in Neurosciences* vol. 32 160–169 (2009).

70. Davis, G. E. & Senger, D. R. Endothelial extracellular matrix: Biosynthesis, remodeling, and functions during vascular morphogenesis and neovessel stabilization. *Circulation Research* vol. 97 1093–1107 (2005).

71. Bergers, G. & Song, S. The role of pericytes in blood-vessel formation and maintenance. *Neuro-Oncology* vol. 7 452–464 (2005).

72. Condren, A. B. *et al.* Perivascular Mural Cells of the Mouse Choroid Demonstrate

Morphological Diversity That Is Correlated to Vasoregulatory Function. *PLoS One* **8**, (2013).

73. Herman, I. M. & D'amore, P. A. Microvascular pericytes contain muscle and nonmuscle actins. *J. Cell Biol.* **101**, 43–52 (1985).

74. Sims, D. E. Diversity within pericytes. in *Clinical and Experimental Pharmacology and Physiology* vol. 27 842–846 (Clin Exp Pharmacol Physiol, 2000).

75. Devor, A. *et al.* Suppressed neuronal activity and concurrent arteriolar vasoconstriction may explain negative blood oxygenation level-dependent signal. *J. Neurosci.* **27**, 4452–4459 (2007).

76. Hill, R. A. *et al.* Regional Blood Flow in the Normal and Ischemic Brain Is Controlled by Arteriolar Smooth Muscle Cell Contractility and Not by Capillary Pericytes. *Neuron* **87**, 95–110 (2015).

77. Peppiatt, C. M., Howarth, C., Mobbs, P. & Attwell, D. Bidirectional control of CNS capillary diameter by pericytes. *Nature* **443**, 700–704 (2006).

78. Gerhardt, H. & Betsholtz, C. Endothelial-pericyte interactions in angiogenesis. *Cell and Tissue Research* vol. 314 15–23 (2003).

79. Zhai, X. *et al.* Astrocytes Regulate Angiogenesis Through the Jagged1-Mediated Notch1 Pathway After Status Epilepticus. *Mol. Neurobiol.* **53**, 5893–5901 (2016).

80. Thomas, W. E. Brain macrophages: On the role of pericytes and perivascular cells. *Brain Research Reviews* vol. 31 42–57 (1999).

81. Morizawa, Y. M. *et al.* Reactive astrocytes function as phagocytes after brain ischemia via

ABCA1-mediated pathway. *Nat. Commun.* **8**, (2017).

82. Al-Ali, S. Y., Al-Zuhair, A. G. H. & Dawod, B. Ultrastructural study of phagocytic activities of young astrocytes in injured neonatal rat brain following intracerebral injection of colloidal carbon. *Glia* **1**, 211–218 (1988).

83. Ikeshima-Kataoka, H. & Yasui, M. Correlation between astrocyte activity and recovery from blood-brain barrier breakdown caused by brain injury. *Neuroreport* **27**, 894–900 (2016).

84. Faraco, G. *et al.* Perivascular macrophages mediate the neurovascular and cognitive dysfunction associated with hypertension. *J. Clin. Invest.* **126**, 4674–4689 (2016).

85. Faraco, G., Park, L., Anrather, J. & Iadecola, C. Brain perivascular macrophages: characterization and functional roles in health and disease. *J. Mol. Med. (Berl).* **95**, 1143–1152 (2017).

86. Merlini, M. *et al.* Fibrinogen Induces Microglia-Mediated Spine Elimination and Cognitive Impairment in an Alzheimer's Disease Model. *Neuron* **101**, 1099-1108.e6 (2019).

87. Andersen, H. H., Johnsen, K. B. & Moos, T. Iron deposits in the chronically inflamed central nervous system and contributes to neurodegeneration. *Cell. Mol. Life Sci.* **71**, 1607–22 (2014).

88. Herz, J., Filiano, A. J., Smith, A., Yogev, N. & Kipnis, J. Myeloid Cells in the Central Nervous System. *Immunity* vol. 46 943–956 (2017).

89. Erdö, F., Denes, L. & De Lange, E. Age-associated physiological and pathological

changes at the blood-brain barrier: A review. *Journal of Cerebral Blood Flow and Metabolism* vol. 37 4–24 (2017).

90. Montagne, A. *et al.* Blood-Brain barrier breakdown in the aging human hippocampus. *Neuron* **85**, 296–302 (2015).

91. Sweeney, M. D., Sagare, A. P. & Zlokovic, B. V. Blood-brain barrier breakdown in Alzheimer disease and other neurodegenerative disorders. *Nature Reviews Neurology* vol. 14 133–150 (2018).

92. Hametner, S. *et al.* Iron and neurodegeneration in the multiple sclerosis brain. *Ann. Neurol.* **74**, 848–61 (2013).

93. Kim, E., Yang, J., Park, K. W. & Cho, S. Inhibition of VEGF Signaling Reduces Diabetes-Exacerbated Brain Swelling, but Not Infarct Size, in Large Cerebral Infarction in Mice. *Transl. Stroke Res.* **9**, 540–548 (2018).

94. Coucha, M., Abdelsaid, M., Ward, R., Abdul, Y. & Ergul, A. Impact of metabolic diseases on cerebral circulation: Structural and functional consequences. *Compr. Physiol.* **8**, 773–799 (2018).

95. Eknoyan, G. & Nagy, J. A history of diabetes mellitus or how a disease of the kidneys evolved into a kidney disease. *Adv. Chronic Kidney Dis.* **12**, 223–229 (2005).

96. Medvei, V. C. *The History of Clinical Endocrinology: A Comprehensive Account of Endocrinology from the Earliest Times to the Present Day.* (The Parthenon Publishing Group Inc. , 1993).

97. Karamanou, M. Milestones in the history of diabetes mellitus: The main contributors.

World J. Diabetes **7**, 1 (2016).

98. Sanders, L. J. From Thebes to Toronto and the 21st Century: An Incredible Journey. *Diabetes Spectr.* **15**, 56–60 (2002).

99. Loriaux, D. L. Diabetes and The Ebers Papyrus. *Endocrinologist* **16**, 55–56 (2006).

100. Valenti, G. History of Diabetes Insipidus. *Ital. J. Nephrol.* **33**, 33–38 (2016).

101. Fujiwara, T. M. & Bichet, D. G. Molecular biology of hereditary diabetes insipidus. *J. Am. Soc. Nephrol.* **16**, 2836–2846 (2005).

102. Canadian Diabetes Association. Types of Diabetes. https://www.diabetes.ca/about-diabetes/what-is-diabetes (2020).

103. Bonifacio, E., Hummel, M., Walter, M., Schmid, S. & Ziegler, A. G. IDDM1 and multiple family history of type 1 diabetes combine to identify neonates at high risk for type 1 diabetes. *Diabetes Care* **27**, 2695–2700 (2004).

104. Hyttinen, V., Kaprio, J., Kinnunen, L., Koskenvuo, M. & Tuomilehto, J. Genetic liability of type 1 diabetes and the onset age among 22, 650 young Finnish twin pairs: A nationwide follow-up study. *Diabetes* **52**, 1052–1055 (2003).

105. Dotta, F. *et al.* Coxsackie B4 virus infection of β cells and natural killer cell insulitis in recent-onset type 1 diabetic patients. *Proc. Natl. Acad. Sci. U. S. A.* **104**, 5115–5120 (2007).

106. Warram, J. H., Krolewski, A. S. & Kahn, C. R. Determinants of IDDM and Perinatal Mortality in Children of Diabetic Mothers. *Diabetes* **37**, 1328–1334 (1988).

107. Mehers, K. L. & Gillespie, K. M. The genetic basis for type 1 diabetes. *Br. Med. Bull.* **88**,

115–129 (2008).

108. Opie, E. L. ON THE RELATION OF CHRONIC INTERSTITIAL PANCREATITIS TO THE ISLANDS OF LANGERHANS AND TO DIABETES MELLITUS. *J Exp Med* **5**, 397–428 (1901).

109. Nerup, J., Andersen, O. O., Bendixen, G., Egeberg, J. & Poulsen, J. E. Anti-pancreatic cellular hypersensitivity in diabetes mellitus. *Diabetes* **20**, 424–427 (1971).

110. Gepts, W. Pathologic anatomy of the pancreas in juvenile diabetes mellitus. *Diabetes* **14**, 619–633 (1965).

111. Da Silva Xavier, G. The Cells of the Islets of Langerhans. *J. Clin. Med.* **7**, 54 (2018).

112. Vardanyan, R. & Hruby, V. Hyperglycemic and Hypoglycemic Drugs. in *Synthesis of Best-Seller Drugs* 419–458 (Elsevier, 2016). doi:10.1016/b978-0-12-411492-0.00026-2.

113. Fernandes-Santos, C. *et al.* Amylin acts in the central nervous system to increase sympathetic nerve activity. *Endocrinology* **154**, 2481–2488 (2013).

114. Weiss, M., Steiner, D. F. & Philipson, L. H. *Insulin Biosynthesis, Secretion, Structure, and Structure-Activity Relationships*. *Endotext* (MDText.com, Inc., 2000).

115. Sima, A. A. F. *et al.* C-peptide prevents and improves chronic Type I diabetic polyneuropathy in the BB/Wor rat. *Diabetologia* **44**, 889–897 (2001).

116. Huang, S. & Czech, M. P. The GLUT4 Glucose Transporter. *Cell Metab.* **5**, 237–252 (2007).

117. Saltiel, A. R. & Kahn, C. R. Insulin signalling and the regulation of glucose and lipid metabolism. *Nature* **414**, 799–806 (2001).

118. Satoh, T. Molecular mechanisms for the regulation of insulin-stimulated glucose uptake by small guanosine triphosphatases in skeletal muscle and adipocytes. *International Journal of Molecular Sciences* vol. 15 18677–18692 (2014).

119. Adeva-Andany, M. M., Pérez-Felpete, N., Fernández-Fernández, C., Donapetry-García, C. & Pazos-García, C. Liver glucose metabolism in humans. *Bioscience Reports* vol. 36 416 (2016).

120. Saltiel, A. R. New perspectives into the molecular pathogenesis and treatment of type 2 diabetes. *Cell* **104**, 517–529 (2001).

121. Saini, V. Molecular mechanisms of insulin resistance in type 2 diabetes mellitus. *World J. Diabetes* **1**, 68–75 (2010).

122. Nakae, J. *et al.* Regulation of insulin action and pancreatic β-cell function by mutated alleles of the gene encoding forkhead transcription factor Foxo1. *Nat. Genet.* **32**, 245–253 (2002).

123. Dey, D. *et al.* Inhibition of insulin receptor gene expression and insulin signaling by fatty acid: Interplay of PKC isoforms therein. *Cell. Physiol. Biochem.* **16**, 217–228 (2005).

124. Moeschel, K. *et al.* Protein kinase C-zeta-induced phosphorylation of Ser318 in insulin receptor substrate-1 (IRS-1) attenuates the interaction with the insulin receptor and the tyrosine phosphorylation of IRS-1. *J. Biol. Chem.* **279**, 25157–25163 (2004).

125. Um, S. H. *et al.* Absence of S6K1 protects against age- and diet-induced obesity while enhancing insulin sensitivity. *Nature* **431**, 200–205 (2004).

126. DiMauro, S. & Schon, E. A. Mitochondrial Respiratory-Chain Diseases. *N. Engl. J. Med.*

348, 2656–2668 (2003).

127. Ibrahim, A. S. *et al.* Retinal microglial activation and inflammation induced by amadori-glycated albumin in a rat model of diabetes. *Diabetes* **60**, 1122–1133 (2011).

128. Megherbi, S.-E. *et al.* Association Between Diabetes and Stroke Subtype on Survival and Functional Outcome 3 Months After Stroke: Data From the European BIOMED Stroke Project. *Stroke* **34**, 688–694 (2003).

129. Laing, S. P. *et al.* Mortality from cerebrovascular disease in a cohort of 23 000 patients with insulin-treated diabetes. *Stroke* **34**, 418–21 (2003).

130. The Diabetes Control and Complications Trial Research Group *et al.* The Effect of Intensive Treatment of Diabetes on the Development and Progression of Long-term Complications in Insulin-dependent Diabetes Mellitus. *N. Engl. J. Med.* **329**, 977–986 (2017).

131. Elsamahy, M. H., Elhenawy, Y. I. & Altayeb, N. Long-term prognosis of type 1 diabetes in relation to the clinical characteristics at the onset of diabetes. *Egypt. Pediatr. Assoc. Gaz.* **65**, 90–94 (2017).

132. Peters, A. *et al.* The selfish brain: Competition for energy resources. *Neuroscience and Biobehavioral Reviews* vol. 28 143–180 (2004).

133. Gibbs, E. L., Lennox, W. G., Nims, L. F. & Gibbs, F. A. ARTERIAL AND CEREBRAL VENOUS BLOOD ARTERIAL-VENOUS DIFFERENCES IN MAN. *J. Biol. Chem.* **144**, 325–332 (1942).

134. Howarth, C., Gleeson, P. & Attwell, D. Updated energy budgets for neural computation in

the neocortex and cerebellum. *Journal of Cerebral Blood Flow and Metabolism* vol. 32 1222–1232 (2012).

135. Lu, L. *et al.* Suppression of GLUT1; A new strategy to prevent diabetic complications. *J. Cell. Physiol.* **228**, 251–257 (2013).

136. Benarroch, E. E. Brain glucose transporters: Implications for neurologic disease. *Neurology* **82**, 1374–1379 (2014).

137. Pardridges, W. M., Boado, R. J. & Farrell, C. R. *Brain-type Glucose Transporter (GLUT-1) Is Selectively Localized to the Blood-Brain Barrier STUDIES WITH QUANTITATIVE WESTERN BLOTTING AND IN SITU HYBRIDIZATION'*. *THE JOURNAL OF BIOLOGICAL CHEMISTRY* vol. 265 http://www.jbc.org/ (1990).

138. Nelson, C. P. & Hindson, D. A. Inhibition of Polymorphonuclear Leukocyte Respiratory Burst by Elevated Glucose Concentrations in Vitro. *Diabetes* **38**, 1031–1035 (1989).

139. Pettersson, U. S. *et al.* Increased recruitment but impaired function of leukocytes during inflammation in mouse models of type 1 and type 2 diabetes. *PLoS One* **6**, e22480 (2011).

140. Tesfamariam, B. & Cohen, R. A. Free radicals mediate endothelial cell dysfunction caused by elevated glucose. *Am. J. Physiol. - Hear. Circ. Physiol.* **263**, (1992).

141. Abedin, M. J., Kashio, Y., Seki, M., Nakamura, K. & Hirashima, M. Potential roles of galectins in myeloid differentiation into three different lineages. *J. Leukoc. Biol.* **73**, 650–656 (2003).

142. Brownlee, M. Biochemistry and molecular cell biology of diabetic complications. *Nature* **414**, 813–820 (2001).

143. Mergenthaler, P., Lindauer, U., Dienel, G. A. & Meisel, A. Sugar for the brain: The role of glucose in physiological and pathological brain function. *Trends in Neurosciences* vol. 36 587–597 (2013).

144. Yenari, M. A. & Giffard, R. G. Ischemic vulnerability of primary murine microglial cultures. *Neurosci. Lett.* **298**, 5–8 (2001).

145. Voloboueva, L. A., Emery, J. F., Sun, X. & Giffard, R. G. Inflammatory response of microglial BV-2 cells includes a glycolytic shift and is modulated by mitochondrial glucose-regulated protein 75/mortalin. *FEBS Lett.* **587**, 756–762 (2013).

146. Sonneville, R. *et al.* Impact of Hyperglycemia on Neuropathological Alterations during Critical Illness. *J. Clin. Endocrinol. Metab.* **97**, 2113–2123 (2012).

147. Quan, Y., Jiang, C. T., Xue, B., Zhu, S. G. & Wang, X. High glucose stimulates TNFα and MCP-1 expression in rat microglia via ROS and NF-κB pathways. *Acta Pharmacol. Sin.* **32**, 188–193 (2011).

148. Tomlinson, D. R. & Gardiner, N. J. Glucose neurotoxicity. *Nat. Rev. Neurosci.* **9**, 36–45 (2008).

149. Prasad, S., Sajja, R. K., Naik, P. & Cucullo, L. Diabetes Mellitus and Blood-Brain Barrier Dysfunction: An Overview. *J. Pharmacovigil.* **02**, (2014).

150. Shah, K., DeSilva, S. & Abbruscato, T. The role of glucose transporters in brain disease: Diabetes and Alzheimer's disease. *International Journal of Molecular Sciences* vol. 13 12629–12655 (2012).

151. Badr, G. A., Tang, J., Ismail-Beigi, F. & Kern, T. S. Diabetes downregulates GLUT1

expression in the retina and its microvessels but not in the cerebral cortex or its microvessels. *Diabetes* **49**, 1016–1021 (2000).

152. Seaquist, E. R., Tkac, I., Damberg, G., Thomas, W. & Gruetter, R. Brain glucose concentrations in poorly controlled diabetes mellitus as measured by high-field magnetic resonance spectroscopy. *Metabolism.* **54**, 1008–1013 (2005).

153. Kreis, R. & Ross, B. D. Cerebral metabolic disturbances in patients with subacute and chronic diabetes mellitus: Detection with proton MR spectroscopy. *Radiology* **184**, 123–130 (1992).

154. Greene, D. A. & Winegrad, A. I. In vitro studies of the substrates for energy production and the effects of insulin on glucose utilization in the neural components of peripheral nerve. *Diabetes* **28**, 878–887 (1979).

155. Thiagarajan, R., Varsha, M. K. N. S., Srinivasan, V., Ravichandran, R. & Saraboji, K. Vitamin K1 prevents diabetic cataract by inhibiting lens aldose reductase 2 (ALR2) activity. *Sci. Rep.* **9**, 1–14 (2019).

156. Brownlee, M. The pathobiology of diabetic complications: A unifying mechanism. *Diabetes* **54**, 1615–1625 (2005).

157. Shanmugam, N., Reddy, M. A., Guha, M. & Natarajan, R. High glucose-induced expression of proinflammatory cytokine and chemokine genes in monocytic cells. *Diabetes* **52**, 1256–1264 (2003).

158. Guha, M., Bai, W., Nadler, J. L. & Natarajan, R. Molecular mechanisms of tumor necrosis factor α gene expression in monocytic cells via hyperglycemia-induced oxidant stress-

dependent and - independent pathways. *J. Biol. Chem.* **275**, 17728–17739 (2000).

159. Pendyala, S. & Natarajan, V. Redox regulation of Nox proteins. *Respir. Physiol. Neurobiol.* **174**, 265–271 (2010).

160. Van Dyken, P. & Lacoste, B. Impact of Metabolic Syndrome on Neuroinflammation and the Blood–Brain Barrier. *Front. Neurosci.* **12**, 930 (2018).

161. Zhang, X., Dong, F., Ren, J., Driscoll, M. J. & Culver, B. High dietary fat induces NADPH oxidase-associated oxidative stress and inflammation in rat cerebral cortex. *Exp. Neurol.* **191**, 318–325 (2005).

162. Nishikawa, T., Brownlee, M. & Araki, E. Mitochondrial reactive oxygen species in the pathogenesis of early diabetic nephropathy. *J. Diabetes Investig.* **6**, 137–139 (2015).

163. Green, K., Brand, M. D. & Murphy, M. P. Prevention of Mitochondrial Oxidative Damage As A Therapeutic Strategy in Diabetes. *Diabetes* **53**, S110–S118 (2004).

164. Obrosova, I. G. *et al.* Oxidative-nitrosative stress and poly(ADP-ribose) polymerase (PARP) activation in experimental diabetic neuropathy: The relation is revisited. *Diabetes* **54**, 3435–3441 (2005).

165. Obrosova, I. G. *et al.* An aldose reductase inhibitor reverses early diabetes-induced changes in peripheral nerve function, metabolism, and antioxidative defense. *FASEB J.* **16**, 123–125 (2002).

166. Winterbourn, C. C. Toxicity of iron and hydrogen peroxide: the Fenton reaction. *Toxicol. Lett.* **82**–**83**, 969–974 (1995).

167. Tucsek, Z. *et al.* Obesity in aging exacerbates blood-brain barrier disruption,

neuroinflammation, and oxidative stress in the mouse hippocampus: Effects on expression of genes involved in beta-amyloid generation and Alzheimer's disease. *Journals Gerontol. - Ser. A Biol. Sci. Med. Sci.* **69**, 1212–1226 (2014).

168. Nishikawa, T. *et al.* Normalizing mitochondrial superoxide production blocks three pathways of hyperglycaemic damage. *Nature* **404**, 787–790 (2000).

169. Beckman, J. S. Oxidative damage and tyrosine nitration from peroxynitrite. *Chem. Res. Toxicol.* **9**, 836–844 (1996).

170. Joshi, M. S. *et al.* Nitric oxide is consumed, rather than conserved, by reaction with oxyhemoglobin under physiological conditions. *Proc. Natl. Acad. Sci. U. S. A.* **99**, 10341–10346 (2002).

171. Mates, Jose, M. Antioxidant enzymes and their implications in pathophysiologic processes. *Front. Biosci.* **4**, D339-45 (1999).

172. Furukawa-Hibi, Y., Kobayashi, Y., Chen, C. & Motoyama, N. FOXO transcription factors in cell-cycle regulation and the response to oxidative stress. *Antioxidants and Redox Signaling* vol. 7 752–760 (2005).

173. Wells, P. G. *et al.* Oxidative stress in developmental origins of disease: Teratogenesis, neurodevelopmental deficits, and cancer. *Toxicol. Sci.* **108**, 4–18 (2009).

174. Squier, T. C. Oxidative stress and protein aggregation during biological aging. *Exp. Gerontol.* **36**, 1539–1550 (2001).

175. Gandhi, G. K., Ball, K. K., Cruz, N. F. & Dienel, G. A. Hyperglycaemia and Diabetes Impair Gap Junctional Communication among Astrocytes. *ASN Neuro* **2**, (2010).

176. Ignarro, L. J., Byrns, R. E., Buga, G. M. & Wood, K. S. Endothelium-derived relaxing factor from pulmonary artery and vein possesses pharmacologic and chemical properties identical to those of nitric oxide radical. *Circ. Res.* **61**, 866–879 (1987).

177. Mittal, M., Siddiqui, M. R., Tran, K., Reddy, S. P. & Malik, A. B. Reactive oxygen species in inflammation and tissue injury. *Antioxidants Redox Signal.* **20**, 1126–1167 (2014).

178. Choi, Y.-B. *et al.* Molecular basis of NMDA receptor-coupled ion channel modulation by S-nitrosylation. *Nat. Neurosci.* **3**, 15–21 (2000).

179. Huie, R. E. & Padmaja, S. The reaction of no with superoxide. *Free Radic. Res.* **18**, 195–199 (1993).

180. Czapski, G. & Goldstein, S. The role of the reactions of ·NO with superoxide and oxygen in biological systems: A kinetic approach. *Free Radic. Biol. Med.* **19**, 785–794 (1995).

181. Pacher, P., Beckman, J. S. & Liaudet, L. Nitric oxide and peroxynitrite in health and disease. *Physiol. Rev.* **87**, 315–424 (2007).

182. Phares, T. W., Fabis, M. J., Brimer, C. M., Kean, R. B. & Hooper, D. C. A Peroxynitrite-Dependent Pathway Is Responsible for Blood-Brain Barrier Permeability Changes during a Central Nervous System Inflammatory Response: TNF-α Is Neither Necessary nor Sufficient. *J. Immunol.* **178**, 7334–7343 (2007).

183. Mayhan, W. G. Nitric oxide donor-induced increase in permeability of the blood-brain barrier. *Brain Res.* **866**, 101–108 (2000).

184. Frears, E. R., Zhang, Z., Blake, D. R., O'Connell, J. P. & Winyard, P. G. Inactivation of

tissue inhibitor of metalloproteinase-1 by peroxynitrite. *FEBS Lett.* **381**, 21–24 (1996).

185. Tan, K. H., Harrington, S., Purcell, W. M. & Hurst, R. D. Peroxynitrite Mediates Nitric Oxide-Induced Blood-Brain Barrier Damage. *Neurochem. Res.* **29**, 579–587 (2004).

186. Zamanian, J. L. *et al.* Genomic analysis of reactive astrogliosis. *J. Neurosci.* **32**, 6391–6410 (2012).

187. Igarashi, M. *et al.* Glucose or diabetes activates p38 mitogen-activated protein kinase via different pathways. *J. Clin. Invest.* **103**, 185–195 (1999).

188. Natarajan, R., Scott, S., Wei, B., Yerneni, K. K. V. & Nadler, J. Angiotensin II signaling in vascular smooth muscle cells under high glucose conditions. *Hypertension* **33**, 378–384 (1999).

189. Remels, A. H. V., Gosker, H. R., Verhees, K. J. P., Langen, R. C. J. & Schols, A. M. W. J. TNF-α-induced NF-κB activation stimulates skeletal muscle glycolytic metabolism through activation of HIF-1-α. *Endocrinology* **156**, 1770–1781 (2015).

190. Yamakawa, T. *et al.* Intracellular signaling in rat cultured vascular smooth muscle cells: Roles of nuclear factor-κB and p38 mitogen-activated protein kinase on tumor necrosis factor-α production. *Endocrinology* **140**, 3562–3572 (1999).

191. Kim, K., Wass, C., Cross, A. & Opal, S. Modulation of blood-brain barrier permeability by tumor necrosis factor and antibody to tumor necrosis factor in the rat. *Lymph. cytokine Res.* **11**, 293–298 (1992).

192. Dickstein, J. B., Moldofsky, H. & Hay, J. B. Brain-blood permeability: TNF-α promotes escape of protein tracer from CSF to blood. *Am. J. Physiol. - Regul. Integr. Comp.*

Physiol. **279**, (2000).

193. Wright, J. L. & Merchant, R. E. Blood-brain barrier changes following intracerebral injection of human recombinant tumor necrosis factor-α in the rat. *J. Neurooncol.* **20**, 17–25 (1994).

194. Skelly, D. T., Hennessy, E., Dansereau, M. A. & Cunningham, C. A Systematic Analysis of the Peripheral and CNS Effects of Systemic LPS, IL-1B, TNF-α and IL-6 Challenges in C57BL/6 Mice. *PLoS One* **8**, e69123 (2013).

195. Lawrence, T. The nuclear factor NF-kappaB pathway in inflammation. *Cold Spring Harb. Perspect. Biol.* **1**, a001651–a001651 (2009).

196. Degenhardt, T. P., Thorpe, S. R. & Baynes, J. W. Chemical modification of proteins by methylglyoxal. *Cell. Mol. Biol.* **44**, 1139–1145 (1998).

197. Singh, R., Barden, A., Mori, T. & Beilin, L. Advanced glycation end-products: A review. *Diabetologia* **44**, 129–146 (2001).

198. Jakuš, V. & Rietbrock, N. Advanced Glycation End-Products and the Progress of Diabetic Vascular Complications. *Physiol. Res* **53**, 131–142 (2004).

199. Haslbeck, K. M. *et al.* Activation of the RAGE pathway: A general mechanism in the pathogenesis of polyneuropathies? *Neurol. Res.* **29**, 103–110 (2007).

200. Fernyhough, P., Diemel, L. T. & Tomlinson, D. R. Target tissue production and axonal transport of neurotrophin-3 are reduced in streptozocin-diabetic rats. *Diabetologia* **41**, 300–306 (1998).

201. Russell, J. W., Sullivan, K. A., Windebank, A. J., Herrmann, D. N. & Feldman, E. L.

Neurons undergo apoptosis in animal and cell culture models of diabetes. *Neurobiol. Dis.* **6**, 347–363 (1999).

202. Yang, S. H., Sharrocks, A. D. & Whitmarsh, A. J. Transcriptional regulation by the MAP kinase signaling cascades. *Gene* vol. 320 3–21 (2003).

203. Bucala, R., Tracey, K. J. & Cerami, A. Advanced Glycosylation Products Quench Nitric Oxide and Mediate Defective Endothelium-dependent Vasodilatation in Experimental Diabetes. *J. Clin. Invest.* **87**, 432–8 (1991).

204. Wells-Knecht, K. J., Zyzak, D. V., Litchfield, J. E., Thorpe, S. R. & Baynes, J. W. Mechanism of Autoxidative Glycosylation: Identification of Glyoxal and Arabinose as Intermediates in the Autoxidative Modification of Proteins by Glucose. *Biochemistry* **34**, 3702–3709 (1995).

205. Ahmed, N. *et al.* Methylglyoxal-Derived Hydroimidazolone Advanced Glycation End-Products of Human Lens Proteins. *Investig. Ophthalmol. Vis. Sci.* **44**, 5287–5292 (2003).

206. Thornalley, P. J. Modification of the glyoxalase system in human red blood cells by glucose in vitro. *Biochem. J.* **254**, 751–755 (1988).

207. Giardino, I., Edelstein, D. & Brownlee, M. Nonenzymatic glycosylation in vitro and in bovine endothelial cells alters basic fibroblast growth factor activity. A model for intracellular glycosylation in diabetes. *J. Clin. Invest.* **94**, 110–117 (1994).

208. Stitt, A. W. *et al.* Advanced glycation end products (AGEs) co-localize with AGE receptors in the retinal vasculature of diabetic and of AGE-infused rats. *Am. J. Pathol.* **150**, 523–531 (1997).

209. Nakamura, J. *et al.* A protein kinase C-beta-selective inhibitor ameliorates neural dysfunction in streptozotocin-induced diabetic rats. *Diabetes* **48**, 2090–5 (1999).

210. Soulis-Liparota, T., Cooper, M., Papazoglou, D., Clarke, B. & Jerums, G. Retardation by aminoguanidine of development of albuminuria, mesangial expansion, and tissue fluorescence in streptozocin-induced diabetic rat. *Diabetes* **40**, 1328–1334 (1991).

211. Elmarakby, A. A. & Sullivan, J. C. Relationship between oxidative stress and inflammatory cytokines in diabetic nephropathy. *Cardiovasc. Ther.* **30**, 49–59 (2012).

212. Shimizu, F. *et al.* Advanced glycation end-products disrupt the blood-brain barrier by stimulating the release of transforming growth factor-β by pericytes and vascular endothelial growth factor and matrix metalloproteinase-2 by endothelial cells in vitro. *Neurobiol. Aging* **34**, 1902–1912 (2013).

213. Serban, A. I., Stanca, L., Geicu, O. I., Munteanu, M. C. & Dinischiotu, A. RAGE and TGF-β1 cross-talk regulate extracellular matrix turnover and cytokine synthesis in AGEs exposed fibroblast cells. *PLoS One* **11**, e0152376 (2016).

214. Badenhoop, K., Kahles, H. & Penna-Martinez, M. Vitamin d, immune tolerance, and prevention of type 1 diabetes. *Current Diabetes Reports* vol. 12 635–642 (2012).

215. Mastrandrea, L. *et al.* Etanercept treatment in children with new-onset type 1 diabetes: Pilot randomized, placebo-controlled, double-blind study. *Diabetes Care* **32**, 1244–1249 (2009).

216. Feuerer, M., Shen, Y., Littman, D. R., Benoist, C. & Mathis, D. How Punctual Ablation of Regulatory T Cells Unleashes an Autoimmune Lesion within the Pancreatic Islets.

Immunity **31**, 654–664 (2009).

217. Petersen, A. M. W. The anti-inflammatory effect of exercise. *J. Appl. Physiol.* **98**, 1154–1162 (2005).

218. Derewenda, U., Derewenda, Z., Dodson, G. G., Hubbard, R. E. & Korber, F. Molecular structure of insulin: The insulin monomer and its assembly. *Br. Med. Bull.* **45**, 4–18 (1989).

219. Ferreira De Souza, A. M. & López, J. A. Insulin or insulin-like studies on unicellular organisms: A review. *Brazilian Archives of Biology and Technology* vol. 47 973–981 (2004).

220. Ivanova, M. I., Sievers, S. A., Sawaya, M. R., Wall, J. S. & Eisenberg, D. Molecular basis for insulin fibril assembly. *Proc. Natl. Acad. Sci. U. S. A.* **106**, 18990–18995 (2009).

221. Unger, J. W., Livingston, J. N. & Moss, A. M. Insulin receptors in the central nervous system: Localization, signalling mechanisms and functional aspects. *Progress in Neurobiology* vol. 36 343–362 (1991).

222. Unger, J. W., Moss, A. M. & Livingston, J. N. Immunohistochemical localization of insulin receptors and phosphotyrosine in the brainstem of the adult rat. *Neuroscience* **42**, 853–861 (1991).

223. De La Monte, S. M. & Wands, J. R. *Review of insulin and insulin-like growth factor expression, signaling, and malfunction in the central nervous system: Relevance to Alzheimer's disease*. *Journal of Alzheimer's Disease* vol. 7 (2005).

224. Choeiri, C., Staines, W. & Messier, C. Immunohistochemical localization and

quantification of glucose transporters in the mouse brain. *Neuroscience* **111**, 19–34 (2002).

225. Steen, E. *et al.* Impaired insulin and insulin-like growth factor expression and signaling mechanisms in Alzheimer's disease - Is this type 3 diabetes? *J. Alzheimer's Dis.* **7**, 63–80 (2005).

226. Kitabchi, A. E., Umpierrez, G. E., Miles, J. M. & Fisher, J. N. Hyperglycemic crises in adult patients with diabetes. in *Diabetes Care* vol. 32 1335–1343 (American Diabetes Association, 2009).

227. Cooke, D. W. & Plotnick, L. Type 1 diabetes mellitus in pediatrics. *Pediatr. Rev.* **29**, 374–385 (2008).

228. (UKPDS), U. P. D. S. Intensive blood-glucose control with sulphonylureas or insulin compared with conventional treatment and risk of complications in patients with type 2 diabetes (UKPDS 33). *Lancet* **352**, 837–853 (1998).

229. Banting, F. G. & Best, C. H. The internal secretion of the pancreas. *J. Lab. Clin. Med.* **7**, 251–266 (1922).

230. Giakoumidakis, K. *et al.* Effects of intensive glycemic control on outcomes of cardiac surgery. *Hear. Lung J. Acute Crit. Care* **42**, 146–151 (2013).

231. Lim, S. W., van Wijngaarden, P., Harper, C. A. & Al-Qureshi, S. H. Early worsening of diabetic retinopathy due to intensive glycaemic control. *Clin. Experiment. Ophthalmol.* **47**, 265–273 (2019).

232. World Health Organization. Use of Glycated Haemoglobin (HbA1c) in the Diagnosis of

Diabetes Mellitus. *Publications of the World Health Organization* 25 https://www.who.int/diabetes/publications/diagnosis_diabetes2011/en/ (2011).

233. McCance, D. R. *et al.* Comparison of tests for glycated haemoglobin and fasting and two hour plasma glucose concentrations as diagnostic methods for diabetes. *BMJ* **308**, 1323–8 (1994).

234. Ceriello, A. The emerging challenge in diabetes: The 'metabolic memory'. *Vascular Pharmacology* vol. 57 133–138 (2012).

235. Mordes, J. P., Bortell, R., Blankenhorn, E. P., Rossini, A. A. & Greiner, D. L. Rat models of type 1 diabetes: genetics, environment, and autoimmunity. *ILAR journal / National Research Council, Institute of Laboratory Animal Resources* vol. 45 278–291 (2004).

236. Mansford, K. R. & Opie, L. Comparison of metabolic abnormalities in diabetes mellitus induced by streptozotocin or by alloxan. *Lancet* **1**, 670–671 (1968).

237. Hanafusa, T. *et al.* The NOD mouse. *Diabetes Res. Clin. Pract.* **24**, S307–S311 (1994).

238. Yoshioka, M., Kayo, T., Ikeda, T. & Koizumi, A. A novel locus, Mody4, distal to D7Mit189 on chromosome 7 determines early-onset NIDDM in nonobese C57BL/6 (Akita) mutant mice. *Diabetes* **46**, 887–894 (1997).

239. Novikova, L. *et al.* Variations in rodent models of type 1 diabetes: Islet morphology. *J. Diabetes Res.* **2013**, (2013).

240. Yoon, J. W. & Jun, H. S. Cellular and molecular pathogenic mechanisms of insulin-dependent diabetes mellitus. in *Annals of the New York Academy of Sciences* vol. 928 200–211 (New York Academy of Sciences, 2001).

241. Makino, S., Muraoka, Y., Kishimoto, Y. & Hayashi, Y. Genetic analysis for insulitis in NOD mice. *Jikken Dobutsu.* **34**, 425–431 (1985).

242. Ohsugi, T. & Kurosawa, T. Increased incidence of diabetes mellitus in specific pathogen-eliminated offspring produced by embryo transfer in NOD mice with low incidence of the disease. *Lab. Anim. Sci.* **44**, 386–388 (1994).

243. King, A. J. F. The use of animal models in diabetes research. *British Journal of Pharmacology* vol. 166 877–894 (2012).

244. Shoda, L. K. M. *et al.* A comprehensive review of interventions in the NOD mouse and implications for translation. *Immunity* vol. 23 115–126 (2005).

245. von Herrath, M. & Nepom, G. T. Animal models of human type 1 diabetes. *Nature Immunology* vol. 10 129–132 (2009).

246. Pearson, T., Greiner, D. L. & Shultz, L. D. Humanized SCID mouse models for biomedical research. *Current Topics in Microbiology and Immunology* vol. 324 25–51 (2008).

247. Mathews, C. E., Langley, S. H. & Leiter, E. H. New mouse model to study islet transplantation in insulin-dependent diabetes mellitus. *Transplantation* **73**, 1333–1336 (2002).

248. Baek, H. S. & Yoon, J. W. Direct involvement of macrophages in destruction of β-cells leading to development of diabetes in virus-infected mice. *Diabetes* **40**, 1586–1597 (1991).

249. Craighead, J. E. & McLane, M. F. Diabetes mellitus: Induction in mice by

encephalomyocarditis virus. *Science (80-.).* **162**, 913–914 (1968).

250. Jun, H. S. & Yoon, J. W. A new look at viruses in type 1 diabetes. *Diabetes/Metabolism Research and Reviews* vol. 19 8–31 (2003).

251. Ohashi, P. S. *et al.* Ablation of 'tolerance' and induction of diabetes by virus infection in viral antigen transgenic mice. *Cell* **65**, 305–317 (1991).

252. Lenzen, S. The mechanisms of alloxan- and streptozotocin-induced diabetes. *Diabetologia* vol. 51 216–226 (2008).

253. Szkudelski, T. The mechanism of alloxan and streptozotocin action in B cells of the rat pancreas. *Physiol. Res.* **50**, 537–546 (2001).

254. Cnop, M. *et al.* Mechanisms of pancreatic beta-cell death in type 1 and type 2 diabetes: many differences, few similarities. *Diabetes* **54**, S97-107 (2005).

255. Mathews, C. E. & Leiter, E. H. Constitutive differences in antioxidant defense status distinguish alloxan-resistant and alloxan-susceptible mice. *Free Radic. Biol. Med.* **27**, 449–455 (1999).

256. Muller, Y. D. *et al.* Immunosuppressive effects of streptozotocin-induced diabetes result in absolute lymphopenia and a relative increase of T regulatory cells. *Diabetes* **60**, 2331–2340 (2011).

257. Van Belle, T. L., Taylor, P. & von Herrath, M. G. Mouse models for Type 1 Diabetes. *Drug Discovery Today: Disease Models* vol. 6 41–45 (2009).

258. Mittelbronn, M., Dietz, K., Schluesener, H. J. & Meyermann, R. Local distribution of microglia in the normal adult human central nervous system differs by up to one order of

magnitude. *Acta Neuropathol.* **101**, 249–255 (2001).

259. Bisht, K. *et al.* Dark microglia: A new phenotype predominantly associated with pathological states. *Glia* **64**, 826–839 (2016).

260. Masuda, T., Sankowski, R., Staszewski, O. & Prinz, M. Microglia Heterogeneity in the Single-Cell Era. *Cell Rep.* **30**, 1271–1281 (2020).

261. Stratoulias, V., Venero, J. L., Tremblay, M. & Joseph, B. Microglial subtypes: diversity within the microglial community. *EMBO J.* **38**, e101997 (2019).

262. Derecki, N. C. *et al.* Wild-type microglia arrest pathology in a mouse model of Rett syndrome. *Nature* **484**, 105–109 (2012).

263. Halder, S. K. & Milner, R. Chronic mild hypoxia accelerates recovery from preexisting EAE by enhancing vascular integrity and apoptosis of infiltrated monocytes. *Proc. Natl. Acad. Sci. U. S. A.* **117**, 11126–11135 (2020).

264. Ajami, B., Bennett, J. L., Krieger, C., McNagny, K. M. & Rossi, F. M. V. V. Infiltrating monocytes trigger EAE progression, but do not contribute to the resident microglia pool. *Nat. Neurosci.* **14**, 1142–1149 (2011).

265. Otxoa-de-Amezaga, A. *et al.* Microglial cell loss after ischemic stroke favors brain neutrophil accumulation. *Acta Neuropathol.* **137**, 321–341 (2019).

266. Simard, A. R., Soulet, D., Gowing, G., Julien, J. P. & Rivest, S. Bone marrow-derived microglia play a critical role in restricting senile plaque formation in Alzheimer's disease. *Neuron* **49**, 489–502 (2006).

267. El Khoury, J. *et al.* Ccr2 deficiency impairs microglial accumulation and accelerates

progression of Alzheimer-like disease. *Nat. Med.* **13**, 432–438 (2007).

268. Mildner, A. *et al.* Microglia in the adult brain arise from Ly-6ChiCCR2+ monocytes only under defined host conditions. *Nat. Neurosci.* **10**, 1544–1553 (2007).

269. Galloway, D. A., Phillips, A. E. M., Owen, D. R. J. & Moore, C. S. Phagocytosis in the brain: Homeostasis and disease. *Front. Immunol.* **10**, 790 (2019).

270. Greenhalgh, A. D. & David, S. Differences in the phagocytic response of microglia and peripheral macrophages after spinal cord Injury and its effects on cell death. *J. Neurosci.* **34**, 6316–6322 (2014).

271. Mills, S. *et al.* Fractalkine-induced microglial vasoregulation occurs within the retina and is altered early in diabetic retinopathy. *bioRxiv* 2020.06.15.151464 (2020) doi:10.1101/2020.06.15.151464.

272. Nicolls, M. R., Haskins, K. & Flores, S. C. Oxidant Stress, Immune Dysregulation, and Vascular Function in Type I Diabetes. *Antioxid. Redox Signal.* **9**, 879–889 (2007).

273. Kamata, K. & Kobayashi, T. Changes in superoxide dismutase mRNA expression by streptozotocin-induced diabetes. *Br. J. Pharmacol.* **119**, 583–9 (1996).

274. Junker, U., Jaggi, C., Bestetti, G. & Rossi, G. L. Basement membrane of hypothalamus and cortex capillaries from normotensive and spontaneously hypertensive rats with streptozotocin-induced diabetes. *Acta Neuropathol.* **65**, 202–208 (1985).

275. Halder, S. K. & Milner, R. A critical role for microglia in maintaining vascular integrity in the hypoxic spinal cord. *Proc. Natl. Acad. Sci. U. S. A.* **116**, 26029–26037 (2019).

276. Goldmann, T. *et al.* Origin, fate and dynamics of macrophages at central nervous system

interfaces. *Nat. Immunol.* **17**, 797–805 (2016).

277. Steptoe, R. J., Holt, P. G. & McMenamin P G. Functional studies of major histocompatibility class II-positive dendritic cells and resident tissue macrophages isolated from the rat iris. *Immunology* **85**, 630–637 (1995).

278. McMenamin, P. G., Crewe, J., Morrison, S. & Holt, P. G. Immunomorphologic studies of macrophages and MHC class II-positive dendritic cells in the iris and ciliary body of the rat, mouse, and human eye. *Investig. Ophthalmol. Vis. Sci.* **35**, 3234–3250 (1994).

279. Brissette-Storkus, C. S., Reynolds, S. M., Lepisto, A. J. & Hendricks, R. L. *Identification of a Novel Macrophage Population in the Normal Mouse Corneal Stroma*.

280. Tremblay, M. È., Lecours, C., Samson, L., Sánchez-Zafra, V. & Sierra, A. From the Cajal alumni Achúcarro and Río-Hortega to the rediscovery of never-resting microglia. *Frontiers in Neuroanatomy* vol. 9 (2015).

281. Nimmerjahn, A., Kirchhoff, F. & Helmchen, F. Resting Microglial Cells Are Highly Dynamic Surveillants of Brain Parenchyma in Vivo. *Science (80-.).* **308**, 1314–1318 (2005).

282. De Biase, L. M. *et al.* Local Cues Establish and Maintain Region-Specific Phenotypes of Basal Ganglia Microglia. *Neuron* **95**, 341-356.e6 (2017).

283. Ohsawa, K. *et al.* P2Y12 receptor-mediated integrin-β1 activation regulates microglial process extension induced by ATP. *Glia* **58**, 790–801 (2010).

284. Haynes, S. E. *et al.* The P2Y12 receptor regulates microglial activation by extracellular nucleotides. *Nat. Neurosci.* **9**, 1512–1519 (2006).

285. Hanisch, U. K. & Kettenmann, H. Microglia: Active sensor and versatile effector cells in the normal and pathologic brain. *Nature Neuroscience* vol. 10 1387–1394 (2007).

286. Davalos, D. *et al.* Fibrinogen-induced perivascular microglial clustering is required for the development of axonal damage in neuroinflammation. *Nat. Commun.* **3**, 1–15 (2012).

287. Martinez, F. O. & Gordon, S. The M1 and M2 paradigm of macrophage activation: Time for reassessment. *F1000Prime Rep.* **6**, (2014).

288. Nayak, D., Zinselmeyer, B. H., Corps, K. N. & McGavern, D. B. In vivo dynamics of innate immune sentinels in the CNS. *IntraVital* **1**, 95–106 (2012).

289. Régnier-Vigouroux, A. The mannose receptor in the brain. *Int. Rev. Cytol.* **226**, 321–342 (2003).

290. Mato, M. *et al.* Involvement of specific macrophage-lineage cells surrounding arterioles in barrier and scavenger function in brain cortex. *Proc. Natl. Acad. Sci. U. S. A.* **93**, 3269–3274 (1996).

291. Da Mesquita, S. *et al.* Functional aspects of meningeal lymphatics in ageing and Alzheimer's disease. *Nature* **560**, 185–191 (2018).

292. Jais, A. *et al.* Myeloid-Cell-Derived VEGF Maintains Brain Glucose Uptake and Limits Cognitive Impairment in Obesity. *Cell* **165**, 882–895 (2016).

293. Barkauskas, D. S. *et al.* Extravascular CX3CR1+ cells extend intravascular dendritic processes into intact central nervous system vessel lumen. in *Microscopy and Microanalysis* vol. 19 778–790 (NIH Public Access, 2013).

294. He, H. *et al.* Perivascular Macrophages Limit Permeability. *Arterioscler. Thromb. Vasc.*

Biol. **36**, 2203–2212 (2016).

295. Willis, C. L., Garwood, C. J. & Ray, D. E. A size selective vascular barrier in the rat area postrema formed by perivascular macrophages and the extracellular matrix. *Neuroscience* **150**, 498–509 (2007).

296. Schain, A. J. *et al.* Activation of pial and dural macrophages and dendritic cells by cortical spreading depression. *Ann. Neurol.* **83**, 508–521 (2018).

297. Cavaillon, J.-M. The historical milestones in the understanding of leukocyte biology initiated by Elie Metchnikoff. *J. Leukoc. Biol.* **90**, 413–424 (2011).

298. Gordon, S. Phagocytosis: An Immunobiologic Process. *Immunity* vol. 44 463–475 (2016).

299. Wakselman, S. *et al.* Developmental neuronal death in hippocampus requires the microglial CD11b integrin and DAP12 immunoreceptor. *J. Neurosci.* **28**, 8138–8143 (2008).

300. Fourgeaud, L. *et al.* TAM receptors regulate multiple features of microglial physiology. *Nature* **532**, 240–244 (2016).

301. Bergman, M. *et al.* Interaction between phagocytosis and IL-1β production by rat peritoneal macrophages. *Biomed. Pharmacother.* **56**, 159–162 (2002).

302. Park, L. *et al.* Scavenger receptor CD36 is essential for the cerebrovascular oxidative stress and neurovascular dysfunction induced by amyloid-β. *Proc. Natl. Acad. Sci. U. S. A.* **108**, 5063–5068 (2011).

303. Mrdjen, D. *et al.* High-Dimensional Single-Cell Mapping of Central Nervous System Immune Cells Reveals Distinct Myeloid Subsets in Health, Aging, and Disease. *Immunity*

48, 380-395.e6 (2018).

304. Hong, S. *et al.* Complement and microglia mediate early synapse loss in Alzheimer mouse models. *Science (80-.).* **352**, 712–716 (2016).

305. Weinhard, L. *et al.* Microglia remodel synapses by presynaptic trogocytosis and spine head filopodia induction. *Nat. Commun.* **9**, 1228 (2018).

306. Tremblay, M.-È., Lowery, R. L. & Majewska, A. K. Microglial Interactions with Synapses Are Modulated by Visual Experience. *PLoS Biol.* **8**, e1000527 (2010).

307. Fourgeaud, L. *et al.* TAM receptors regulate multiple features of microglial physiology. *Nature* **532**, 240–244 (2016).

308. Jordão, M. J. C. *et al.* Single-cell profiling identifies myeloid cell subsets with distinct fates during neuroinflammation. *Science (80-.).* **363**, eaat7554 (2019).

309. Van Hove, H. *et al.* A single-cell atlas of mouse brain macrophages reveals unique transcriptional identities shaped by ontogeny and tissue environment. *Nat. Neurosci.* doi:10.1038/s41593-019-0393-4.

310. Hickey, W. F. & Kimura, H. Perivascular microglial cells of the CNS are bone marrow-derived and present antigen in vivo. *Science.* **239**, 290–2 (1988).

311. Hickey, W. F., Vass, K. & Lassmann, H. Bone marrow-derived elements in the central nervous system: An immunohistochemical and ultrastructural survey of rat chimeras. *J. Neuropathol. Exp. Neurol.* **51**, 246–256 (1992).

312. Bechmann, I. *et al.* Immune surveillance of mouse brain perivascular spaces by blood-borne macrophages. *Eur. J. Neurosci.* **14**, 1651–8 (2001).

313. Prinz, M., Erny, D. & Hagemeyer, N. Ontogeny and homeostasis of CNS myeloid cells. *Nat. Immunol.* **18**, 385–392 (2017).

314. Ginhoux, F. *et al.* Fate Mapping Analysis Reveals That Adult Microglia Derive from Primitive Macrophages. *Science (80-.).* **330**, 841–845 (2010).

315. Kierdorf, K. *et al.* Microglia emerge from erythromyeloid precursors via Pu.1- and Irf8-dependent pathways. *Nat. Neurosci.* **16**, 273–280 (2013).

316. Gomez Perdiguero, E. *et al.* Tissue-resident macrophages originate from yolk-sac-derived erythro-myeloid progenitors. *Nature* **518**, 547–551 (2015).

317. Schulz, C. *et al.* A Lineage of Myeloid Cells Independent of Myb and Hematopoietic Stem Cells. *Science (80-.).* **336**, 86–90 (2012).

318. Hoeffel, G. *et al.* C-Myb+ Erythro-Myeloid Progenitor-Derived Fetal Monocytes Give Rise to Adult Tissue-Resident Macrophages. *Immunity* **42**, 665–678 (2015).

319. Casano, A. M., Albert, M. & Peri, F. Developmental Apoptosis Mediates Entry and Positioning of Microglia in the Zebrafish Brain. *Cell Rep.* **16**, 897–906 (2016).

320. Bohlen, C. J. *et al.* Diverse Requirements for Microglial Survival, Specification, and Function Revealed by Defined-Medium Cultures. *Neuron* **94**, 759-773.e8 (2017).

321. Buttgereit, A. *et al.* Sall1 is a transcriptional regulator defining microglia identity and function. *Nat. Immunol.* **17**, 1397–1406 (2016).

322. Wong, K. *et al.* Mice deficient in NRROS show abnormal microglial development and neurological disorders. *Nat. Immunol.* **18**, 633–641 (2017).

323. Wang, Y. *et al.* IL-34 is a tissue-restricted ligand of CSF1R required for the development

of Langerhans cells and microglia. *Nat. Immunol.* **13**, 753–760 (2012).

324. Schulz, C. *et al.* A lineage of myeloid cells independent of myb and hematopoietic stem cells. *Science (80-.).* **335**, 86–90 (2012).

325. Tay, T. L. *et al.* A new fate mapping system reveals context-dependent random or clonal expansion of microglia. *Nat. Neurosci.* **20**, 793–803 (2017).

326. Hashimoto, D. *et al.* Tissue-resident macrophages self-maintain locally throughout adult life with minimal contribution from circulating monocytes. *Immunity* **38**, 792–804 (2013).

327. Bennett, M. L. *et al.* New tools for studying microglia in the mouse and human CNS. *Proc. Natl. Acad. Sci. U. S. A.* **113**, E1738–E1746 (2016).

328. Masuda, T. *et al.* Novel Hexb-based tools for studying microglia in the CNS. *Nat. Immunol.* **21**, 802–815 (2020).

329. Shemer, A. *et al.* Engrafted parenchymal brain macrophages differ from microglia in transcriptome, chromatin landscape and response to challenge. doi:10.1038/s41467-018-07548-5.

330. Lawson, L. J., Perry, V. H., Dri, P. & Gordon, S. Heterogeneity in the distribution and morphology of microglia in the normal adult mouse brain. *Neuroscience* **39**, 151–170 (1990).

331. Ren, L. qiang, Lubrich, B., Biber, K. & Gebicke-Haerter, P. J. Differential expression of inflammatory mediators in rat microglia cultured from different brain regions. *Mol. Brain Res.* **65**, 198–205 (1999).

332. Goldmann, T. *et al.* USP18 lack in microglia causes destructive interferonopathy of the

mouse brain. *EMBO J.* **34**, 1612–1629 (2015).

333. Askew, K. *et al.* Coupled Proliferation and Apoptosis Maintain the Rapid Turnover of Microglia in the Adult Brain. *Cell Rep.* **18**, 391–405 (2017).

334. Huang, Y. *et al.* Repopulated microglia are solely derived from the proliferation of residual microglia after acute depletion. *Nat. Neurosci.* **21**, 530–540 (2018).

335. Masuda, T. *et al.* Spatial and temporal heterogeneity of mouse and human microglia at single-cell resolution. *Nature* **566**, 388–392 (2019).

336. Hammond, T. R. *et al.* Single-Cell RNA Sequencing of Microglia throughout the Mouse Lifespan and in the Injured Brain Reveals Complex Cell-State Changes. *Immunity* **50**, 253-271.e6 (2019).

337. Keren-Shaul, H. *et al.* A Unique Microglia Type Associated with Restricting Development of Alzheimer's Disease. *Cell* **169**, 1276-1290.e17 (2017).

338. Tu, P., Gurney, M., Julien, J., Lee, V. & Trojanowski, J. Oxidative stress, mutant SOD1, and neurofilament pathology in transgenic mouse models of human motor neuron disease. *Lab. Investig.* **76**, 441–456 (1997).

339. Safaiyan, S. *et al.* White matter aging drives microglial diversity. *Neuron* (2021) doi:10.1016/j.neuron.2021.01.027.

340. Sousa, C. *et al.* Single-cell transcriptomics reveals distinct inflammation-induced microglia signatures. *EMBO Rep.* **19**, (2018).

341. Cserép, C. *et al.* Microglia monitor and protect neuronal function through specialized somatic purinergic junctions. *Science (80-.).* **367**, 528–537 (2020).

342. Császár, E. *et al.* Microglia control cerebral blood flow and neurovascular coupling via P2Y12R-mediated actions. *bioRxiv* 2021.02.04.429741 (2021) doi:10.1101/2021.02.04.429741.

343. Hayashi, Y., Ishibashi, H., Hashimoto, K. & Nakanishi, H. Potentiation of the NMDA receptor-mediated responses through the activation of the glycine site by microglia secreting soluble factors. *Glia* **53**, 660–668 (2006).

344. Coull, J. A. M. *et al.* BDNF from microglia causes the shift in neuronal anion gradient underlying neuropathic pain. *Nature* **438**, 1017–1021 (2005).

345. Sparrow, J. R. Inducible nitric oxide synthase in the central nervous system. *J. Mol. Neurosci.* **5**, 219–229 (1994).

346. Grossmann, R. *et al.* Juxtavascular microglia migrate along brain microvessels following activation during early postnatal development . *Glia* **37**, 229–240 (2002).

347. Lassmann, H., Zimprich, F., Vass, K. & Hickey, W. F. Microglial cells are a component of the perivascular glia limitans. *J. Neurosci. Res.* **28**, 236–243 (1991).

348. Kurz, H. Physiology of angiogenesis. *Journal of Neuro-Oncology* vol. 50 17–35 (2000).

349. Risau, W. Mechanisms of angiogenesis. *Nature* vol. 386 671–674 (1997).

350. Eilken, H. M. & Adams, R. H. Dynamics of endothelial cell behavior in sprouting angiogenesis. *Current Opinion in Cell Biology* vol. 22 617–625 (2010).

351. Fantin, A. *et al.* Tissue macrophages act as cellular chaperones for vascular anastomosis downstream of VEGF-mediated endothelial tip cell induction. *Blood* **116**, 829–840 (2010).

352. Rymo, S. F. *et al.* A two-way communication between microglial cells and angiogenic sprouts regulates angiogenesis in aortic ring cultures. *PLoS One* **6**, e15846 (2011).

353. Checchin, D., Sennlaub, F., Levavasseur, E., Leduc, M. & Chemtob, S. Potential role of microglia in retinal blood vessel formation. *Investig. Ophthalmol. Vis. Sci.* **47**, 3595–3602 (2006).

354. Kubota, Y. *et al.* M-CSF inhibition selectively targets pathological angiogenesis and lymphangiogenesis. *J. Exp. Med.* **206**, 1089–1102 (2009).

355. Tata, M., Ruhrberg, C. & Fantin, A. Vascularisation of the central nervous system. *Mechanisms of Development* vol. 138 26–36 (2015).

356. Zhang, Y. *et al.* Apoptosis of Endothelial Cells Contributes to Brain Vessel Pruning of Zebrafish During Development. *Front. Mol. Neurosci.* **11**, 222 (2018).

357. Franco, C. A. *et al.* Dynamic Endothelial Cell Rearrangements Drive Developmental Vessel Regression. *PLoS Biol.* **13**, e1002125 (2015).

358. Kochhan, E. *et al.* Blood Flow Changes Coincide with Cellular Rearrangements during Blood Vessel Pruning in Zebrafish Embryos. *PLoS One* **8**, e75060 (2013).

359. Chen, Q. *et al.* Haemodynamics-Driven Developmental Pruning of Brain Vasculature in Zebrafish. *PLoS Biol.* **10**, e1001374 (2012).

360. Lang, R. A. & Bishop, J. M. Macrophages are required for cell death and tissue remodeling in the developing mouse eye. *Cell* **74**, 453–462 (1993).

361. Lobov, I. B. *et al.* WNT7b mediates macrophage-induced programmed cell death in patterning of the vasculature. *Nature* **437**, 417–421 (2005).

362. Varol, C., Mildner, A. & Jung, S. Macrophages: Development and tissue specialization. *Annual Review of Immunology* vol. 33 643–675 (2015).

363. Stevens, B. *et al.* The Classical Complement Cascade Mediates CNS Synapse Elimination. *Cell* **131**, 1164–1178 (2007).

364. Hoeffel, G. & Ginhoux, F. Fetal monocytes and the origins of tissue-resident macrophages. *Cell. Immunol.* **330**, 5–15 (2018).

365. Akashi, K., Traver, D., Miyamoto, T. & Weissman, I. L. A clonogenic common myeloid progenitor that gives rise to all myeloid lineages. *Nature* **404**, 193–197 (2000).

366. Passlick, B., Flieger, D. & Ziegler-Heitbrock, H. Identification and characterization of a novel monocyte subpopulation in human peripheral blood. *Blood* **74**, 2527–2534 (1989).

367. Serbina, N. V. & Pamer, E. G. Monocyte emigration from bone marrow during bacterial infection requires signals mediated by chemokine receptor CCR2. *Nat. Immunol.* **7**, 311–317 (2006).

368. Ley, K., Laudanna, C., Cybulsky, M. I. & Nourshargh, S. Getting to the site of inflammation: the leukocyte adhesion cascade. *Nat. Rev. Immunol.* **7**, 678–689 (2007).

369. Springer, T. A. Traffic signals for lymphocyte recirculation and leukocyte emigration: The multistep paradigm. *Cell* vol. 76 301–314 (1994).

370. Ostermann, G., Weber, K. S. C., Zernecke, A., Schröder, A. & Weber, C. JAM-I is a ligand of the β2 integrin LFA-I involved in transendothelial migration of leukocytes. *Nat. Immunol.* **3**, 151–158 (2002).

371. Massena, S. *et al.* A chemotactic gradient sequestered on endothelial heparan sulfate

induces directional intraluminal crawling of neutrophils. *Blood* **116**, 1924–1931 (2010).

372. Man, S., Ubogu, E. E. & Ransohoff, R. M. Inflammatory cell migration into the central nervous system: A few new twists on an old tale. in *Brain Pathology* vol. 17 243–250 (John Wiley & Sons, Ltd, 2007).

373. Gray, S. M. & Barrett, E. J. The Blood-Brain Barrier in Diabetes Mellitus. in *Type 2 Diabetes and Dementia* 211–229 (Elsevier Inc., 2018). doi:10.1016/B978-0-12-809454-9.00011-1.

374. Toft-Hansen, H. *et al.* Metalloproteinases Control Brain Inflammation Induced by Pertussis Toxin in Mice Overexpressing the Chemokine CCL2 in the Central Nervous System. *J. Immunol.* **177**, 7242–7249 (2006).

375. Varvel, N. H. *et al.* Microglial repopulation model reveals a robust homeostatic process for replacing CNS myeloid cells. *Proc. Natl. Acad. Sci. U. S. A.* **109**, 18150–18155 (2012).

376. Wilkinson, F. L. *et al.* Busulfan conditioning enhances engraftment of hematopoietic donor-derived cells in the brain compared with irradiation. *Mol. Ther.* **21**, 868–876 (2013).

377. Kierdorf, K., Katzmarski, N., Haas, C. A. & Prinz, M. Bone Marrow Cell Recruitment to the Brain in the Absence of Irradiation or Parabiosis Bias. *PLoS One* **8**, e58544 (2013).

378. Brehm, M., Schiller, E. & Zeller, W. J. Quantification of reactive oxygen species generated by alveolar macrophages using lucigenin-enhanced chemiluminescence - methodical aspects. *Toxicol. Lett.* **87**, 131–138 (1996).

379. Waddington, R. J., Moseley, R. & Embery, G. Reactive oxygen species: A potential role in the pathogenesis of periodontal diseases. *Oral Diseases* vol. 6 138–151 (2000).

380. Stranahan, A. M., Hao, S., Dey, A., Yu, X. & Baban, B. Blood-brain barrier breakdown promotes macrophage infiltration and cognitive impairment in leptin receptor-deficient mice. *J. Cereb. Blood Flow Metab.* **36**, 2108–2121 (2016).

381. Mildner, A. *et al.* Distinct and non-redundant roles of microglia and myeloid subsets in mouse models of Alzheimer's disease. *J. Neurosci.* **31**, 11159–11171 (2011).

382. Ajami, B., Bennett, J. L., Krieger, C., Tetzlaff, W. & Rossi, F. M. V. Local self-renewal can sustain CNS microglia maintenance and function throughout adult life. *Nat. Neurosci.* **10**, 1538–1543 (2007).

383. Shih, A. Y., Hyacinth, I., Hartmann, D. A. & Van Veluw, S. J. Rodent models of cerebral microinfarct and microhemorrhage. *Stroke* **49**, 803–810 (2018).

384. Shinohara, M. *et al.* Overexpression of glyoxalase-I in bovine endothelial cells inhibits intracellular advanced glycation endproduct formation and prevents hyperglycemia-induced increases in macromolecular endocytosis. *J. Clin. Invest.* **101**, 1142–1147 (1998).

385. Baynes, J. W. & Thorpe, S. R. Role of oxidative stress in diabetic complications: A new perspective on an old paradigm. *Diabetes* vol. 48 1–9 (1999).

386. Haneda, M. *et al.* Abnormalities in protein kinase C and MAP kinase cascade in mesangial cells cultured under high glucose conditions. *J. Diabetes Complications* **9**, 246–8 (1995).

387. Purves, T. *et al.* A role for mitogen-activated protein kinases in the etiology of diabetic

neuropathy. *FASEB J.* **15**, 2508–2514 (2001).

388. Haneda, M. *et al.* Mitogen-activated protein kinase cascade is activated in glomeruli of diabetic rats and glomerular mesangial cells cultured under high glucose conditions. *Diabetes* **46**, 847–53 (1997).

389. Siperstein, M. D., Unger, R. H. & Madison, L. L. Studies of muscle capillary basement membranes in normal subjects, diabetic, and prediabetic patients. *J. Clin. Invest.* **47**, 1973–1999 (1968).

390. Bendayan, M., Bouchard, P. & Ghitescu, L. D. Morpho-functional studies of the blood-brain barrier in streptozotocin-induced diabetic rats. *Diabetologia* **45**, 1017–1025 (2002).

391. Hawkins, B. T., Lundeen, T. F., Norwood, K. M., Brooks, H. L. & Egleton, R. D. Increased blood–brain barrier permeability and altered tight junctions in experimental diabetes in the rat: contribution of hyperglycaemia and matrix metalloproteinases. *Diabetologia* **50**, 202–211 (2006).

392. Byon, I. S. *et al.* Effect of angiotensin ii type 1 receptor blocker and angiotensin converting enzyme inhibitor on the intraocular growth factors and their receptors in streptozotocin-induced diabetic rats. *Int. J. Ophthalmol.* **10**, 896–901 (2017).

393. Kim, J. H., Kim, J. H., Yu, Y. S., Cho, C. S. & Kim, K. W. Blockade of angiotensin II attenuates VEGF-mediated blood-retinal barrier breakdown in diabetic retinopathy. *J. Cereb. Blood Flow Metab.* **29**, 621–628 (2009).

394. Kawamura, H. *et al.* Effects of angiotensin II on the pericyte-containing microvasculature of the rat retina. *J. Physiol.* **561**, 671–683 (2004).

395. van Veluw, S. J. *et al.* Different microvascular alterations underlie microbleeds and microinfarcts. *Ann. Neurol.* **86**, 279–292 (2019).

396. Wang, Z., Soo, Y. O. Y. & Mok, V. C. T. Cerebral microbleeds: Is antithrombotic therapy safe to administer? *Stroke* vol. 45 2811–2817 (2014).

397. Taqueti, V. R. & Di Carli, M. F. Coronary Microvascular Disease Pathogenic Mechanisms and Therapeutic Options: JACC State-of-the-Art Review. *Journal of the American College of Cardiology* vol. 72 2625–2641 (2018).

398. Anderson, T. J. Assessment and treatment of endothelial dysfunction in humans. *J. Am. Coll. Cardiol.* **34**, 631–638 (1999).

399. Fazekas, F. *et al.* Histopathologic analysis of foci of signal loss on gradient-echo T2*-weighted MR images in patients with spontaneous intracerebral hemorrhage: Evidence of microangiopathy-related microbleeds. *Am. J. Neuroradiol.* **20**, 637–642 (1999).

400. Fisher, M., French, S., Ji, P. & Kim, R. C. Cerebral microbleeds in the elderly: a pathological analysis. *Stroke* **41**, 2782–5 (2010).

401. Uetani, H. *et al.* Prevalence and topography of small hypointense foci suggesting microbleeds on 3T susceptibility-weighted imaging in various types of dementia. *Am. J. Neuroradiol.* **34**, 984–989 (2013).

402. Milner, R. *et al.* Increased expression of fibronectin and the α5β1 integrin in angiogenic cerebral blood vessels of mice subject to hypobaric hypoxia. *Mol. Cell. Neurosci.* **38**, 43–52 (2008).

403. Hassler, O. Blood Supply to Human Spinal Cord: A Microangiographic Study. *Arch.*

Neurol. **15**, 302–307 (1966).

404. Auriat, A. M. *et al.* Ferric iron chelation lowers brain iron levels after intracerebral hemorrhage in rats but does not improve outcome. *Exp. Neurol.* **234**, 136–143 (2012).

405. Rosidi, N. L. *et al.* Cortical Microhemorrhages Cause Local Inflammation but Do Not Trigger Widespread Dendrite Degeneration. *PLoS One* **6**, e26612 (2011).

406. Lee, S. H. *et al.* Dynamic temporal change of cerebral microbleeds: Long-Term Follow-Up MRI study. *PLoS One* **6**, (2011).

407. Jeon, S. B. *et al.* Rapid appearance of new cerebral microbleeds after acute ischemic stroke. *Neurology* **73**, 1638–1644 (2009).

408. Cordonnier, C. *et al.* Prevalence and severity of microbleeds in a memory clinic setting. *Neurology* **66**, 1356–1360 (2006).

409. Martinez-Ramirez, S., Greenberg, S. M. & Viswanathan, A. Cerebral microbleeds: overview and implications in cognitive impairment. *Alzheimers. Res. Ther.* **6**, 33 (2014).

410. Poels, M. M. F. *et al.* Prevalence and risk factors of cerebral microbleeds: An update of the rotterdam scan study. in *Stroke* vol. 41 (Stroke, 2010).

411. DiSabato, D. J., Quan, N. & Godbout, J. P. Neuroinflammation: the devil is in the details. *J. Neurochem.* **139**, 136–153 (2016).

412. Banks, W. A., Kastin, A. J. & Broadwell, R. D. Passage of cytokines across the blood-brain barrier. *Neuroimmunomodulation* **2**, 241–8 (1995).

413. Pan, W. *et al.* Cytokine signaling modulates blood-brain barrier function. *Curr. Pharm. Des.* **17**, 3729–40 (2011).

414. Prinz, M. & Priller, J. The role of peripheral immune cells in the CNS in steady state and disease. *Nat. Neurosci.* **20**, 136–144 (2017).

415. Chai, J. & Song, Q. Quantitative and Multiplexed Study of Endothelial Cell Inflammation. *Cell Biochem. Biophys.* **70**, 1783–1790 (2014).

416. Pieper, G. M. & Peltier, B. A. Amelioration by L-arginine of a dysfunctional arginine/nitric oxide pathway in diabetic endothelium. *J. Cardiovasc. Pharmacol.* **25**, 397–403 (1995).

417. Pieper, G. M. Acute amelioration of diabetic endothelial dysfunction with a derivative of the nitric oxide synthase cofactor, tetrahydrobiopterin. *J. Cardiovasc. Pharmacol.* **29**, 8–15 (1997).

418. Lefer, D. J. *et al.* Leukocyte-endothelial cell interactions in nitric oxide synthase- deficient mice. *Am. J. Physiol. - Hear. Circ. Physiol.* **276**, (1999).

419. Song, J. *et al.* Focal MMP-2 and MMP-9 Activity at the Blood-Brain Barrier Promotes Chemokine-Induced Leukocyte Migration. *Cell Rep.* **10**, 1040–1054 (2015).

420. Paré, A. *et al.* IL-1β enables CNS access to CCR2hi monocytes and the generation of pathogenic cells through GM-CSF released by CNS endothelial cells. *Proc. Natl. Acad. Sci. U. S. A.* **115**, E1194–E1203 (2018).

421. Pitocco, D. *et al.* The effects of calcitriol and nicotinamide on residual pancreatic β-cell function in patients with recent-onset Type 1 diabetes (IMDIAB XI). *Diabet. Med.* **23**, 920–923 (2006).

422. Asahara, T. *et al.* Isolation of putative progenitor endothelial cells for angiogenesis.

Science (80-.). **275**, 964–967 (1997).

423. Russo, M. V., Latour, L. L. & McGavern, D. B. Distinct myeloid cell subsets promote meningeal remodeling and vascular repair after mild traumatic brain injury article. *Nat. Immunol.* **19**, 442–452 (2018).

424. Tammela, T. *et al.* VEGFR-3 controls tip to stalk conversion at vessel fusion sites by reinforcing Notch signalling. *Nat. Cell Biol.* **13**, 1202–1213 (2011).

425. Jolivel, V. *et al.* Perivascular microglia promote blood vessel disintegration in the ischemic penumbra. *Acta Neuropathol.* **129**, 279–295 (2015).

426. Chiu, I. M. *et al.* A neurodegeneration-specific gene-expression signature of acutely isolated microglia from an amyotrophic lateral sclerosis mouse model. *Cell Rep.* **4**, 385–401 (2013).

427. Jung, S. *et al.* Analysis of fractalkine receptor CX(3)CR1 function by targeted deletion and green fluorescent protein reporter gene insertion. *Mol. Cell. Biol.* **20**, 4106–4114 (2000).

428. Karunanayake, E. H., Baker, J. R. J., Christian, R. A., Hearse, D. J. & Mellows, G. Autoradiographic study of the distribution and cellular uptake of (14C)-streptozotocin in the rat. *Diabetologia* **12**, 123–128 (1976).

429. Arison, R. N., Ciaccio, E. I., Glitzer, M. S., Cassaro, J. A. & Pruss, M. P. Light and electron microscopy of lesions in rats rendered diabetic with streptozotocin. *Diabetes* **16**, 51–56 (1967).

430. Yamamoto, H., Uchigata, Y. & Okamoto, H. Streptozotocin and alloxan induce DNA

strand breaks and poly(ADP-ribose) synthetase in pancreatic islets. *Nature* **294**, 284–286 (1981).

431. Reeson, P., Jeffery, A. & Brown, C. E. Illuminating the Effects of Stroke on the Diabetic Brain: Insights From Imaging Neural and Vascular Networks in Experimental Animal Models. *Diabetes* **65**, 1779–88 (2016).

432. Allen Mouse Brain Atlas. Slc2a2 - RP_050315_01_E04 - sagittal. *Allen Institute for Brain Science* https://mouse.brain-map.org/experiment/show/69015679 (2021).

433. Sun, P. *et al.* Streptozotocin impairs proliferation and differentiation of adult hippocampal neural stem cells in vitro-correlation with alterations in the expression of proteins associated with the insulin system. *Front. Aging Neurosci.* **10**, 145 (2018).

434. LinShin Canada Inc. LinBit Product Instructions. *LinShin Canada, Inc.* http://www.linshincanada.com/linbit.html (2016).

435. Alavi, A. *et al.* Diabetic foot ulcers: Part I. Pathophysiology and prevention. *Journal of the American Academy of Dermatology* vol. 70 1.e1-1.e18 (2014).

436. Brem, H. & Tomic-Canic, M. Cellular and molecular basis of wound healing in diabetes. *Journal of Clinical Investigation* vol. 117 1219–1222 (2007).

437. Unger, M. S., Schernthaner, P., Marschallinger, J., Mrowetz, H. & Aigner, L. Microglia prevent peripheral immune cell invasion and promote an anti-inflammatory environment in the brain of APP-PS1 transgenic mice. *J. Neuroinflammation* **15**, 274 (2018).

438. Cakman, I., Kirchner, H. & Rink, L. Zinc supplementation reconstitutes the production of interferon-α by leukocytes from elderly persons. *J. Interf. Cytokine Res.* **17**, 469–472

(1997).

439. Gray, P. W. & Goeddel, D. V. Structure of the human immune interferon gene. *Nature* **298**, 859–863 (1982).

440. Elmore, M. R. P. *et al.* Colony-stimulating factor 1 receptor signaling is necessary for microglia viability, unmasking a microglia progenitor cell in the adult brain. *Neuron* **82**, 380–397 (2014).

441. Erblich, B., Zhu, L., Etgen, A. M., Dobrenis, K. & Pollard, J. W. Absence of colony stimulation factor-1 receptor results in loss of microglia, disrupted brain development and olfactory deficits. *PLoS One* **6**, e26317 (2011).

442. MW, V. *et al.* Prevalence and risk factors of cerebral microbleeds: the Rotterdam Scan Study. *Neurology* **70**, 1208–14 (2008).

443. Zhan, L. *et al.* A MAC2-positive progenitor-like microglial population is resistant to CSF1R inhibition in adult mouse brain. *Elife* **9**, e51796 (2020).

444. Lee, J., Sohn, E. H., Oh, E. & Lee, A. Y. Characteristics of Cerebral Microbleeds. *Dement. Neurocognitive Disord.* **17**, 73 (2018).

445. Renard, D. Cerebral microbleeds: a magnetic resonance imaging review of common and less common causes. *Eur. J. Neurol.* **25**, 441–450 (2018).

446. Perry, V. H. & Gordon, S. Macrophages and microglia in the nervous system. *Trends Neurosci.* **11**, 273–277 (1988).

447. Yu, C., Roubeix, C., Sennlaub, F. & Saban, D. R. Microglia versus Monocytes: Distinct Roles in Degenerative Diseases of the Retina. *Trends Neurosci.* **43**, 433–449 (2020).

448. Utz, S. G. *et al.* Early Fate Defines Microglia and Non-parenchymal Brain Macrophage Development. *Cell* **181**, 557-573.e18 (2020).

449. Ajami, B. *et al.* Single-cell mass cytometry reveals distinct populations of brain myeloid cells in mouse neuroinflammation and neurodegeneration models. *Nat. Neurosci.* **21**, 541–551 (2018).

450. Paschalis, E. I. *et al.* Permanent neuroglial remodeling of the retina following infiltration of CSF1R inhibition-resistant peripheral monocytes. *Proc. Natl. Acad. Sci. U. S. A.* **115**, E11359–E11368 (2018).

451. Fiala, M. *et al.* Ineffective phagocytosis of amyloid-beta by macrophages of Alzheimer's disease patients. *J. Alzheimers. Dis.* **7**, 221–32; discussion 255-62 (2005).

452. Rangasamy, S. *et al.* Chemokine mediated monocyte trafficking into the retina: Role of inflammation in alteration of the blood-retinal barrier in diabetic retinopathy. *PLoS One* **9**, e108508 (2014).

453. Le Marer, N. GALECTIN-3 expression in differentiating human myeloid cells. *Cell Biol. Int.* **24**, 245–251 (2000).

454. Frith, J. C., Mönkkönen, J., Blackburn, G. M., Russell, R. G. G. & Rogers, M. J. Clodronate and liposome-encapsulated clodronate are metabolized to a toxic ATP analog, adenosine 5'-(β,γ-dichloromethylene) triphosphate, by mammalian cells in vitro. *J. Bone Miner. Res.* **12**, 1358–1367 (1997).

455. Lehenkari, P. P. *et al.* Further insight into mechanism of action of clodronate: Inhibition of mitochondrial ADP/ATP translocase by a nonhydrolyzable, adenine-containing

metabolite. *Mol. Pharmacol.* **61**, 1255–1262 (2002).

456. Berg, J. T., Lee, S. T., Thepen, T., Lee, C. Y. & Tsan, M. F. Depletion of alveolar macrophages by liposome-encapsulated dichloromethylene diphosphonate. *J. Appl. Physiol.* **74**, 2812–2819 (1993).

457. Huitinga, I., van Rooijen, N., de Groot, C. J. A., Uitdehaag, B. M. J. & Dijkstra, C. D. Suppression of experimental allergic encephalomyelitis in lewis rats after elimination of macrophages. *J. Exp. Med.* **172**, 1025–1033 (1990).

458. Polfliet, M. M. J. *et al.* A method for the selective depletion of perivascular and meningeal macrophages in the central nervous system. *J. Neuroimmunol.* **116**, 188–195 (2001).

459. Weinger, J. G. *et al.* Loss of the receptor tyrosine kinase Axl leads to enhanced inflammation in the CNS and delayed removal of myelin debris during Experimental Autoimmune Encephalomyelitis. *J. Neuroinflammation* **8**, (2011).

460. Nam, K. N. *et al.* Effect of high fat diet on phenotype, brain transcriptome and lipidome in Alzheimer's model mice. *Sci. Rep.* **7**, 1–13 (2017).

461. Chistiakov, D. A., Killingsworth, M. C., Myasoedova, V. A., Orekhov, A. N. & Bobryshev, Y. V. CD68/macrosialin: Not just a histochemical marker. *Lab. Investig.* **97**, 4–13 (2017).

462. Holness, C. & Simmons, D. Molecular cloning of CD68, a human macrophage marker related to lysosomal glycoproteins. *Blood* **81**, 1607–1613 (1993).

463. Filipello, F. *et al.* The Microglial Innate Immune Receptor TREM2 Is Required for Synapse Elimination and Normal Brain Connectivity. *Immunity* **48**, 979-991.e8 (2018).

464. Frediani, B. & Bertoldi, I. Clodronate: new directions of use. *Clin. Cases Miner. Bone Metab.* **12**, 97 (2015).

465. Khan, S. A. *et al.* Duration of response with oral clodronate in Paget's disease of bone. *Bone* **18**, 185–190 (1996).

466. McCloskey, E. *et al.* Clodronate reduces vertebral fracture risk in women with postmenopausal or secondary osteoporosis: Results of a double-blind, placebo-controlled 3-year study. *J. Bone Miner. Res.* **19**, 728–736 (2004).

467. Lalancette-Hébert, M. *et al.* Galectin-3 is required for resident microglia activation and proliferation in response to ischemic injury. *J. Neurosci.* **32**, 10383–10395 (2012).

468. Reichert, F. & Rotshenker, S. Galectin-3 (MAC-2) Controls Microglia Phenotype Whether Amoeboid and Phagocytic or Branched and Non-phagocytic by Regulating the Cytoskeleton. *Front. Cell. Neurosci.* **13**, 90 (2019).

469. Wattananit, S. *et al.* Monocyte-Derived Macrophages Contribute to Spontaneous Long-Term Functional Recovery after Stroke in Mice. *J. Neurosci.* **36**, 4182–4195 (2016).

470. Werner, Y. *et al.* Cxcr4 distinguishes HSC-derived monocytes from microglia and reveals monocyte immune responses to experimental stroke. *Nat. Neurosci.* **23**, 351–362 (2020).

471. Shen, J. *et al.* In vivo immunostaining demonstrates macrophages associate with growing and regressing vessels. *Investig. Ophthalmol. Vis. Sci.* **48**, 4335–4341 (2007).

472. Poché, R. A., Hsu, C. W., McElwee, M. L., Burns, A. R. & Dickinson, M. E. Macrophages engulf endothelial cell membrane particles preceding pupillary membrane capillary regression. *Dev. Biol.* **403**, 30–42 (2015).

473. Korn, C. & Augustin, H. G. Mechanisms of Vessel Pruning and Regression. *Dev. Cell* **34**, 5–17 (2015).

474. Höhn, A., Jung, T., Grimm, S. & Grune, T. Lipofuscin-bound iron is a major intracellular source of oxidants: Role in senescent cells. *Free Radic. Biol. Med.* **48**, 1100–1108 (2010).

475. TERMAN, A. & BRUNK, U. T. Lipofuscin: Mechanisms of formation and increase with age. *APMIS* **106**, 265–276 (1998).

476. Moreno-García, A., Kun, A., Calero, O., Medina, M. & Calero, M. An overview of the role of lipofuscin in age-related neurodegeneration. *Front. Neurosci.* **12**, 464 (2018).

477. Rotshenker, S. The role of Galectin-3/MAC-2 in the activation of the innate-immune function of phagocytosis in microglia in injury and disease. *J. Mol. Neurosci.* **39**, 99–103 (2009).

478. Takahashi, K., Rochford, C. D. P. & Neumann, H. Clearance of apoptotic neurons without inflammation by microglial triggering receptor expressed on myeloid cells-2. *J. Exp. Med.* **201**, 647–657 (2005).

479. Yao, H. *et al.* Distinct Signaling Pathways Regulate TREM2 Phagocytic and NFκB Antagonistic Activities. *Front. Cell. Neurosci.* **13**, (2019).

480. Ishimoto, Y., Ohashi, K., Mizuno, K. & Nakano, T. Promotion of the uptake of PS liposomes and apoptotic cells by a product of growth arrest-specific gene, gas6. *J. Biochem.* **127**, 411–417 (2000).

481. Grommes, C. *et al.* Regulation of microglial phagocytosis and inflammatory gene expression by Gas6 acting on the Axl/Mer family of tyrosine kinases. *J. NeuroImmune*

Pharmacol. **3**, 130–140 (2008).

482. Sawaya, A. P. *et al.* Deregulated immune cell recruitment orchestrated by FOXM1 impairs human diabetic wound healing. *Nat. Commun.* **11**, (2020).

483. Stratoulias, V., Venero, J. L., Tremblay, M. & Joseph, B. Microglial subtypes: diversity within the microglial community. *EMBO J.* **38**, (2019).

484. Cianchetti, F. A., Kim, D. H., Dimiduk, S., Nishimura, N. & Schaffer, C. B. Stimulus-Evoked Calcium Transients in Somatosensory Cortex Are Temporarily Inhibited by a Nearby Microhemorrhage. *PLoS One* **8**, (2013).

485. Taylor, S. L. *et al.* VEGF can protect against blood brain barrier dysfunction, dendritic spine loss and spatial memory impairment in an experimental model of diabetes. *Neurobiol. Dis.* **78**, 1–11 (2015).

486. Zhan, L., Sohn, P. D., Zhou, Y., Li, Y. & Gan, L. A Mac2-positive progenitor-like microglial population survives independent of CSF1R signaling in adult mouse brain. *bioRxiv* 722090 (2019) doi:10.1101/722090.

487. Greenberg, S. M. *et al.* Cerebral microbleeds: a guide to detection and interpretation. *Lancet Neurol.* **8**, 165–174 (2009).

488. Bennett, F. C. *et al.* A Combination of Ontogeny and CNS Environment Establishes Microglial Identity. *Neuron* **98**, 1170-1183.e8 (2018).

489. Lambert, J. C. *et al.* Meta-analysis of 74,046 individuals identifies 11 new susceptibility loci for Alzheimer's disease. *Nat. Genet.* **45**, 1452–1458 (2013).

490. Colonna, M. & Butovsky, O. Microglia Function in the Central Nervous System During

Health and Neurodegeneration. *Annu. Rev. Immunol.* **35**, 441–468 (2017).

491. Fahrenhold, M. *et al.* TREM2 expression in the human brain: a marker of monocyte recruitment? *Brain Pathol.* **28**, 595–602 (2018).

492. Lemke, G. & Rothlin, C. V. Immunobiology of the TAM receptors. *Nat. Rev. Immunol.* **8**, 327–336 (2008).

493. Brenig, R. *et al.* Expression of AXL receptor tyrosine kinase relates to monocyte dysfunction and severity of cirrhosis. *Life Sci. Alliance* **3**, e201900465 (2020).

494. Walter, J. The triggering receptor expressed on myeloid cells 2-a molecular link of neuroinflammation and neurodegenerative diseases. *J. Biol. Chem.* **291**, 4334–41 (2016).

495. Fourgeaud, L. *et al.* TAM receptors regulate multiple features of microglial physiology. *Nature* **532**, 240–244 (2016).

496. Otero, K. *et al.* Macrophage colony-stimulating factor induces the proliferation and survival of macrophages via a pathway involving DAP12 and β-catenin. *Nat. Immunol.* **10**, 734–743 (2009).

497. Damisah, E. C. *et al.* Astrocytes and microglia play orchestrated roles and respect phagocytic territories during neuronal corpse removal in vivo. *Sci. Adv.* **6**, eaba3239 (2020).

498. Zarruk, J. G., Greenhalgh, A. D. & David, S. Microglia and macrophages differ in their inflammatory profile after permanent brain ischemia. *Exp. Neurol.* **301**, 120–132 (2018).

499. Greenhalgh, A. D. *et al.* Peripherally derived macrophages modulate microglial function to reduce inflammation after CNS injury. *PLOS Biol.* **16**, e2005264 (2018).

500. Wald, C. & Corinna, W. U. Of mice and women: The bias in animal models. *Science* vol. 327 1571–1572 (2010).

501. Machida, T., Yonezawa, Y. & Noumura, T. Age-associated changes in plasma testosterone levels in male mice and their relation to social dominance or subordinance. *Horm. Behav.* **15**, 238–245 (1981).